NOVEL COATING TECHNOLOGIES FOR ELECTRICAL STEELS

PhD thesis

Vishu Goel

A thesis submitted to the Cardiff University in candidature for the degree of Doctor of Philosophy

May 2016

Wolfson Centre for Magnetics
Cardiff School of Engineering
Cardiff University
Wales, United Kingdom

Acknowledgement

This work was funded by Cardiff University's president scholarship and co-sponsored by Tata steel RD&T Warwick and Cogent Power Ltd. Newport. I am grateful for their support, in terms of finance, resources and technical advice. The work was carried out at Wolfson Centre for Magnetics, school of engineering, Cardiff University.

I wish to thank my supervisors Dr. Philip Anderson and Dr. Jeremy Hall for their continuous support throughout the project. Their guidance, enthusiasm, encouragement and advice were all I need to finish the project. I am also grateful to Mr. Keith Jenkins, Dr. Fiona Robinson Prof. Siva Bohm and Dr. Sreedhara Sarma for providing me with timely resources and support for the work.

I am grateful to Dr. Dan Reed for helping me use the magnetic particle measurement system and atomic force microscopy. I appreciate the support provided by Dr. Emmanuel Brousseau and Dr. Alastair Clarke for their assistance in using the surface roughness analysis facilities in the university. I admire the help of Dr. Paul Williams in using the vibrating sample magnetometer. I am also thankful to mechanical and electrical workshop staff for sorting out my requests as early as possible.

I would like to thank my colleagues in Wolfson centre, Dr. Mahesh Kumar Mani, Dr. Tomasz Kutrowski, Dr. Christopher Harrison, Dr. Teeraphon Phophongviwat, Mr. Amar albaaji, Mr. Hamid, Mrs. Sahar and Mr. David Okhiria for their help and motivation provided during the course of my research.

My parents Mr. Suresh Kumar and Mrs. Usha Rani are the pillars of my success and I would take this opportunity to thank them. I owe my gratitude to my wife, Dr. Mania who has consistently supported and motivated me throughout my research. Last but not the least I thank my friends and relatives for being there with me from the beginning to the end.

Summary

Power loss in transformer cores accounts for approximately 5% of the energy lost as heat. The loss could be reduced by improving the secondary recrystallization methods, grain orientation control, increasing the electrical resistivity of the steel, reducing the thickness of laminations, manipulating the domain structure and applying coatings. Coating grain oriented electrical steel (GOES) helps in reducing the loss by providing electrical resistance, improving the surface roughness and applying beneficial tensile stress.

In this work a range of coatings were explored that can be economically applied on GOES to reduce power loss and magnetostriction in working transformers. Coatings were investigated using a range of coating processes including electroless plating, thermal evaporation physical vapour deposition and electron beam physical vapour deposition.

The coatings were characterised using a range of processes including Single Strip Testing (SST), Magnetostriction measurement, Vibrating Sample Magnetometer (VSM), magnetic domain imaging, Optical microscopy, Scanning Electron Microscopy (SEM), Energy Dispersive X-ray Spectroscopy (EDS), X-ray Diffraction (XRD), Surface profilometry, Atomic force microscopy and Raman spectroscopy.

Co-Ni-P applied on GOES improved the magnetic properties by applying beneficial tensile stress which aligns the domains in the direction of magnetization and by improving the surface roughness which reduces the number of pinning sites on the surface of steel. The magnetostriction was improved due to the effect of beneficial tensile stress. Similarly Co-P-CNT applied on GOES reduced the power loss by improving the surface roughness. CrN, CrAlN, TiAlN improved the power loss and magnetostriction as tensile stress was applied by the coatings which reduced the domain width and hence loss was reduced. The reduction in magnetostriction was due to the high value of Young's modulus of the coatings as compared to GOES which did not allow the steel to expand under the influence of applied magnetic field. The ceramic coatings could be directly employed in the production line replacing the phosphate coating unit with the Chemical/Physical vapour deposition.

Table of Contents

1. Introduction

Electrical steels are used in the core of transformers, generators and motors. These steels are of two types; grain-oriented electrical steel and non-oriented electrical steel.

Grain-oriented electrical steel (GOES) is a special type of cold rolled electrical steel made up of 3% silicon in iron and used in the core of transformers where the grains are oriented in the direction of rolling resulting in superior magnetic properties in that direction. Non-oriented electrical steel is mostly used in motors and generators where they have a cubic texture with (001) and (110) planes parallel to plane of the sheet and uniformly distributed [100] direction.

The AC magnetization of electrical steel can lead to generation of heat and sound which in turn increases the power loss in terms of anomalous, eddy currents and hysteresis loss [1]. Domestic power is provided at very low voltages of around 220-240V but is transmitted at 400,000V from electric power stations and this voltage cannot be directly provided to the houses. Transformers are therefore used to step up/down the voltage. A typical power system diagram is shown in Figure 1.1 which shows the generation, transmission and consumption of power and the use of transformers from the power generation unit to the residential/industrial areas to save the losses from low voltage transmission. There is a problem of transformer hum noise associated with the cyclic magnetization and demagnetization caused due to magnetostriction (change in length of material in the magnetic field) which may be irritating to the local residences. Noise isolating enclosures can be built which attenuate the noise but these introduce significant extra expense. The optimum solution is to control magnetostriction by altering the material properties. Coatings can reduce magnetostriction by eliminating the surface closure domains [2].

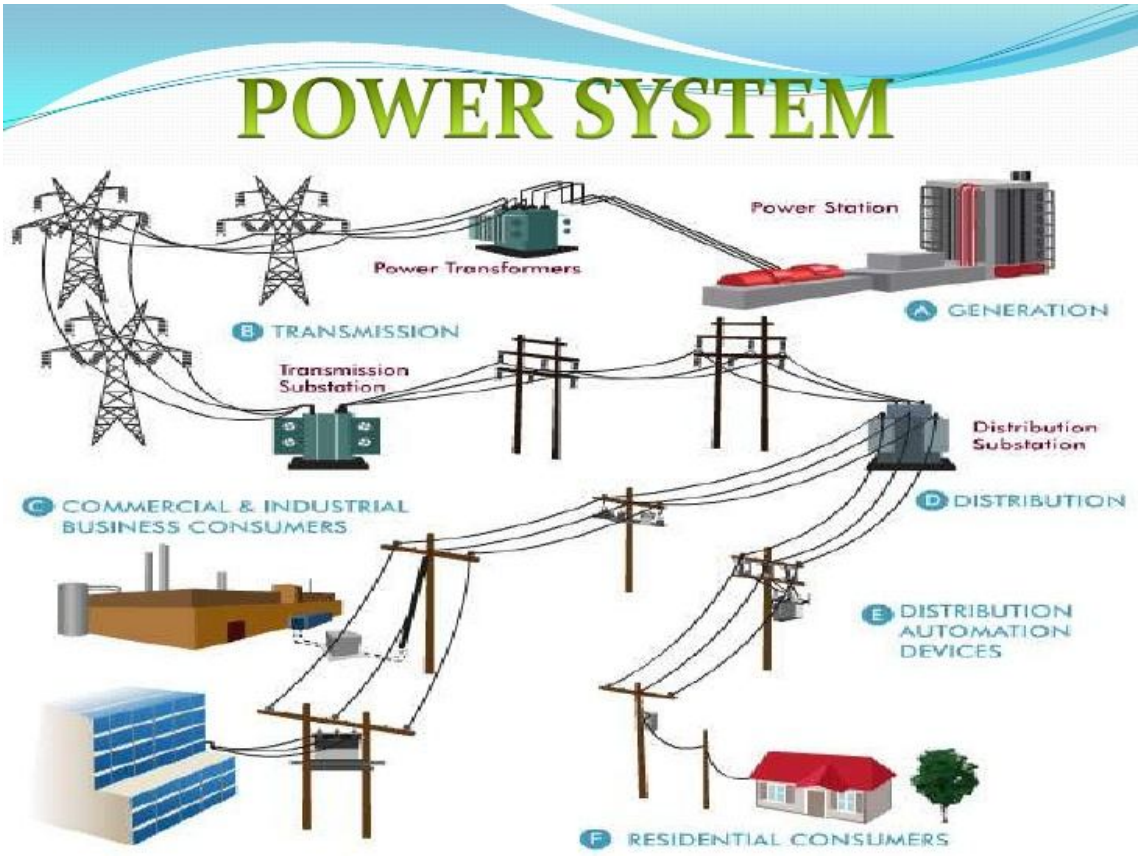

Figure 1.1 shows the usage of transformers in each and every stage of power transmission.

Conventional coatings can reduce the power loss and magnetostriction at zero stress but as the applied compressive stress increases it becomes difficult to control the overall loss and magnetostriction which is directly proportional to compressive stress. Compressive stress is very harmful and tensile stress is beneficial in terms of power loss and magnetostriction. Stresses develop in the transformer during manufacture due to clamping of laminations, temperature gradient across the laminations or damage in the laminations. To reduce this, coatings can be applied which could provide additional tensile stress to compensate the compressive stress.

An effective coating on grain oriented electrical steel provides sufficient tension and insulation to reduce the power loss and magnetostriction. In addition to that, the magnetic activity and thinness improves the stacking factor. The conventional coating system of forsterite and aluminium orthophosphate has thickness in the range of 4-8 microns which means that the stacking factor (amount of magnetic material in the core) is 96 % as the coatings are non-magnetic which reduces the permeability and saturation.

The improvement in power loss due to the beneficial stress in the coatings ranges from 4-6 % and the magnetostriction is zero με for up to 3 MPa of compressive stress.

The aim of this work is to explore a range of novel coatings, magnetic and non-magnetic, ranging from a few hundred nanometres to a few microns that could be applied on grain oriented electrical steel using various coating technologies to get better properties than the conventional coatings. These aimed coatings would have the benefits of increased stacking factor due to the reduction in thickness of coatings also magnetic coatings would be explored to develop coatings with increased permeability, and stacking factor of 98-99% is desired. Improvement in power loss of 10-15 % is aimed and magnetostriction of zero με at 10 MPa of compressive stress is targeted.

The improved coatings would have an effect on the overall efficiency of the transformer and an improvement of 1% would have a significant effect on the power that is lost in millions of transformers used in the world and it will lead to a cost saving of trillions of pounds per year. The amount of CO_2 emitted per kWh is 0.527 kg [3] and saving the energy lost in the transformers would result in reduced emissions and cleaner atmosphere. A considerable reduction in transformer noise due to zero magnetostriction in the transformer would result in reduced noise pollution.

1.1 References

[1] C. R. Boon and J. A. Robey, "Effect of domain-wall motion on power loss in grainoriented silicon-iron sheet," *Proceedings of the IEEE,* vol. 115, pp. 1535-1540, October 1968.

[2] P. I. Anderson, A. J. Moses, and H. J. Stanbury, "Assessment of the Stress Sensitivity of Magnetostriction in Grain-Oriented Silicon Steel " *IEEE Transactions on Magnetics,* vol. 43, pp. 3467-3476, 2007.

[3] DEFRA, "Act on CO2 Calculator: Public Trial Version Data, Methodology and Assumptions Paper," June 2007.

2 Literature Review

2.1 Ferromagnetism

Ferromagnetism is a property exhibited by some materials which can retain the magnetic behaviour after the removal of magnetic field. The electrons spin and orbit around the nucleus to generate magnetic field. In general, the electrons in atoms cancel each other's magnetic field but in a few atoms the resultant magnetic field is not zero and in these atoms a long range order is formed by unpaired electron spins lined parallel to each other and this region is called as a domain. Each domain is aligned in such a way that the resultant magnetic field is zero for the material. In the presence of applied field the domains align themselves in the direction of magnetisation and there is net resultant magnetic field.

2.2 Energies associated with magnetization

The magnetic material, either magnetised or demagnetised, maintains a state of minimum energy and maximum stability in the absence of external force. There are several energies that play an important role in determining the state of the material. Some of the energies are discussed below.

2.2.1 Magnetocrystalline Anisotropy energy

Above the Curie temperature (T_c) the magnetic moments are randomly arranged and the net magnetic moment is zero. As the material is cooled below T_c spontaneous magnetisation occurs and the magnetic moments arrange themselves in the easy axis of magnetization [1]. The resultant magnetic moment is a positive value. The material is no longer isotropic and the energy associated with this phenomenon is known as magnetocrystalline anisotropy energy.

Magnetic materials are generally anisotropic; which means that they show variation in properties in different directions. For example, <001> is considered as the easy magnetization direction and <111> is considered the hardest for a single crystal of iron. If the grains are oriented in <001> it is more easily magnetized provided the field is in the

same direction. The easy axis of magnetization for nickel is <111> which is exactly opposite to that of iron. Figure 2.1 shows the relation between orientation and magnetization. In grain oriented electrical steel the cubic crystals are aligned on edges with the (110) plane of cube aligned along the sheet plane and <100> axis parallel to the rolling direction. The magnetocrystalline anisotropy energy of it can be calculated by the equation as shown below

$$E_k = K_0 + K_1(\alpha_1^2\alpha_2^2+\alpha_2^2\alpha_3^2+\alpha_3^2\alpha_1^2) + K_2(\alpha_1^2\alpha_2^2\alpha_3^2) \quad (2.1)$$

Where

K_1 and K_2 are the anisotropy constants of first and second order

α1, α2, α3 are the direction cosines of magnetisation in <100> directions

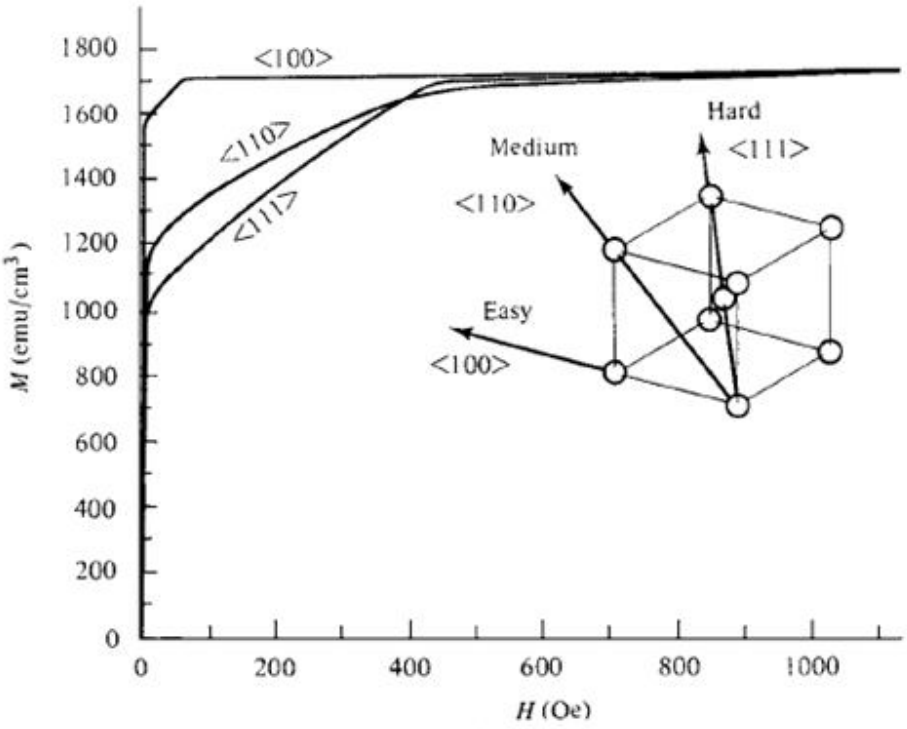

Figure 2.1 Magnetization curves for single crystals of iron [2].

2.2.2 Magnetoelastic energy

The magnetic anisotropy and ferromagnetism develops due to atomic moment interactions and these interactions also strain the lattice anisotropically [3]. On heating a single magnetic domain above Curie temperature the thermal agitation of atoms overcomes the exchange interaction and hence the ferromagnetic properties disappear. Cooling it again would strain the lattice in the direction of magnetisation as shown in Figure 2.2 and the energy associated with this strain is called magnetoelastic energy and it can be calculated for an isotropic material from the equation below.

$$E_\lambda = -\frac{3}{2}\lambda_s \sigma sin^2\theta \tag{2.2}$$

Where

θ is the angle between direction of magnetisation and stress σ

λ_s is the saturation magnetostriction

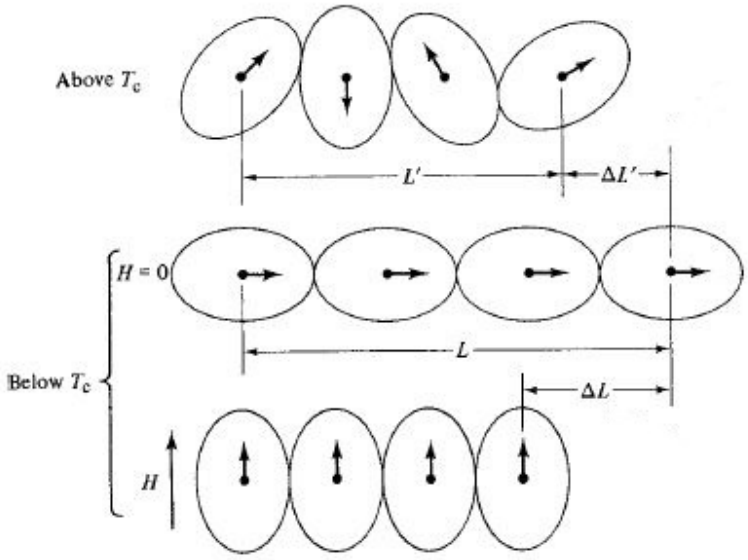

Figure 2.2 Inducing magnetoelastic energy in the material

2.2.3 Magnetostatic energy

In a ferromagnetic material the magnetocrystalline anisotropy energy aligns the domains in one direction but this increases magnetostatic energy in the material by the creation of free poles as shown in Figure 2.3 and there is a demagnetising field associated with it as shown in the equation below:

$$E_m = \frac{1}{2} N_D M^2 \tag{2.3}$$

Where

E_m is the magnetostatic energy

N_D is the demagnetisation factor

M is the magnetisation of the sample.

The geometry of the sample influences the demagnetising factor as for a very long and thin sample N_D is zero but for a thick and short specimen N_D is large.

To reduce the magnetostatic energy domains of opposite magnetisation are formed as shown in Figure 2.4. The extent of H field is now decreased as the opposite poles are close to each other. Increasing the number of reverse domains reduced the magnetostatic energy but at the cost of adding domain wall energy discussed below.

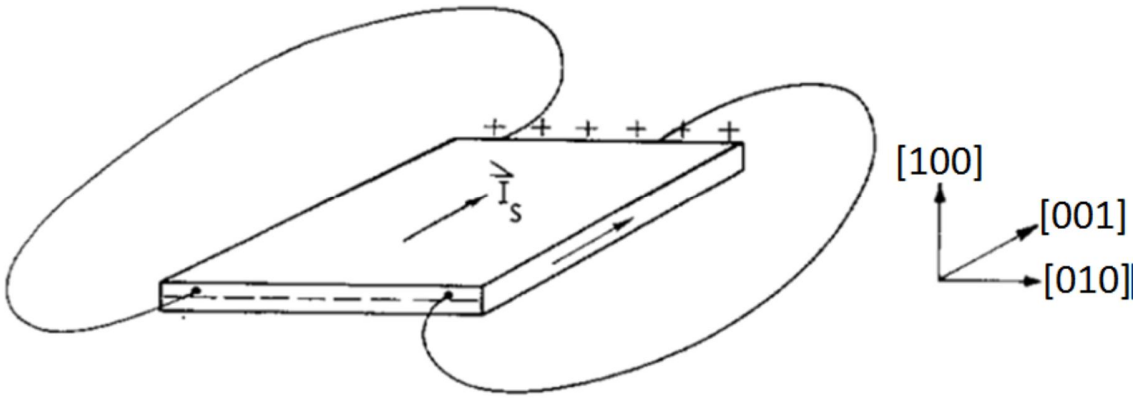

Figure 2.3 Magnetostatic charges in ferromagnetic sheet along [001] direction [3]

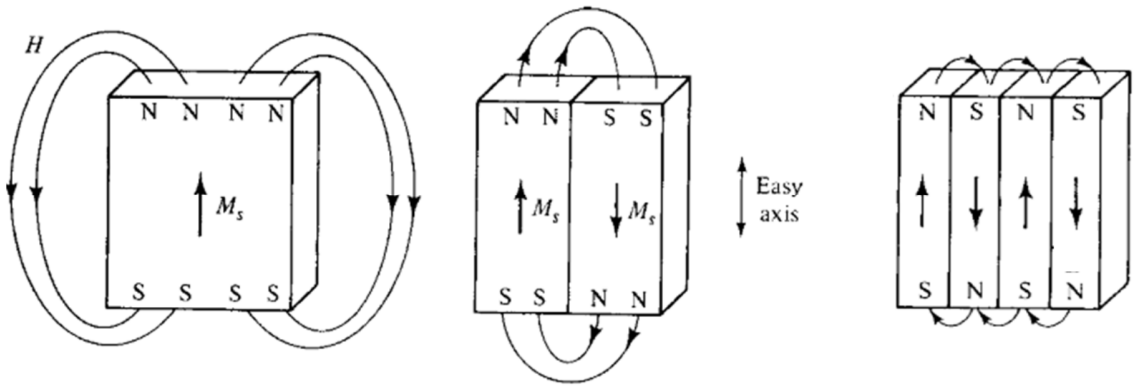

Figure 2.4 Reduction of magnetostatic energy by domain division [2]

2.2.4 Domain wall energy

A domain wall is the interface between two regions of differently oriented magnetisations. Figure 2.5 shows a Bloch wall transition where the rotation of magnetization is normal to the plane of domain wall and these types of walls are found in materials where the size of the material is larger than the width of the wall. Another type of wall known as Neel wall has the rotation of magnetization along the plane of the domain wall and these types of walls are found in very thin films where the thickness is very small as compared to the exchange length. The domain wall has stored energy in it referred to as domain wall energy. The width of the wall is determined on the basis of two energies; anisotropy and exchange energy. The anisotropy energy tends to align all the moments in easy axis of magnetisation and hence reduces the domain wall width. The exchange energy (the energy associated with aligning all the magnetic moments in one direction) tends to increase the wall width so as to reduce the angle between adjacent moments. A compromise is reached by minimising the overall energy of the material. The domain wall could be a 180° or 90°.

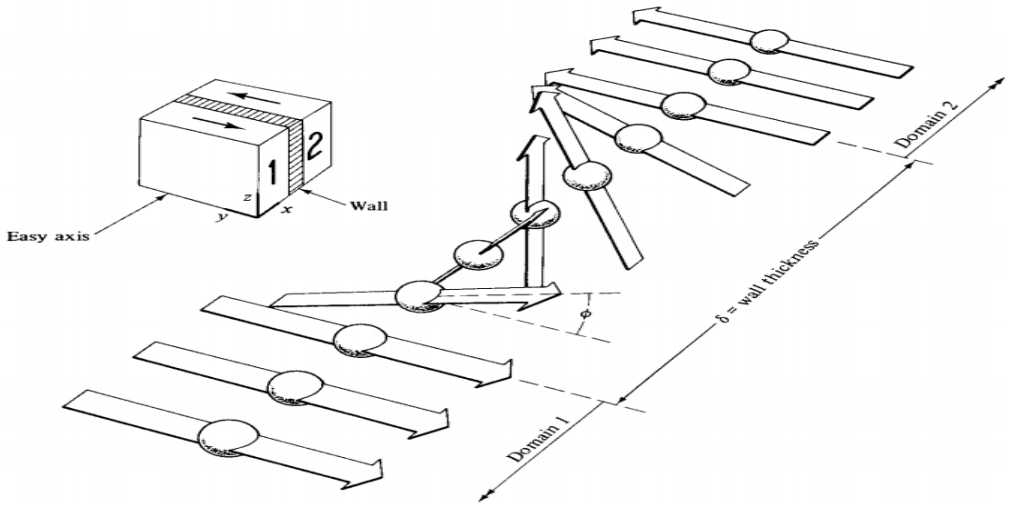

Figure 2.5 Representation of 180° domain wall(Bloch wall) in a magnetic material [2]

2.3 Magnetostriction

The increase or decrease in length of a material when placed in magnetic field is termed as magnetostriction. The representation of magnetostriction (λ) is shown in equation

$$\lambda = \frac{\Delta L}{L} \tag{2.4}$$

Where

ΔL is the change in length

L is the original length

Magnetostriction occurs in two forms:-

1. Volume magnetostriction in which the magnetisation of the material results in change of the volume, this effect is not common at small magnetic fields (< 2 T).

2. Longitudinal magnetostriction is also called as Joule effect in which the length of a material changes under applied magnetic field and is the type considered in this work. If there is increase in the size of a material then it is termed as positive magnetostriction e.g. iron and cobalt whereas if the length decreases then it is called negative magnetostriction e.g. nickel. It is dependent upon stress and magnetic flux density. Compressive stress

increases it whereas tensile stress decreases and it increases with increase in magnetic flux density. The typical values of magnetostriction at zero stress for GOES with a coating is less than 1 μϵ but at compressive stress of 10 MPa the value increases to 20-25 μϵ and a tensile stress of 10 MPa reverses it to a very small negative value of less than 0.5 μϵ.

2.4 Power loss

Electrical steels undergo cycles of magnetization and demagnetization which in turn dissipate energy. The difference between the input and output power is termed as power loss. The advancement in production methods after 1934 when GOES was discovered has reduced losses but still around 5 % [4] of the input power is lost in the transformer which is due to the core loss and copper loss. Core loss is due to the hysteresis, eddy and anomalous loss in the transformer whereas the copper loss is due to the resistance in the transformer windings. The losses can also be categorised into load and no-load losses; the losses in the coil of the transformer is called load losses whereas the losses in the core of the transformer are called no-load losses. The core loss is subdivided into three categories as follows:

2.4.1 Hysteresis loss

The area of the B-H curve is equal to the hysteresis loss if measured at 0 Hz frequency, for transformer steels. In cyclic magnetisation the domain walls move constantly backwards and forwards although these walls may be pinned by defects such as dislocations, grain boundary, impurity or imperfection. Hysteresis loss occurs when these walls are annihilated, moved or created. Although it is said that hysteresis loss is independent of frequency, practically it does depend upon frequency. The frequency determines the number of domain walls in motion which determines the hysteresis loss [4].

In Figure 2.6 when the magnetic field is initially increased, the magnetization is reversible until a certain point after which further increase would result in an irreversible magnetization. Point **a** in the loop denotes saturation induction which means that further increase in magnetic field will not affect the magnetic flux density to a large extent. When the magnetization is reduced to zero from **a,** the magnetic flux density doesn't become zero but some magnetism is retained in the material which is called as remanence. If the magnetic field is applied in the negative direction it goes to point $\mathbf{H_c}$ called the coercivity

which denotes the amount of magnetic field required to reduce the magnetisation to zero. Point **d** is known as the saturation flux density in the negative direction. Hence a cyclic loop is formed which is known as the hysteresis loop.

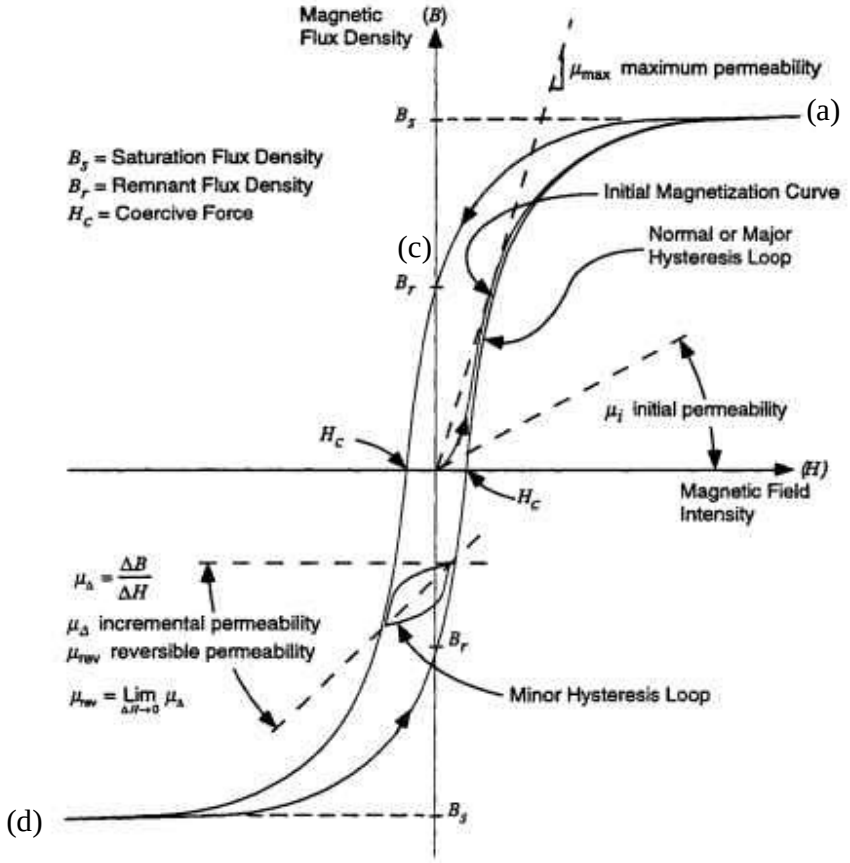

Figure 2.6 Hysteresis curve for a magnetic material

2.4.2 Eddy current loss

A change in magnetic field produces an opposing induced voltage as per Faraday's law. This induced emf will produce currents not contributing to the output power and lost as heat. This energy lost is called eddy current loss. It makes a significant share of the total loss. A thinner laminated sheet, higher silicon content and small grain size decrease eddy currents. As the thickness of the sheets is reduced, the electrons are restricted within the laminations and hence wider current loops are avoided, overall reducing the eddy currents as shown in Figure 2.7. The reduction of thickness sounds promising but also has many disadvantages: firstly, secondary-recrystallization behaviour becomes unstable as the

product becomes thinner; secondly, hysteresis loss increases as the sheet thickness is reduced because the surface roughness contribute a major share of loss at reduced thickness [5]; thirdly, there is a reduction in the stacking factor (section 2.4.6); fourthly, there is a deterioration of shape and appearance. Therefore, a balance has to be obtained for optimum thickness. The resistivity of steel can be enhanced by increasing the silicon content and it helps to reduce the eddy currents, Chun [6] increased the silicon content from 0.21 to 2 % in electrical steel and increased the resistivity from 15 to 38 μΩ-cm.

The eddy currents assuming uniform magnetic field, uniform material and no skin effect are calculated by the equation [7]:-

$$P_e = \Pi^2 B_p^2 d^2 f^2 / 6k\rho D \qquad (2.5)$$

Where,

P_e is the eddy current loss per unit mass (W/kg),
B_p is the peak magnetic field (T),
d is the thickness of the sheet or diameter of the wire (m),
f is the frequency (Hz),
k is a constant equal to 1 for a thin sheet and 2 for a thin wire,
ρ is the resistivity of the material (Ω m), and
D is the density of the material (kg/m^3).

It can be seen that the eddy currents are directly proportional to square of frequency and magnetic flux density.

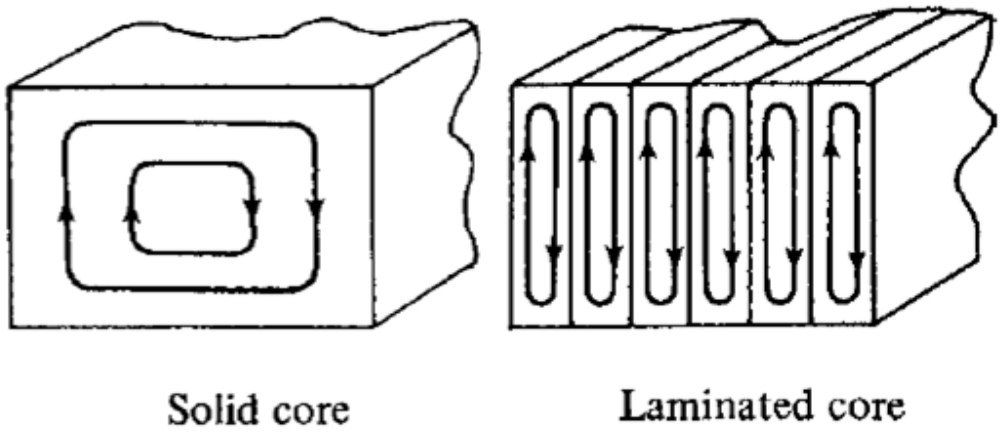

Figure 2.7 A schematic representation of reduction of eddy currents by laminations

2.4.3 Anomalous loss

Initially the difference between the practical loss and the theoretical loss was related to the flux harmonics which occur due to the non-linear B-H relationship. Brailsford et al. [8] proved that the extra loss could not be all due to the flux harmonics by modelling of thin ferromagnetic laminations. To explain the anomalous loss, Agarwal et al. [9] brought in the factor of domain wall bowing. According to this effect the centre of the wall moved slower than the surface and hence the difference between practical and theoretical loss was termed as anomalous loss. Anomalous loss could be 50% of the total loss at frequencies of 50 and 60 Hz [10].

Anomalous losses depend upon the grain size; a smaller grain size reduces the domain width. The domain width depends upon two energies; magnetostatic and domain wall energy. Minimising the sum of both energies determines the domain width, which is proportional to square root of grain size [11]. As the domain width is smaller hence the domain wall travels less distance in the given time, this reduces the velocity of walls and minimises the anomalous loss.

2.4.4 Power loss model

The amount of energy wasted at specific frequency and flux density is the total power loss in a transformer core. The power loss was separated firstly by Steinmetz [12]. The hysteresis and eddy current component were explained by Jordan [13] and the anomalous

loss was introduced by Bertotti [14]. A brief explanation of the various components of the static loss model developed by Bertotti is given below. The power loss separation is shown in the Figure 2.8.

The model used in this work for loss separation was proposed by Ionel et al. [15] . The hysteresis loss coefficient is dependent upon frequency and magnetic flux whereas the eddy current and anomalous loss coefficient is only dependent upon magnetic flux. The core loss equation is

$$W = k_h f B^{\alpha} + k_e f^2 B^2 + K_a f^{1.5} B^{1.5} \quad (2.6)$$

where

W is the total loss, $k_h f B^{\alpha}$ is the hysteresis loss component, $k_e f^2 B^2$ is the eddy current and $K_a f^{1.5} B^{1.5}$ is the anomalous loss component. The loss per cycle is given by

$$W/f = k_h B^{\alpha} + k_e f B^2 + K_a f^{0.5} B^{1.5} \quad (2.7)$$

Equation (2.7) can be compared to a quadratic equation of the type $a + bx + cx^2$ as shown in (2.8) assuming k_h, k_a,, k_e and α are constants independent of frequency and magnetic flux density. The coefficients of $f^{0.5}$ can be found by plotting a fitting curve.

$$W = a + bf^{0.5} + cf \quad (2.8)$$

Where

$a = k_h B^{\alpha}$ $b = k_a B^{1.5}$ $c = k_e B^2$

The values can be plotted over a range of frequencies from 10 Hz to 1000 Hz to get a good fitting of the curve.

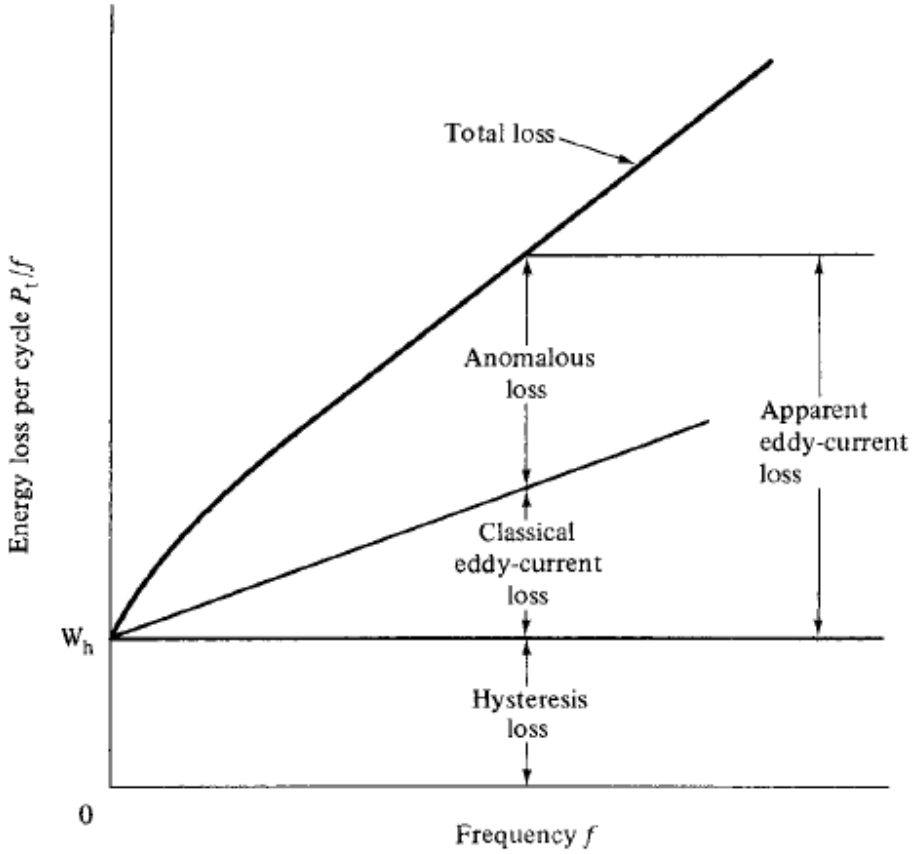

Figure 2.8 Conventional separation of losses in transformer steels [2].

2.4.5 Factors affecting loss

2.4.5.1 Grain size

Grain size is a critical factor in magnetic materials. It varies with the amount of cold work done and upon subsequent annealing temperature and time. A large grain tends to have beneficial effect on magnetic permeability because it will have uniformly orientated domains throughout and a small field is required to align them but it will also have wide domain wall spacing which increases loss. The wide domain spacing requires the walls to move rapidly at higher frequencies to revert to the initial state. Energy is dissipated in creation of new walls or there is bowing in the walls due to large distance between the walls. On the other hand a small grain size will limit the anomalous losses (as the domain wall velocity will be small) but it will have a large proportion of grain boundaries which limit the domain wall motion by pinning [16]. A balance has to be reached on the size of

grain that is optimum for loss minimization however the domains can be refined (narrowed) to reduce losses.

2.4.5.2 Impurity content

If there are foreign impurities present in the material it will affect the magnetic properties substantially as explained below. The impurities are present as precipitates of metal sulphides, carbides or nitrides and their size vary from 10-400 nm.

Aluminium nitride (AlN) and manganese sulphide (MnS) precipitates are useful inhibitors allowing preferential grain growth in the easy magnetization direction. Too much precipitation hinders domain wall movement by pinning the walls.

Silicon: The amount of silicon content determines the magnetic permeability and eddy currents observed. Addition of silicon raises the A_3 (upper critical temperature 910 °C for 0% alloy addition) and lowers the A_4 (1395 °C for 0% alloy addition) temperature as shown in Figure 2.9, forming a gamma loop at 2.5% silicon and 1170˚C. As silicon content is increased further, no change in phase occurs while cooling from high temperature. In this process all forms of grain refinement are restricted and the desired large grains are obtained. More silicon reduces the eddy currents to a large extent. Silicon increases permeability in low magnetic fields but decreases it at high magnetic fields. The brittleness of the material increases as the amount of silicon increases, so rolling becomes a problem once silicon exceeds 3%. It transforms harmful carbides to graphite which is beneficial.

Carbon is useful in getting a sharp crystallographic orientation simultaneously with large cold reduction. It is harmful in the form of pearlite as it mixes with iron to form undesired products and affects the magnetic properties also if present in the solid solution it precipitates with the passage of time and this process is known as magnetic aging which affects the domain wall motion and hence increases the losses.

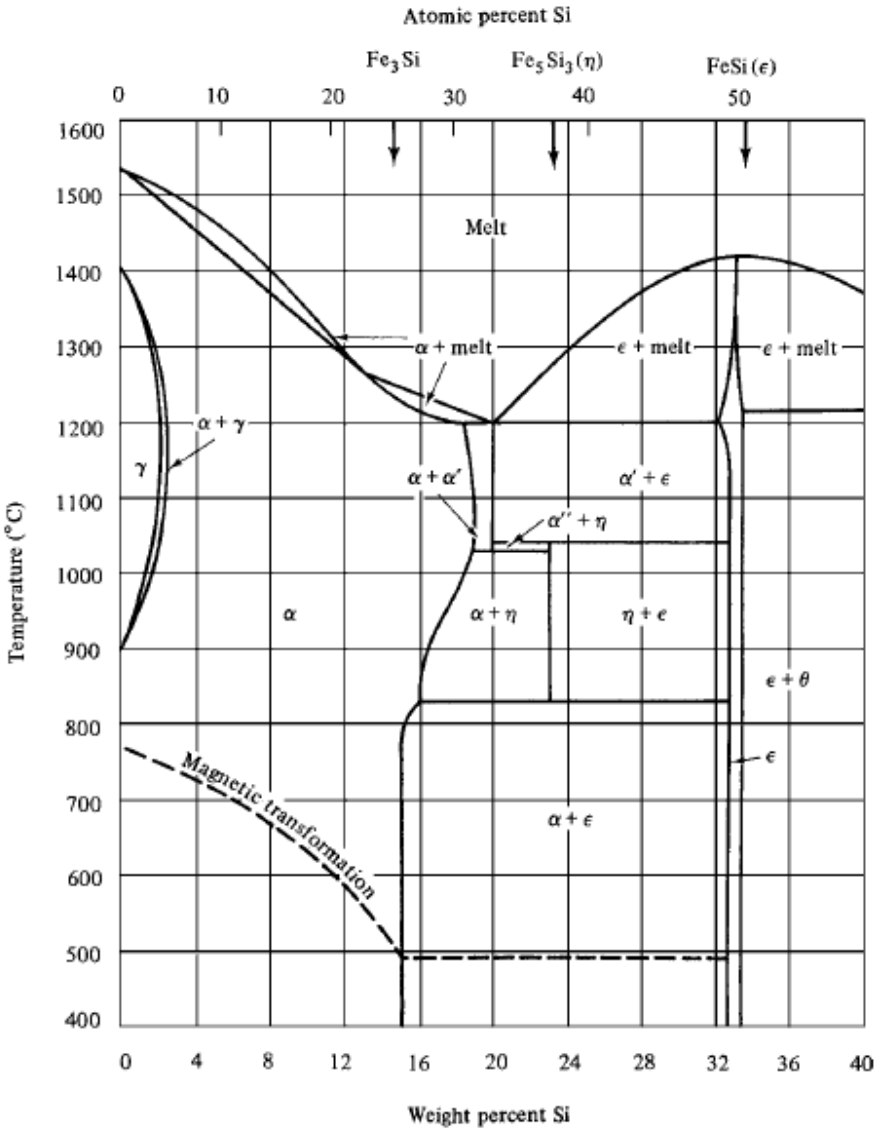

Figure 2.9 Iron-Silicon equilibrium diagram[2].

2.4.6 Stacking factor

Transformers are made up of iron sheets laminated together to reduce eddy currents. These laminations are made up of non-magnetic material so it does not contribute to magnetic flux and hence the term stacking factor was introduced to calculate the magnetic material in the transformers. Stacking factor is the ratio of magnetic to total material in the core of a transformer. It is an important criterion for calculating the magnetic flux density in a transformer core. The conventional coating of forsterite and aluminium ortho-phosphate are non-magnetic and hence the stacking factor of a transformer is always less than 100%. On

increasing the stacking factor the permeability of the transformer increases as more magnetic material is present in the given area.

2.5 Effect of stress on the magnetic properties

Mechanical stress of any kind affects the magnetic domain structure and hence the magnetic properties largely depend upon the type of stress. The GOES has main and supplementary domain structure. The closure domain structures which retain the flux inside the material by forming a closed loop are known as supplementary domain structures. Power loss depends upon these structures. The domain structure changes on the application of stress which can change the magnetic behaviour of the material [3]. Anderson [17] has summarised the effect of stress on different magnetic properties of GOES in the rolling direction. From Figure 2.10 it can be seen that tensile stress can be beneficial in reducing loss and magnetostriction whereas compressive stress increases the loss and magnetostriction. In case of permeability the optimum value is slightly in the compressive stress region.

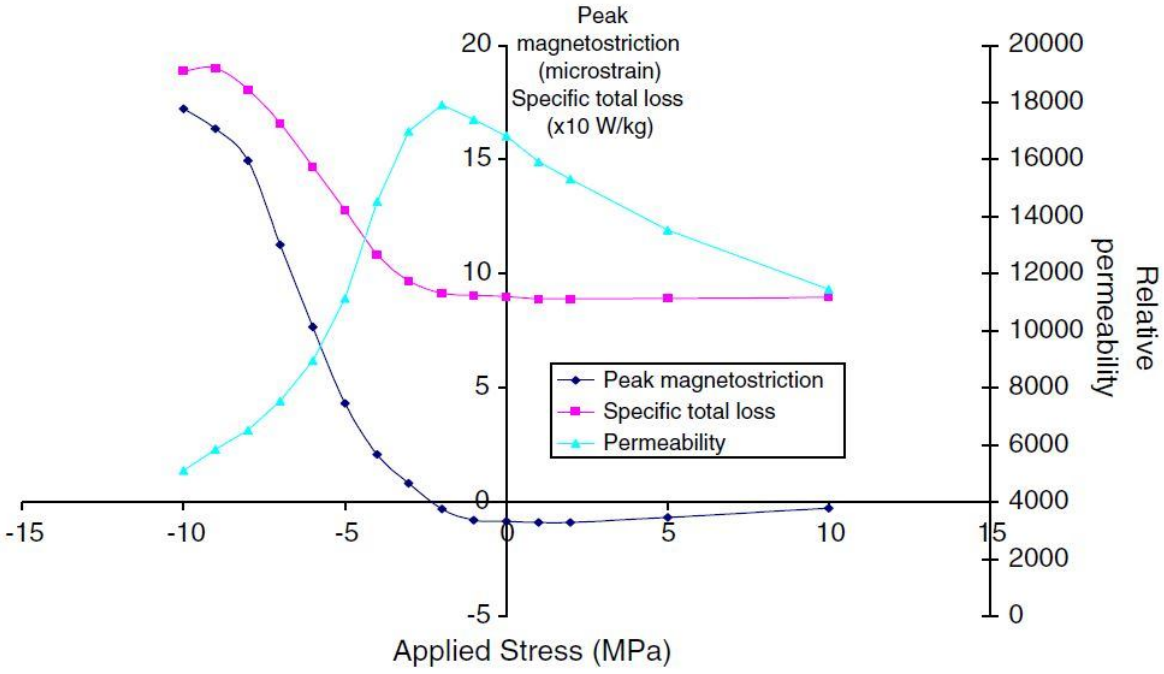

Figure 2.10 A graph representing effect of stress on various magnetic properties [17]

2.5.1 Tensile stress in the rolling direction of GOES

Application of tensile stress parallel to the rolling direction tends to lower the magnetoelastic energy of the longitudinal domains and increase the energy of transverse domains. To maintain the overall energy to a minimum value the domains perpendicular to the direction of magnetization are annihilated as those domains have high magnetoelastic energy [16] shown in Figure 2.11. The magnetostatic energy increases as the longitudinal domains grow so to keep this energy minimum the domain wall spacing is reduced as shown in Figure 2.12. The anomalous loss is reduced as the domain wall velocity is reduced. Hence a very small amount of magnetic field is required to align the domains in the direction of field.

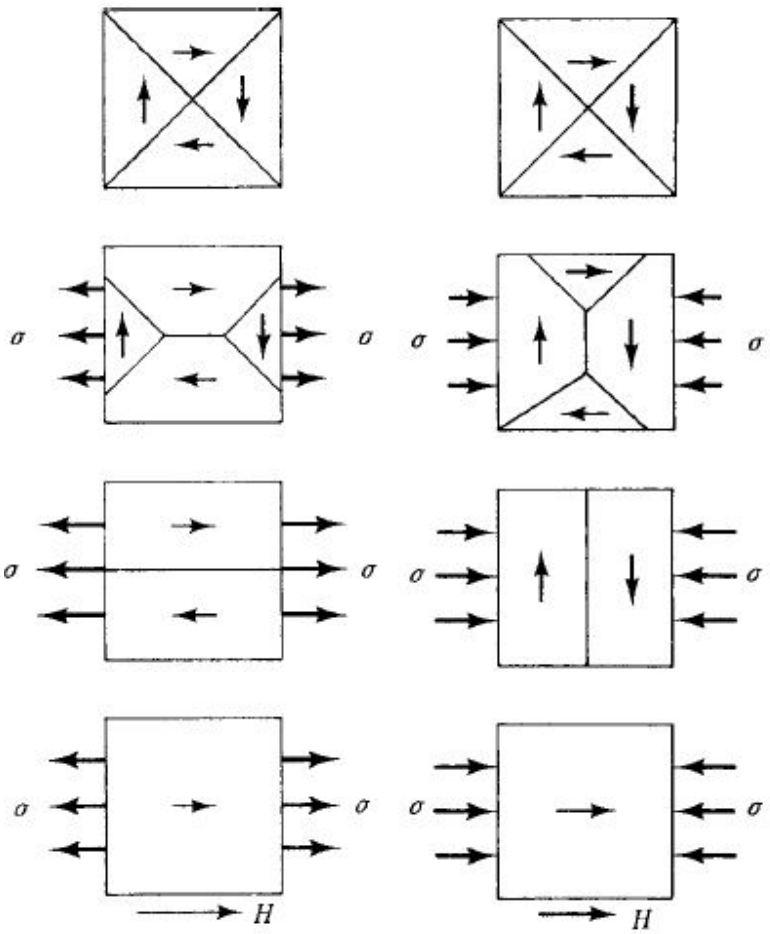

Figure 2.11 Tensile and compressive stress effect on magnetization of a material [2]

Shilling [16] made the observations below which are very useful in understanding the power loss and magnetostriction of magnetic materials under application of stress.

1. The 180˚ walls that were oriented nearly perfect got closer (i.e. wall spacing was reduced) and similarly all the daggers, chevrons & lancet combs shown in Figure 2.12 in the orientation were removed by the application of tensile stress in the demagnetized state.
2. The defects like daggers, chevrons & lancet combs which have disappeared during application of stress in the demagnetized state reappeared once the material was magnetized which produced negative magnetostriction.

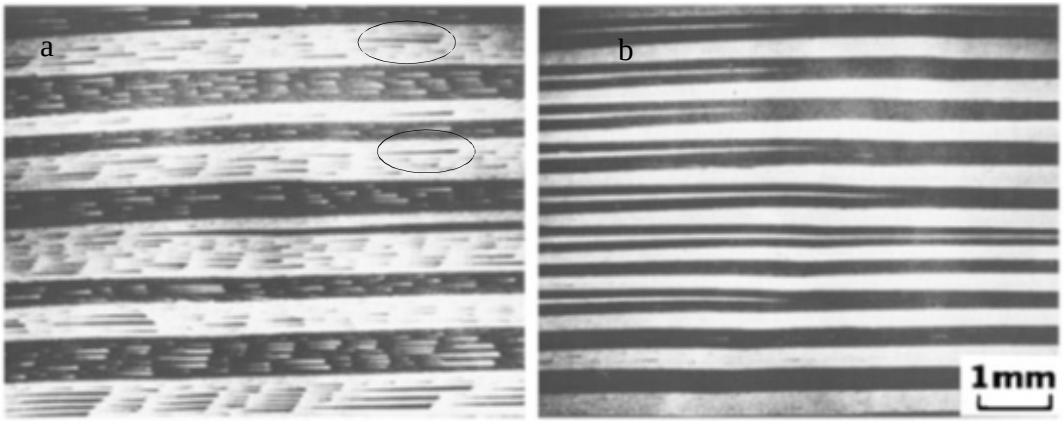

Figure 2.12 Narrowing of 180° domain under applied stress and lancet combs shown in (a) [18]

2.5.2 Compressive stress in rolling direction of GOES

The effect of compressive stress in rolling direction is the reverse of the effect of tensile stress as shown in Figure 2.11. Compressive stress in rolling direction tends to increase the magnetoelastic energy of longitudinal domains and reduce the energy of transverse domains. As a result, the transverse domains grow at the expense of longitudinal domains and a large amount of magnetic field is required to align the domains in the direction of magnetic field. The domains in compressive stress can form two types of stress patterns known as stress pattern I [19] shown in Figure 2.13 and stress pattern II [20] shown in Figure 2.14. In stress pattern I the domains align from [001] direction to [100] direction and also small flux closure domains are formed. Under very high compression the stress pattern

can change from stress pattern I to stress pattern II. In this the main domain stays aligned in the [100] direction but the domain wall align themselves 45° to the rolling direction.

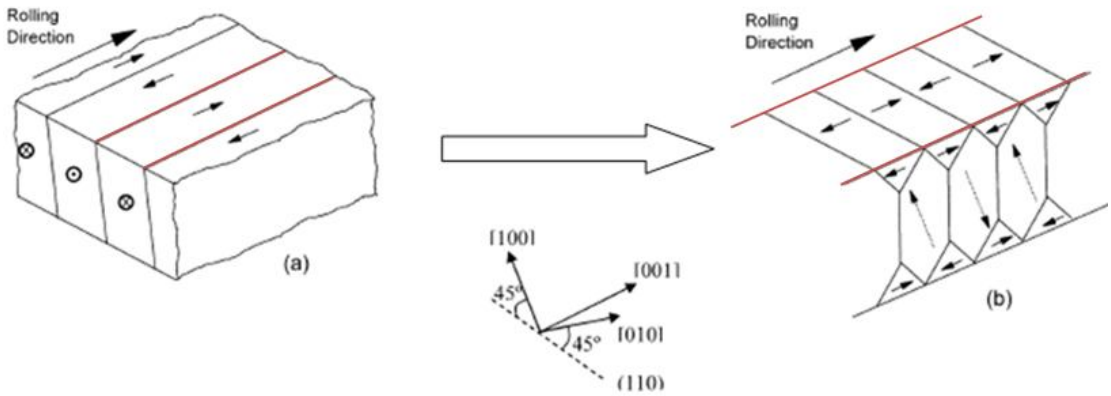

Figure 2.13 Compressive stress applied on material (a) unstressed (b) stress pattern I [21]

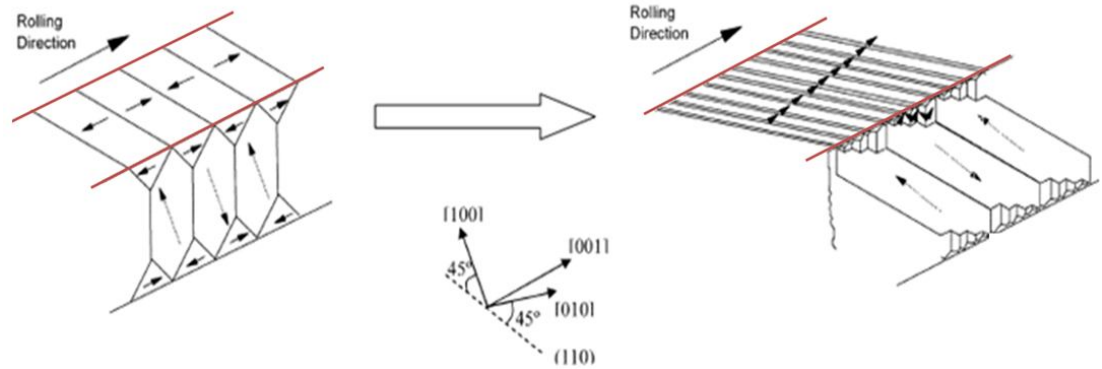

Figure 2.14 Large compressive stress converts the material from (a) Stress Pattern I to (b) Stress Pattern II [21]

2.5.3 Tensile and compressive stress in the transverse direction

The effect of tensile stress in the transverse direction is same as the effect of compressive stress in the rolling direction and the effect of compressive stress in the transverse direction is same as the effect of tensile stress in the rolling direction. The effect of longitudinal stress on GOES is double in magnitude to that of transverse stress [22] due to the difference in Young's modulus in the rolling (113GPa) and transverse (195GPa) direction.

2.6 Electrical steel production and development

Electrical steels (Fe-3wt. %Si) are mostly used in the core of transformers, generators and motors. Figure 2.15 shows the evolution of electrical steel in the 20th century. The development of electrical steel started with Hadfield's production of 3% silicon steel, which had a significant effect on loss reduction in 1903 [23]. Advancement in material processing reduced the impurity content in steel which had a sizeable enhancement in magnetic properties. Development of cold rolling process further reduced the thickness and better magnetic propertied could be achieved.

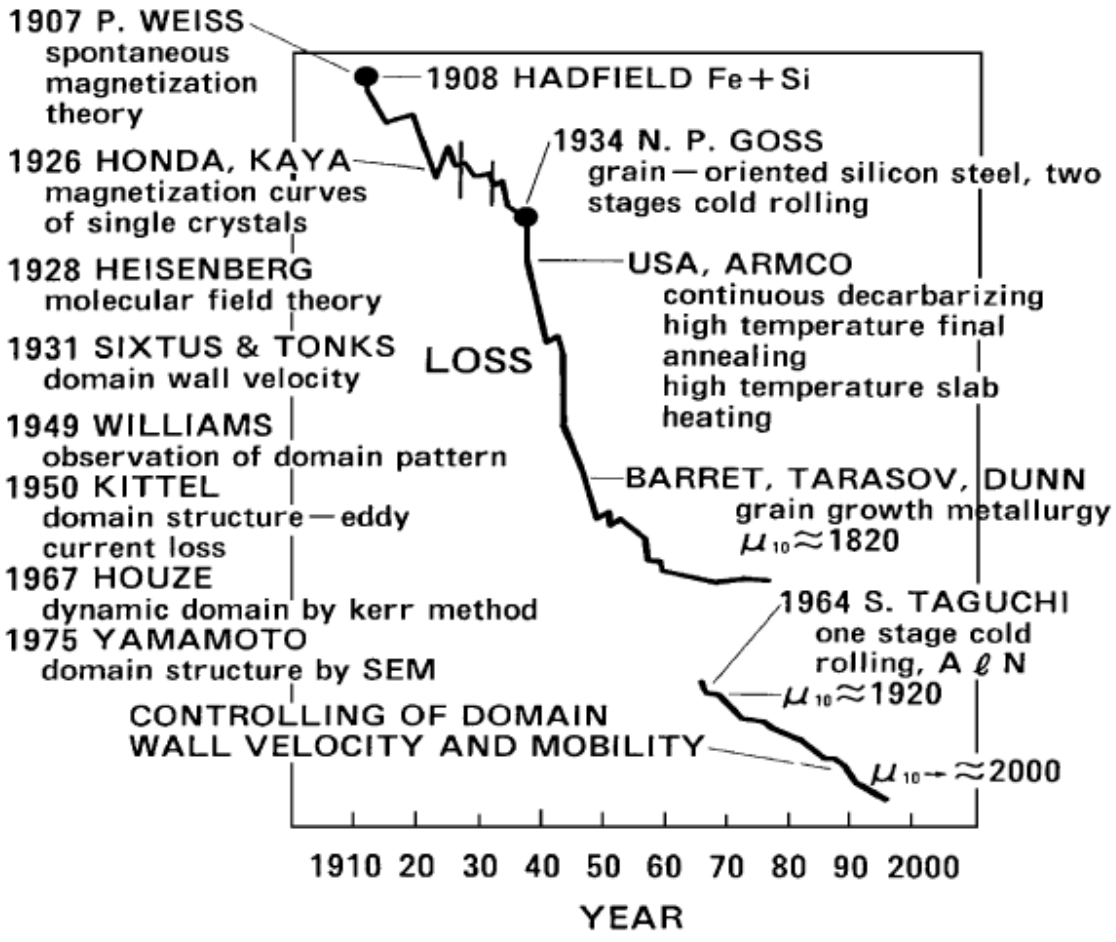

Figure 2.15 Historical development of core loss reduction in electrical steel [18].

It was not until 1934 when Goss developed the idea from the works of Beck [24] and Ruder [25] that iron has high magnetic permeability in certain crystallographic directions and planes. In this type of steel, the grains are oriented such that the <100> direction is parallel to the direction of rolling and the (110) planes are parallel to the surface of sheet. The process involved two stage cold reduction and intermediate annealing, followed by decarburization, batch annealing and flattening. Modern day production of electrical steel still relies on this texture which is commonly known as Goss texture and the steel is popularly called Grain Oriented (GO) steel. It is purely a matter of coincidence that expanding "GOSS" comes out to be Grain Oriented Silicon Steel.

Nippon steel produced a new type of high permeability steel known as HiB [26] . The manufacturing process was different from the Goss steel as only one cold rolling reduction was applied, and using aluminium nitride (AlN) as the primary inhibitor along with manganese sulphide (MnS) as the secondary. The angle of orientation with the rolling direction was decreased from 7˚ to 3˚ but the grain size increased from 0.3mm to 1 cm [27].

Introduction of stress coatings facilitated further reduction in power loss and magnetostriction. The ever increasing demand to increase efficiency led to new domain refining techniques, and Nippon steel developed laser scribing [28] where in losses were found to be 0.85 W/Kg at 1.7T for a thickness of 0.23mm. These losses were 5-8% less than the unscratched HiB steel [27]. A recoat on the damaged surface was necessary as the coating vaporized. Other methods have also been employed to achieve the same where grooves were made on steel on which the ceramic coating was deposited [29]. The grooves were able to refine domains and the ceramic coating was able to apply tension on the GOES substrate.

The current coating system is a two layer coating system where in a forsterite (Mg_2SiO_4) layer is formed first and finally a layer of aluminium orthophosphate coating is applied. The thickness of conventional coating is around 4 μm as can be seen in Figure 2.16. The coating application processes are discussed in detail below:-

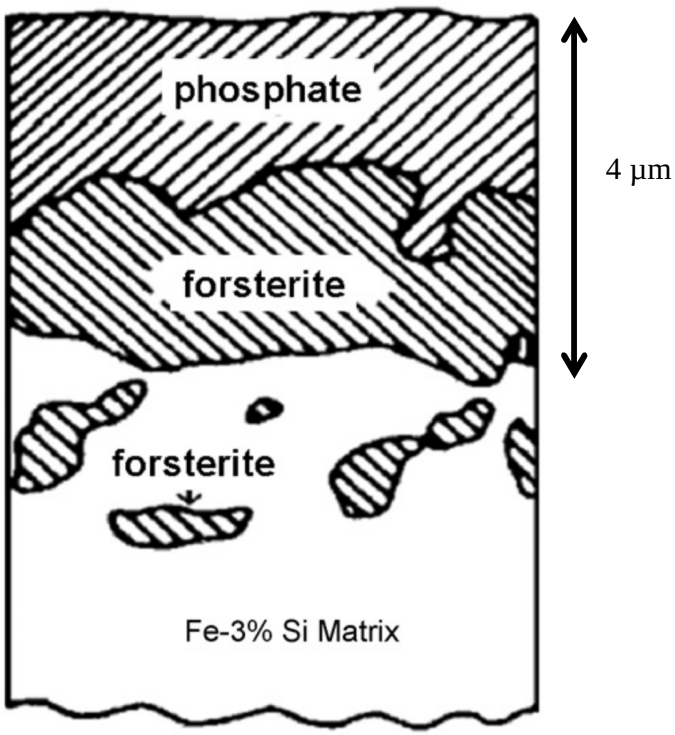

Figure 2.16 Conventional coated Iron-3% Silicon showing layers of phosphate and forsterite.

2.6.1 Forsterite layer formation

The decarburisation of steel and subsequent process of applying MgO coat is shown in Figure 2.17. The formation of the forsterite layer is a two-step process. On the surface of electrical steel, iron reacts with silicon and oxygen to form fayalite. This fayalite reacts with magnesium oxide (MgO) along with silicon dioxide (SiO_2) to form florisil (Mg_2SiO_3). The florisil reacts with excess SiO_2 to form forsterite as shown in equations 2.9 and 2.10 below.

$$MgO + Fe_2SiO_4 + SiO_2 \longrightarrow Mg_2SiO_3 + SiO_2 \quad (2.9)$$

$$Mg_2SiO_3 + SiO_2 \longrightarrow Mg_2SiO_4 \quad (2.10)$$

The application of magnesium oxide (MgO) coating during the decarburising stage helps in serving the following purposes.

1. During high temperature annealing, there is a high risk of sheets sticking together, so MgO is added as a separator which prevents sticking.

2. It forms an insulating glass film in the subsequent process by reaction with fayalite and forms forsterite (Mg_2SiO_4).
3. It facilitates sulphur removal through the forsterite layer which is absorbed in the coating.

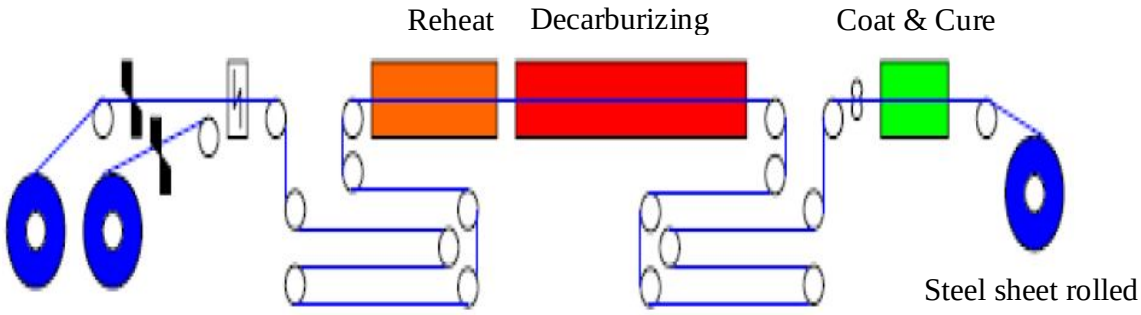

Figure 2.17 Decarburisation annealing with MgO coating [30].

The forsterite layer is formed in the high temperature coil annealing process which is shown in Figure 2.18. The harmful impurities are removed by treating the sheet at 1190˚C for a period of 24-28 hours in dry hydrogen and nitrogen when they get absorbed by the coating. To prevent the absorption of nitrogen, boron is added to steel melt. It helps in the formation of glass film at lower temperatures.

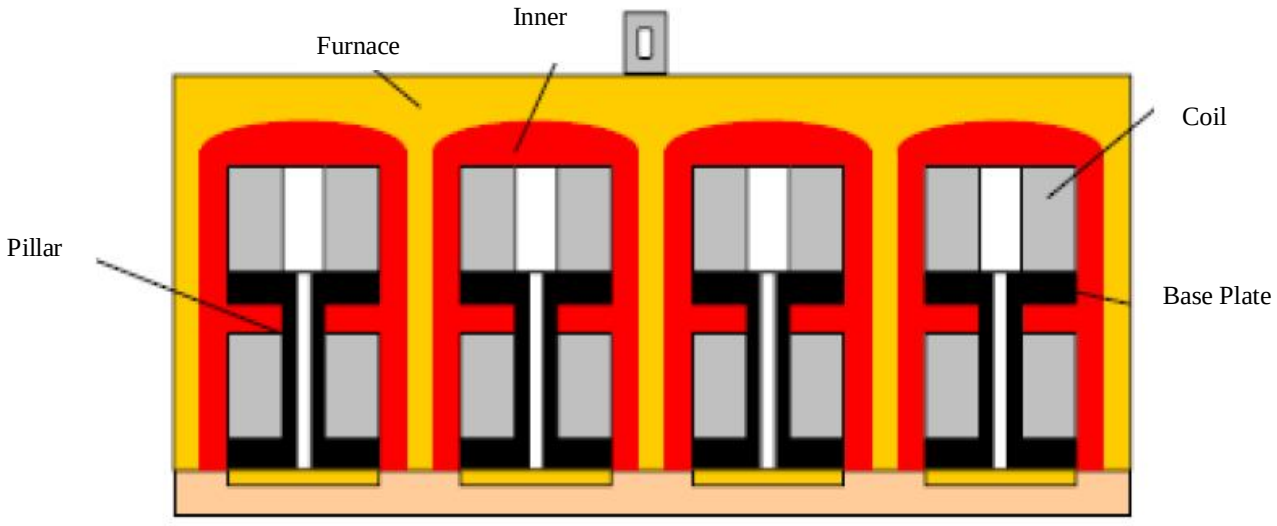

Figure 2.18 High Temperature Coil Annealing [30].

2.6.2 Thermal Flattening and Finish Coating

A tension is applied to the strip on the thermal flattening line as shown in Figure 2.19, taking care of the excessive stress which can damage the GOSS texture. It is normally carried out at a temperature of 840-860˚C in an atmosphere of nitrogen and 2-4% hydrogen. A solution made up by mixing colloidal silica and aluminium orthophosphate in water is coated as a final coating to provide additional insulation to the strip. The hard and soft coating rollers control the thickness, accumulation and uniformity of the coating which is then cured in the gas curing ovens at 350-450 °C. Infrared detection gauges based upon the principle of gradual discolouration of coatings are used to measure the thickness of cured layers and any uncured or over-cured layers are easily detected. The transformer oil does not affect the coating in any way and the coatings are corrosion resistant, stable and show good adherence with steel. The steel sheets are trimmed and wound into a coil in the end of the line.

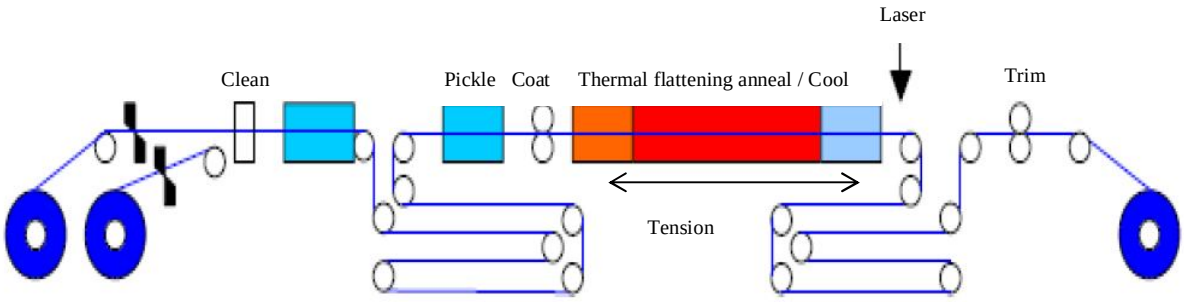

Figure 2.19 Thermal flattening and final coating [30].

2.6.2.1 Mechanism of stress in insulation coating

The coating applies tension on steel in two ways [31]:

1. Isotropic tension is applied by the coating on steel due to the difference in contractions between the coating and steel.
2. The uniaxial tension applied to steel in the rolling direction is held by the coating and a tension of 1.2 MPa was measured.

Anderson [17] has proposed four different mechanisms of stress of which two are stated above and the other two are stated below:

1. During high temperature coil annealing, the coil due to large mass causes widening of the base but this is restricted due to the tight wound and this causes transverse compression.
2. The interlaminar compression perpendicular to the plane acting on waviness in the strip causes longitudinal compression.

Washko et al [32] suggested that coating applied biaxial tensile stress to steel with more strain in rolling direction than in the transverse direction and the effectiveness of the stress by the coating on steel for power loss reduction depends upon the orientation of the grains with a poorly oriented grains showing lesser or no improvement in power loss as compared to perfectly oriented grains. An applied stress of 6.9 MPa on conventional grain oriented (CGO) showed loss improvement of less than 3 % whereas the same stress applied on high permeability (HiB) steel showed an improvement of 10-14% [33].

2.6.2.2 Manufacturing of insulation coating

Nippon steel corp. [34] applied a coating with 4-16 weight % colloidal silica, 3-24 weight % aluminium phosphate and 0.2-4.5 weight % of compound from the group of chromic anhydride and chromate with or without boric acid of 1 to 5 grams and cured it at 350 °C to achieve a coating deposition of 4 gm/m^2 on one side with a power loss reduction of 5 % and magnetostriction reduction of 15 $\mu\epsilon$ at compressive stress of 30 kg/cm^2. The reason for reduction in power loss and magnetostriction by the coating was due to the low thermal expansion coefficient of silica in colloidal silica and also due to the super micro-granular nature of it which removes the unevenness in the surface.

Armco steel corp. [35] coated a solution of silica and potassium oxide in the ratio 2:1 to 2.5:1 on glass coating with or without the phosphate coating and annealed it at 550 ° to 900 °C in the atmosphere of dry nitrogen and hydrogen in the ratio 9:1 to develop a coating of thickness 0.04 mm to 0.2 mm with reduction in power loss by 4-5 % and magnetostriction reduction of 50 $\mu\epsilon$ at no applied stress. The improvement was due to the low coefficient of thermal expansion which imparts tensile stress and high resistivity of the coating.

JFE steel corp. [36] produced a chrome free coating with a solution of phosphates from the group of Al, Mg, Ca, Ba, Sr, Zn and Mn with colloidal silica of 0.5 to 10 mol and one

element from Mg, Sr, Zn , Ba and Ca with 0.02 to 2.5 mol in relation to PO_4:1 mol in phosphates with a thickness of 3µm on one side and achieved 8 MPa of tension in the coating and a stacking factor of 97-98%. The tension developed in the coating was due to the difference in thermal expansion coefficient and the amount of tension developed depend upon the thickness of the coating with thinner coating applying less tension than thick coating.

2.7 Influence of Coatings on electrical steel

Efforts are being made to produce high performance electrical steels through several methods including better secondary recrystallization methods [37], grain orientation control [38], increasing the electrical resistivity, gauge reduction [39] and understanding the magnetic domain structure [16, 40, 41] perhaps the greatest gains can be made by employing effective stress coatings [5, 42] which can play a dominant role in minimizing losses and magnetostriction. While manufacturing a transformer, the steel sheets are free from any stress but compressive stress develops in the process which increases magnetostriction, if we can induce tensile stress in the sheet, compressive stress developed will be counter balanced. This is the reason for the application of coatings which can apply tensile stress on steel.

Power losses can be minimised by exploiting the surface of grain oriented electrical steel [43]. The surface roughness can be manipulated or surface stress could be varied to bring down the overall power loss by using coatings. Wada et al. [44] had shown that power losses could be reduced by 30-40 % on improving the surface roughness. Tensile stress is beneficial to reduce power losses. Conventionally, coatings which have low coefficient of thermal expansion when cooled from high temperature are used since they contract less than the substrate. This difference in cooling applies a tensile stress on the substrate.

Coating the steel helps in reducing both the losses and the magnetostriction. Coating minimises the eddy current loss by providing insulation resistance and reduces the hysteresis and anomalous loss by improving the surface roughness [44] and beneficial tensile stress [5] to the substrate. A higher surface roughness increases the number of free poles. These free poles pin the domain wall motion. The number of mobile domains

reduces and it leads to inhomogeneous domain wall motion. Freeing up these domains leads to significant amount of energy loss. Improvement in surface roughness would lead to an increase in the number of mobile domains and reduce the energy consumption which reduces the total loss. Tensile stress imparted from the coating on the steel sheet eliminates the surface closure domains whereas losses are reduced as tensile stress helps in narrowing the domain wall spacing which decreases the anomalous loss. The reverse happens when compressive stress is applied on GOES. According to Kuppers et al. [45] the coercivity of the magnetic material can be reduced by eliminating the supplementary structures and hence the hysteresis loss can be improved. The refinement in hysteresis loss is due to reduction in the surface closure domains.

There are a number of alternative methods that can be used to apply a coating on the surface of steel sheet such as sol gel [46], CVD [47], PVD [48], plasma spraying, wet coating, printing, electroless and electro chemical plating. The desirable properties [49] in a coating are insulation resistance, heat resistance, chemical resistance, punchability, weldability, corrosion resistance, burn out characteristics, resistance to compression, coating thickness, surface roughness and scratch resistance.

Yamaguchi et. al. [47] have deposited titanium carbide (TiC) coating of 1 μm thickness on 0.23 mm thick grain oriented electrical steel and found that the coating was effective in reducing losses up to 0.586 W/kg. The coating was deposited by chemical vapour deposition and it was found that the eddy current loss was reduced by the coating whereas no effect on hysteresis loss was noticed. The coating was deposited after removing the insulation and tension coating also the samples were chemically polished which improves the surface roughness of GOES as shown in Figure 2.20. The W_h and W_e in the figure is the hysteresis and eddy current loss separated. There was no change in power loss after putting the insulation coating and annealing.

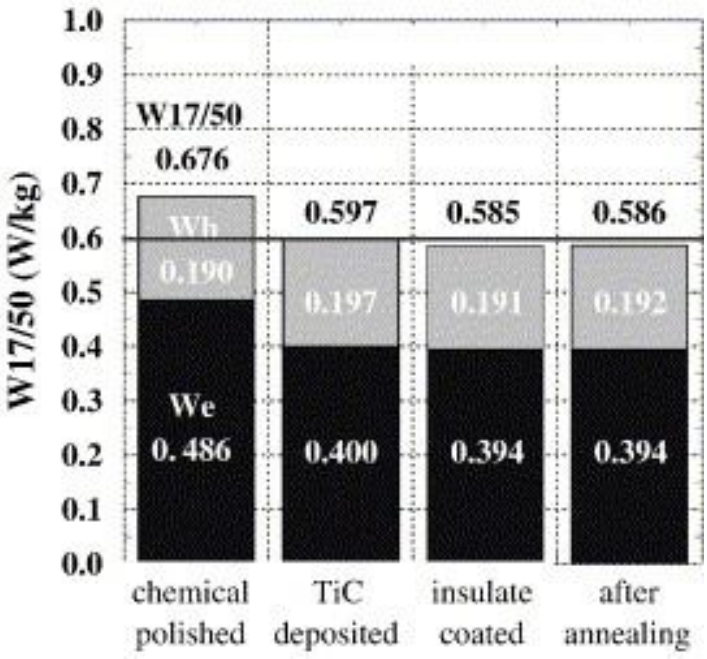

Figure 2.20 Dependence of hysteresis and eddy current loss on different processes.

Nishiike et. al. [50] combined the effect of surface roughness and tensile stress and measured a loss of 0.6 W/kg. The GOES was chemically polished to surface roughness R_a of 0.05 μm and stressed to tensile stress of 45 MPa. It was shown that the reduction of power loss was due to the increase in the number of mobile domain walls by polishing and also due to the application of tensile stress which reduced the eddy current loss. The application of tensile stress was divided into two parts. Below 10 MPa tensile stresses, the mechanism of loss reduction was due to reduction in domain size and above 10 MPa, the rotation of magnetization in the direction of rolling improved performance of electrical steel. It was also shown that above 10 MPa the power loss was saturated and parallel to the horizontal axis of tension.

2.8 References

[1] S. Chikazumi, "Physics of magnetism," *Robert E. Krieger Publishing Company,* 1978.

[2] B. C. a. C. Graham, "Introduction to magnetic material," *John Wiley & Sons,* 2009.

[3] J. W. Shilling and G. L. Houze, "Magnetic Properties and Domain Structure in Grain-Oriented 3 % Si-Fe," *IEEE Transactions on Magnetics,* vol. MAG-10, pp. 195-223, 1974.

[4] A. J. Moses, "Energy efficient electrical steels: Magnetic performance prediction and optimization," *Scripta Materialia,* vol. 67, pp. 560-565, 2012.

[5] T. Yamamoto and T. Nozawa, "Effects of Tensile Stress on Total Loss of Single Crystals of 3% Silicon-Iron," *Journal of Applied Physics,* vol. 41, pp. 2981-2984, June 1970.

[6] C.-K. Hou, "Effect of silicon on the loss separation and permeability of laminated steels " *Journal of Magnetism and Magnetic Materials,* vol. 162, pp. 280-290, 1996.

[7] F. Fiorillo, "Measurement and characterization of magnetic materials," *Elsevier Academic Press,* p. 31, 2004.

[8] F. Brailsford and J. M. Burgess, "Internal waveform distortion in silicon-iron laminations for magnetization at 50 c/s," *J.M Proceedings, IEEE* vol. 108, pp. 458-462, 1961.

[9] P. D. Agarwal and L. Rabins, "Rigorous solution of eddy current losses in rectangular bar for single plane domain wall model," *Journal of Applied Physics,* vol. 31, p. 246S, 1960.

[10] S. Taguchi, "Review of the recent development of electrical sheet steel in Japan," *Trans. Iron Steel Inst. Jpn.,* vol. 17, pp. 604-615, 1977.

[11] J. B. Goodenough, "A Theory of Domain Creation and Coercive Force in Polycrystalline Ferromagnetics," *Physical review* vol. 95, p. 917, 1954.

[12] C. P. Steinmetz, "On the law of hysteresis," *Proceedings of the IEEE,* vol. 72, pp. 196-221, February 1984.

[13] H. Jordan, "Die ferromagnetischen konstanten fur schwache wechselfelder," *Elektr. Nach. Techn.,* vol. 1, p. 8, 1924.

[14] G. Bertotti, "General properties of power losses in soft ferromagnetic materials," *IEEE Transactions on Magnetics,* vol. 24, pp. 621-630, January 1988.

[15] D. M. Ionel, M. Popescu, S. J. Dellinger, T. J. E. Miller, R. J. Heideman, and M. I. McGilp, "On the Variation With Flux and Frequency of the Core Loss Coefficients in Electrical Machines," *IEEE transactions on industry applications,* vol. 42, pp. 658-667, 2006.

[16] J. W. Shilling, "Domain Structure During Magnetization of Grain-Oriented 3% Si-Fe as a function of Applied Tensile Stress," *Journal of Applied Physics,* vol. 42, pp. 1787-1789, 15 Mach 1971.

[17] P. Anderson, "A novel method of measurement and characterisation of magnetostriction in electrical steels," *Cardiff University, Thesis,* 2000.

[18] Z. Xia, Y. Kang, and Q. Wang, "Developments in the production of grain-oriented electrical steel," *Journal of Magnetism and Magnetic Materials,* vol. 320, p. 3229, 2008.

[19] L. J. Dijkstra and U. M. Martius, "Domain patterns in silicon iron under stress," *Review of modern physics,* vol. 25, pp. 146-150, 1953.

[20] W. D. Corner and J. J. Mason, "Effect of stress on domain structure of goss textured silicon iron," *British Journal of Applied Physics,* vol. 15, pp. 709-722, 1964.

[21] P. I. Anderson, A. J. Moses, and H. J. Stanbury, "Assessment of the Stress Sensitivity of Magnetostriction in Grain-Oriented Silicon Steel " *IEEE Transactions on Magnetics,* vol. 43, pp. 3467-3476, 2007.

[22] P. J. Banks and E. Rawlinson, "Dynamic magnetostriction and mechanical strain in oriented 3% silicon iron sheet subject to combined longitudinal and transverse stresses," *Proceedings of the Institution of Electrical Engineers-London,* vol. 114, pp. 1537-1546, 1967.

[23] R. A. Hadfield, "Magnetic composition and method of making same," *US Patent 745829 A,* 1903.

[24] Beck.K, "The magnetic properties of Fe crystals at ordinary temperature," *Zurich Naturforsch Ges.,* vol. 66, pp. 116-186, 1918.

[25] W. E. Ruder, "Magnetisation and crystal orientation," *Trans. Am. Soc. Steel Treating* vol. 8, pp. 23-29, 1920.

[26] H. J. E and L. M. F, "Process of increasing the permeability of oriented silicon steels," *US Patent 2599340 A*, 1952.

[27] A. J. Moses, "Electrical steels : past, present and future developments," *IEEE proceedings*, vol. 137, pp. 233-245, 1990.

[28] G. L. Neiheisel, "Laser treatment of electrical steel and optical scanning assembly therefore," *Us Patent 4468551 A*, 1984.

[29] Y. Inokuti, Chuo-Ku, and Chiba-Shi, "Ultra low iron loss undirectional silicon steel sheet," *European patent*, vol. EP0910101A1, 1999.

[30] M. Cichuta, "Trends and developments in grain oriented steels," *Internal presentation of Cogent Power Ltd*, 2009.

[31] A. J. Moses, S. M. Pegler, and J. E. Thompson, "Role of phosphate coating in determining the magnetic properties of Goss-oriented silicon iron," *proceedings of the IEEE*, vol. 119, 1972.

[32] S. D. Washko and E. G. Choby, "Evidence for the effectiveness of stress coatings in improving tfe magnetic properties of high perwability 3% si-fe," *IEEE transactions on magnetics*, vol. Mag-15, 1979.

[33] T. Yamamoto, S. Taguchi, A. Sakakura, and T. Nozawa, "Magnetic Properties of Grain-Oriented Silicon Steel with High Permeability Orientcore HI-B " *IEEE transactions on magnetics*, vol. 8, pp. 677-681, 1972.

[34] O. Tanaka, T. Yamamoto, and T. Takata, "Method for forming an insulating film on an oriented silicon steel sheet," *US Patent 3856568 A*, 1974.

[35] D. M. Kohler, "Potassium silicate coated silicon steel," *US patent 3522113*, 1968.

[36] M. Takashima, M. Muraki, M. Watanabe, and T. Shigekuni, "Treatment solution for insulation coating for grain oriented electrical steel sheet and method for producing grain oriented electrical steel sheet having insulation coating," *US Patent 8535455 B2*, 2013.

[37] T. Steven, A. Moses, J. Hall, and K. Jenkins, "The effect of precipitate size on magnetic domain behavior in grain-oriented electrical steels," *Journal of Applied Physics*, vol. 107, p. 09A307, 2010.

[38] J.-T. Park and J. A. Szpunar, "Effect of initial grain size on texture evolution and magnetic properties in nonoriented electrical steels," *Journal of Magnetism and Magnetic Materials,* vol. 321, pp. 1928-1932, 2009.

[39] H. Haiji, K. Okada, T. Hiratani, M. Abe, and M. Ninomiya, "Magnetic properties and workability of 6.5% Si steel sheet," *Journal of Magnetism and Magnetic Materials,* vol. 160, pp. 109-114, 1996.

[40] C. R. Boon and J. A. Robey, "Effect of domain-wall motion on power loss in grainoriented silicon-iron sheet," *Proceedings of the IEEE,* vol. 115, pp. 1535-1540, October 1968.

[41] M. Yabumoto, Y. Matsuo, H. Kobayashi, and T. Nozawa, "Relation between dynamic domian wall movement and crystal orientation in advanced grain-oriented silicon steel," *Journal of Applied Physics,* vol. 64, pp. 5364-5366, 1988.

[42] R. Langman, "The Effect of Stress on the Magnetization of Mild Steel at Moderate Field Strengths," *IEEE Transactions on Magnetics,* vol. MAG-21, pp. 1314-1320, 1985.

[43] B. Weidenfeller and W. Riehemann, "Effects of surface treatments on the hysteresis losses of GO iron silicon steel," *Journal of Magnetism and Magnetic Materials,* vol. 292, pp. 210-214, 2005.

[44] T. Wada, T. Nozawa, and T. Takata, "Method for producing a super low watt loss grain oriented electrical steel sheet," *US Patent,* vol. 3932236, January 13, 1976.

[45] D. Küppers, J. Kranz, and A. Hubert, "Coercivity and Domain Structure of Silicon-Iron Single Crystals " *Journal of Applied Physics,* vol. 39, p. 608, 1968.

[46] T. Olding, M. Sayer, and D. Barrow, "Ceramic sol–gel composite coatings for electrical insulation," *Thin Solid Films,* vol. 398-399, pp. 581-586, 2001.

[47] H. Yamaguchi, M. Muraki, and M. Komatsubara, "Application of CVD method on grain-oriented electrical steel," *Surface & Coatings Technology,* vol. 200, pp. 3351-3354, 2006.

[48] X. D. He, X. Li, and Y. Sun, "Microstructure and magnetic properties of high silicon electrical steel produced by electron beam physical vapor deposition," *Journal of Magnetism and Magnetic Materials,* vol. 320, pp. 217-221, 2008.

[49] G. Loisos, A. J. Moses, and P. Beckley, "Electrical stress on electrical steel coatings," *Journal of Magnetism and Magnetic Materials*, vol. 254–255, pp. 340-342, 2003.

[50] U. Nishiike, T. Kan, and A. Honda, "Influence of surface properties on the stress magnetization properties of grain-oriented silicon steel," *IEEE transactions on magnetics in Japan*, vol. 8, p. 777, 1993.

3 Coating Techniques

3.1 Electroless plating

Electroless plating is a commonly used technique for coating a wide variety of materials. It is a coating technique in which the metal to be deposited is reduced on the substrate with the help of a reducing agent. The process is auto-catalytic as no external current is supplied for the process to take place. The process is monitored by supplying metal ions or reducing agent. The substrate is made the cathode and the metal salt as anode. The exact process parameters for electroless deposition were given by Brenner and Riddell [1]. Electroless process offers the given below advantages compared to other coating processes.

1. The coating is uniformly distributed throughout the substrate as entire surface acts as nucleation sites for coating to grow.
2. The plating rates are fast because the reduction of metallic ions is an auto-catalytic process.
3. The magnetic properties can be varied widely by changing the pH of the solution.
4. The coatings are resistant to corrosion due to the presence of phosphorus.
5. The coatings are brighter in colour, offer good wear and abrasion resistance and favour weldability and solderability.

Depending on the surface of the substrate the electroless deposition can start spontaneously or needs surface active agents which can initiate the nucleation on the substrate. The Group VIII metals (Fe, Ni, Co, Pd, Pt, Rh) require no surface activation.

3.1.1 Constituents of electroless plating solution

Electroless plating bath consists of several components of which the metal ions are the source of plating metal, the electrons used for the reduction process are provided by the reducing agent, the complexants stabilize the solution, the accelerators activate the reducing agent, the buffers control the pH of the solution, the stabilizers prevent the breakdown of the solution and the wetting agents increase the wettability of the surfaces [2]. Some of the components are described in detail below:

3.1.1.1 Metallic ions

A salt solution of the metals is usually used as a source of metal ions for example nickel sulphate or cobalt sulphate is used for nickel and cobalt respectively. These ions in the bath are reduced to their respective metals and hence deposited on the substrate.

3.1.1.2 Reducing agents

The purpose of introducing the reducing agents is to reduce the metallic ions to the metal on the surface of the material. The choice of reducing agent is based upon the composition of the coating. Sodium hypophosphite is used for phosphorus based coating and amine boranes are used for boron based coating.

3.1.1.3 Complexing agents

Complexing agents are added in the electroless bath to maintain the pH of the bath. It arrests the precipitation of metallic salts which would otherwise stop the coating reaction. The free ions concentration in the solution is maintained by the complexing agents [3].

3.1.1.4 Stabilizers

Stabilizers prevent the spontaneous decomposition of the bath and help in making the bath stable. Stabilizers also control the plating reaction so excess usage of stabilizers may be harmful in terms of poor deposits and bath life.

3.1.1.5 Energy

All processes require energy to proceed and electroless plating is no different. The desired energy is supplied in the form of heat energy by raising the temperature of bath. The kinetics of the reaction and the deposition rate are determined by the amount of

energy supplied. Higher energy leads to poor microstructural deposit and low energy may not be sufficient to start the process.

Electroless plating can be used to coat nickel, cobalt, copper & silver. Pure nickel is highly conductive and thus a nickel coating would lead to generation of eddy currents if coated on electrical steels. Alloying it with phosphorus, boron, cobalt & tungsten can significantly affect the final properties [4, 5]. The saturation magnetization of cobalt (2T) is much higher than that of nickel (0.6T) so, increasing cobalt content can result in better magnetic properties as shown in Figure 3.1. Addition of phosphorus or boron to the nickel coating increases the overall resistivity. The desired coatings produced should have the characteristics of high magnetic permeability and resistivity.

3.1.2 Electroless plating of Co-Ni-P

Co-Ni-P has high saturation magnetization of 15 emu/g as shown in Figure 3.1 based upon nickel to cobalt ratio [4]. The resistivity of these coatings ranges from (7.9 to 13.6 x 10^{-7} Ωm) depending upon the amount of cobalt used and is higher than the typical 3% Si steel coatings (4.5 x 10^{-7} Ωm). P. Chivavibul et al. [6] produced an electroless Ni-Co-P (56–59% Ni, 32–35% Co, and 8–10% P by mass) coating of 1 micron thickness on non-oriented electrical steel and found that the coating was effective in reducing losses by up to 4% at a magnetic flux density of 0.3 T and frequency of 400Hz. The coating was able to provide insulation resistance and minimize the eddy current loss at higher frequencies to reduce the overall loss. As the thickness of the coating was increased there was an increase in the hysteresis loss. This was because the soft magnetic coating was part of the power loss measurement, and so the loss from the coating also contributes to the power loss. The loss of the coating must be significantly higher than the substrate.

Ni-Co-P coating was not chosen because of the low saturation magnetization of the coating and no stresses were generated in the coating after the deposition. Co-Ni-P was chosen based upon experimental evidence to generate stress in the coating and also upon its tendency to alter the final magnetic properties such as the coercivity and hysteresis loss [7].

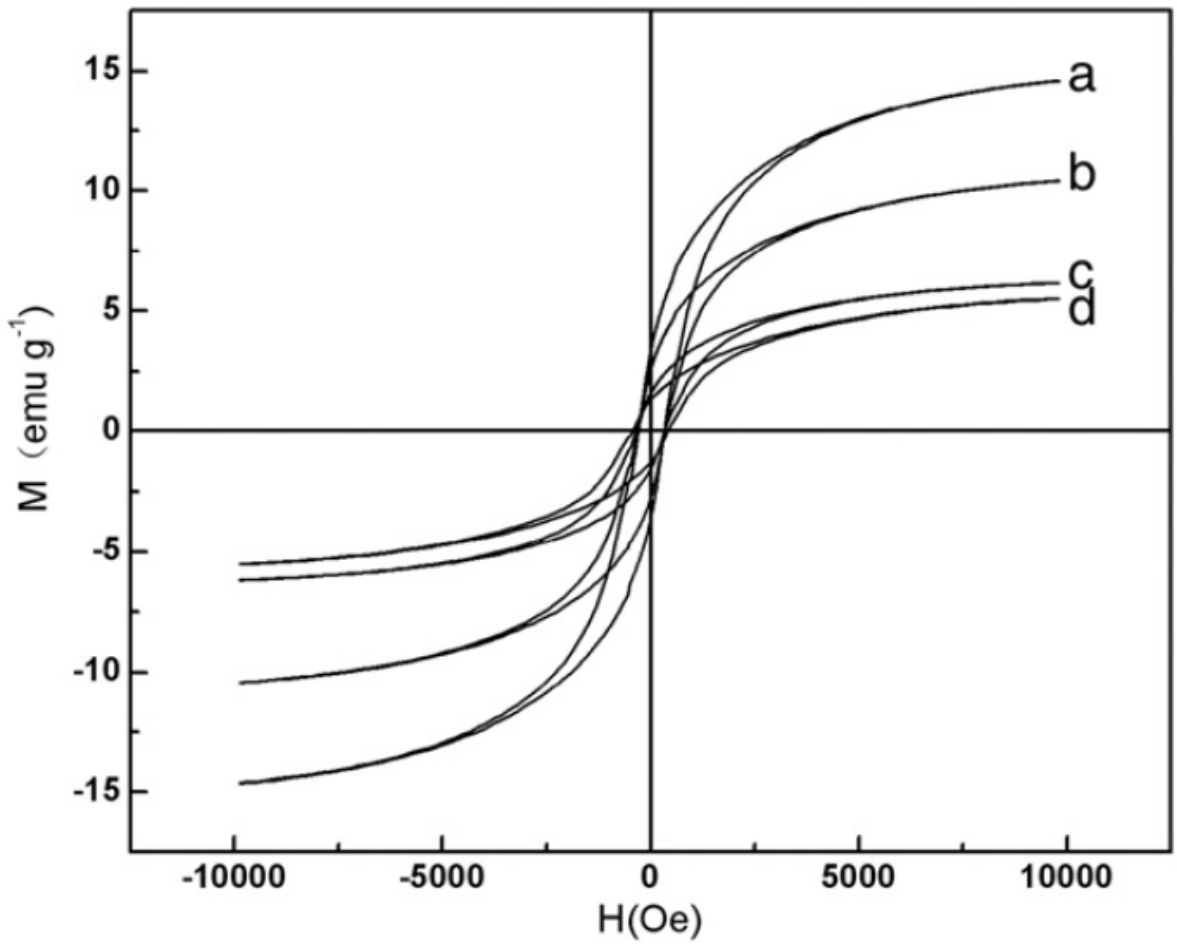

Figure 3.1 Hysteresis loops for different Ni^{2+}/Co^{2+} mole ratios (a) 1:4; (b) 1:1.5; (c) 1:1; and (d) 4:1 [4].

3.1.2.1 Stress in electroless depositions of Co-Ni-P

Stresses develop in the electroless plating and are generated either due to the difference in coefficient of thermal expansion between the substrate and the coating or in the deposition process. There are several theories proposed explaining the development of stress [3, 8, 9].

During deposition the particles deposit at few places rather than forming a uniform atomic layer [3]. The coating grows at those few places only. The surface tension binds the particles together. Rearrangement of these atoms due to surface tension changes the interatomic distance and hence develop tensile or compressive stress depending on the increase or decrease in the interatomic distance. Minimizing the coagulation could reduce the amount of tensile stress and by introducing phosphorus the stress can be changed from tensile to compressive as can be seen in the Figure 3.2.

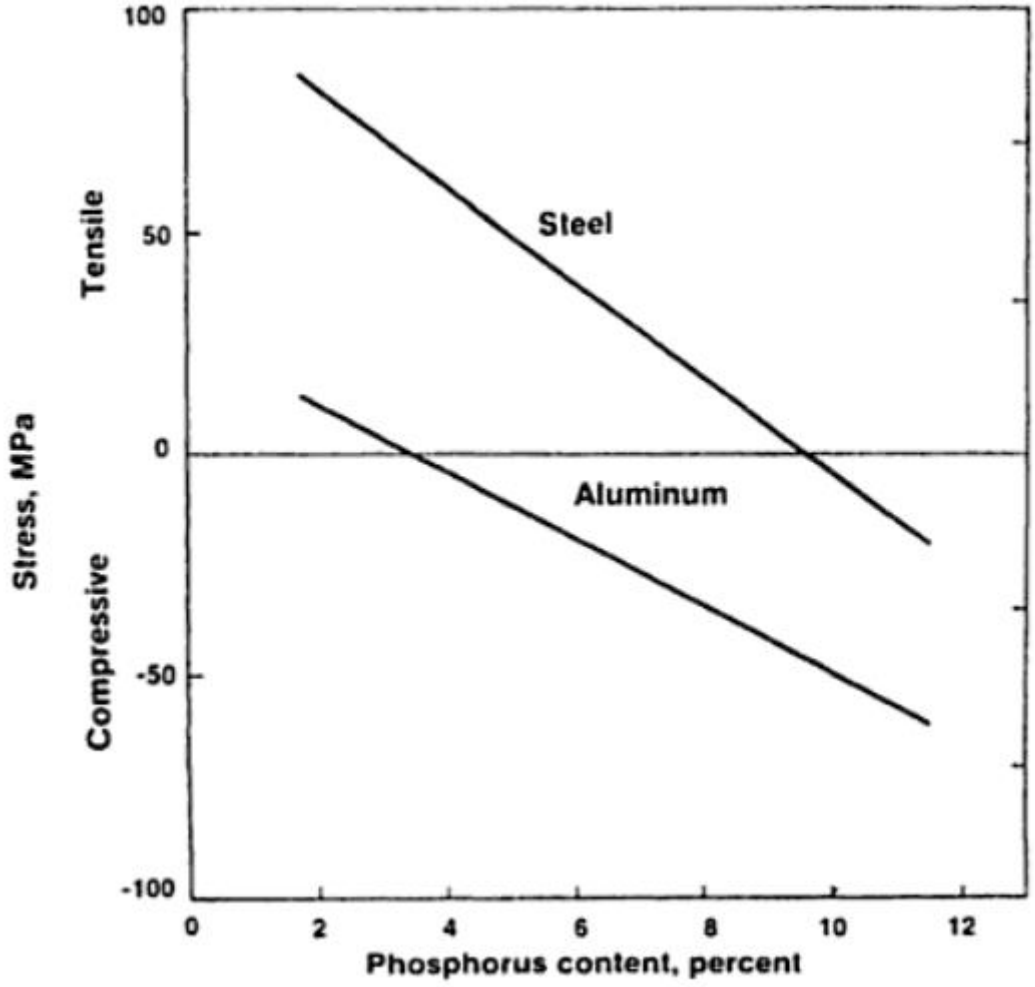

Figure 3.2 Variation in stress generated depending upon the amount of phosphorus in the coating.

Another theory behind the generation of stress in the coating was explained by Bozorth [8]. In the deposition process hydrogen is co-deposited along with metal atoms. The structure of metal during deposition is stretched due to the presence of hydrogen as compared to pure metal structure. As the coating layers continue to be deposited, the hydrogen starts to diffuse out and the layers begun to be in the state of tension. After few layers have been deposited a stress difference is set up between the layers. The compressive stress in the innermost layer is maximum and it decreases as with the adjacent layers. Sometimes the stress is so high that rearrangement of atoms occurs and hence the peaks are shifted when analysed with the X-rays.

Duncan and Moiseev [9, 10] have explained the origin of stress in the coating with relation to microstructure. Any nickel plating consists of two phases known as the beta (β) or the gamma (γ) phase. The phosphorus content determines the amount of these

phases. Below 5 % phosphorus the phase is entirely β, above 8.5% phosphorus the phase is entirely γ and in between 5 to 8.5% the microstructure consists of both β and γ. β phase is a crystalline solid solution of phosphorus in nickel whereas γ is an amorphous phase. Both the individual phases alone are coherent, ductile and impart compressive stress but the two phases together makes the structure incoherent, brittle and provides a tensile stress to the coating.

All the above theories complement each other and will be used to explain the development of stress in electroless coatings.

In the Ni-P phase diagram [3], phosphorus has no solid solubility in nickel at room temperature. The electroless plating is performed at temperature no greater than 100 °C so it doesn't permit sufficient diffusion of atoms to form intermetallic compounds like Ni_3P. Hence layers of nickel atoms are laid on the substrate and the phosphorus atoms are trapped in these layers without a uniform distribution which leads to microcrystalline deposit formation and an amorphous coating.

3.1.2.2 Stress in transverse cut samples

In Figure 3.3 GOES samples cut in transverse and rolling direction are shown where x and y refer to the axis direction. Assuming isotropic stress was applied by the coating on GOES, the stress in the transverse direction was equal to the stress in the rolling direction as shown in equation 3.1. The stress was equal to the product of strain and Young's modulus as shown in equation 3.2. The Young's modulus in the rolling and transverse direction of HiB steel was 114 GPa and 195 GPa respectively [11]. Substituting the value of Young's modulus in equation 3.2 we get equation 3.3 and 3.4. From equation 3.4 it can be seen that the strain in the rolling direction was almost double the strain in transverse direction which shows that upon application of stress the domains would always narrow in the rolling direction and it does not depend upon the cutting direction.

$$\sigma_T = \sigma_R \tag{3.1}$$

$$\epsilon_T E_T = \epsilon_R E_R \tag{3.2}$$

$$\epsilon_T \times 195 = \epsilon_R \times 114 \tag{3.3}$$

$$\epsilon_T = 0.58 \times \epsilon_R \tag{3.4}$$

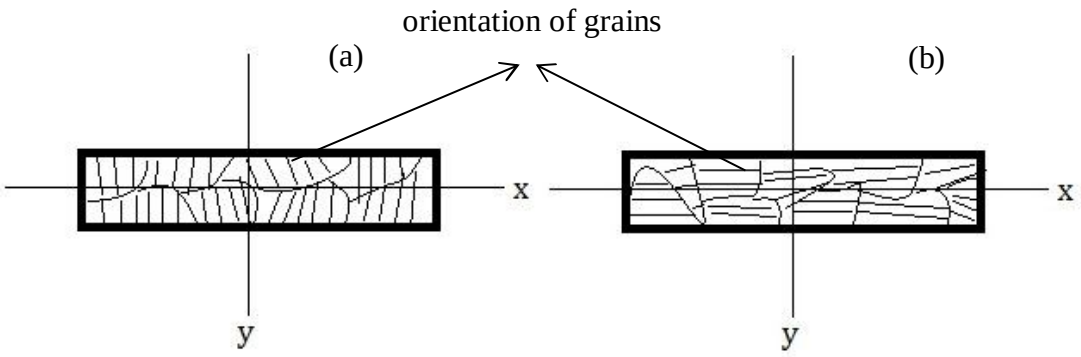

Figure 3.3 grain oriented electrical steel cut in the transverse direction (a) and rolling direction (b).

3.1.3 Electroless plating of Co-P-CNT

Carbon Nanotubes (CNTs) are known for their mechanical properties such as high strength, elastic modulus, elastic strain bearing tendency [12, 13], flexibility [14] and many other properties which make them favourable for a number of applications. The calculation of the theoretical Young's modulus of single walled CNT of 5 GPa [15] and bending strength of 14.2 GPa [16] make it ideal for use in a composite coating. CNTs are mostly used in composite coatings for improving the tribological properties of the material [17-21]. Chen et al. [17] has shown that the addition of CNTs in the coating increases the hardness of the coating. Wang et al. [18] found that the surface roughness of Ni-P-CNT coated sample was between 100 to 300 nm. Alishahi et al. [22] reported that wear properties of the surface could be enhanced by an improvement in surface roughness from CNT coating. The surface roughness of Ni-P and Ni-P-CNT coated sample was shown to be 192 nm to 129 nm respectively it was also shown that the corrosion resistance of Ni-P coatings was improved with the incorporation of CNTs due to their high chemical stability.

Wada et al. [23] had shown that power losses could be reduced by 30-40 % on improving the surface roughness. Improving the surface roughness with a non-magnetic coating would not contribute to an improvement in magnetic properties of the material as the magnetic path on the surface of grain oriented electrical steel remains the same so a magnetic material could only be used. Cobalt was chosen as it is magnetically active and has a comparable saturation magnetization of 167 emu to that of iron (221 emu). The electrical and magnetic properties can change widely upon depositing the composite coating of the CNTs with cobalt [21].

3.2 Physical Vapour Deposition (PVD)

PVD is a coating deposition process used to deposit films of thickness ranging from nanometres to few microns [24]. All PVD methods use the same principle of deposition and the fundamental steps are as follows:-

1. The material to be deposited is vaporised.
2. The vaporised material is transported to the substrate.
3. The vaporised material condenses on the substrate to develop the coating.

There are various PVD methods used for depositing thin films as discussed below:-

1. Thermal evaporation
2. Sputtering
3. Electron beam

3.2.1 Thermal evaporation

In this process the coating material to be deposited is evaporated by passing electric current thorough a tungsten boat (high melting point) containing the material [25] as shown in Figure 3.4. Heat is generated in the boat due to the passage of current and can be expressed by equation 3.5.

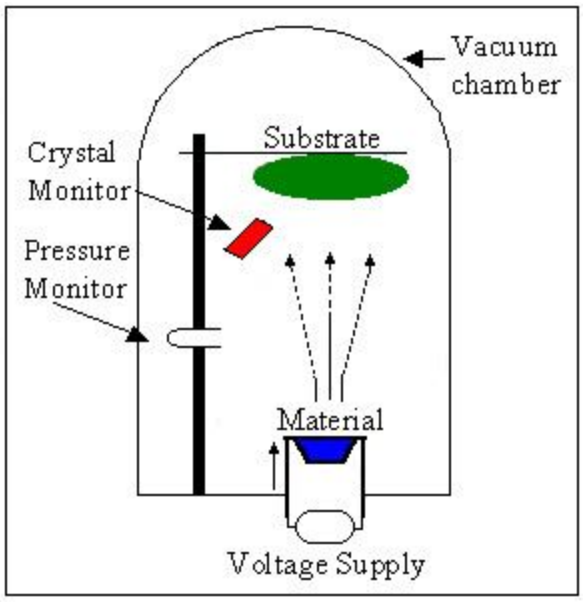

Figure 3.4 A schematic representation of the thermal evaporation system.

$$H = I^2Rt \quad (3.5)$$

Where

H is the heat energy generated in Joules

I is the current passed through the boat in Amps

R is the resistance in the circuit in Ohms

t is the heating time in seconds

This heat melts the source material which evaporates in the presence of a full or partial vacuum. The substrate is placed in the path of vapours and these vapours condense on the surface to form a thin film. The deposition rates are faster than sputtering and the substrate is not damaged as compared to sputter deposition where the high speed atoms affect the substrate properties when they impinge the surface. The disadvantage of using this process is that the substrate has to be kept in the path of deposition. Ceramic materials cannot be evaporated as the boats used for evaporation are made up of ceramics and would melt along with the material, For longer (> 100 mm) substrates the deposition is not uniform as it tends to be thicker closer to the target and thinner everywhere else. The deposition follows a parabolic profile, concentrated more in the centre and less on the sides.

3.2.2 Sputtering

Sputtering is a technique in which high energy ions are bombarded on the target and ejects the material atoms which get deposited on the substrate. The kinetic energy of the ions is very high as compared to the binding energy of the atoms due to which the atoms get ejected. To generate these high energy ions the chamber is evacuated and filled with argon gas. This argon gas is subjected to strong electromagnetic field leading to generation of plasma. This plasma contains high energy ions required for bombardment. The main advantage of this process is that the melting point of the target material is not a constraint. Since the sputtered particles impinge the substrate the bonding between the coating and the substrate is strong as compared to thermal evaporation. The disadvantages include impure deposition due to the presence of sputtered gases in the film, difficult to control layer growth and contamination due to random movement of sputtered particles.

3.2.3 Electron beam physical vapour deposition (EB-PVD)

In this process, high energy beams produced by electron guns are focused on ingot material which melts and evaporates to be deposited on the substrate. A simplified diagram of EB-PVD is shown in Figure 3.5. The kinetic energy of the electron beam strikes the target material and converts into heat energy. This heat energy melts and evaporates the target material. The substrate could also be cleaned and preheated with a high energy beam which enhances the bonding between the substrate and the coating [26].

The advantages of the process include high deposition rates, manipulation of the composition and microstructure, low impurity content and ability to develop alternating layers of coatings. The shortcomings of the process include that it is a line of sight method, wear and tear of the electron gun film leads to non-uniform evaporation and constraints on using some materials like aluminium nitride which decomposes and titanium (IV) oxide which reduces to titanium (II) oxide and titanium.

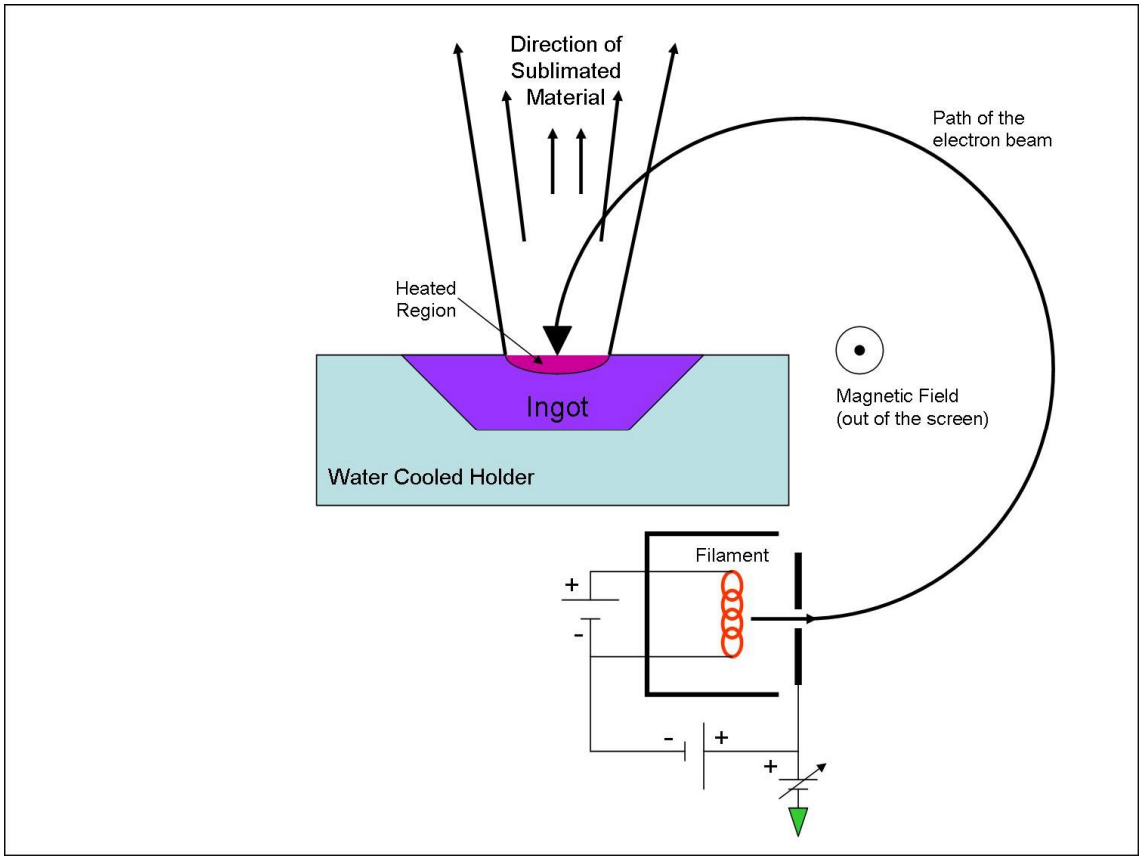

Figure 3.5 A schematic representation of electron beam-physical vapour deposition.

3.2.4 PVD of Ceramics

Ceramics are inorganic, non-metallic crystalline solids exhibiting impressive properties like oxidation resistance, corrosion resistance, high strength, low coefficient of thermal expansion and higher electrical resistivity. These properties of ceramics can be employed for coating electrical steel where eddy currents are curtailed by superior insulation and magnetostriction is limited with the stress applied by the coating having low coefficient of thermal expansion and hence reducing the both the loss and magnetostriction in the transformers. Ceramics can be oxides, nitrides, carbides or composites depending upon the desired properties. Figure 3.6 gives idea about the coefficient of thermal expansion for a few metals and ceramics. An effective coating system will have the ability to provide high insulation resistance and control hysteresis loss and magnetostriction through mechanisms such as tensile stress. Current coatings utilise a differential thermal contraction with the substrate to create tensile stress on cooling from high temperature. The coefficient of thermal expansion of silicon steel is 13×10^{-6}/K. Based upon the desired properties of electrical steel coatings, three coatings namely CrN, CrAlN and TiAlN were suggested.

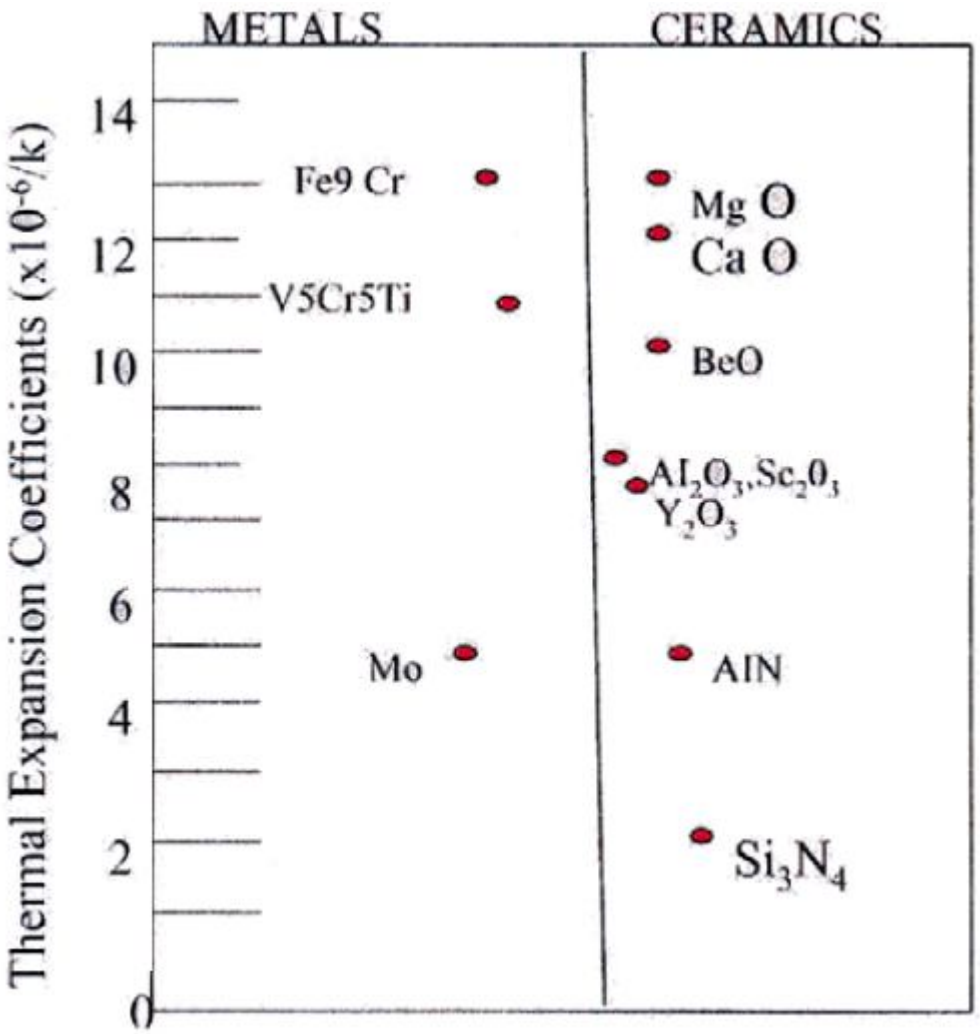

Figure 3.6 Thermal expansion coefficients for various metals and ceramics [27].

3.2.4.1 Chromium Nitride by PVD

Table 3.1 CrN electrical resistivity with varying parameters [28].

Sample No.	Argon (sccm)	Nitrogen (sccm)	Thickness (nm)	Deposition rate (A°/(kW. min))	Resistivity (m Ω cm)
1	112	0	1115	1115	0.0185
2	90	22	797	797	0.0960
3	67	45	735	735	0.1600
4	50	62	562	562	1.0000
5	38	74	516	516	28.7000

Pure chromium has an electrical resistivity of 6.3 x 10^{-4} Ω cm. On addition of nitrogen up to 60% the resistivity increases to 1.16 Ω cm and then decreases[29]. Hou [28] performed series of tests to increase the resistivity of CrN and Table 3.1 was produced. It is clear that the electrical resistivity can be increased by increasing the nitrogen content.

Inokuti et. al. [30] experimented with a number of different ceramic coatings and suggested TiN and CrN as potential coatings that can be used to restrict losses in electrical steels. Figure 3.7 shows graphs for magnetic flux density on the top and iron losses at the bottom with 'P' as the silicon sheet and 'C' as the ceramic coating. The iron loss $W_{17/50}$*(W/* kg) means the losses were calculated at 1.7 T magnetic flux density and 50 Hz frequency. The magnetic field strength was 800 A/m. The magnetic flux density improved marginally while losses were reduced to a larger extent by using TiN or CrN coatings. CrN coatings impart lower residual compressive stresses than TiN but CrN showed higher electrical resistivity than TiN [31].

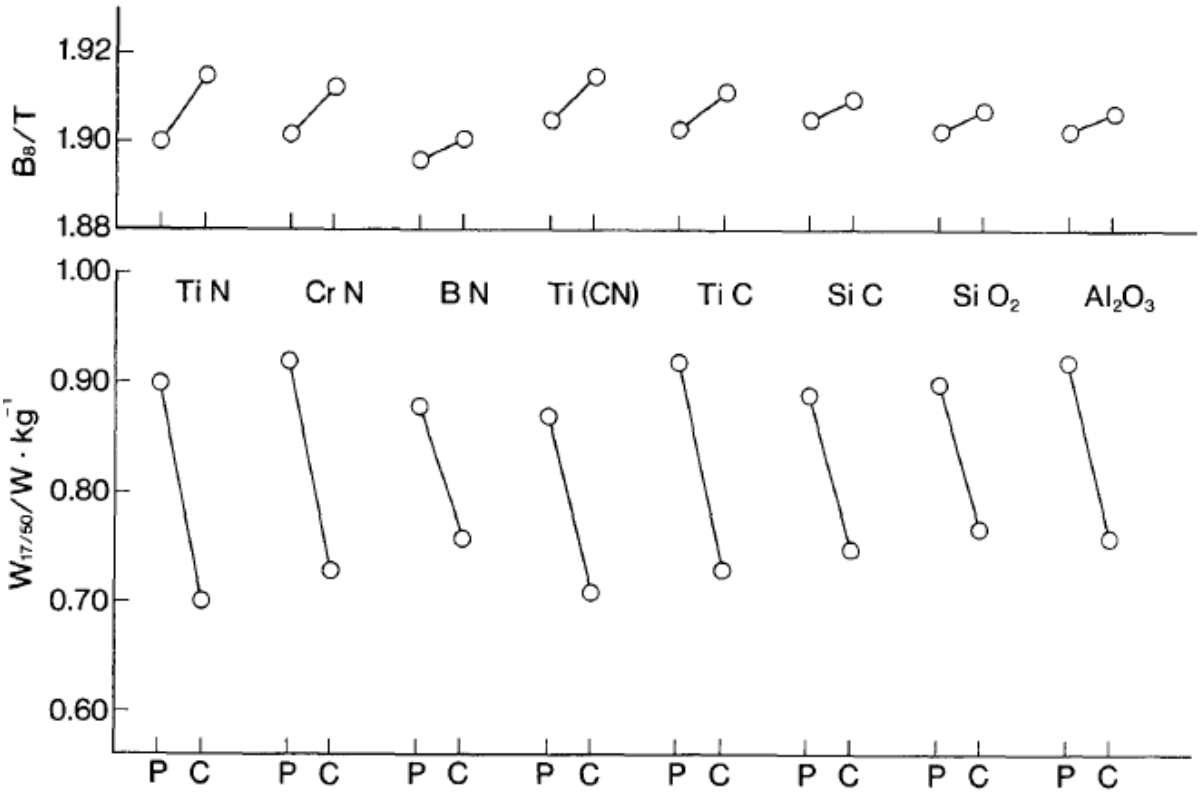

Figure 3.7 Variations in magnetic flux density B_8(T) and iron loss $W_{17/50}$*(W/* kg) for the grain oriented silicon steel product *(P)* and ceramic coatings (C) of TiN, CrN, BN, Ti(CN), TiC, SiC, $Si0_2$ and Al_20_3 [30].

3.2.4.2 Chromium Aluminium Nitride (CrAlN) by PVD

CrAlN is a ternary nitride coating mostly used to enhance the wear resistance of cutting tools as the coating is considered to be very hard. The residual compressive stress generated by $Cr_{1-x}Al_xN$ coating is quoted in the range of 4.5 to 5.6 GPa based upon the type of deposition process, parameters and chemical composition of the coating [32]. Reiter et. al. [33] varied the aluminium content in the coating and found that a compressive residual stress of around 5 GPa and microhardness of 37000 N/mm^2 were observed at x=0.46. Aluminium atoms get dissolved in the fcc-CrN lattice and strain it; this hinders the movement of dislocation and increases hardness and residual compressive stress. The resistivity of the $Cr_{1-x}Al_xN$ coating depends upon the amount of aluminium content in the coating and increases from 3.5×10^{-3} to $2 \times 10^{-1}\Omega m$ for x=0 to x=0.55 [34] respectively at room temperature. The large value of resistivity and compressive stress could be very beneficial for grain oriented electrical steel coating.

3.2.4.3 Titanium Aluminium Nitride (TiAlN) by PVD

The properties of $Ti_{1-x}Al_xN$ are similar to that of CrAlN coating. Incorporation of x= 0.12 aluminium in the crystal structure of TiN reduces the lattice parameter and grain size, and also the orientation of TiN changes from (200) to random orientation. The mircohardness increases from 1400 to 2800 HK (Knoop hardness) [35]. The decrease in grain size hinders the movement of dislocations and random orientation has large angle grain boundaries which require a large amount of stress to move the dislocations from one grain to another hence the hardness increases. The generation of residual stress in this coating is due to lattice strain by replacement of Ti atoms with Al atoms [36]. The values of compressive stress reported by Ahlgren et. al [37] were 1.7 and 5 GPa for a substrate bias voltage of 40 and 70-200 V respectively.

3.3 Chemical Vapour Deposition (CVD)

In this type of deposition process precursor gases react and decompose on substrate surfaces which are heated to desired temperatures and a coating is formed by chemical reaction of the gases on the surface. The undesired products formed as a result of these reactions are removed. Although the original CVD processes were based on heating the substrate recently low temperature CVD deposition [38] has been demonstrated.

The fundamental steps in a CVD technique are as follows and shown in Figure 3.8:-

1. The chemical gases diffuse into the surface of the substrate.
2. The diffused gases get absorbed by the surface.
3. The absorbed gases react with the surface to form the coating.
4. The by-products get desorbed from the surface.
5. The by-products are removed from the chamber.

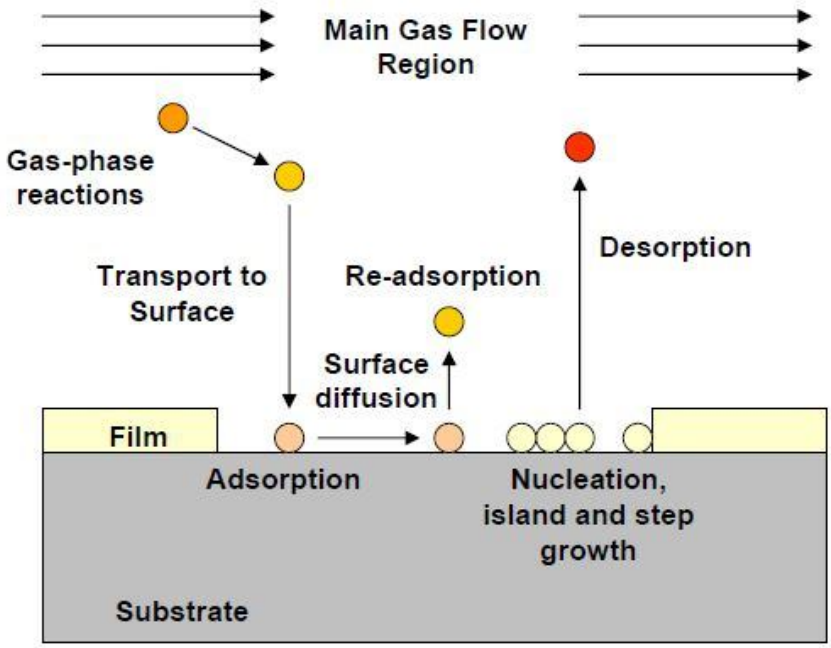

Figure 3.8 A schematic representation of CVD process.

CVD processes are classified into various types but only Plasma-Enhanced Chemical Vapor Deposition is discussed in detail because it is a low temperature and low cost deposition process for depositing Diamond Like Carbon (DLC) coatings.

3.3.1 Plasma-Enhanced Chemical Vapour Deposition (PECVD)

The purpose of introducing PECVD was to deposit coatings on substrates at low temperature. The reaction rate is not controlled by heat energy but by plasma (an ionised gas) created by Radio Frequency or Direct Current discharge between electrodes. In PECVD the gas mixture is converted in to plasma so the gas contains ions, neutral atoms, molecules and other excited species as can be seen in Figure 3.9. These excited species are absorbed on the surface, react with the substrate and are deposited on it. The reaction can occur at low temperatures as these reactive species have high energy to collide with the substrate and release heat. The process offers the

advantage of good bonding with the substrate, uniformity of deposition and low pinhole density.

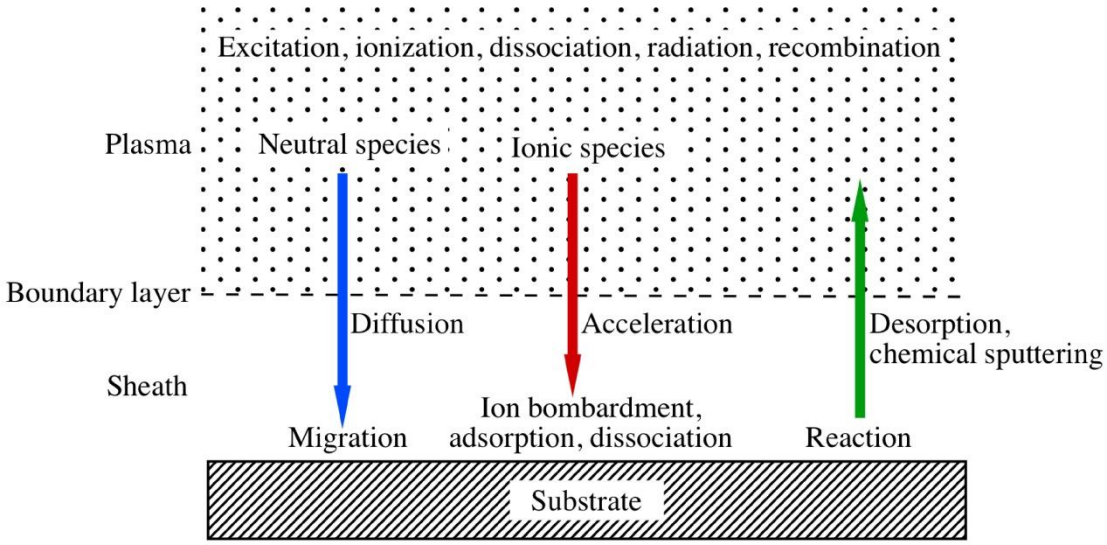

Figure 3.9 Mechanism of PECVD process.

3.3.2 Diamond Like Carbon by PECVD

Recently, many researchers have investigated the properties of Diamond Like Carbon (DLC). The coating has found numerous applications in relation to mechanical and tribological properties [39, 40]. It showed higher hardness, higher electrical insulation [41] (10^2–10^{16} Ω cm) and chemical inertness. The high internal stress demonstrated by coating is considered as a limitation for all coating applications except for electrical steel. A high compressive stress (0.5 to 7 GPa) applied by the coating can be very beneficial to electrical steel sheets wherein power loss and magnetostriction is reduced by a resultant tensile stress on the sheet as illustrated in the Figure 3.10.

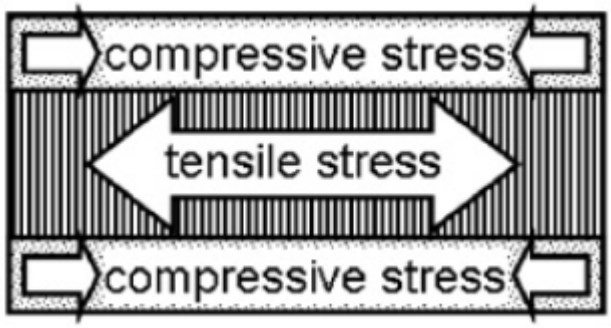

Figure 3.10 Resultant tensile stress on substrate by compressive stress coating [42].

DLC coating doesn't adhere properly to the substrate. Numerous alloying elements like Si, N, B, F, P and many more have been tried to improve the adhesion and other properties of the coatings. It has been observed that DLC has excellent bonding with carbide and silicide substrates. Depositing an amorphous silicon layer on the metal (silicide promoter) is very helpful in promoting adhesion [40]. The presence of hydrogen in the coating increases the electrical resistance to a large extent. Nitrogen addition to the DLC can reduce the compressive stress without affecting the mechanical properties but it increases the electrical conductivity by promoting the formation of sp^2 hybridisation through graphitization. Incorporation of nickel in DLC led to ferromagnetic behaviour of the coating [43]. The bonding between the substrate and the coating was improved as surface roughness was increased by increasing the nickel content.

Schuhmacher et. al. [44] developed an amorphous carbon-hydrogen network insulation coating to be used on electrical steel sheets. The coating was very effective in reducing the power loss in electrical steel as shown in Figure 3.11. Si-C:H were used as an interlayer to augment adhesion.

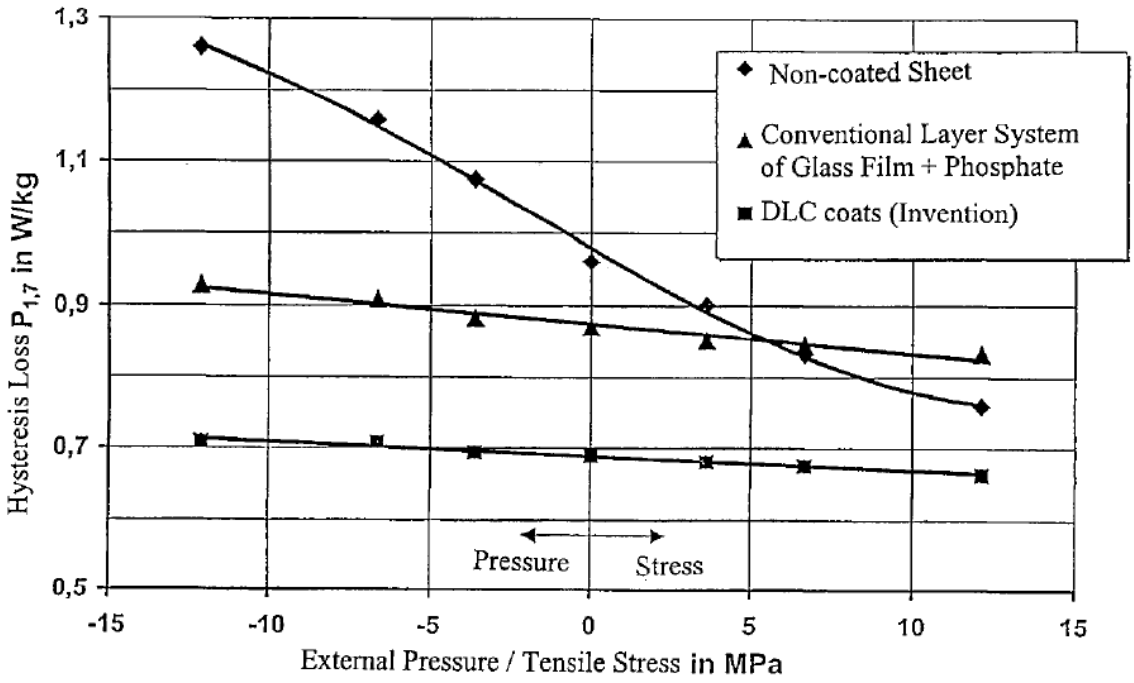

Figure 3.11 Hysteresis loss as a function of tensile stress for various coated and uncoated steel [44].

Numerous techniques for example pulsed laser deposition, radio frequency Plasma enhanced chemical vapour deposition (rf PECVD), sputtering, and filtered cathodic vacuum arc can be used to apply DLC coating on the substrate. The rf PECVD is a low cost deposition system used to deposit DLC coatings at relatively low temperatures. Clay et. al [38] had reported the formation of DLC coatings on silicon substrate using three different combination of gases (CH_4/He, CH_4/Ar and CH_4/N) and shown that a mixture of methane and helium gas had shown higher resistivity values and improved adhesion to the substrate.

3.4 Summary

Coatings on GOES can be deposited by a number of techniques including electroless/electrochemical plating, physical/chemical vapour deposition and sol-gel method. All these methods will be attempted to produce coatings on GOES with lower power loss and magnetostriction. The suitable coatings will be further explored on industrial scale using the facilities in Tata steel and Cogent.

3.5 References

[1] A. Brenner and G. E. Riddell, "Deposition of nickel and cobalt by chemical reduction," *J. Res. Nat. Bus. Stand. ,* vol. 39, pp. 385-395, 1947.

[2] P. Sahoo and S. K. Das, "Tribology of electroless nickel coatings – A review," *Materials & Design,* vol. 32, p. 1760, 2011.

[3] G. O. Mallory and J. B. Hajdu, "Electroless Plating Fundamentals & Applications," *American electroplaters and surface finishers society,* vol. chapter 4, pp. 121-122, 1990.

[4] J. Pang, Q. Li, W. Wang, X. Xu, and J. Zhai, "Preparation and characterization of electroless Ni–Co–P ternary alloy on fly ash cenospheres," *Surface & Coatings Technology,* vol. 205, pp. 4237-4242, 2011.

[5] Z. Xiao-Yun, G. Zhong_Cheng, and X. R. Dong, "Process and properties of electroless Ni-W-B amorphous electrical resistance film," *Transactions Nonferrous Metals Socity of China,* vol. 14, pp. 144-146, 2004.

[6] P. Chivavibul, M. Enoki, S. Konda, Y. Inada, T. Tomizawa, and AkiraToda, "Reduction of core loss in non-oriented (NO) electrical lsteel by electroless-plated magnetic coating," *Journal of Magnetism and Magnetic Materials,* vol. 323, pp. 306-310, 2011.

[7] D. H. Kim, K. Aoki, and O. Takano, "Soft Magnetic Films by Electroless Ni-Co-P Plating," *Journal of the electrochemical society,* vol. 142, pp. 3763-3767, 1995.

[8] R. M. Bozorth, "The orientations of crystals in electrodeposited metals," *Physics Review,* vol. 26, p. 390, 1925.

[9] R. N. Duncan, "Metallurgical Structure of EN Deposit," *Plating and surface finishing,* vol. 83, p. 65, 1996.

[10] V. P. Moiseev, "Technique to define atomic structure precipitation of chemically restored nickel," *Izvestiya Akademii Nauk SSSR Physics,* vol. 26, p. 378, 1962.

[11] P. Klimczyk, "Novel Techniques for Characterisation and Control of Magnetostriction in G.O.S.S," *PhD Thesis, Cardiff University, Cardiff*, 2012.

[12] G. Overney, W. Zhong, and D. Tomamek, "Structural rigidity and low frequency vibrational modes of long carbon tubules," *Z physics D,* vol. 27, pp. 93-96, 1993.

[13] J. P. Salvetat, J. M. Bonard, N. H. Thomson, A. J. Kulik, L. Forr´o, W. Benoit, *et al.*, "Mechanical properties of carbon nanotubes," *Applied Physics A,* vol. 69, pp. 255-260, 1999.

[14] S. Iijima, "Structural flexibility of carbon nanotubes," *Journal of Chemical Physics,* vol. 104, pp. 2089-2092, 1 February 1996.

[15] M. M. J. Treacy, T. W. Ebbesen, and J. M. Gibson, "Exceptionally high Young's modulus observed for individual carbon nanotubes," *Nature,* vol. 381, pp. 678-680, 1996.

[16] E. W. Wong, P. E. Sheehan, and C. M. Lieber, "Nanobeam mechanics: elasticity, strength and toughness of nanorods and nanotubes," *Science,* vol. 277, pp. 1971-1975, 1997.

[17] W. X. Chen, J. P. Tu, Z. D. Xu, W. L. Chen, X. B. Zhang, and D. H. Cheng, "Tribological properties of Ni–P-multi-walled carbon nanotubes electroless composite coating," *Materials Letters,* vol. 57, pp. 1256-1260, 2003.

[18] L. Y. Wang, J. P. Tu, W. X. Chen, Y. C. Wang, X. K. Liu, C. Olk, *et al.*, "Friction and wear behavior of electroless Ni-based CNT composite coatings," *Wear,* vol. 254, pp. 1289–1293, 2003.

[19] W. X. Chen, J. P. Tu, H. Y. Ga, Z. D. Xu, Q. G. Wang, J. Y. Lee, *et al.*, "Electroless preparation and tribological properties of Ni-P-Carbon nanotube composite coatings under lubricated condition," *Surface and Coatings Technology,* vol. 160, pp. 68-73, 2002.

[20] X. H. Chen, C. S. Chen, H. N. Xiao, H. B. Liu, L. P. Zhou, S. L. Li, *et al.*, "Dry friction and wear characteristics of nickel/carbon nanotube electroless composite deposits," *Tribology International,* vol. 39, pp. 22–28, 2006.

[21] X. Chen, J. Xia, J. Peng, W. Li, and S. Xie, "Carbon-nanotube metal-matrix composites prepared by electroless plating," *Composites Science and Technology,* vol. 60, pp. 301-306, 2000.

[22] M. Alishahi, S. M. Monirvaghefi, A. Saatchi, and S. M. Hosseini, "The effect of carbon nanotubes on the corrosion and tribological behavior of electroless Ni–P–CNT composite coating," *Applied Surface Science,* vol. 258, pp. 2439-2446, 2012.

[23] T. Wada, T. Nozawa, and T. Takata, "Method for producing a super low watt loss grain oriented electrical steel sheet," *US Patent,* vol. 3932236, January 13, 1976.

[24] D. M. Mattox, "Handbook of physical vapor deposition (pvd) processing- Film formation, adhesion, surface preparation and contamination control," *Noyes Publications Westwood, New Jersey, U.S.A.*, 1998.

[25] R. F. Bunshah, J. John M. Blocher, T. D. Bonifield, J. G. Fish, P. B. Ghate, B. E. Jacobson, *et al.*, "Deposition technologies for films and coatings-Development and applications," *Noyes Publications Westwood, New Jersey, U.S.A.*, 1982.

[26] J. Singh, F. Quli, D. E. Wolfe, J. T. Schriempf, and J. Singh, "An overview: Electron beam-physical vapor deposition technology- present and future applications," *The Applied Research Laboratory, The Pennsylvania State University, USA*, 1999.

[27] D. L. Smith, J.-H. Park, I. Lyublinski, V. Evtikhin, A. Perujo, H. Glassbrenner, *et al.*, "Progress in coating development for fusion systems," *Fusion Engineering and Design*, vol. 61-62, pp. 629-641, 2002.

[28] Y. HOU, "Aluminum Nitride and Chromium Nitride Thin Films for Strain Gauge Application," *Masters Thesis, Delft University of Technology*, 2010.

[29] G. A. Zhang, P. X. Yan, P. Wang, Y. M. Chen, and J. Y. Zhang, "Influence of nitrogen content on the structural, electrical and mechanical properties of CrNx thin films," *Materials Science and Engineering A*, vol. 460-461, pp. 301-305, 2007.

[30] Y. Inokuti, K. Suzuki, and Y. Kobayashi, "Grain Oriented Silicon Steel Sheet with New Ceramic Films Characterized by Ultra-Low Iron Loss," *Materials Transactions, JIM*, vol. 33, No. 10, pp. 946-952, 1992.

[31] B. Navingek, P. Panjan, and A. Cvelbar, "Characterization of low temperature CrN and TiN (PVD) hard coatings," *Surface and Coatings Technology*, vol. 74-75, pp. 155-161, 1995.

[32] G. S. Kim and S. Y. Lee, "Microstructure and mechanical properties of AlCrN films deposited by CFUBMS," *Surface & Coatings Technology*, vol. 201, pp. 4361-4366, 2006.

[33] A. E. Reiter, V. H. Derflinger, B. Hanselmann, T. Bachmann, and B. Sartory, "Investigation of the properties of $Al_{1-x}Cr_xN$ coatings prepared by cathodic arc evaporation," *Surface & Coatings Technology*, vol. 200, pp. 2114-2122, 2005.

[34] R. Sanjine´s, O. Banakh, C. Rojas, P. E. Schmid, and F. Le´vy, "Electronic properties of Cr1yxAlxN thin films deposited by reactive magnetron sputtering," *Thin Solid Films*, vol. 420-421, pp. 312-317, 2002.

[35] K. H. Kim and S. H. Lee, "Comparative studies of TiN and _ AlxN by plasma-assisted chemical vapor deposition using a TiCla/A1C13/N2/H2/Ar gas mixture," *Thin Solid Films*, vol. 283, pp. 165-170, 1996.

[36] S.-Y. Yoon, J.-K. Kim, and K. H. Kim, "A comparative study on tribological behavior of TiN and TiAlN coatings prepared by arc ion plating technique," *Surface & Coatings Technology*, vol. 161, pp. 237-242, 2002.

[37] M. Ahlgren and H. Blomqvist, "Influence of bias variation on residual stress and texture in TiAlN PVD coatings," *Surface & Coatings Technology,* vol. 200, pp. 157-160, 2005.

[38] K. J. Clay, S. P. Speakman, N. A. Morrison, N. Tomozeiu, W. I. Milne, and A. Kapoor, "Material properties and tribological performance of rf-PECVD deposited DLC coatings," *Diamond and Related Materials,* vol. 7, pp. 1100-1107, 1998.

[39] J. Robertson, "Diamond-like amorphous carbon," *Material science and engineering R,* vol. 37 (4–6), pp. 129-281, 2002.

[40] C. Donnet, "Recent progress on the tribology of doped diamond-like and carbon alloy coatings: a review," *Surface & Coatings Technology,* vol. 100-101, pp. 180-186, 1998.

[41] A. Grill, "Diamond-like carbon: state of the art," *Diamond and Related Materials,* vol. 8, pp. 428-434, 1999.

[42] E. Beyer, L.Lahn, C.Schepers, and T.Stucky, "The influence of compressive stress applied by hard coatings on the power loss of grain oriented electrical steel sheet," *Journal of Magnetism and Magnetic Materials,* vol. 323, pp. 1985-1991, 2011.

[43] R. Paul, M. K. Sharma, R. Chatterjee, S. Hussain, R. Bhar, and A. K. Pal, "Ferromagnetism in nanocrystalline nickel incorporated diamond-like carbon thin films," *Applied Surface Science,* vol. 258, pp. 5850-5857, 2012.

[44] B. Schuhmacher, K. Guenther, H. Hingmann, K. Bewilogua, C.-P. Klages, H. Dimigen*, et al.*, "Grain oriented magnetic steel sheet comprising an electrically insulating coating," *US Patent 7169479 B2,* 2007.

4 Experimental Procedure

4.1 Introduction

This chapter describes the procedures followed for producing a range of coatings on GOES. Coatings were produced using electroless plating and PVD techniques which are described in sections 3.1 and 3.2. The range of analytical systems used to characterise the coatings are then described in sections 4.08 to 4.21.

4.2 Electroless Co-Ni-P coating on GOES

Table 4.1 Electroless plating bath conditions

Composition	**grams/litre**
Nickel sulphate	7.5
Cobalt sulphate	15.0
Sodium hypophosphite	25.0
Trisodium citrate	50.0
Boric acid	30.0
pH 9.0 Temperature 60 ±5°C	

GOES samples were coated with Co-Ni-P using electroless plating. The electroless bath was prepared in deionized water. The composition of the bath and the operating conditions were referred from [1] and modified to reduce the particle size of deposition which reduces power loss as shown in Table 4.1. The chemicals were added whilst the solution was magnetically stirred. The pH of solution was measured by pocket PTTestr 35 pH meter manufactured by Oakton instruments with resolution of 0.1 and it was calibrated using National Institute of Standards and Technology (NIST) buffer solutions of pH 4.01, 7, 10. The pH of the solution was controlled by adding ammonium hydroxide. All pH values quoted are room temperature values. The temperature of bath was raised after ensuring the desired pH value because the pH value is dependent upon

temperature. GOES samples were thoroughly cleaned with ethanol to remove any oil, grease, hand stains and dried by hot blower. The samples were immersed into the solution after it attained the desired temperature. To study the effect of coating thickness on the substrate, four samples were immersed in the plating solution and were removed at 20, 35, 50, and 90 min and were given the sample id's Ni1, Ni2, Ni3 and Ni4 respectively. The samples were cleaned with acetone and dried after removal from the solution. To ascertain the effect of pH on the power loss, five samples were prepared with pH step size 0.4 varying from 7.8 to 9.4 these samples were given the samples id's NipH1, NipH2, NipH3, NipH4 and NipH5. All five samples were immersed for 90 min duration.

The deposition of coating starts with the dehydrogenation of hypophosphite which provides the hydride ion (4.1). The deposition of nickel and cobalt on the surface of grain-oriented electrical steel was triggered by the reduction of nickel and cobalt ions by the hydride ion as shown in reactions (4.2) & (4.3) [2]. These deposited particles act as nucleation sites for further deposition of coating and hence the time period of coating dictates the thickness of coating deposited.

$$H_2PO_2^- + H_2O \rightarrow H^+ + HPO_3^{2-} + 2H \quad (4.1)$$

$$Ni^{2+} + 2H \rightarrow Ni^0 + 2H^+ \quad (4.2)$$

$$Co^{2+} + 2H \rightarrow Co^0 + 2H^+ \quad (4.3)$$

4.3 Electroless Co-P-CNT coating on GOES

Table 4.2 Bath Composition and conditions

Chemical Reagent	Concentrations (g/l)
Cobalt sulphate	14.0
Sodium hypophosphite	25.0
Trisodium citrate	45.0
MWCNT	0.2
pH at 25 °C	9.7
Temperature	62 ± 1 °C

The MWCNTs used in coating the samples were supplied by M/s Haydale Ltd UK. The MWCNTs were used in the as prepared condition (not functionalised). GOES sheets were cut into 0.3mm x 30mm x 75mm samples. The coating solution was prepared in deionised water. Samples were thoroughly cleaned with ethanol to remove dust, grease and dried by blowing hot air. The composition of the bath was taken from [3] and modified by adding 0.2 g/l of MWCNT's in the solution as the best results were obtained at this composition by trial and error. The modified bath and operating conditions are shown in Table 4.2. The solution was stirred with a magnetic stirrer to suspend the MWCNT's in the solution. The pH of the solution was maintained by adding ammonia hydroxide. The solution was heated using the heating element in the magnetic stirrer. The samples were then immersed in the plating bath at a temperature of 50 °C and the final bath temperature recorded was 62 ± 1 °C. Samples were coated with Co-P-CNT coating for 60 (CoP1) & 80 (CoP2) minutes to study the effect of coating thickness on the improvement of power loss. Samples were also coated without CNT's in the plating solution (CoP3) to study the effect of Co-P coating on grain oriented electrical steel.

4.4 Electroless Co-Ni-B coating on GOES

Table 4.3 The composition of the Co-Ni-B plating bath.

Composition	Grams/litre
Nickel sulphate	13.0
Cobalt sulphate	14.0
Tri sodium citrate	27.0
Dimethylamine borane	1.4
pH 8.0 & 8.8	
Temperature 57±3 °C	

Co-Ni-B coating on grain oriented electrical steel was deposited with pH values of 8 and 8.8 given the sample identity of NiB1 and NiB2 respectively. The coating was deposited for a time period of 60 minutes. The bath conditions were taken from [4] as shown in Table 4.3. The remaining procedure was similar to that described in section 4.2.

4.5 Coating removal procedure

Grain oriented (Fe- 3%Si) samples (0.3mm x 30mm x 305mm) were supplied by Cogent Power Limited, Newport. The samples had two coatings; forsterite and aluminium orthophosphate described in section 2.6.1 and 2.6.2. The two layer coating system was removed by immersing the samples in a solution of 7.5% sulphuric acid + 1% Hydrofluoric acid for approximately 10 minutes at a temperature of 75 °C and then placing the samples in 4% Nitric acid solution for approximately 7 minutes. The samples were dried in front of hot air blower to avoid rust formation and immediately packed in anti-corrosive paper.

4.6 Pre-treatments

Electroless plating can only be done on the catalytic surfaces. To develop a coating on a glass slide the surface has to be pre-treated. Pre-treatment involves three steps.

Rough Surface: Initially the surface is roughened by scratching it with 220 grit abrasive paper. A rough surface ensures good bonding between the coating and the substrate by trapping the particles in the surface grooves and also it increases the surface area so the number of active sites for nucleation increases. Surfaces could also be roughened by acid etching.

Sensitisation: In this process the surface of the glass slide was dipped in a 300 ml deionised water solution of 7.5 gm of tin (II) chloride and 12 ml of hydrochloric acid for 30 minutes at a temperature of 25-30 °C until the Sn^{2+} particles were deposited on the surface of the sample.

Activation: To activate the surface a solution of 300 ml of deionised water was prepared with 0.1 gm of palladium (II) chloride and 0.75 ml of hydrochloric acid. The glass slide was dipped in this solution for 30 minutes and the temperature of the solution was maintained between 25-30 °C. The palladium particles (Pd^{2+}) were deposited over the already deposited Sn^{2+} particles. These palladium particles act as catalytic sites for nucleation. The coating starts to develop on these sites.

4.7 Ceramic coatings

4.7.1 Chromium Nitride (CrN)

CrN coatings were deposited on GOES by electron beam physical vapour deposition (EB-PVD) in vacuum at Wallwork Ltd., Cambridge. The samples were vapour blasted to remove any dust/grease from the surface and were then put in the PVD chamber for coating. The chamber was evacuated and filled with argon. The surface of GOES was then sputter cleaned at 450 °C removing any oxide layer present and enhancing the bonding capabilities of the steel for further deposition. The surface temperature increased due to plasma heating of the surface. The deposition of pure chromium initiated upon focusing the electron beam on the chromium target melting and then evaporating the chromium billet for a period of 5-10 minutes. Nitrogen was introduced in the chamber at a flow rate of 80 ml/min for 60 minutes which reacted with Cr depositing as CrN on the substrate surface and the thickness of the coating was measured using a plasma gauge.

4.7.2 Chromium Aluminium Nitride (CrAlN)

The procedure for depositing the CrAlN coatings was same as above except few addition steps as follows. Two billets one made of chromium and another made of aluminium was used in the process. The deposition temperature was between 350-450 ˚C. Initially pure chromium was deposited on the substrate. Nitrogen was injected in the chamber with a flow rate of 110 ml/min. The chromium and aluminium shutters were open and closed respectively and vice versa to get the final deposition of CrAlN. The whole process took around 6 hours and spectrometer was used to monitor the reaction mechanism.

4.7.3 Titanium Aluminium Nitride (TiAlN)

The procedure for deposition of this coating was same as CrAlN expect that the chromium was replaced with titanium and the substrate temperature was raised to around 480 ˚C during the deposition.

4.8 Power loss testing

The specific total loss was measured with an in house single strip tester (SST) [5] which uses a LabVIEW program to measure the magnetic properties as shown in Figure 4.1.

The system consists of a computer with LabVIEW version 8.5 supplied by National Instruments, a NI PCI-6120 data acquisition card, a power amplifier, 1 Ω shunt resistor and air-flux compensated single strip tester shown in Figure 4.2. Epstein strip (305 mm x 30 mm x 0.3 mm) was placed between two yokes (made of grain oriented electrical steel). The number of turns in the primary and secondary winding was 865 and 250 respectively. The strips were magnetised by passing current in the primary winding. The power loss was calculated by the equation below.

$$P = \frac{1}{\rho . f} \int H . \frac{db}{dt} dt \tag{4.4}$$

P = power loss (W/kg)

ρ = density of the sample (kg/m^3)

f = frequency (Hz)

h = magnetic field strength (A/m)

b = magnetic flux density (T)

t = time (s)

Samples were tested from a magnetic flux density of 0.1T to 1.7T at a magnetic field of 800 A/m for a frequency of 50Hz.

Figure 4.1 Single strip tester for measuring the power loss.

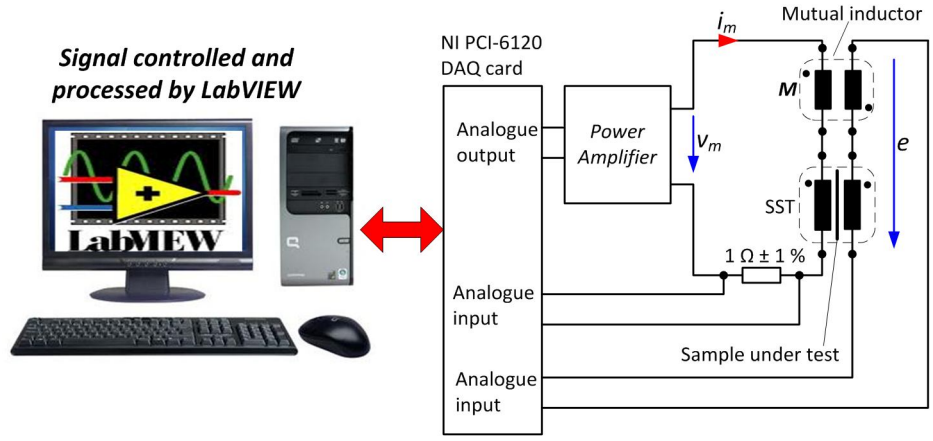

Figure 4.2 Schematic diagram of the single strip tester system.

4.9 Magnetostriction measurement

The magnetostriction measurements were made on a magnetostriction measurement system using the procedure described in [6] and shown in Figure 4.3. The Epstein strip was inserted in between the primary and secondary windings and a tufnol strip was placed on top of the Epstein strip to ensure that the sample stays flat throughout the experiment. The sample was clamped from one side and another end was free to expand under the applied magnetic field and was connected to accelerometer, load cell and pneumatic cylinders. Pneumatic cylinders were used to apply stress on the sample within the range of 10 to -10 MPa. The instantaneous magnetostriction was measured by the accelerometer.

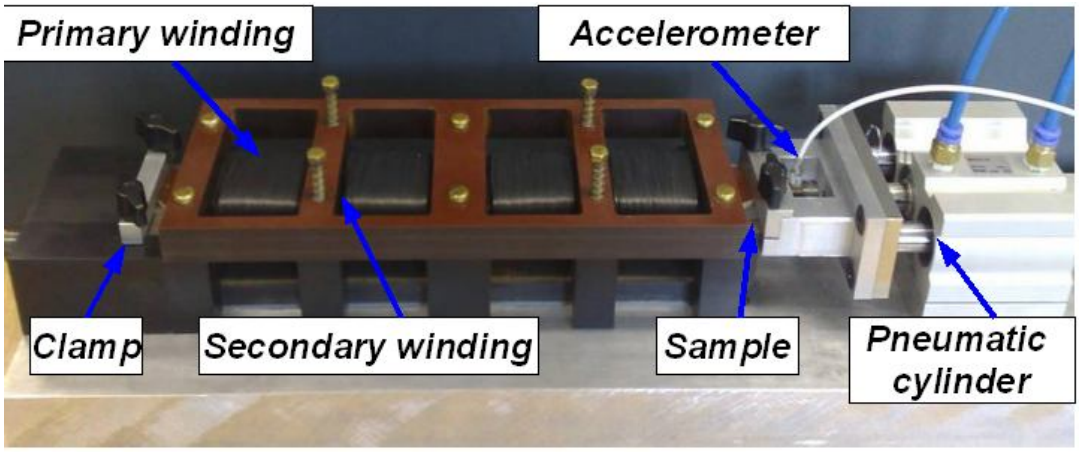

Figure 4.3 Magnetostriction measurement system

4.10 Uncertainty measurements

To gain a reasonable confidence in the measurements of the power loss and magnetostriction results, uncertainty was calculated according to the UKAS document M3003 [7].

The measurement of uncertainty for y depends upon number of factors and can be considered as a function of x as follows:

$$y = f(x1, x2, \ldots xn) \tag{4.5}$$

The average value of the given function can be calculated using the formula

$$\bar{x} = \frac{1}{n}\sum_{i=1}^{n} x_i \tag{4.6}$$

The standard deviation S is calculated by

$$s = \sqrt{\frac{\sum_{i=1}^{n}(x_i - \bar{x})^2}{n-1}} \tag{4.7}$$

The uncertainty can then be calculated by

$$u(y) = \frac{s}{\sqrt{n}} \tag{4.8}$$

The calculation of sensitivity coefficient is based upon the equation given below

$$c_i = \frac{\partial y}{\partial x_i} \tag{4.9}$$

The uncertainty components are characterised by two types of probability distribution. Normal distributions are related to standard calibration and known repeatability whereas rectangular distributions are used when only the upper and lower limits are known for the instrument.

The standard uncertainty calculated is

$$U_i = \frac{u(y)c_i}{k_{95}} \tag{4.10}$$

The degrees of freedom (V_i) of individual uncertainty measurements are combined to calculate the effective degrees of freedom (V_{eff}) as shown below.

$$V_{eff} = \frac{u^4(y)}{\sum_{i=1}^{N} \frac{U_i^4(y)}{v_i}} \tag{4.11}$$

The combined standard uncertainty is

$$U_c(y) = \sum_{i=1}^{n} \sqrt{U_i} \tag{4.12}$$

To calculate the final expanded uncertainty it is multiplied with coverage factor (k_{95}) of 2 to get 95% confidence in the results. When k_{95} is 2, V_{eff} is infinity

$$U_e(y) = k_{95} U_c(y) \tag{4.13}$$

Table 4.4 Determination of uncertainty in the measurement of stress.

Source of uncertainty	**±%**	**Probability distribution**	**Divisor**	**Ci**	**Ui ±%**	**Vi or Veff**
load cell calibration	0.200	Normal	2.0000	1.0	0.10000	∞
load cell drift	0.050	Rectangular	1.7321	1.0	0.02887	∞
Mass (Balance calibration)	0.010	Normal	2.0000	1.0	0.00500	∞
Length (Rule calibration)	0.025	Normal	2.0000	1.0	0.01250	∞
DAQ calibration	0.150	Normal	2.0000	1.0	0.07500	∞
variation in stress	0.500	Rectangular	1.7321	1.0	0.28867	∞
Repeatability	0.500	Rectangular	1.7321	1.0	0.28868	∞
Sum of squares					0.18330	
Combined uncertainty					0.42814	
Expanded uncertainty at 95% confidence level					0.85627	
Rounded uncertainty					0.86	

Table 4.5 Determination of uncertainty in the measurement of magnetic flux density.

Source of uncertainty	±%	Probability distribution	Divisor	Ci	Ui ±%	Vi or Veff
Frequency meter calibration	0.010	Normal	2.0000	1.0	0.00500	∞
Frequency setting	0.010	Rectangular	1.7321	1.0	0.00577	∞
Mass (Balance calibration)	0.010	Normal	2.0000	1.0	0.00500	∞
Length (Rule calibration)	0.025	Normal	2.0000	1.0	0.01250	∞
DAQ calibration	0.150	Normal	2.0000	1.0	0.07500	∞
air flux	0.060	Rectangular	1.7321	1.0	0.03464	∞
Repeatability	0.050	Rectangular	1.7321	1.0	0.02887	∞
Sum of squares					0.00790	
Combined uncertainty					0.08887	
Expanded uncertainty at 95% confidence level					0.17774	
Rounded uncertainty					0.18	

Table 4.6 Determination of uncertainty in the measurement of magnetostriction.

Source of uncertainty	±%	Probability distribution	Divisor	Ci	Ui ±%	Vi or Veff
Accelerometer calibration	0.200	Normal	2.0000	1.0	0.10000	∞
uncertainty in stress	0.860	Normal	2.0000	2.0	0.86000	∞
uncertainty in B	0.180	Normal	2.0000	25.1	2.25900	∞
Mass (Balance calibration)	0.010	Normal	2.0000	1.0	0.00500	∞
Length (Rule calibration)	0.025	Normal	2.0000	1.0	0.01250	∞
DAQ calibration	0.150	Normal	2.0000	1.0	0.07500	∞
Repeatability	0.500	Rectangular	1.7321	1.0	0.28868	∞
Sum of squares					5.94182	
Combined uncertainty					2.43758	
Expanded uncertainty at 95% confidence level					4.87517	
Rounded uncertainty					4.88	

Table 4.7 Determination of uncertainty in the measurement of magnetic flux density.

Source of uncertainty	±%	Probability distribution	Divisor	Ci	Ui ±%	Vi or Veff
Voltmeter calibration	0.120	Normal	2.0000	1	0.06000	∞
Voltmeter drift	0.020	Rectangular	1.7321	1	0.01155	∞
Frequency meter calibration	0.010	Normal	2.0000	1	0.00500	∞
Frequency setting	0.010	Rectangular	1.7321	1	0.00577	∞
Mass calibration	0.010	Normal	2.0000	1	0.00500	∞
Length calibration	0.025	Normal	2.0000	1	0.01250	∞
Length reading uncertainty	0.070	Rectangular	1.7321	1	0.04041	∞
Epstein frame air flux	0.060	Rectangular	1.7321	1	0.03464	∞
Repeatability	0.050	Rectangular	1.7321	1	0.02887	∞
Sum of squares					0.00764	
Combined uncertainty					0.08740	
Expanded uncertainty					0.17481	
Rounded uncertainty					0.18	

Table 4.8 Determination of uncertainty in the measurement of power loss.

Source of uncertainty	±%	Probability distribution	Divisor	Ci	Ui ±%	Vi or Veff
Wattmeter calibration	0.250	Normal	2.0000	1.0	0.12500	∞
Wattmeter uncorrected errors	0.020	Rectangular	1.7321	1.0	0.01155	∞
Wattmeter drift	0.020	Rectangular	1.7321	1.0	0.01155	∞
Frequency meter calibration	0.010	Normal	2.0000	1.0	0.00500	∞
Frequency setting	0.010	Rectangular	1.7321	1.0	0.00577	∞
Mass calibration	0.010	Normal	2.0000	1.0	0.00500	∞
Epstein dimensions	0.100	Normal	2.0000	1.0	0.05000	
Length calibration	0.025	Normal	2.0000	1.0	0.01250	∞
Uncertainty in flux	0.180	Rectangular	1.7321	3.6	0.37411	∞
Repeatability	0.400	Rectangular	1.7321	1.0	0.23094	∞
Sum of squares					0.21192	
Combined uncertainty					0.46035	
Expanded uncertainty					0.92071	
Rounded uncertainty					0.92	∞

Table 4.4-Table 4.6 shows the calculation of uncertainty in magnetostriction which was determined considering the uncertainty in stress and magnetic flux density and multiplied with the sensitivity factor. These uncertainties were then added to the total uncertainty for the calculation of magnetostriction. Similarly for the calculation of uncertainty in power loss the uncertainty in magnetic flux was calculated and followed the same procedure as described above shown in Table 4.7– Table 4.8.

4.11 Magnetic domain viewer

The magnetic domains were imaged with a magnetic pattern viewer [8] shown in Figure.4.4. A coil was wound around the circular ring and it was connected to DC power supply. The iron oxide powder was suspended in distilled water in between the plastic sheet and the white membrane. Electric current was passed through the circular ring which sets up perpendicular magnetic field. As the angle of orientation of electrical steel was not zero the magnetisation of N-S and S-N domains rotate towards and away from the surface respectively which modifies the stray profile. The S-N domains attract more ferromagnetic particles in comparison to N-S domains which build the black and white contrast visible to the naked eye and could be imaged by fixing a camera on top of the viewer.

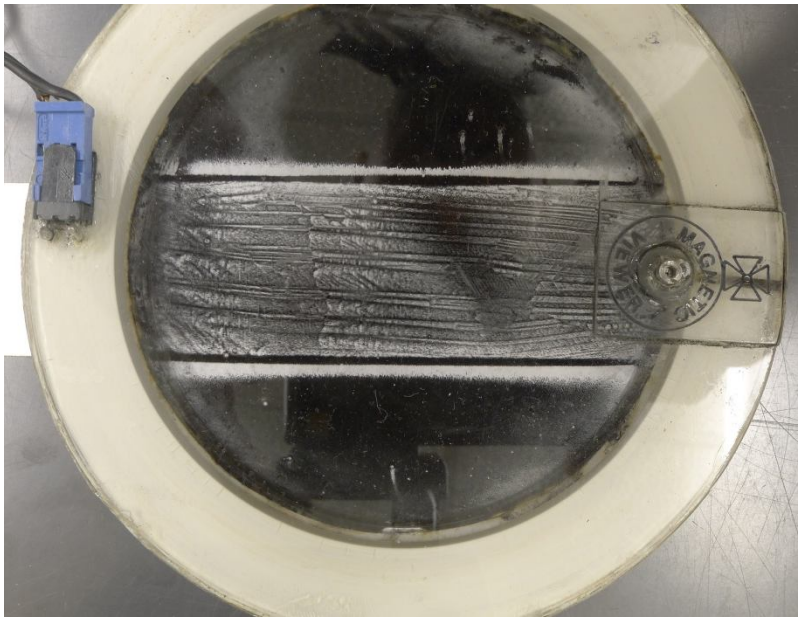

Figure.4.4 Magnetic domain viewer with grain oriented electrical steel sample beneath.

4.12 Vibrating Sample Magnetometer (VSM)

The magnetic properties of the coating were measured at room temperature by VSM. The sample was mounted on a nylon rod attached to vibrating head and a magnetic field by the electromagnet was applied from -15000 to 15000 Oe in a cycle to obtain the B-H loop. The frequency of vibration of the vibrating head was 82 Hz. The magnetic field in the pickup coil varies due to the vibration and an emf was induced according to Faraday's law. This emf was calibrated against a standard nickel sample. Measurements were taken in the plane of coating and perpendicular to the plane of coating by rotating the sample holder.

4.13 Resistivity measurement

The resistivity of the coating was measured by four point probe method. Coated glass strips were connected to Keithley multimeter and a DC current of 1 mA was supplied by a pair of electrodes. The voltage was measured by connecting separate probes distancing 4 cm. To maintain constant distance the glass was marked and it was ensured that the probes touch the marked area. Three readings were noted and the direction was reversed.

4.14 Microscopy

The microscopy images were obtained from a XL30 Environmental Scanning Electron Microscope (ESEM) Field Emission Gun (FEG) to determine the surface morphology and the thickness of the coating. Grain oriented electrical steel samples were polished to a mirror finish and kept in a chamber which was pumped to a pressure of 1.3×10^{-4} mbar. The detector used was a secondary electron and the beam intensity of 10KV was focused onto the surface of a sample. Due to the interaction between the sample and the beam, secondary electrons were emitted which were used to build the topological image of the sample surface. The magnification was varied from 5000-20000x depending upon the thickness and morphology of the coating. The elemental analysis was performed with an Oxford Instruments EDX analysis system. A high energy beam focused on the sample excites and ejected an electron from the inner shell of an atom. This space was filled by an electron from the outer shell having higher energy. During the transition from higher to lower energy, X-rays were emitted which were analysed in the Si-Li detector to understand the chemical nature of the sample.

4.15 Glow Discharge Optical Emission Spectroscopy (GDOES)

The chemical composition during the build-up was measured using GDOES JY 5000RF. In this process coating layers were removed using cathodic sputtering and the atoms removed migrated to plasma were excited by collisions with electrons. These excited atoms emit characteristic spectrum whose intensities were recorded and compared with pre calibrated results to obtain the quantitative analysis. The parameters used for measuring the coating composition were 30 W power and 3.0 mbar pressure, and the sample size was 3mm x 3mm x 0.3 mm strip.

4.16 X-ray Diffraction (XRD)

To study the structure, phases and stress in the coating, XRD was carried out on uncoated and Co-Ni-P coated samples with cobalt radiation at 30kV and 40mA. The scan was performed for 2Θ values between 30° to 90°. The obtained results were then analysed in X'Pert High Score software to identify the crystallographic phases in the coating.

4.17 Stress in coatings calculation

The development of stress in the coatings can be calculated from the XRD results as compressive or tensile stress shift the diffraction peaks as shown below.

The Bragg's equation is:

$$n\lambda = 2d\sin\theta \tag{4.14}$$

where

n is an integer,

λ is the wavelength of incident wave,

d is the spacing between the planes in the atomic lattice,

θ is the angle between the incident ray and the scattering planes

Considering nλ to be constant, increasing the atomic lattice space d would reduce the value of θ. The development of compressive stress in the coating due to an increase in the inter planer distance d would shift the peak towards a lower angle and vice versa.

4.18 Surface profilometer

The surface roughness of the uncoated and coated surfaces was measured by a Talysurf surface profilometer with a resolution of less than 1 nm. The measurements were made in the transverse and rolling direction but only the rolling direction measurements are reported as the length in the transverse direction was small which gave more inaccuracy in results. The measurements were made for a distance of 40 mm for all the samples. The speed of probe was fixed at 0.5 mm/s. The value of roughness reported throughout the thesis is the average roughness (Ra).

4.19 Atomic Force Microscopy (AFM)

AFM was used to observe the surface conditions of the uncoated and coated samples. As prepared Co-Ni-P coated samples (3mm x 3mm x 0.3 mm) were used in the contact mode. The probe connected to the cantilever beam was dragged on the surface of the sample which bends due to variation in the surface conditions. The deflection in the cantilever was detected on the position sensitive photo diode by focusing a laser beam on the cantilever, whose position changed with the deflection in cantilever and generated the topography of the surface. All the scans were performed for a length of 30 µm at a scan rate of 0.1-0.15 Hz generating 128 data points.

4.20 Raman Spectroscopy

To determine the presence of MWCNT's in the coating, samples were analysed using a Renishaw inVia Raman microscope. As prepared Co-P-CNT coated samples (3mm x 3mm x 0.3mm) were excited with a 514 nm argon laser. The power was maintained at 12.5 mW and the spot size was 5 µm. The Raman spectra spanning between 800 and 2100 cm^{-1} was obtained at five different spots.

4.21 High Temperature Annealing Furnace (HTAF)

GOES samples were stress relief annealed in the HTAF. The samples were loaded in the furnace and 10-20 Epstein strips were kept on top of the GOES samples to ensure flatness. The furnace was pumped to a vacuum of 10^{-7} Torr and the samples were heated to 800 °C for 1 hour. The temperature inside the furnace was measured by three thermocouples placed along the furnace tube to ensure uniform temperature distribution.

4.22 References

[1] A. A. Aal, A. Shaaban, and Z. A. Hamid, "Nanocrystalline soft ferromagnetic Ni–Co–P thin film on Al alloy by low temperature electroless deposition," *Applied Surface Science*, vol. 254, pp. 1966–1971, 2008.

[2] A. K. Sharma, M. R. Suresh, H. Bhojraj, H. Narayanamurthy, and R. P. Sahu, "Electroless Nickel Plating on Magnesium Alloy," *Metal Finishing*, vol. 96, pp. 10, 12, 14, 16, 1998.

[3] Z. Li, B. Shen, Y. Deng, L. Liu, and W. Hu, "Preparation and microwave absorption properties of electroless Co–P-coated nickel hollow spheres," *Applied Surface Science*, vol. 255, pp. 4542-4546, 2009.

[4] T. S. N. S. Narayanan, A. Stephan, and S. Guruskanthan, "Electroless Ni–Co–B ternary alloy deposits: preparation and characteristics," *Surface and Coatings Technology*, vol. 179, pp. 56-62, 2004.

[5] P. Anderson, "Measurement techniques for the assessment of materials under complex magnetising conditions," *Electrical review*, vol. 87, pp. 61-64, 2011.

[6] P. I. Anderson, A. J. Moses, and H. J. Stanbury, "Assessment of the Stress Sensitivity of Magnetostriction in Grain-Oriented Silicon Steel " *IEEE Transactions on Magnetics*, vol. 43, pp. 3467-3476, 2007.

[7] U. M3003, "The expression of uncertainity and confidence in measurement," *2nd edition* 2007.

[8] R. J. Taylor and J. A. Watt, "Magnetic pattern viewer," *US Patent*, vol. 5034754 A, 1991.

5 Application of Co-Ni-P/B coating on grain-oriented electrical steel

5.1 Introduction

This chapter provides detailed analysis of electroless plating of Co-Ni-P/B on grain-oriented electrical steel. The aim of the chapter is to discuss the development of new coatings for GOES and two different coatings were attempted namely Co-Ni-P and Co-Ni-B. These coatings produced variable stress and surface roughness which was characterised using Atomic Force Microscopy (AFM). The samples were tested using single strip tester and magnetostriction measurement system to measure the power loss and magnetostriction. The coating was characterised using a number of techniques including Environmental Scanning Electron Microscope (ESEM), Vibrating Sample Magnetometer (VSM), X-ray Diffraction (XRD), magnetic pattern viewer, and profilometer.

5.2 Co-Ni-P coating

Table 5.1 highlights the sample id's along with the time and pH values.

Sample ID	Time for electroless plating (min)	pH of the solution
Ni1	20	9.0
Ni2	35	9.0
Ni3	50	9.0
Ni4/NipH4	90	9.0
NipH1	90	7.8
NipH2	90	8.2
NipH3	90	8.6
NipH5	90	9.4

5.2.1 Influence of deposition time on coating weight

Table 5.1 shows the sample identities with the sample condition. The weight of the coating deposited was proportional to the time for which the samples were kept in the plating solution as shown in Figure 5.1. For the sample Ni1 the deposition weight was 50 ± 2 mg and it increased to 310 ± 6 mg for sample Ni4. The average deposition rate was 3.3 mg/min.

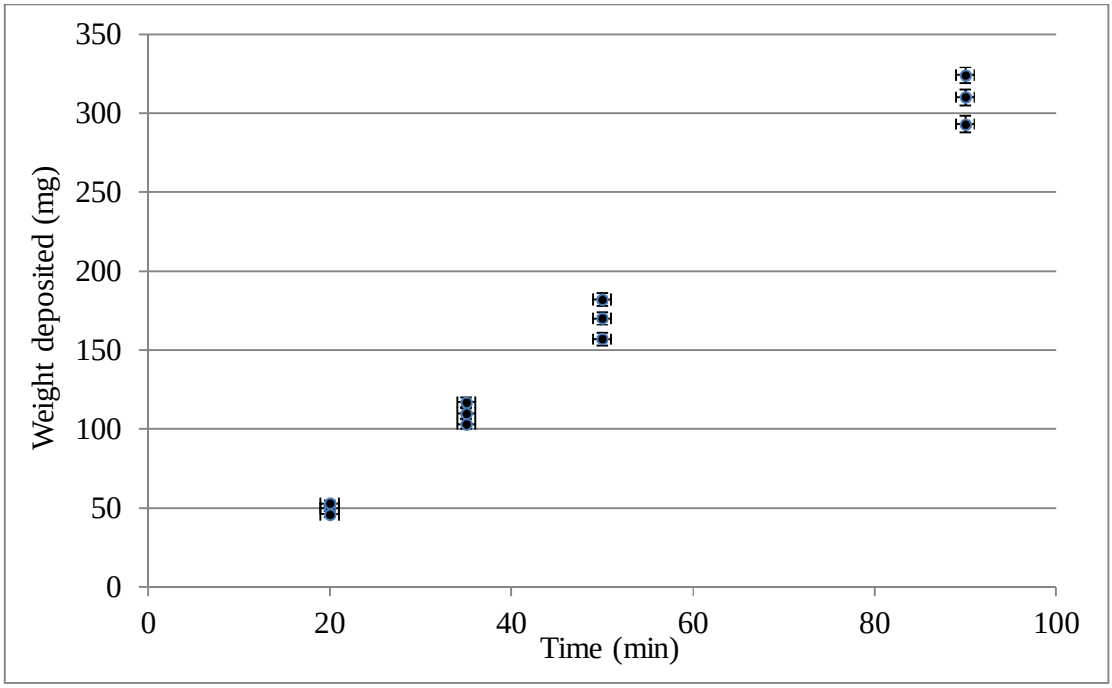

Figure 5.1 Co-Ni-P coating weight deposited compared to different time periods.

5.2.2 Scanning Electron Microscopy

Figure 5.2 shows the SEM image of NipH4. The grey area shows the substrate while the lighter area shows the coating. The coating was uniformly distributed across the sample. No gaps or cracks were found. The thickness of the coating was averaged to be around 2.15±0.15 µm.

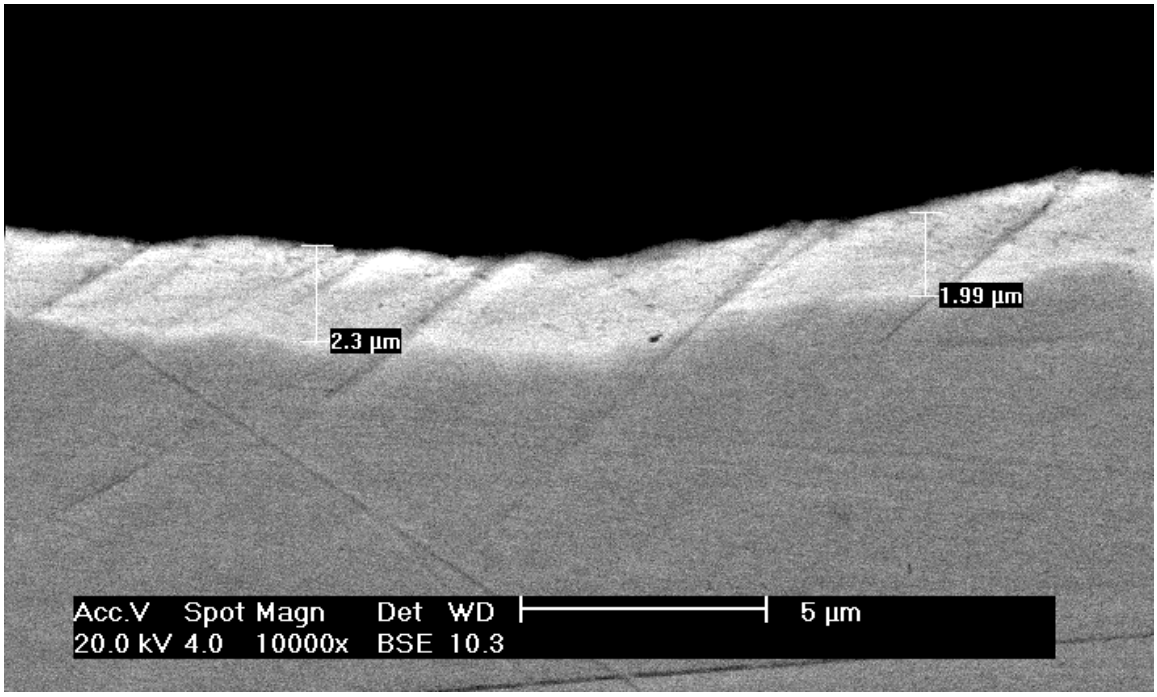

Figure 5.2 Cross section image of the substrate and the coating for sample NipH4.

Figure 5.3 shows five SEM images of the samples NipH1-NipH5 coated with different pH values 7.8, 8.2, 8.6, 9.0 and 9.4.The pH plays a major role in determining the type of coating (hard or soft magnetic) and controls the coating mechanism[1]. At pH value of 1.5 the coating was found to have a coercivity of 11937 A/m and at 3.5 pH value the coating had a coercivity of 47747 A/m [2, 3]. As can be seen from the images at a pH of 7.8 (NipH1) the Co-Ni-P coating coagulates in some areas rather than forming a uniform coating. The nucleation of Ni and Co on the surface of grain-oriented electrical steel was not distributed throughout the sample; instead the metal particles nucleate at a few sites. The coating grows at those sites only. The surface tension binds the particle together and reduces the interatomic spacing. The decrease in interatomic spacing introduces tensile stress in the coating [4] which adversely affected the magnetic properties. As the pH of the

solution was increased there was a reduction in size of the particles and a more uniform coating was formed. At a pH of 9 (NipH4), nucleation occurs throughout the sample and a uniform coating was observed on the substrate and a minimal amount of coagulation was found in the coating. The stress applied by the coating on the substrate was uniform. The pH was increased further and the coating was again found to be coagulated at various places.

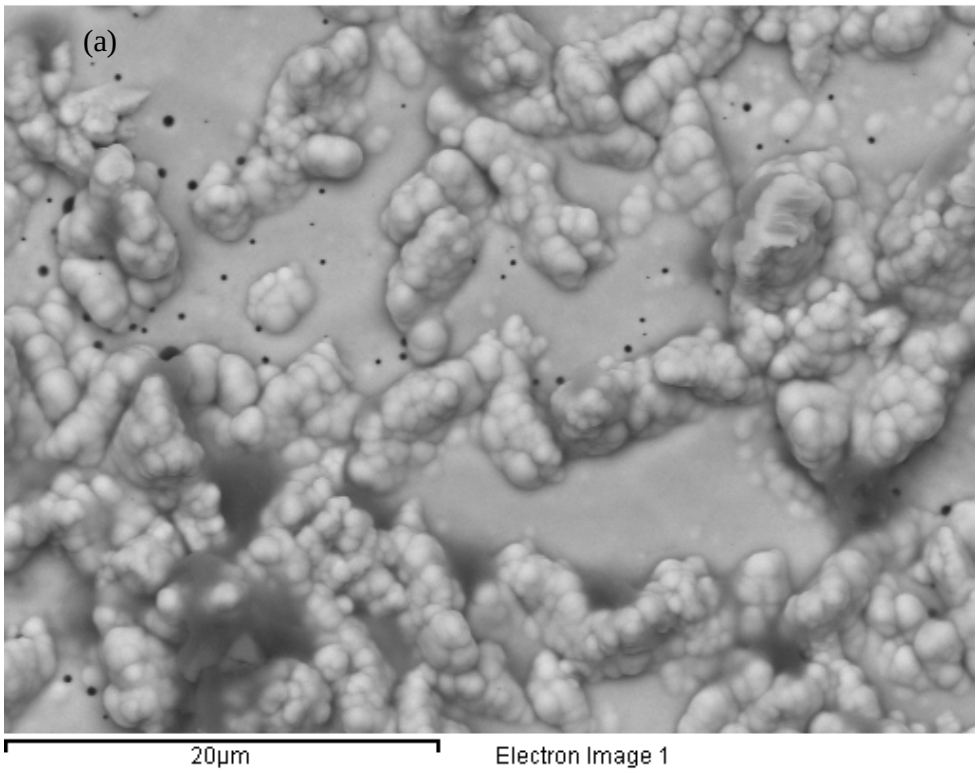

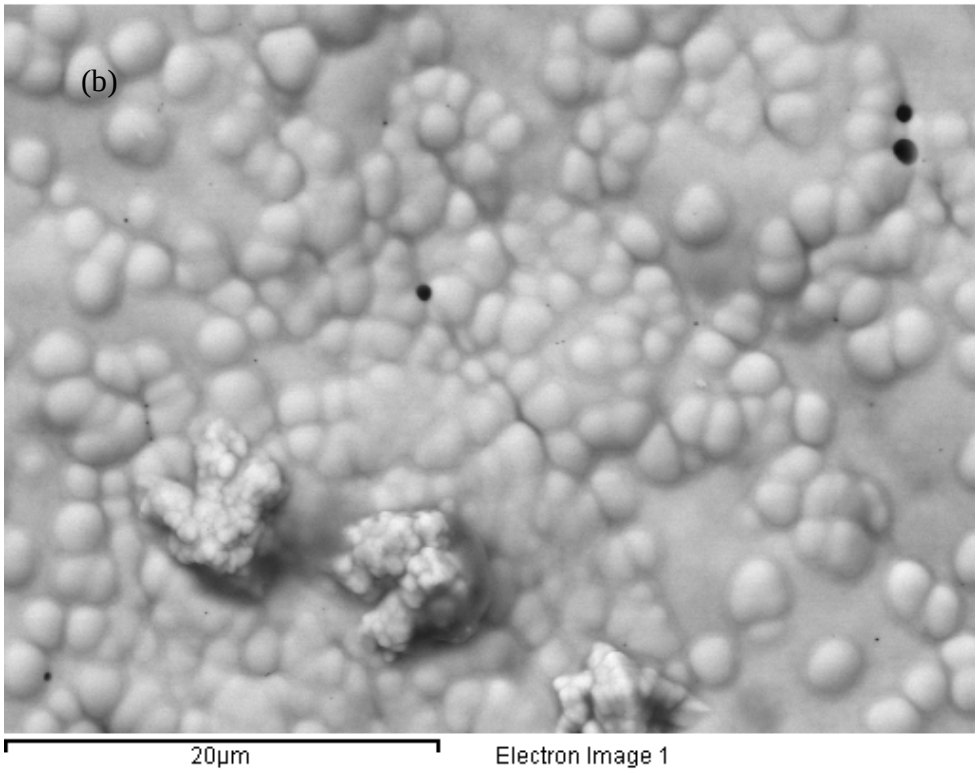
(b)
20µm
Electron Image 1

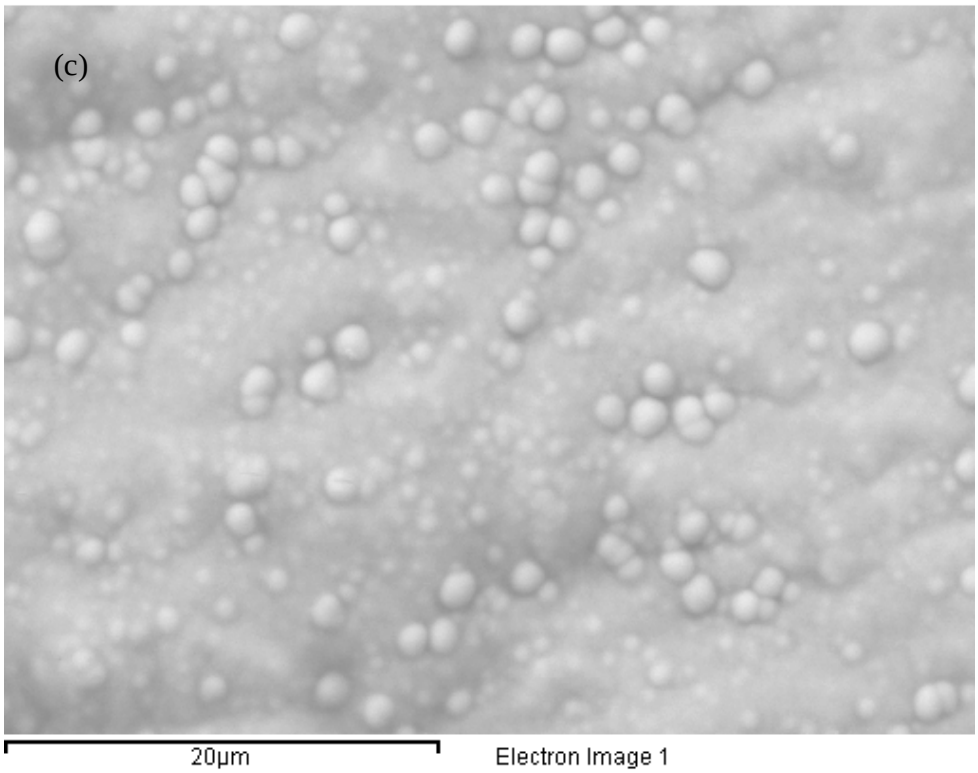
(c)
20µm
Electron Image 1

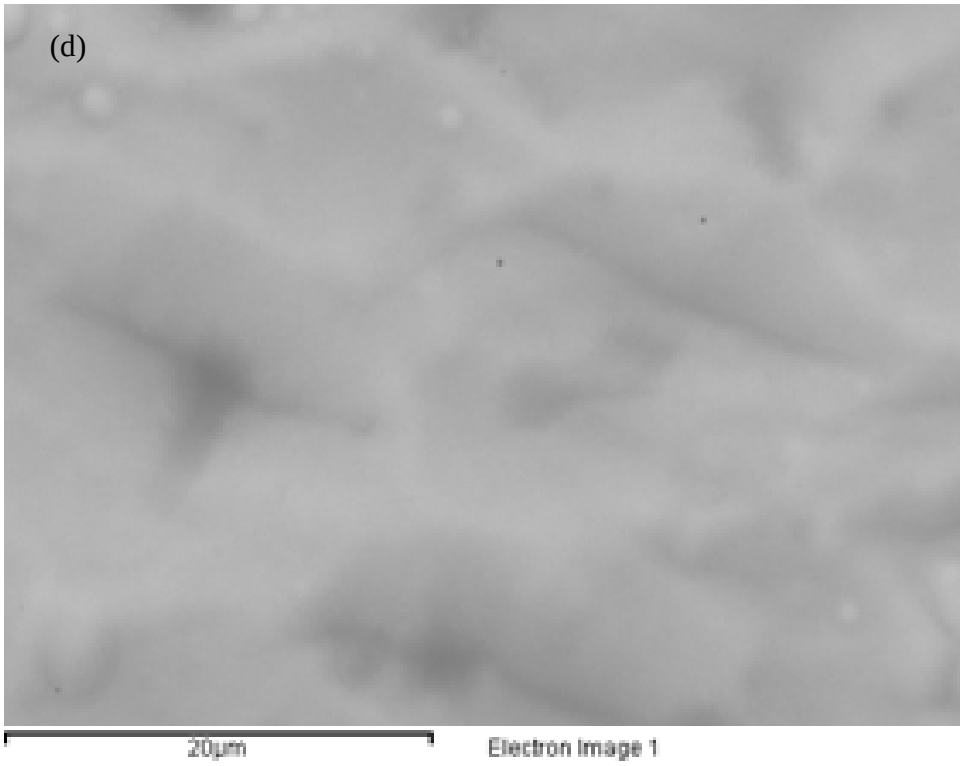

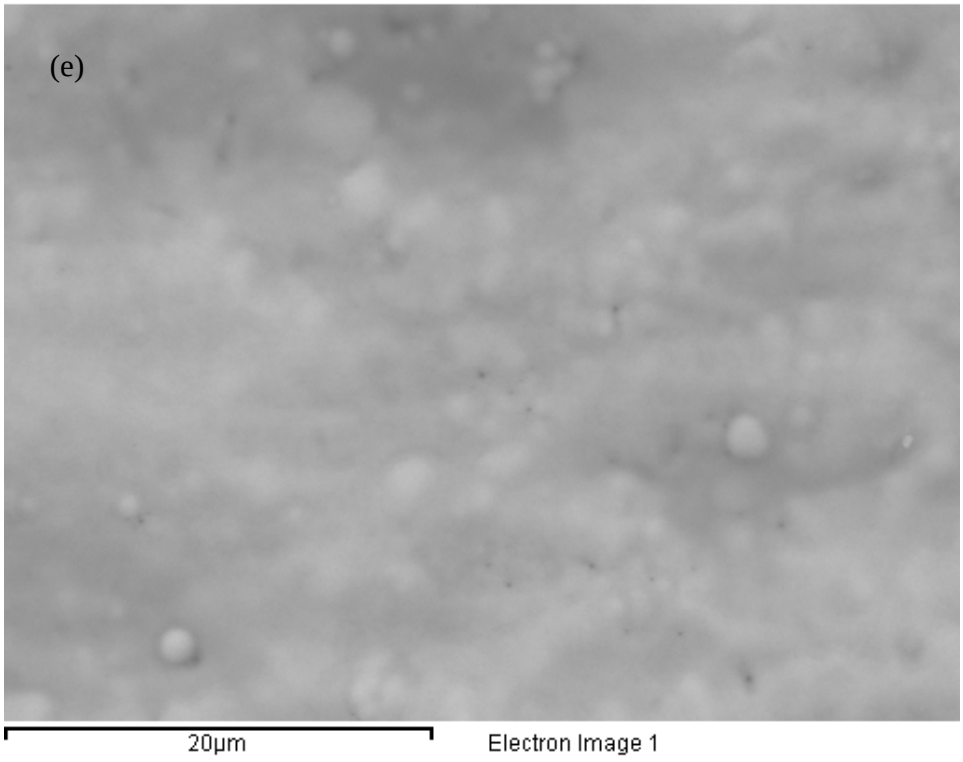

Figure 5.3 SEM images for the samples coated with different pH (a) NipH1 (b) NipH2 (c) NipH3 (d) NipH4 (e) NipH5.

5.2.3 Surface profiling

The surface roughness values in Figure 5.4 support the SEM results. The value of roughness was largely dependent on the pH of the coating solution. The surface of the sample coated with a pH value of 7.8 was found to be rougher than the uncoated sample. The lowest value of roughness was measured at a pH of 9.0.

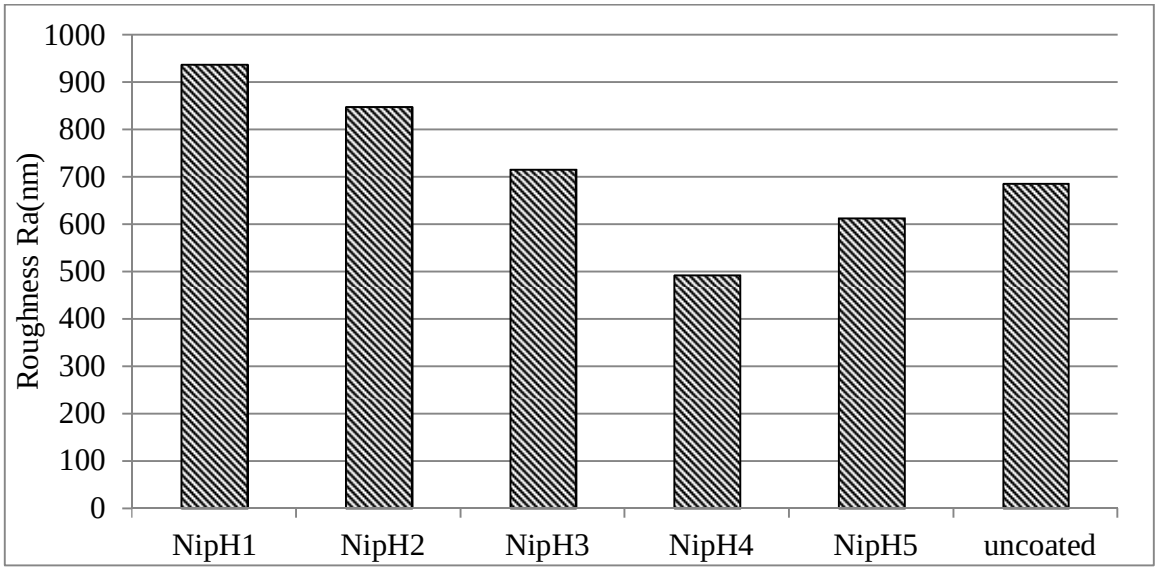

Figure 5.4 Talysurf surface roughness values Co-Ni-P coating at different pH values.

5.2.4 Atomic Force Microscopy (AFM)

AFM was used to study the surface conditions of the uncoated and coated samples. The initial surface roughness affects the final deposited surface finish. Figure 5.5(a-c) shows the uncoated surface (a), NipH1 (b) and NipH4 (c). The uncoated surface shows a wavy pattern with regions of depression and elevation. In sample NipH1 the coating was deposited only at 2-3 spots on the surface as can be seen in Figure 5.5(b). This makes the surface more rough than the uncoated sample. For sample NipH4 the coating was deposited uniformly throughout the surface as shown in Figure 5.5(c) and hence the surface roughness decreases.

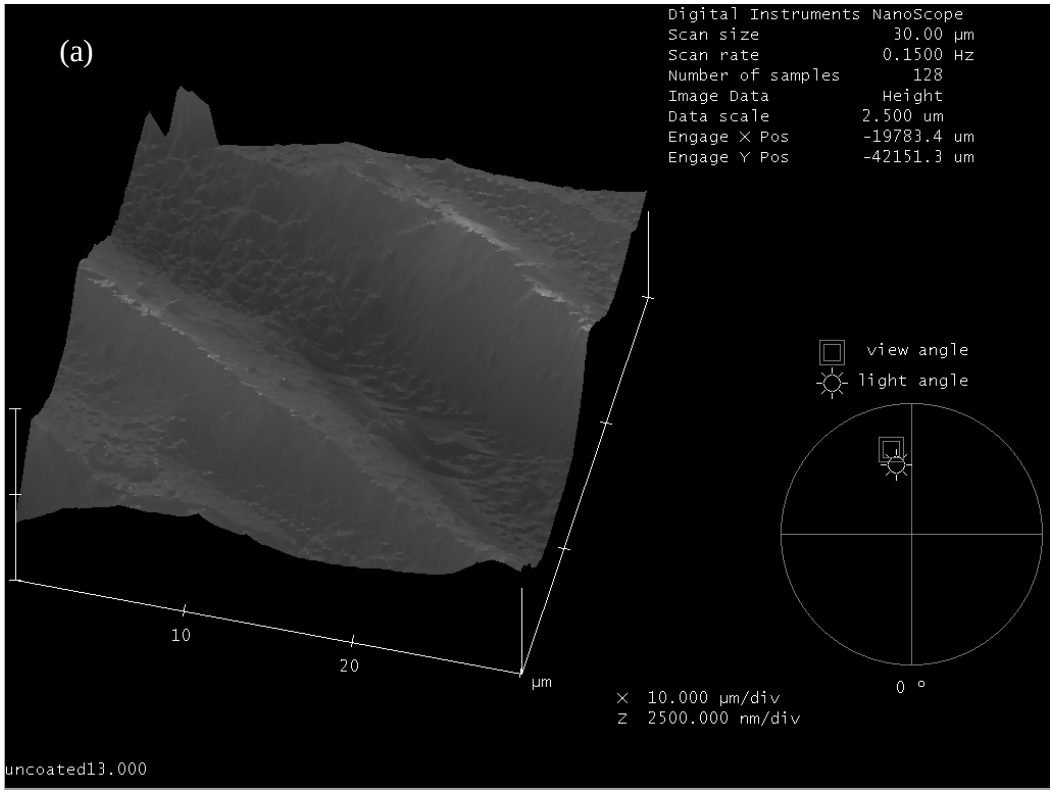
(a)
Digital Instruments NanoScope
Scan size 30.00 µm
Scan rate 0.1500 Hz
Number of samples 128
Image Data Height
Data scale 2.500 um
Engage X Pos -19783.4 um
Engage Y Pos -42151.3 um
view angle
light angle
10
20
µm
0 °
X 10.000 µm/div
Z 2500.000 nm/div
uncoated13.000

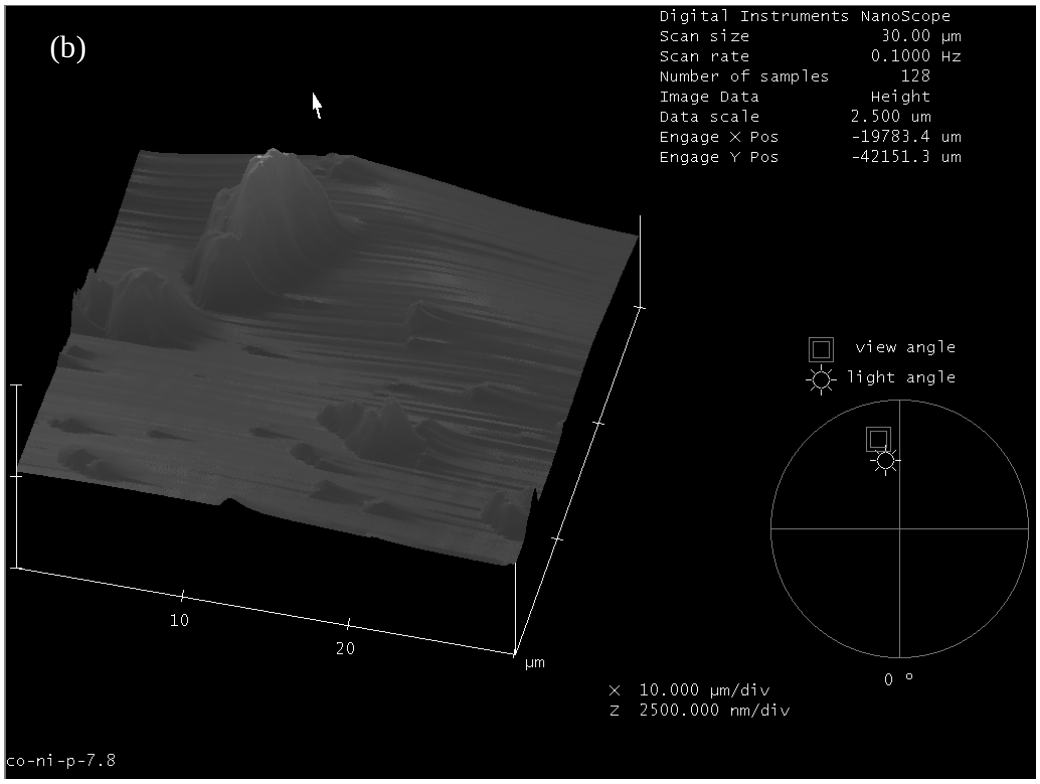
(b)
Digital Instruments NanoScope
Scan size 30.00 µm
Scan rate 0.1000 Hz
Number of samples 128
Image Data Height
Data scale 2.500 um
Engage X Pos -19783.4 um
Engage Y Pos -42151.3 um
view angle
light angle
10
20
µm
0 °
X 10.000 µm/div
Z 2500.000 nm/div
co-ni-p-7.8

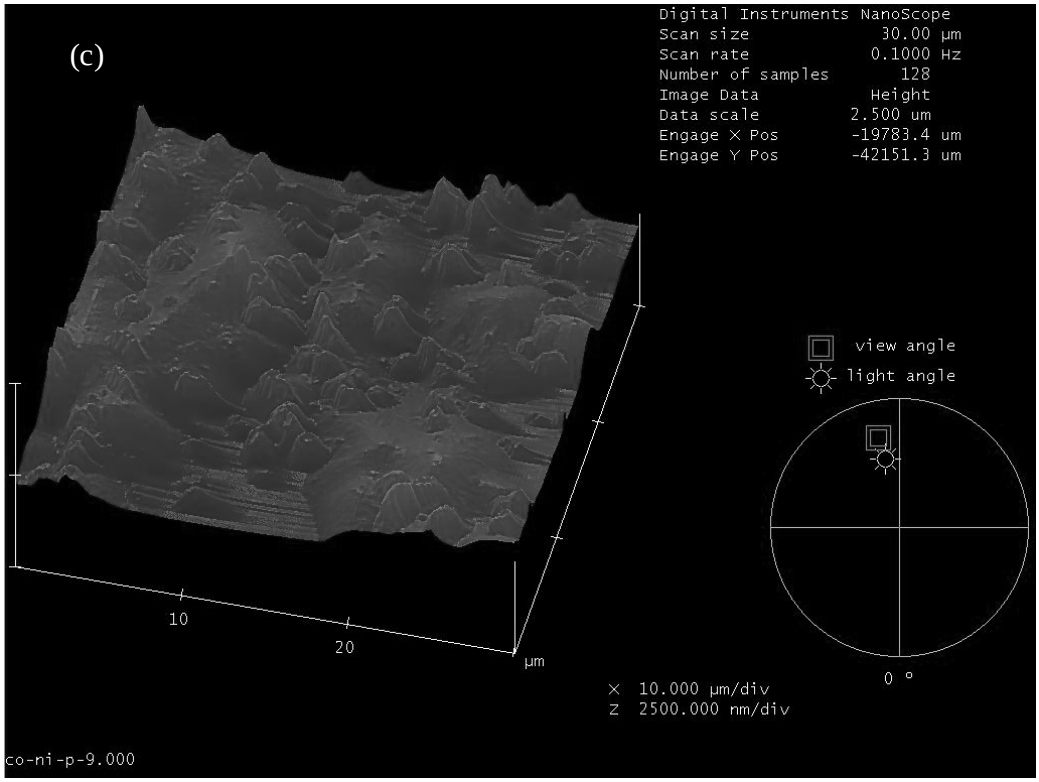

Figure 5.5 AFM images of the (a) uncoated, (b) NipH1 and (c) NipH4 samples.

Table 5.2 Elemental composition (weight %) of the coating for different sample Id's by EDX.

Sample Id	Nickel%	Cobalt%	Phosphorus%	Sodium%
NipH1	41-43	48-50	9-10	0
NipH2	33-35	54-56	9-10	0
NipH3	32-34	55-57	9-10	0
NipH4	29-31	60--62	9-10	0
NipH5	28-30	58-60	7-8	4-5

5.2.5 Effect of pH on coating composition

Table 5.2 highlights the elements present in the coating at different pH values. The cobalt content in the coating increases as the pH was increased and reaches a maximum of 60-62% by weight for NipH4. On the other hand, nickel content decreases. Lew et. al. [2] showed similar results for the relation between pH and chemical composition. The saturation magnetization of cobalt (2 T) is much higher than that of nickel (0.6 T) so, increasing cobalt content can result in better soft magnetic properties. The amount of phosphorus remains relatively unchanged except for NipH5 where sodium was introduced in the coating and influences the stress in the coating.

5.2.6 Magnetic Properties

Figure 5.6(a-b) shows a classical hysteresis loop for Co-Ni-P coating on glass sheet at a pH of 7.8 and 9.0. The B-H loop measured in the VSM shows the coating to be magnetic in nature. The coercivity was calculated to be 2500 A/m and 796 A/m and the saturation magnetization were calculated to be 0.782 T and 0.096 T for the sample NipH1 and NipH4 respectively.

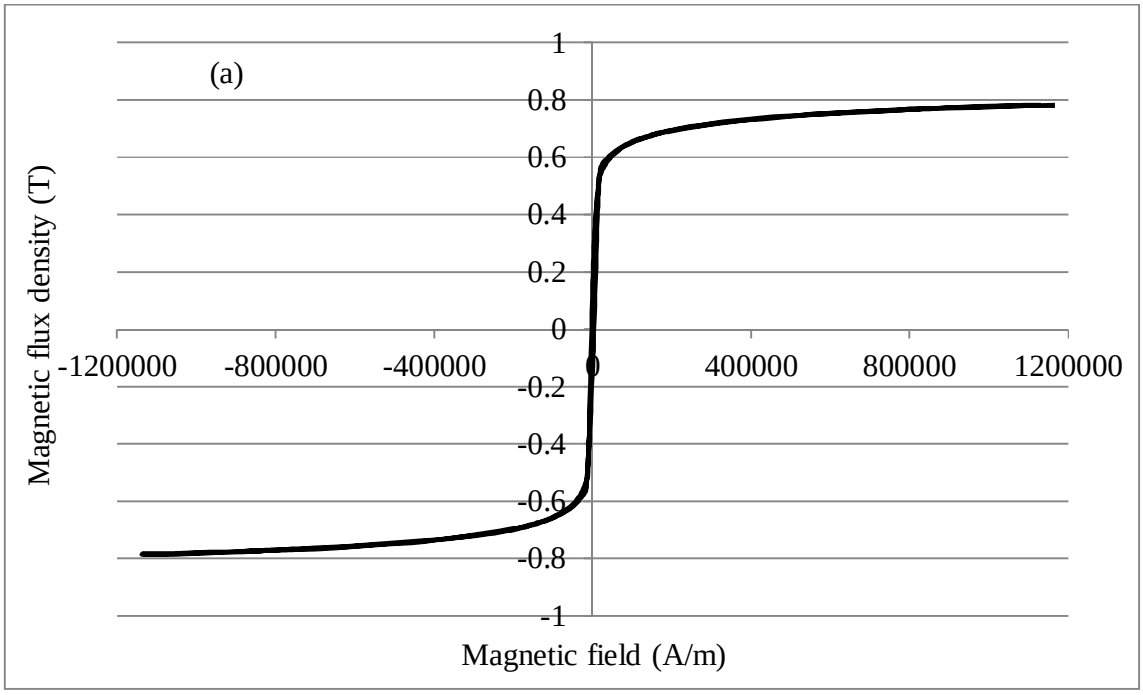

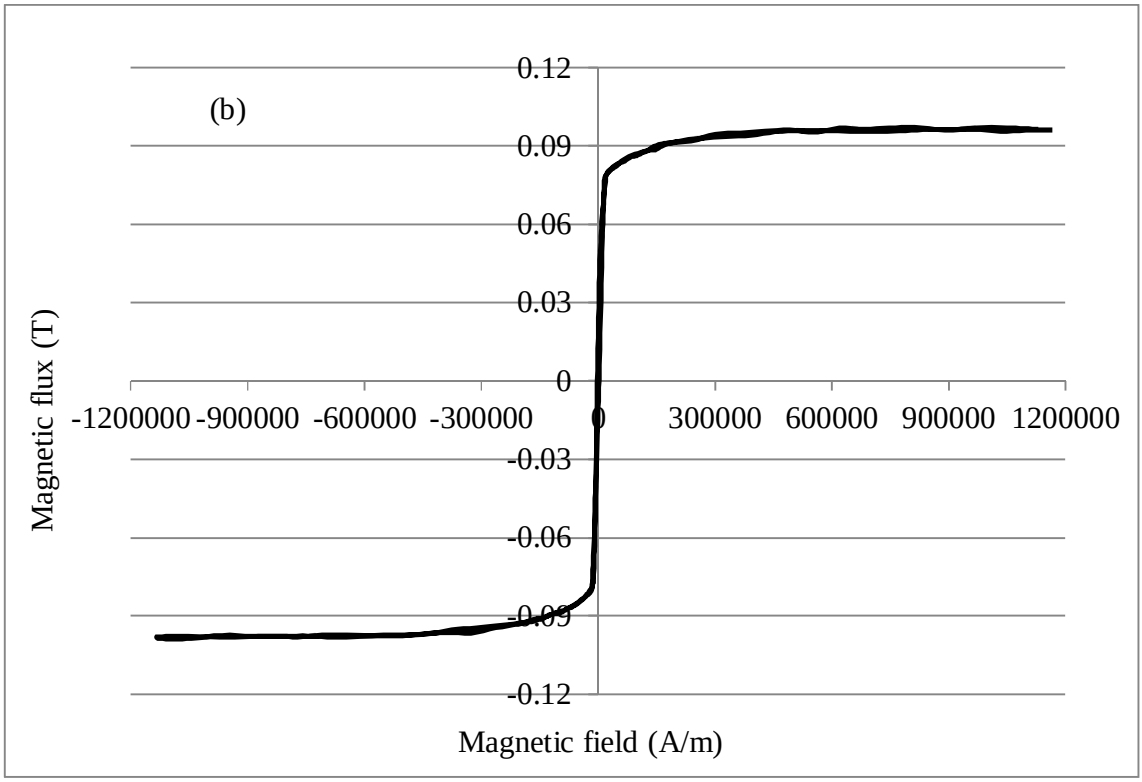

Figure 5.6 Magnetic flux density measured for Co-Ni-P coating (a) NipH1 and (b) NipH4.

The saturation magnetization was measured for all samples (NipH1-NIpH5) in the plane of the coating to understand the nature of the coating as shown in Figure 5.7. From the figure it can be seen that the sample NipH1 shows the highest saturation magnetization and it decreases to a minimum value at pH of 9.4. The high value of saturation magnetization at pH 7.8 proves that, cobalt and nickel did not react with phosphorus and no stress was generated. As the pH value was increased, phosphorus interacted with cobalt and nickel to form either Co-P or Ni-P and stress was developed. The formation of Co-Ni-P compound reduced the saturation magnetization of the coating. At a pH value of 9.4 though we have the minimum saturation which states maximum interaction between the metal atoms and phosphorus but the percentage of phosphorus was decreased which reduces the value of generated stress. The saturation magnetization was also measured perpendicular to the plane of coating and it was 6-10% less as compared to in plane. This was because the domains were aligned along the plane of coating, and large field value was required to rotate them.

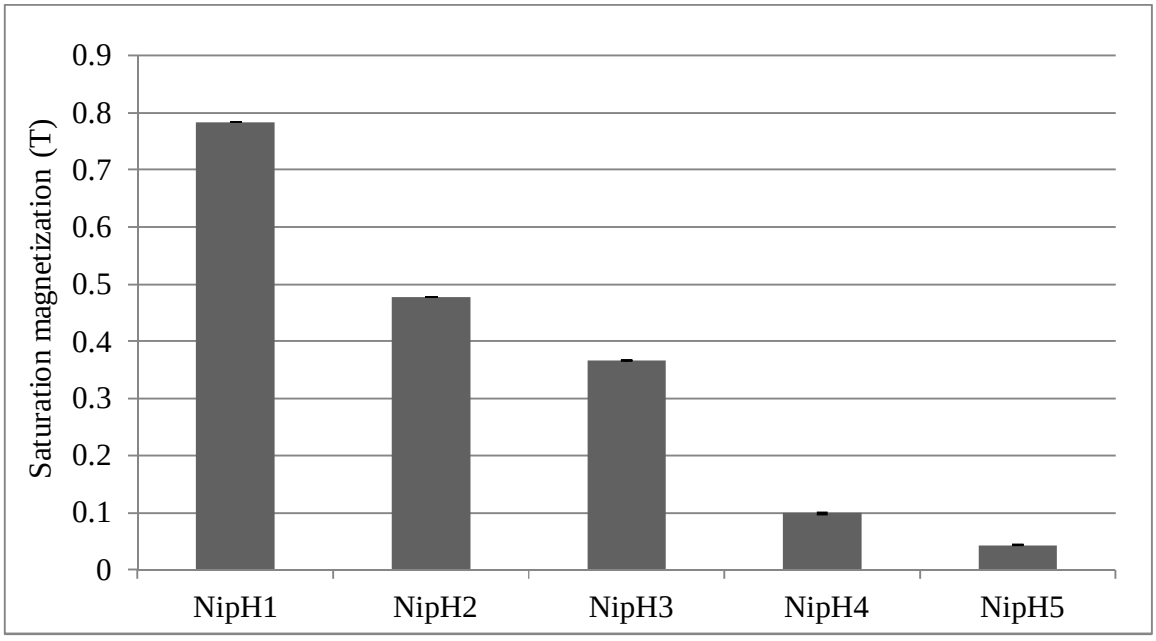

Figure 5.7 Saturation Magnetization measured in VSM at various pH values.

5.2.7 Magnetic Domain Imaging

To study the effect of coating on domain behaviour, the domain images were recorded before and after coating the sample. The magnetic domain imaging clearly shows the narrowing of domains after coating with Co-Ni-P. The average domain width in the blue and yellow rectangular box in Figure 5.8 for the uncoated sample was 0.73 and 0.66 mm as compared to 0.48 and 0.53 mm for the Co-Ni-P coated sample.

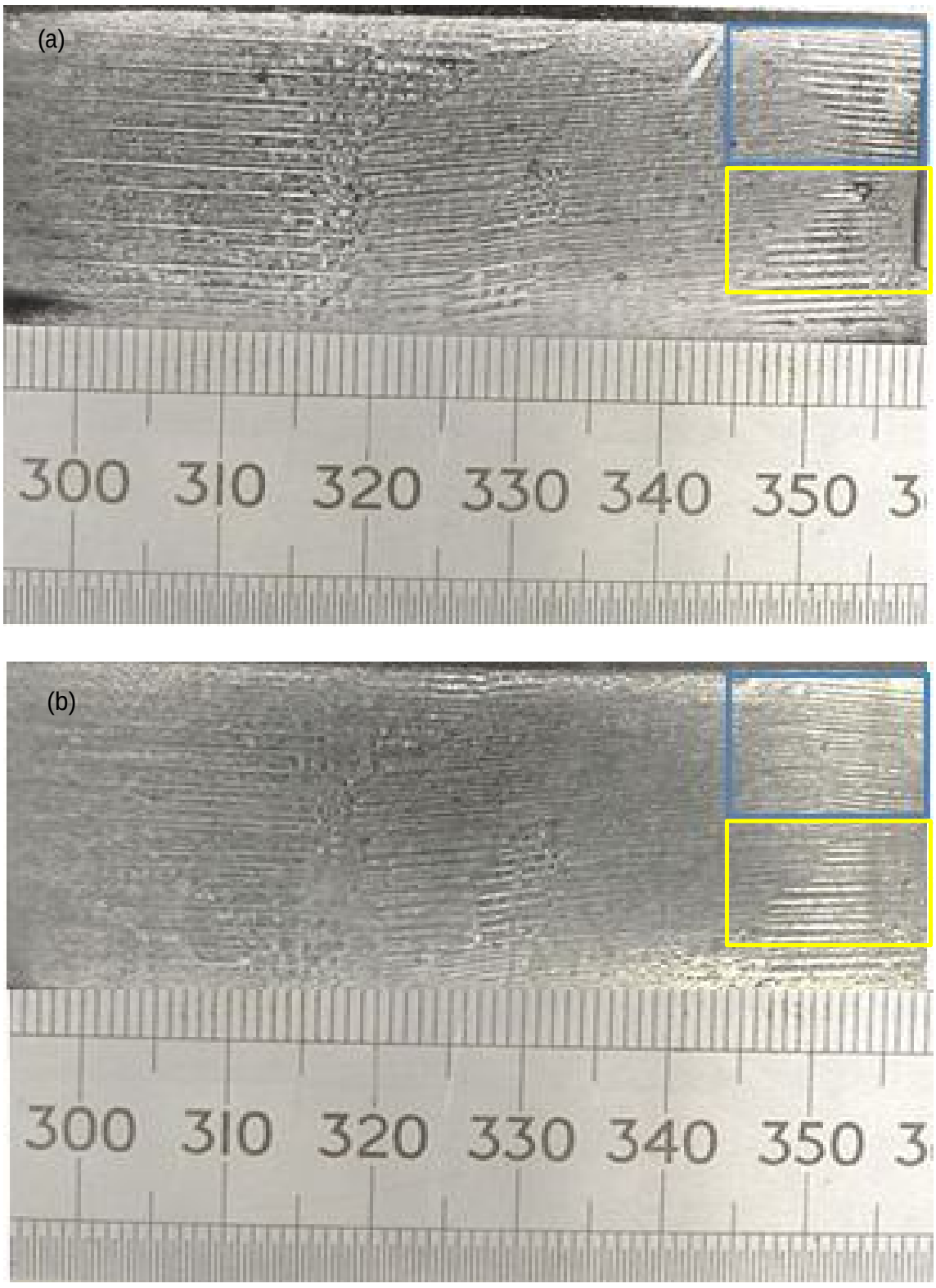

Figure 5.8 Magnetic domain imaging for the (a) uncoated and (b) Co-Ni-P at pH 9 coated sample.

5.2.8 Power loss

Figure 5.9 (a-d) presents the difference in power loss of the coated and uncoated samples for different time duration from 20 to 90 min (Ni1-Ni4). Figure 5.9(a-d) shows that the coating thickness plays a major role in determining the power loss with a thicker coating showing large reduction in power loss compared to a thin coating. For the sample Ni1 the reduction in power loss was around 4-5 %. Sample Ni4 showed a reduction in loss of approximately 9-11 % at 1.5 T as compared to the uncoated sample.

To minimize losses, coating thickness could be increased but the stress decreases as the thickness increases [5] also it leads to unacceptable degradation of permeability shown in Figure 5.10 and stacking factor discussed in section 5.2.10.

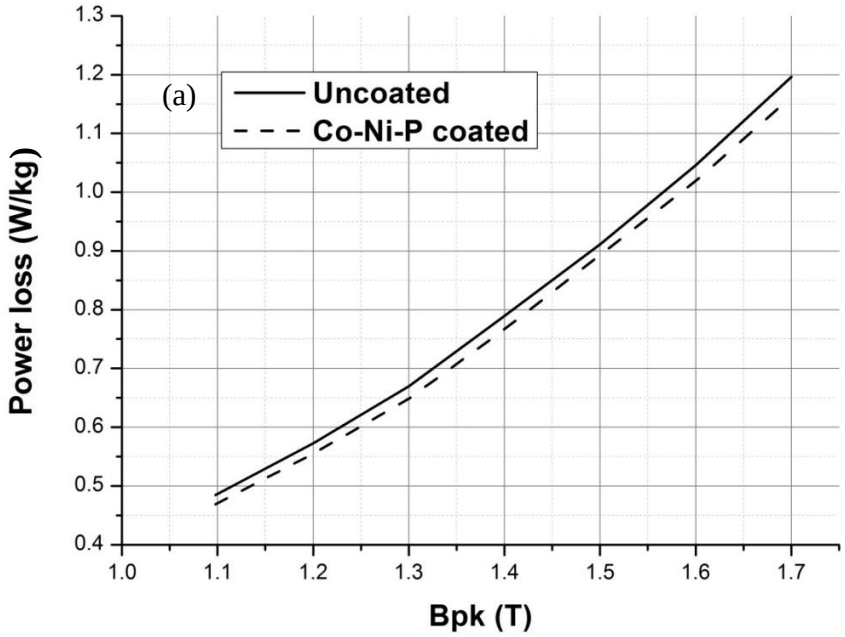

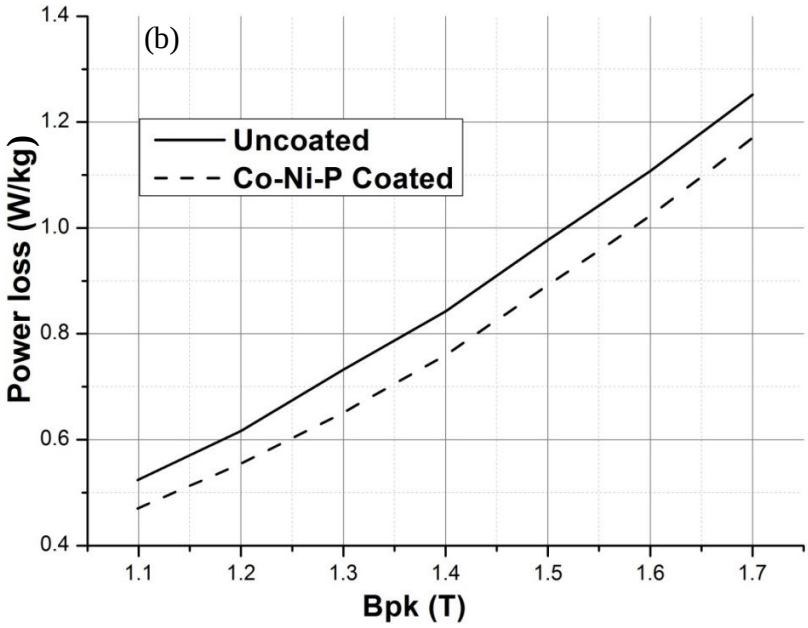
(b)
Uncoated
Co-Ni-P Coated
Power loss (W/kg)
Bpk (T)
1.4
1.2
1.0
0.8
0.6
0.4
1.1
1.2
1.3
1.4
1.5
1.6
1.7

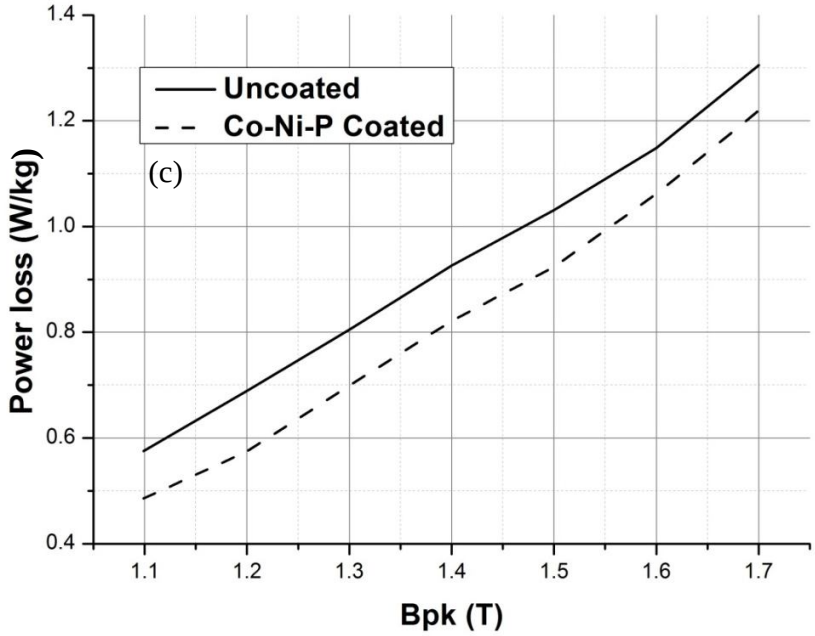
Uncoated
Co-Ni-P Coated
(c)
Power loss (W/kg)
Bpk (T)
1.4
1.2
1.0
0.8
0.6
0.4
1.1
1.2
1.3
1.4
1.5
1.6
1.7

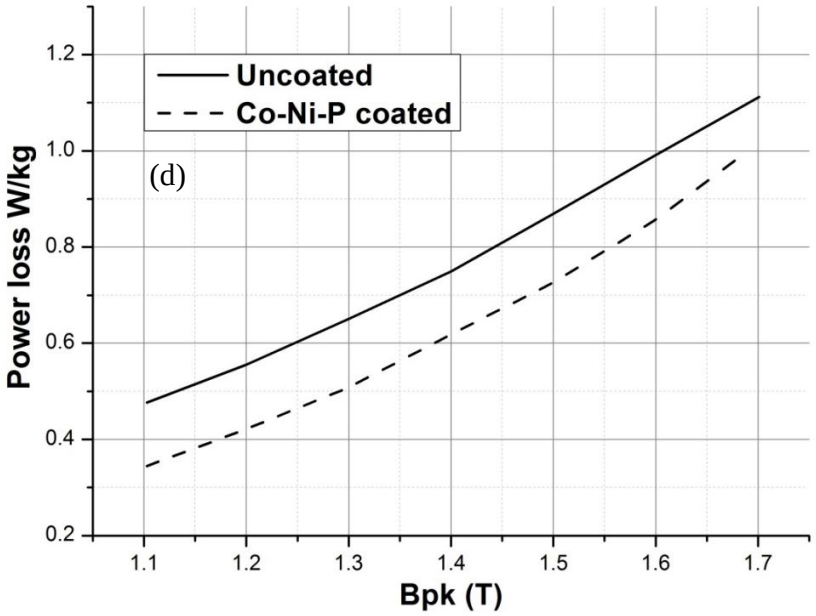

Figure 5.9 Power loss testing for the uncoated and Co-Ni-P coated for different times (a) Ni1 (b) Ni2 (c) Ni3 (d) Ni4.

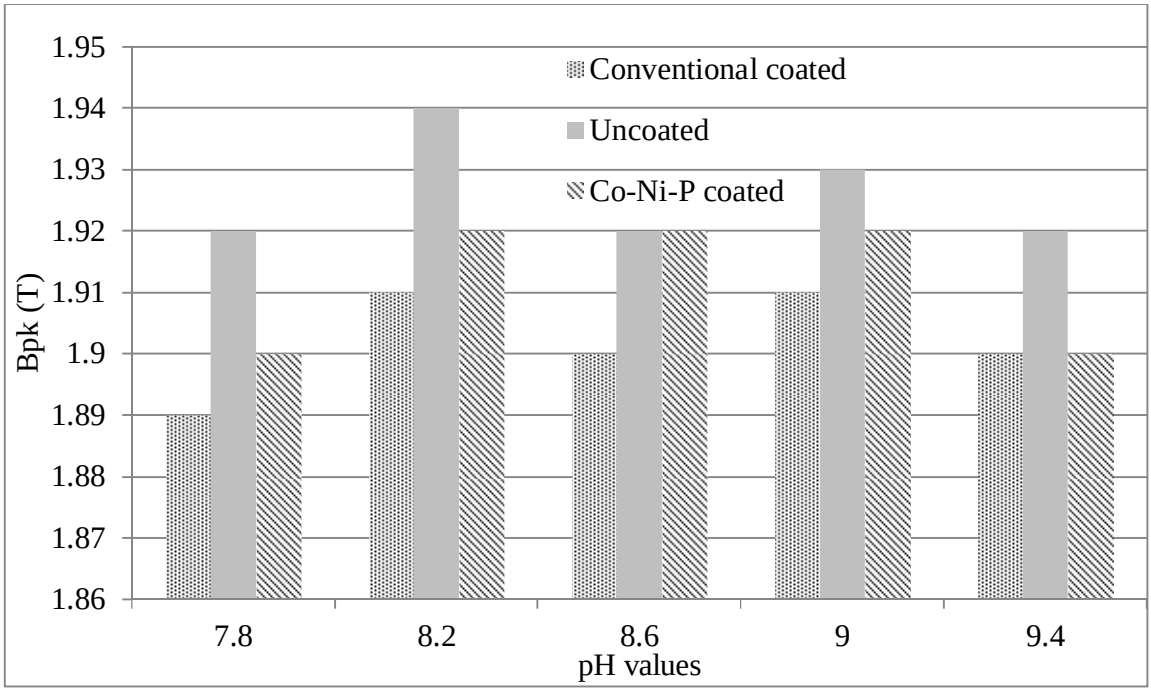

Figure 5.10 Bpk measured at magnetic field strength of 800A/m for different values of pH.

Figure 5.11 shows the power loss results of the conventional, uncoated and Co-Ni-P coated at different pH values. The sample NipH4 shows the highest reduction in power loss because a uniform coating could only be achieved at this value. Changing the pH value either way affects the coating formation which generates compressive stress in the substrate and less improvement in power loss reduction. The surface was also not uniform for other samples and hence it would have more pinning sites to hinder the movement of domain walls in motion which leads to increase in power loss.

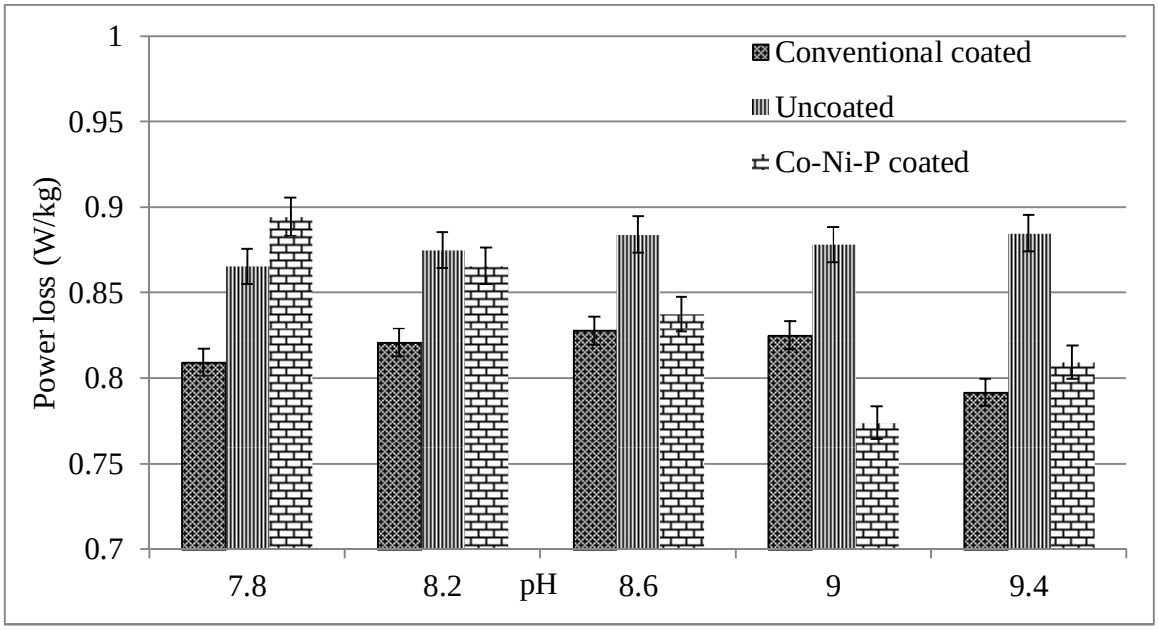

Figure 5.11 The effect of pH on power loss measured at 1.5T and 50Hz frequency.

5.2.9 Stress calculation based on single side coated steel

Song et al. [6] have shown that stress is introduced in the substrate by the Ni-P coating, The stress can be tensile or compressive depending upon the amount of phosphorus in the coating. 8.5 % phosphorus induces compressive stress in the coating [5]. In this case the stress in the coating was compressive as the amount of phosphorus was confirmed to be between 9-10% and hence tensile stress acted on the substrate which was beneficial in terms of power loss reduction and magnetostriction. The reason behind the generation of compressive stress in the coating was explained in section 3.1.2.1.

Samples were also coated on one side to justify the proposed theory of stress development after coating the sample with Co-Ni-P at pH 9.0. Figure 5.12 shows single side coated sample. The sample was coated on the convex side. The results were in agreement with [7] where compressive stress was developed by applying TiN coating. The compressive stress in the coating contracts the sample and sets up tensile stress on the coated surface of the substrate. To balance the stress in the sample it bends. It is important to note that the sample is coated flat and applying a force to the convex (coated) surface sufficient to return it to a perfectly flat state would see the coating return to the compressive stress state.

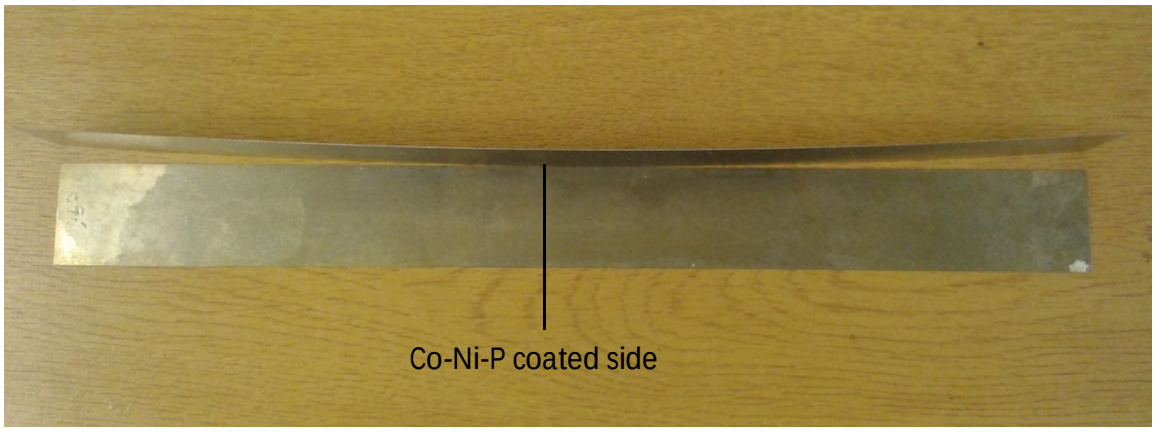

Figure 5.12 Grain oriented electrical coated on one side only.

To measure the stress generated by the coating on GOES, radius of curvature (R) was calculated for the samples coated on single side using the given below equation 5.1 [8].

$$R = \frac{a^2}{2x}, if\ x < a \tag{5.1}$$

Where a, x are defined in Figure 5.13

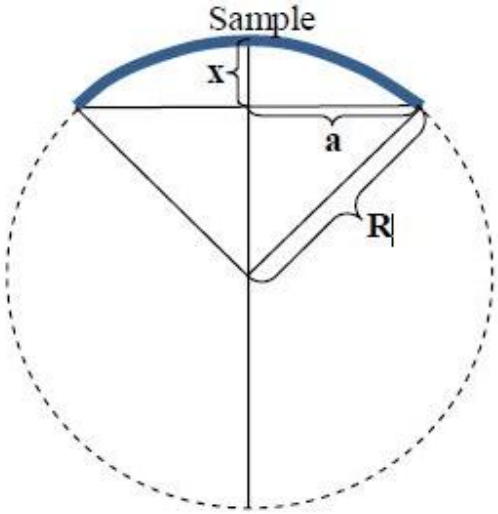

Figure 5.13 Method to calculate the radius of curvature of a strip.

The maximum stress (σ_{max}) was then calculated using equation 5.2

$$\sigma_{max} = \frac{E\,(\frac{t}{2})}{R + \frac{t}{2}} \tag{5.2}$$

The Young's modulus (E) of GOES in rolling direction was 113 GPa,

Thickness of the strip (t) was 0.27 mm,

$$\sigma_{max(Co\text{-}Ni\text{-}P)} = 3.9 \text{ MPa}$$

5.2.10 Loss separation

To understand the mechanism of loss reduction the power loss was separated by the procedure described in section 2.4.4. The value of the correlation coefficient [9] r^2 was 0.9997 and 0.99996 for the uncoated and Co-Ni-P coated samples respectively. Figure 5.14 shows the loss separation data for the uncoated and coated sample. It can be clearly seen from the graph that the coated sample shows a large reduction in anomalous and hysteresis loss.

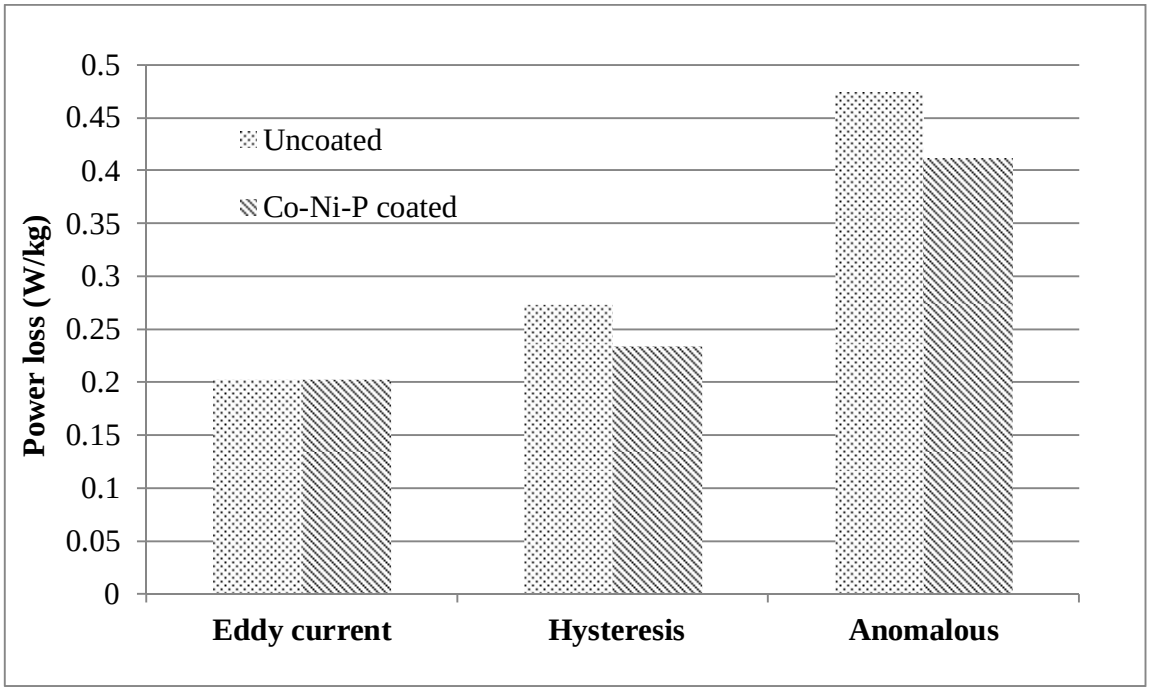

Figure 5.14 Loss separation at a magnetic flux density of 1.5T and 50Hz frequency for Co-Ni-P coated at pH 9.

The decrease in hysteresis loss was due to the improvement in surface roughness [10]. The increase in surface roughness increases the number of free poles on the surface and these free poles pin the domain walls. It leads to a reduction of mobile domains and the motion of domain wall was inhomogeneous [11]. Energy was dissipated in freeing these domain walls and this energy contributes to specific total loss. It was assumed that the enhancement of magnetic properties at pH of 9.0 was due to the improvement in surface roughness by magnetically active coating.

The narrowing of domain width decreases the anomalous loss. The anomalous loss was directly proportional to velocity of the domain wall. As the domain width decreases the walls have to travel a shorter distance within the same time so the velocity of the wall decreases [12].

5.2.11 Stacking factor

The stacking factor calculated for 2 µm thick coating was 98.68 % as compared to 97.36 % for 4 µm thick conventional coating as shown below.

$$stacking\ factor(\%) = (1 - \frac{Non - magnetic\ material\ in\ the\ core}{Total\ material\ in\ the\ transformer}) * 100$$

If the coating was non-magnetic, the thickness of coating on both sides = 4 micron

The thickness of Epstein strip without coating = 300 micron

Total thickness of Epstein strip with coating = 304 micron

$$stacking\ factor(\%) = (1 - \frac{4}{304}) * 100$$

$$stacking\ factor(\%) = (\frac{75}{76}) * 100$$

$$stacking\ factor(\%) = 98.68$$

But as the coating was also magnetic, it would contribute to the stacking factor hence the new value of stacking factor considering the saturation magnetization of Co-Ni-P coating to be 0.096 T and that of GOES to be 1.95 T was 98.74 % as shown below. The increase in stacking factor by the magnetic nature of the coating was found to be insignificant.

$$Net\ magnetic\ contribution\ of\ the\ coating\ as\ compared\ to\ GOES = (\frac{0.096}{1.95}) * 100)$$

$$Net\ magnetic\ contribution\ of\ the\ coating\ as\ compared\ to\ GOES = 4.92\%$$

$$New\ stacking\ factor(\%) = 98.68 + ((\frac{100 - 98.68}{100}) * 4.92)$$

$$New\ stacking\ factor(\%) = 98.745$$

Table 5.3 Stacking factor for different pH values of Co-Ni-P coating

pH	Stacking factor (%)
NipH1	99.20
NipH2	99.00
NipH3	98.93
NipH4	98.75
NipH5	98.71

Stacking factor was also calculated for other coatings based on the results shown in section 5.2.6 as shown in Table 5.3 above. The stacking factor was comparatively better for lower pH values but the coating performance was poor. The reason behind this behaviour is explained in section 5.2.6.

5.2.12 Magnetostriction

Figure 5.15 (a-d) shows the magnetostriction curves for the uncoated and Co-Ni-P coated sample Ni1-Ni4. In Figure 5.15 (a) the change in magnetostriction for the uncoated and Co-Ni-P coated sample was insignificant. As the thickness of the coating increases the magnetostriction begins to reduce and the effect was highest for the sample Ni4. The threshold (point of zero magnetostriction) for uncoated and sample Ni4 was around -1 MPa and -3 MPa respectively. A stress shift of 1.80 ± 0.20 MPa was observed after coating the sample. This shift in the magnetostriction curve towards the left infers that a significant amount of stress was acting on the substrate.

(a)

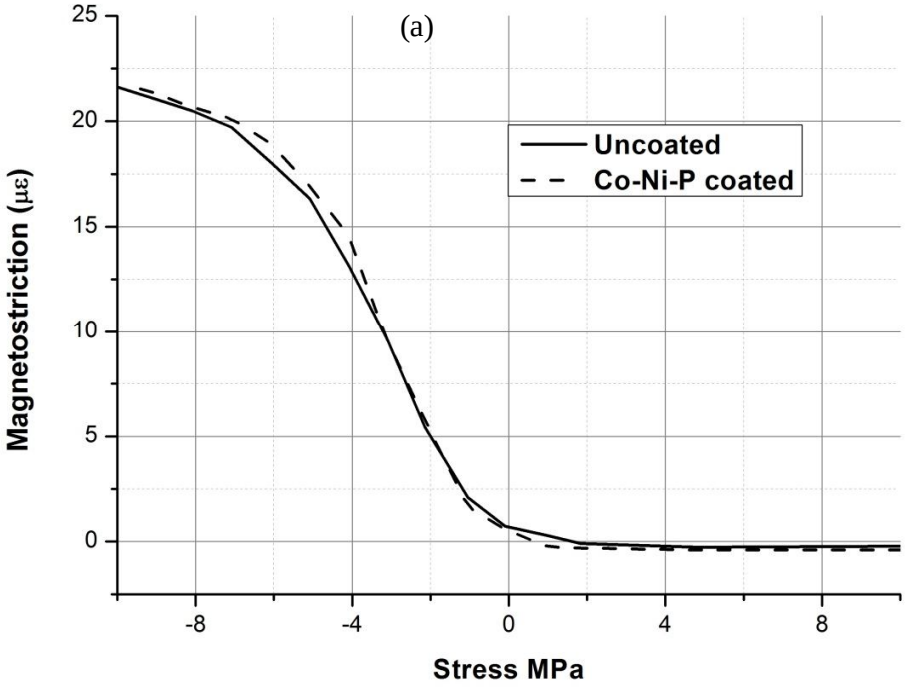
Magnetostriction (με)
Stress MPa
Uncoated
Co-Ni-P coated
25
20
15
10
5
0
-8
-4
0
4
8

(b)

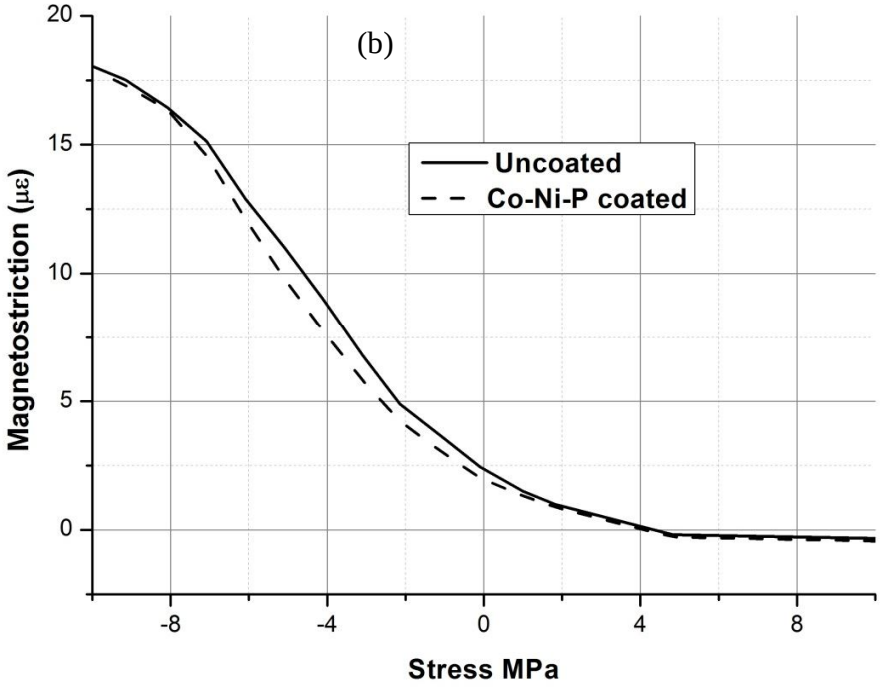
Magnetostriction (με)
Stress MPa
Uncoated
Co-Ni-P coated
20
15
10
5
0
-8
-4
0
4
8

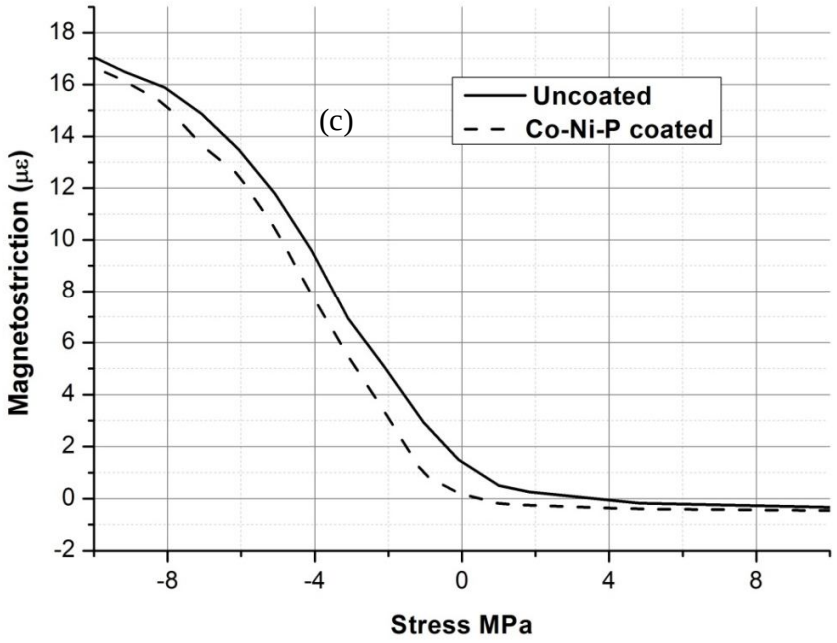

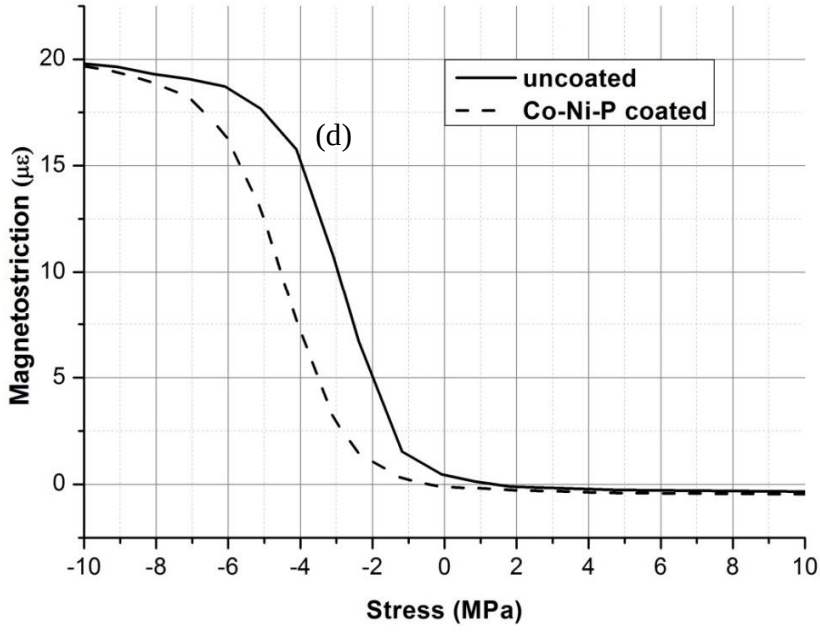

Figure 5.15 Magnetostriction vs Stress for uncoated & Co-Ni-P (a) Ni1 (b) Ni2 (c) Ni3 and (d) Ni4.

5.2.13 X-ray Diffraction

The XRD result in Figure 5.16 shows the uncoated, Ni2 and Ni4 sample. The diffusive broad peaks in the histogram confirms the amorphous or nanocrystalline nature of the coating [13]. The peaks may be Co-P or Co-Ni-P. The sharp peaks that were observed correspond to α-Iron and α-Iron-Cobalt ($Fe_{0.3}Co_{0.7}$). The 110 reflection was shifted towards the lower angle in the coated sample as can be seen in Figure 5.16 Stress was introduced by the coating [6] which expands the lattice of the substrate material.

From Bragg's law [14] the stress shift was interpreted. The shift in peaks towards a lower angle confirmed that the inter planer distance d increases and hence compressive stress developed in the coating. An equivalent tensile stress acted on the grain-oriented electrical steel surface to compensate the compressive residual stresses due to which there was an improvement in magnetic properties.

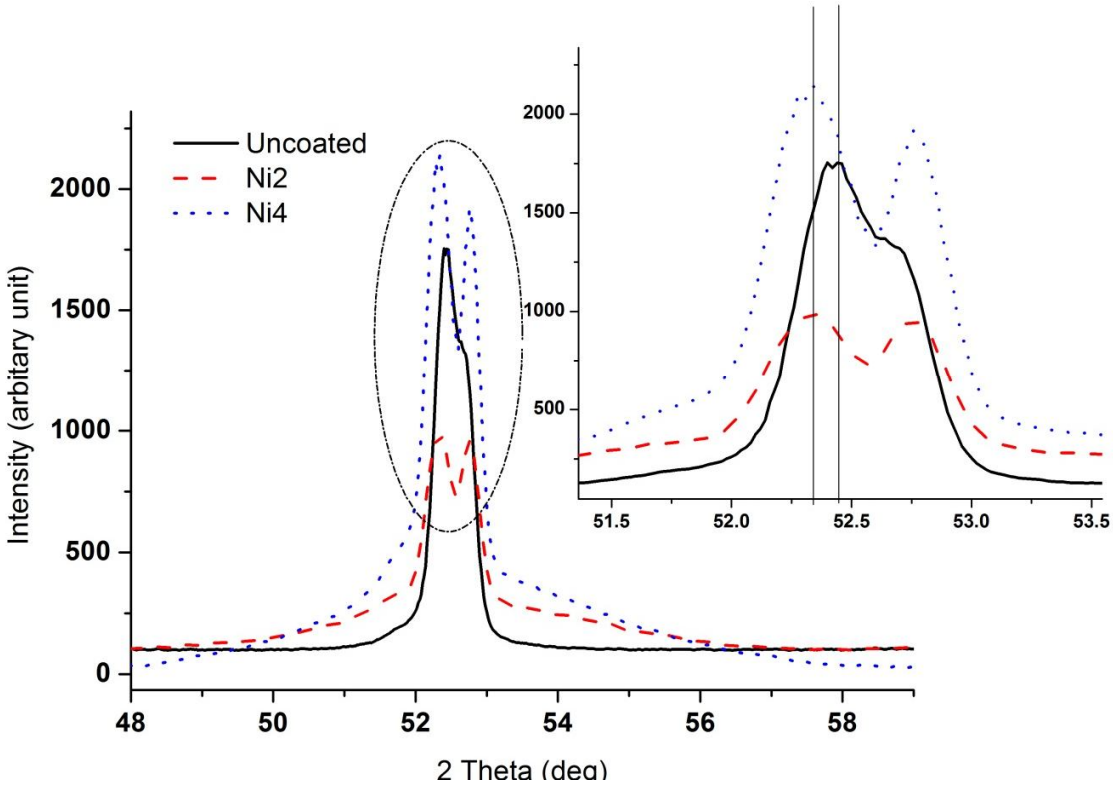

Figure 5.16 XRD of uncoated and Co-Ni-P coated samples at pH 9.

5.2.14 Transverse coated samples

To understand whether the applied stress by Co-Ni-P coating on grain oriented electrical was isotropic or not, samples were cut in the direction perpendicular to the rolling direction and coated with Co-Ni-P. In the transverse samples the grains were oriented along the width of the strip. Magnetic domain imaging was carried to view the domain behaviour. The magnetic domain imaging for the uncoated and Co-Ni-P coated sample is presented in Figure 5.17. The average domain width before and after coating was 0.71 mm and 0.6mm respectively. The domains narrow after coating and it was similar to the results observed for the rolling direction cut samples which endorses the calculation in section 3.1.2.2 and hence the coating applies isotropic stress.

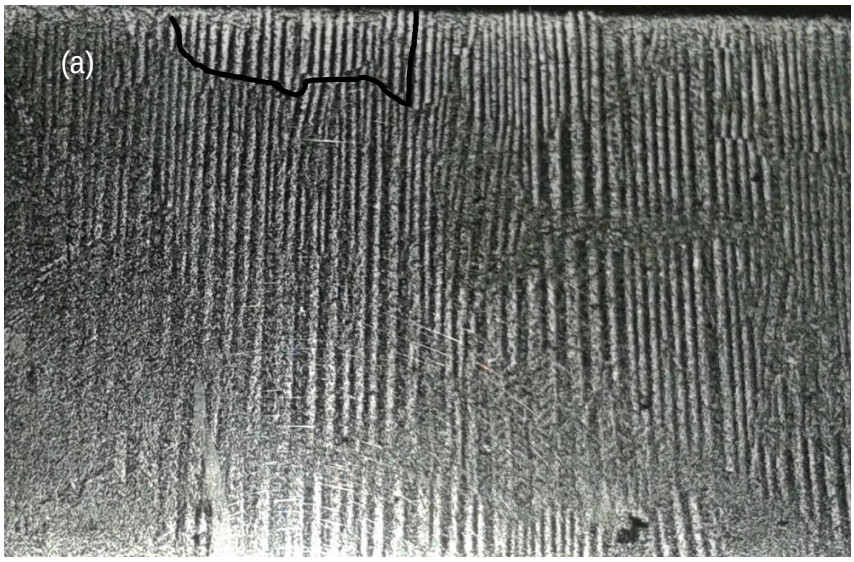

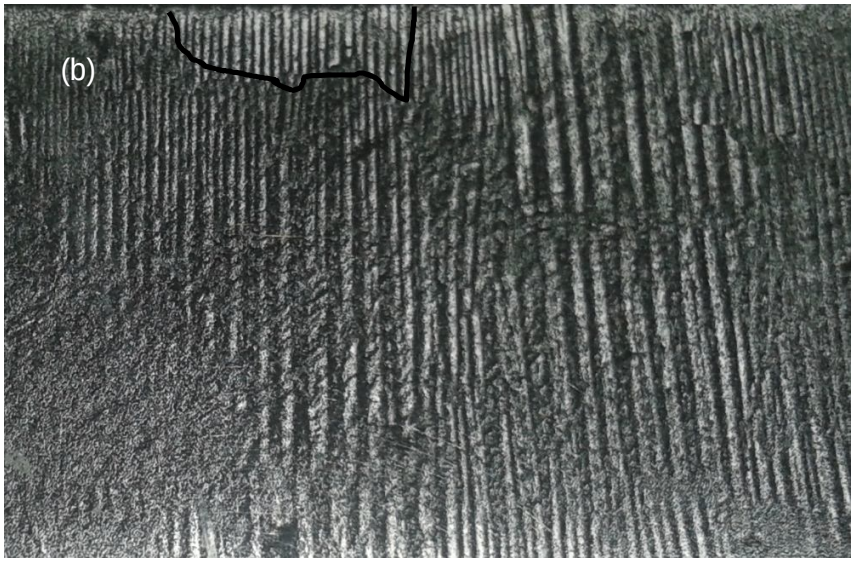

Figure 5.17 Magnetic domain images for the transverse cut (a) uncoated and (b) Co-Ni-P coated sample showing domain narrowing in the box.

The results of the uncoated and transverse cut Co-Ni-P coated sample are shown in Figure 5.18. From the graph it can be seen clearly that the Co-Ni-P coating increases the power loss at all values of magnetic flux density. This behaviour was expected because the narrowing of domains in the transverse direction would require a large magnetic field to rotate the domains in the rolling direction and hence the loss would increase.

The magnetostriction values for the uncoated and transverse cut Co-Ni-P coated sample are shown in Figure 5.19. The magnetostriction curves were shifted towards the right. The stress shift was measured to be about 3 MPa. The shift in the magnetostriction curves was because the coating applied a stress to the substrate which made domains in this direction energetically favourable and increased the magnetostriction.

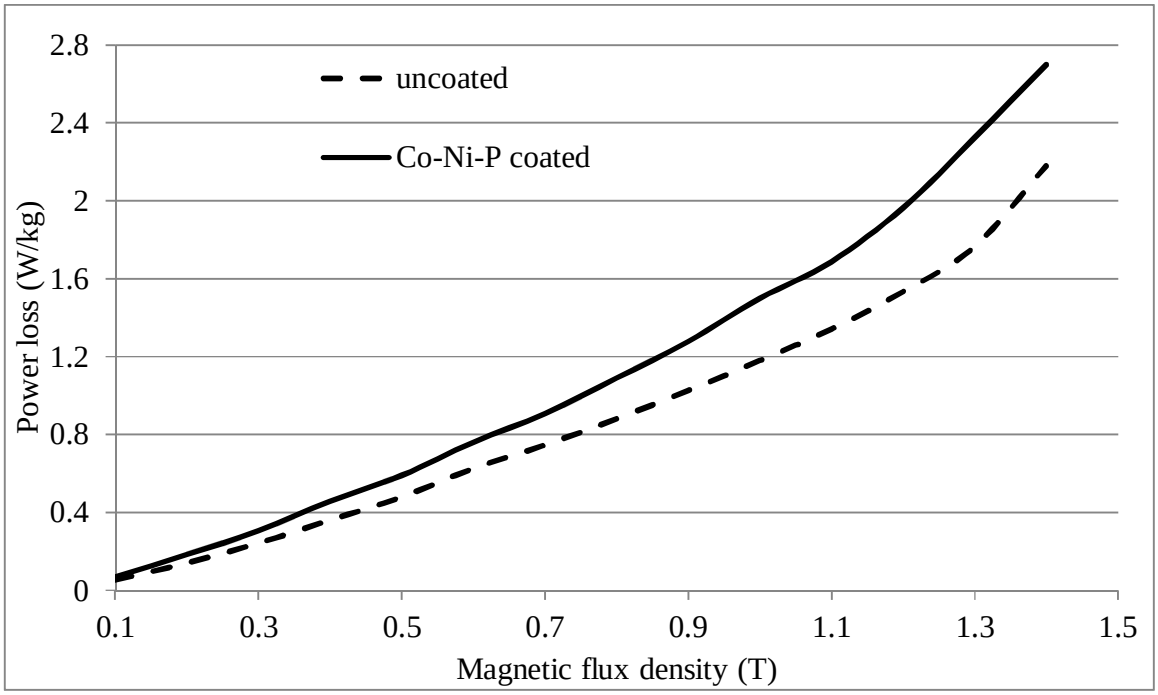

Figure 5.18 Power loss results for the uncoated and transverse cut Co-Ni-P coated samples at 50 Hz frequency.

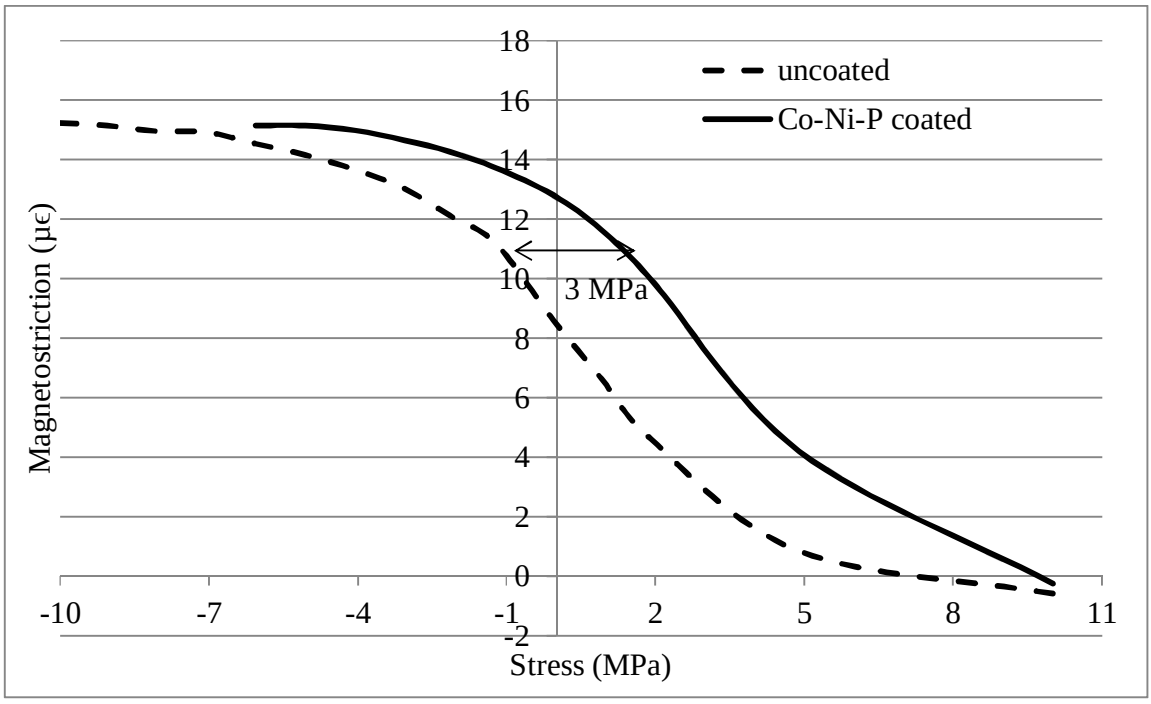

Figure 5.19 Magnetostriction curves for uncoated and transverse cut Co-Ni-P coated samples at a magnetic flux density of 1.3 T and 50 Hz frequency.

5.2.15 Stress and magnetic properties in rolling and transverse direction for Co-Ni-P coating

Stresses affect the domain structure by changing the free energy of the material with the addition or reduction of magnetoelastic energy. Tensile stress reduces the free energy and narrows the domain width whereas compressive stress increases it and sets stress pattern in the material [15]. Co-Ni-P coating applied a tensile stress of 3.9 MPa on GOES which reduced the free energy and narrowed the domains. The domains with perfect orientation were narrowed from a domain width of 0.73 mm to 0.48 mm whereas those with slight misorientation were narrowed from 0.66 mm to 0.53 mm. A larger tensile stress is required to narrow all the domains in oriented and misoriented directions because a smaller tensile stress narrows domain that are in near perfect orientation and a large stress would be required to align the highly misoriented domains in the direction of rolling and then narrowing [16]. The power loss separation graph showed a combined reduction in hysteresis and anomalous loss which was due to the improvement in surface roughness and narrowing of domain width by the coating [11]. The effect of stress on power loss was isolated by calculating the contribution of different losses before and after coating and the percentage of anomalous loss improvement was noted to be 4-6 % which affects the domain narrowing due to stress. The tensile stress of 3.9 MPa shifted the magnetostriction curve by 1.80 MPa because the applied tensile stress was divided between the elimination of surface closure domains which affects both the power loss and magnetostriction, and domain narrowing which effects only the power loss and this value was half the value of applied stress. The results were in agreement with Moses [17] where 6 MPa of stress resulted in a stress shift of 3 MPa.

The stress from the coating in the transverse direction narrowed the domains from 0.71 mm to 0.60 mm which was half the value as compared to that observed in the rolling direction and this was due to the difference in Young's modulus of the steel in rolling and transverse direction. The power loss increased by 30 % for 1.3 T magnetic flux density which was expected as tensile stress in transverse direction has similar effect as compressive stress in rolling direction [18]. The magnetostriction increased by a stress shift of 3 MPa as tensile

stress in transverse direction promoted narrowing of domains and it became harder to magnetise in the direction of magnetization.

5.3 Co-Ni-B coating

Table 5.4 highlights the sample id's along with the time and pH values.

Sample ID	Time for electroless plating (min)	pH of the solution
NiB1	60	8.0
NiB2	60	8.8

5.3.1 Deposition and characterisation of Co-Ni-B

Table 5.4 shows the sample id's for Co-Ni-B coating at different pH and time. The deposition of the coating starts with the reduction of Ni and Co on the surface of electrical steel whereas boron atoms get trapped in between Co and Ni atoms to produce Co-Ni-B.

Figure 5.20 shows the optical microscopy image of the substrate and the coating. The coating was uniformly distributed across the surface and the thickness was measured to be 2.36 ± 0.24 μ. SEM images of sample NiB1 and NiB2 were taken to understand the morphology of the coating growth as shown in Figure 5.21 and Figure 5.22 respectively. The composition of the coating for sample NiB1 was 71-73 weight percent of cobalt, 27-28 weight percent of nickel and around 1 weight percentage of boron. The composition of sample NiB2 was 81-83 weight percent cobalt, 16-17 weight percent nickel and around 1 weight percent of boron. The weight percent of boron did not change with the change in pH value. In NiB1 there was agglomeration in a few places whereas in NiB2 the coating was found to be completely agglomerated a one place only.

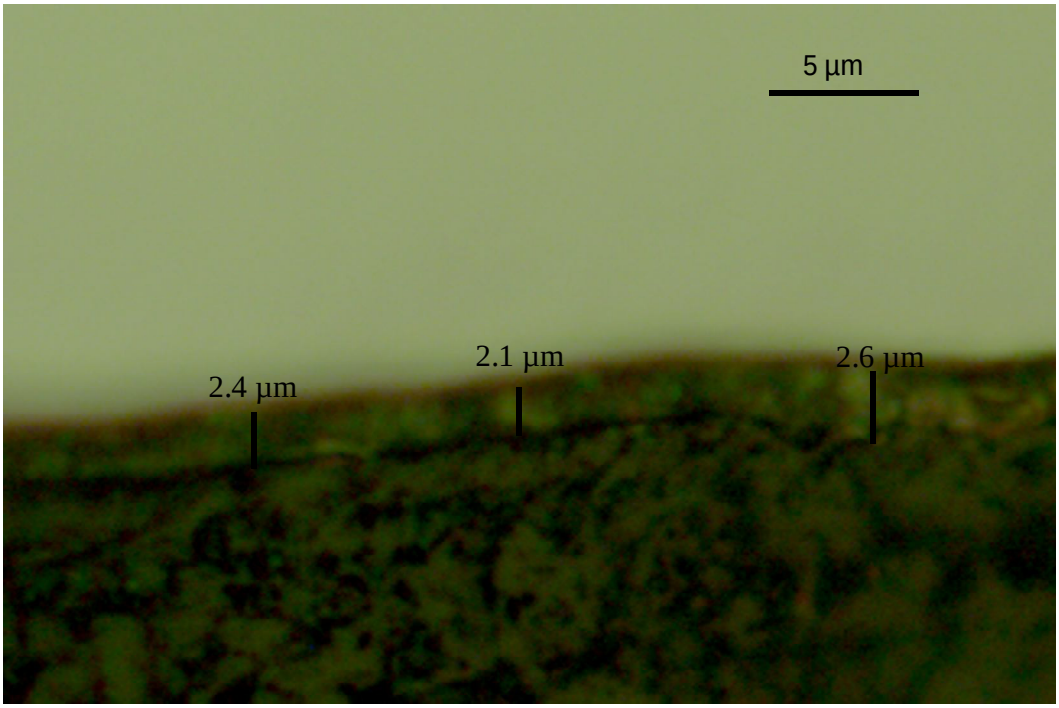

Figure 5.20 Optical Microscope image showing the thickness of Co-Ni-B coating.

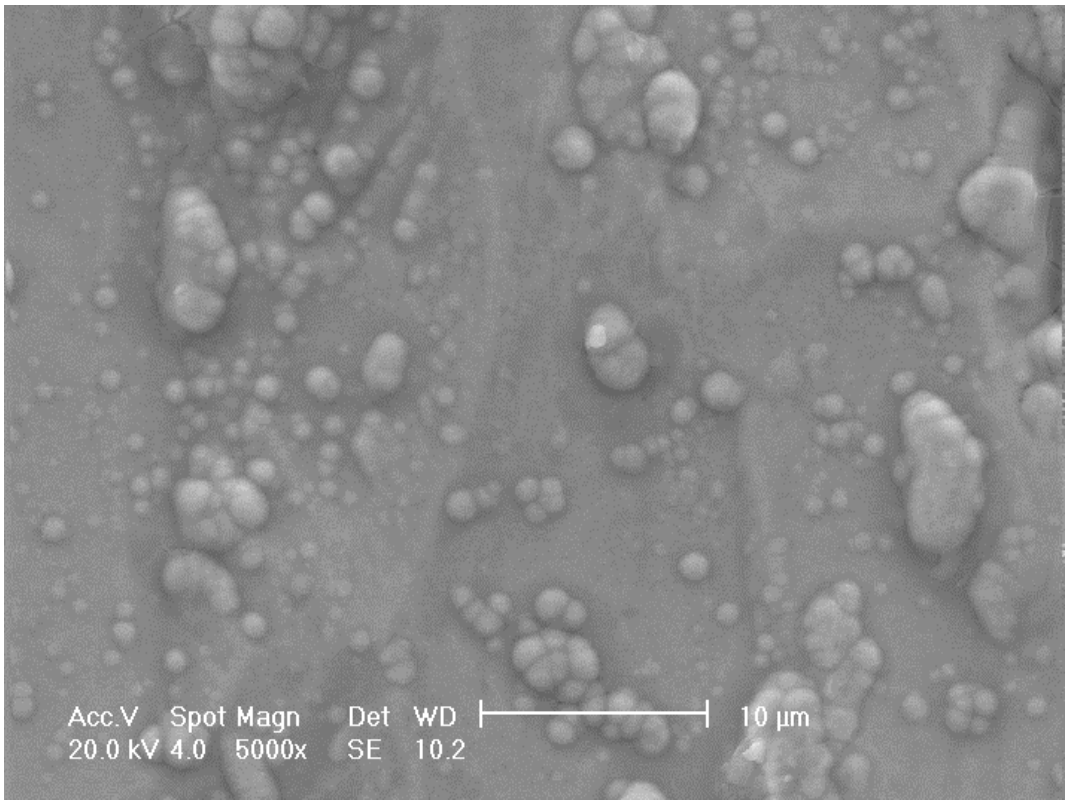

Figure 5.21 SEM image of a sample NiB1.

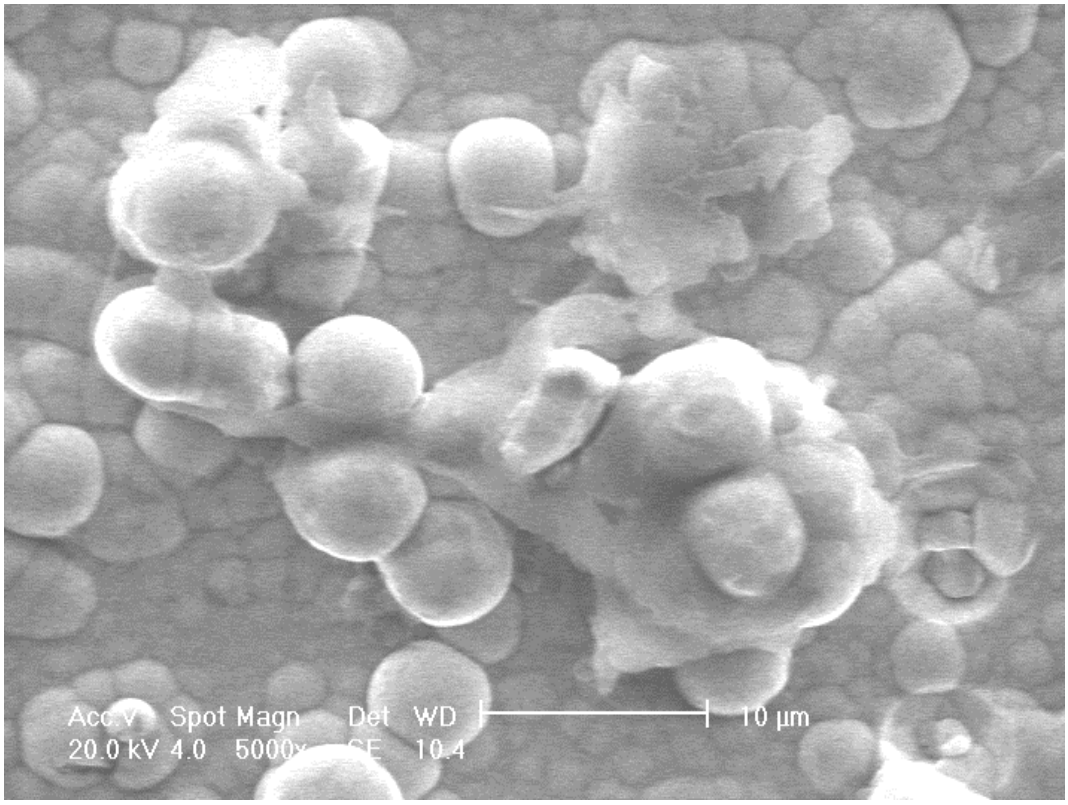

Figure 5.22 SEM image of sample NiB2.

5.3.2 Stress in Co-Ni-B coating

Stresses develop in Co-Ni-B electroless plating. Agarwala et. al. [19] had reported a tensile stress of 500 MPa in 0.5-1 weight percent B coating. Lee et. al. [20] had shown that the tensile stress in the coating increased linearly with increase in boron content. During the deposition the coating starts to grow at few places also known as the activation sites, further development of the coating occurs at these sites only. As the coating grows it coagulates at several places. Due to surface tension the particles are pulled inside and this decrease the interatomic distance between the atoms thus introduces tensile stress in the coating.

To ascertain the type of stress applied by Co-Ni-B coating on the sample, GOES sample was coated on one side. It was observed that the sample bent with the coating on the inside and the uncoated surface on the outside as shown in Figure 5.23. The stress applied by the coating on GOES was calculated to be 11 MPa based on method explained in section 5.2.9. The coating produced a tensile stress which in turn induced compressive stress in the substrate to keep the sum total of all stresses to zero. Compressive stress in the rolling

direction is very harmful for grain oriented electrical steel as it increases the power loss and magnetostriction as described in section 2.5.2.

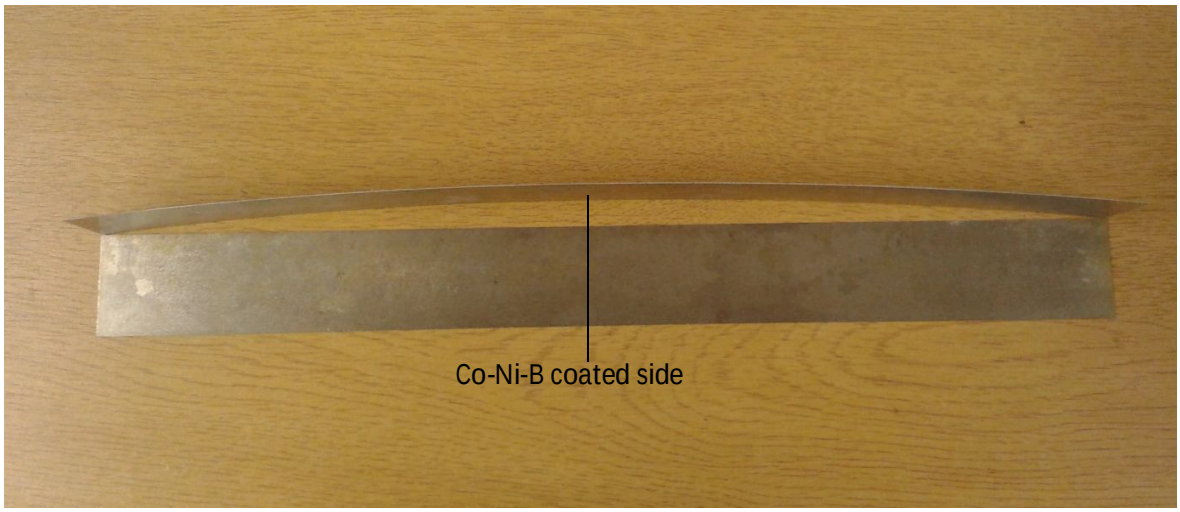

Figure 5.23 Shows the electrical steel sample coated on only one side.

5.3.3 Magnetic domain imaging

Magnetic domain images were taken before and after coating the sample. Figure 5.24 (a) shows the domain pattern for the uncoated sample and Figure 5.24 (b) shows the domain image for the sample coated with Co-Ni-B. In the uncoated sample the domains are clearly visible and they are aligned in the direction of rolling. Co-Ni-B coated sample showed no visible domain pattern as it was completely removed by tensile stress in the coating. The domains form a stress pattern I where the main domains rotate from [001] to [100] direction and the flux closure domains were aligned in the same direction [001].

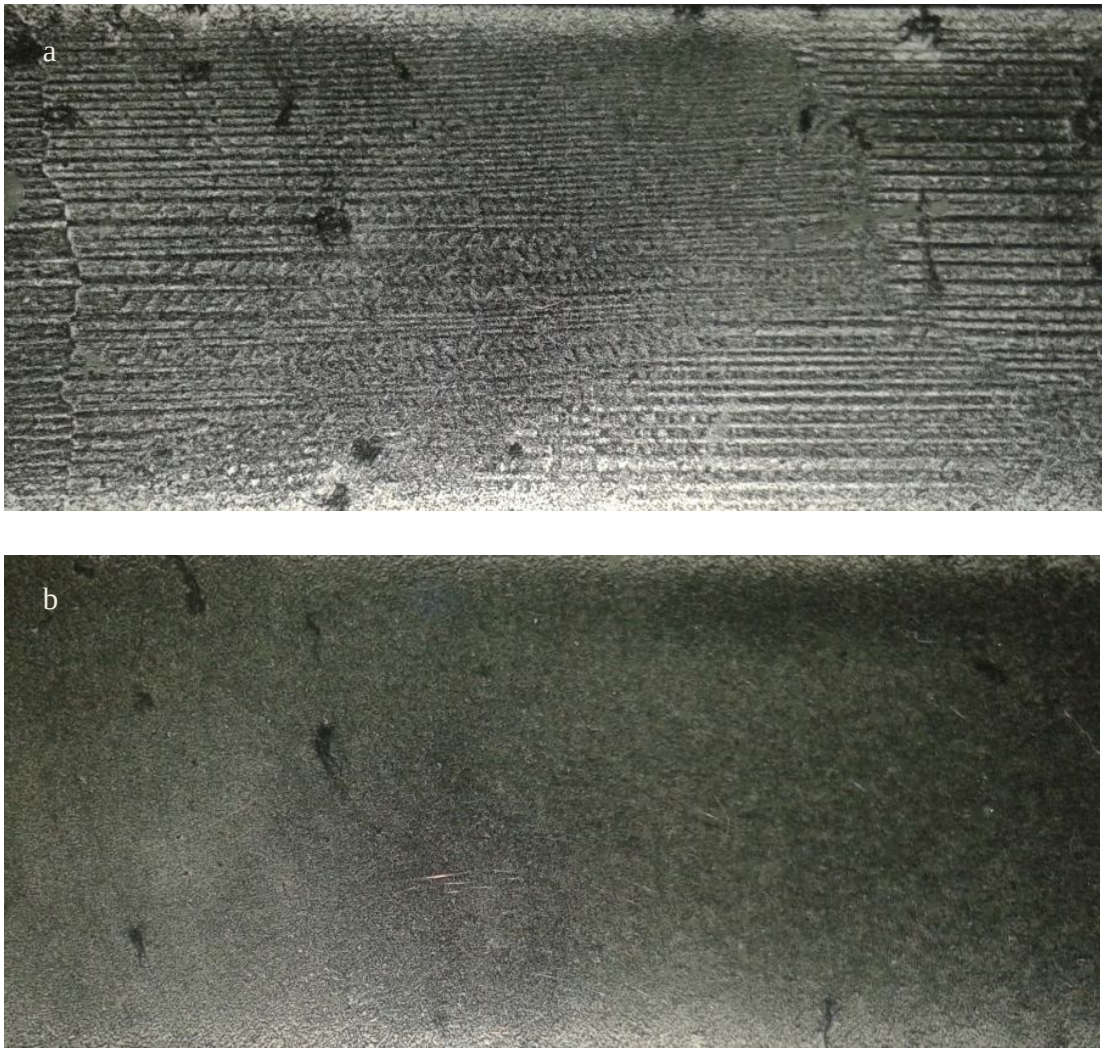

Figure 5.24 Magnetic domain imaging of uncoated (a) and Co-Ni-B (b) coated sample.

5.3.4 Power loss testing

To study the effect of coating on power losses, the samples were tested in the single strip tester. Figure 5.25 show that the uncoated sample had lower power loss as compared to the coated sample for all values of magnetic flux density.

The power loss results for samples NiB1 and NiB2 are shown in Figure 5.26. It can be seen from the figure that the power loss increased more significantly in a NiB2 because the coating was completely agglomerated at a single point with a particle size approximately 10 µm and this increased the roughness and produced a large amount of stress in the coating.

In NiB1 the coating was agglomerated at few places throughout the sample and hence the stress generated was less as the agglomerated particle size was small.

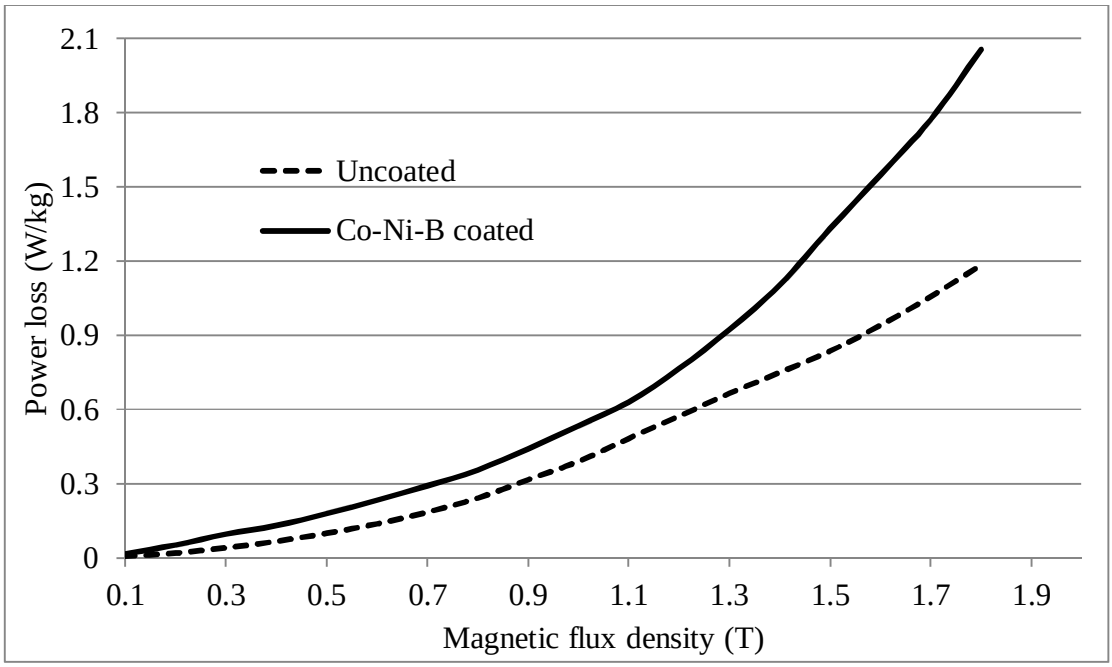

Figure 5.25 power loss values are plotted against the magnetic flux density.

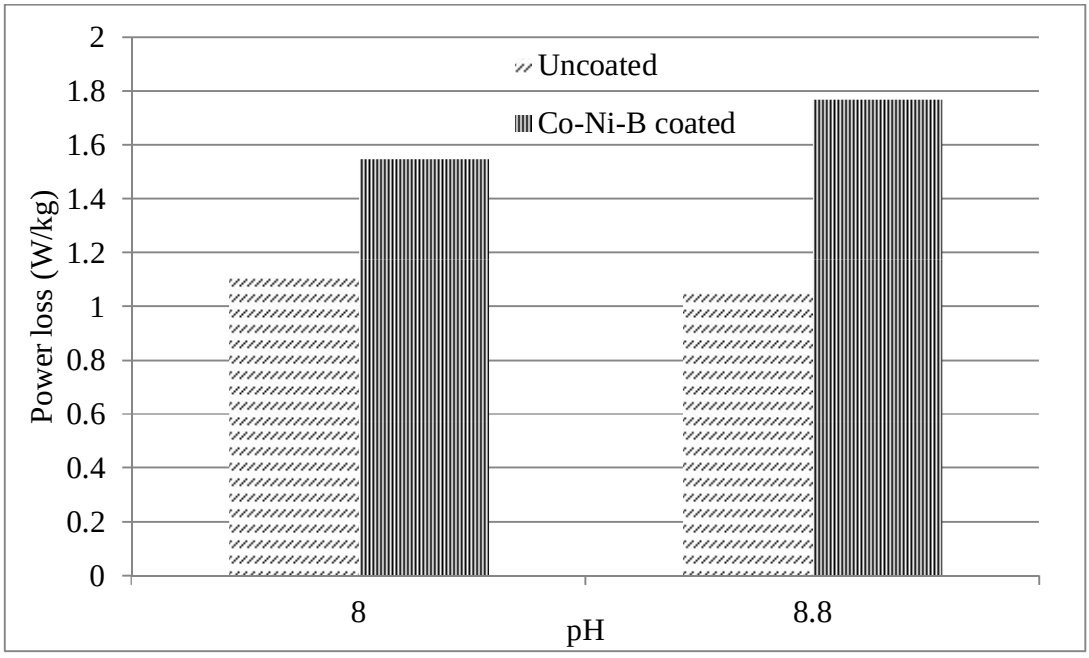

Figure 5.26 Power loss results of uncoated and Co-Ni-B coated sample at two different pH values.

5.3.5 Loss separation

Using the method described in section 2.4.4 the loss values were plotted from a frequency of 10 Hz to 1000 Hz and fitted with a correlation coefficient better than 0.999 as shown in Figure 5.27. After coating the sample the anomalous loss increased as expected because the tensile stress in the coating applies compressive stress on the substrate. This compressive stress in the substrate leads to stress pattern I where the main domains rotate perpendicular to the direction of magnetization. A significant amount of energy was required to align the domains in the direction of magnetization. The effect was exactly opposite to that observed in Co-Ni-P coating where the anomalous and hysteresis loss decreased due to the application of tensile stress on the substrate and improved surface roughness.

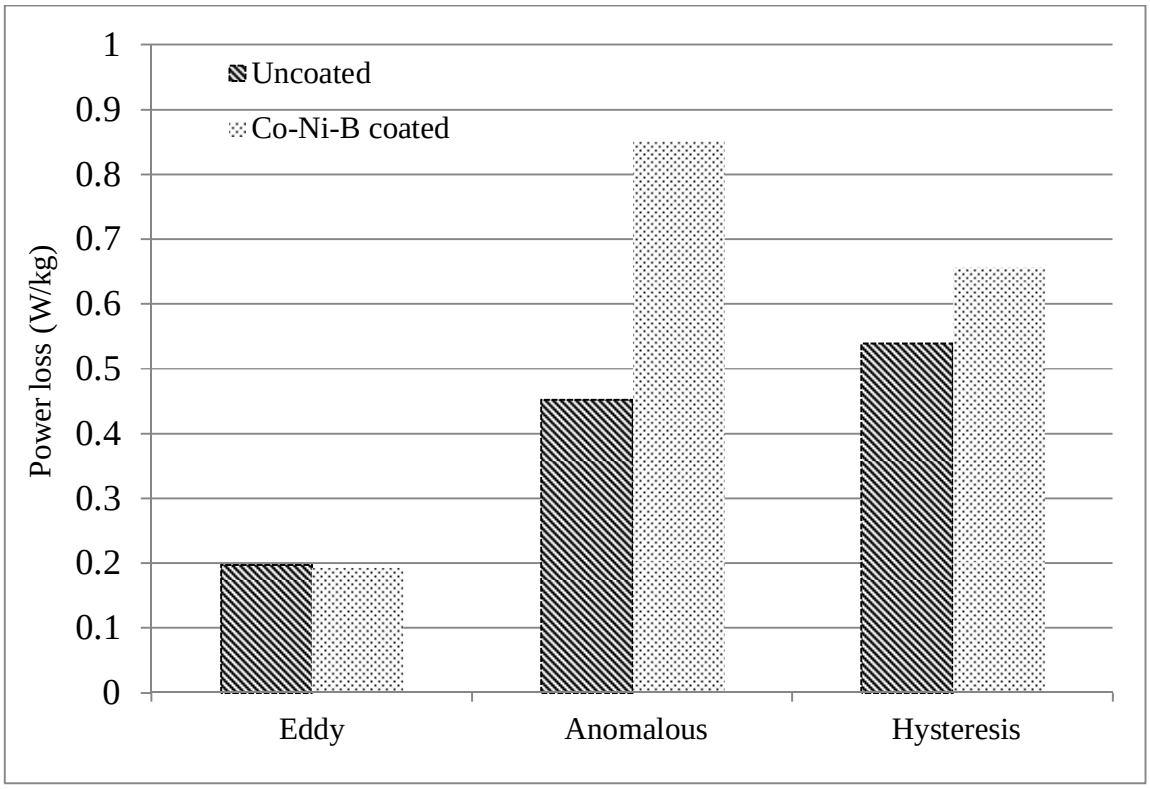

Figure 5.27 Power loss separation for the uncoated and Co-Ni-B coated sample.

5.3.6 Magnetostriction testing

The effect of Co-Ni-B coating on the magnetostriction is shown in Figure 5.28. The magnetostriction curves shift towards the right after coating the sample with Co-Ni-B. This means that the effect of magnetostriction increases after coating. The point of threshold

magnetostriction was shifted from 6 MPa in the uncoated sample to -1 MPa in the sample coated with Co-Ni-B. A compressive stress shift of 7MPa was observed. The reason behind the stress shift was related to the domain behaviour. The domains were aligned in the direction of rolling before coating. After coating the sample the domains rotate in a direction perpendicular to that of rolling as, explained in section 2.7.

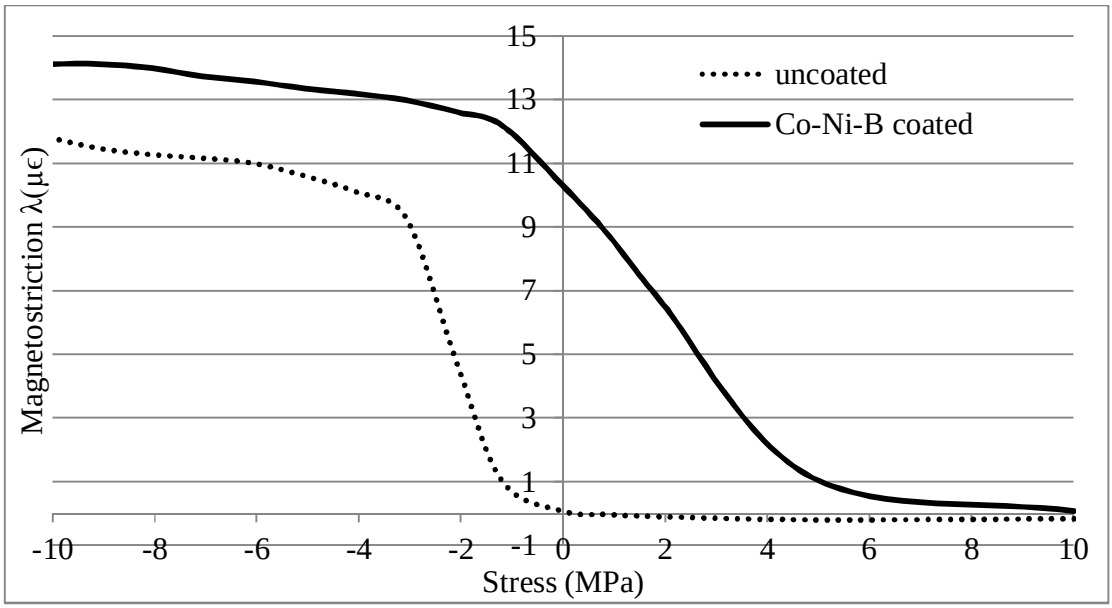

Figure 5.28 Stress vs magnetostriction curve for uncoated and Co-Ni-B coated sample.

5.3.7 Transverse properties

GOES samples cut in a direction perpendicular to the rolling direction were also coated with Co-Ni-B to understand the nature of stress applied by the coating. The results for power loss and magnetostriction are shown in Figure 5.29 and Figure 5.30 respectively. After coating the samples with Co-Ni-B coating the power loss and magnetostriction reduced because the coating applies tensile stress on the substrate and domains that were aligned in the transverse direction were oriented in the direction of applied magnetic field due to this stress. The reverse trend was seen for the Co-Ni-P coating where the power loss and magnetostriction increased after coating. The reason for this behaviour was explained in section 5.2.13.

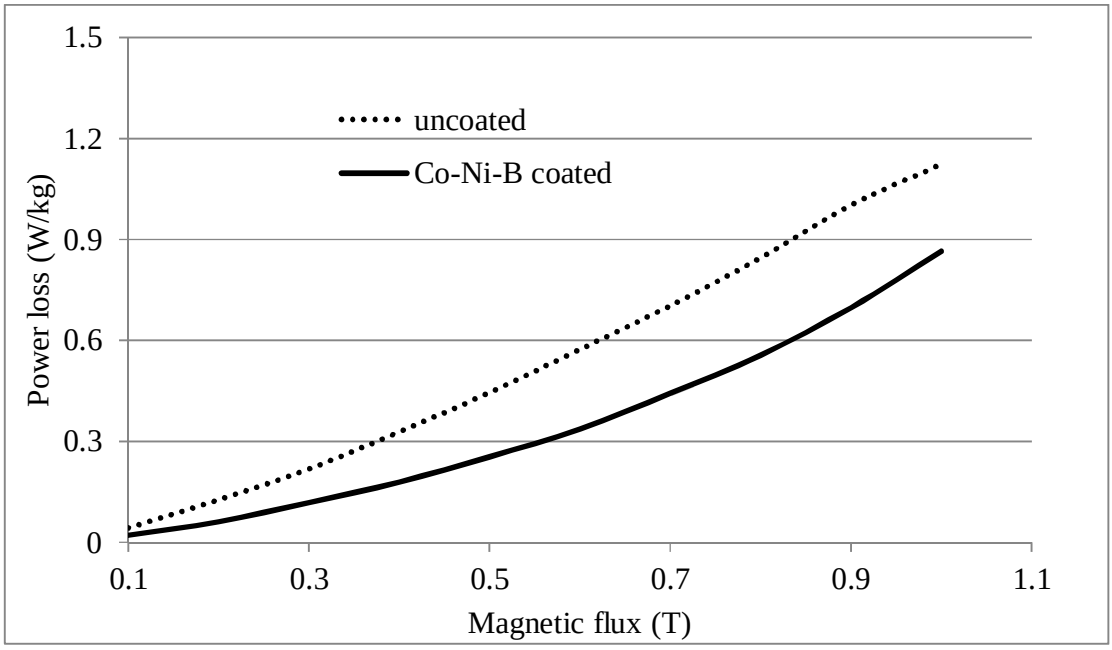

Figure 5.29 Power loss of a transverse sample coated with Co-Ni-B.

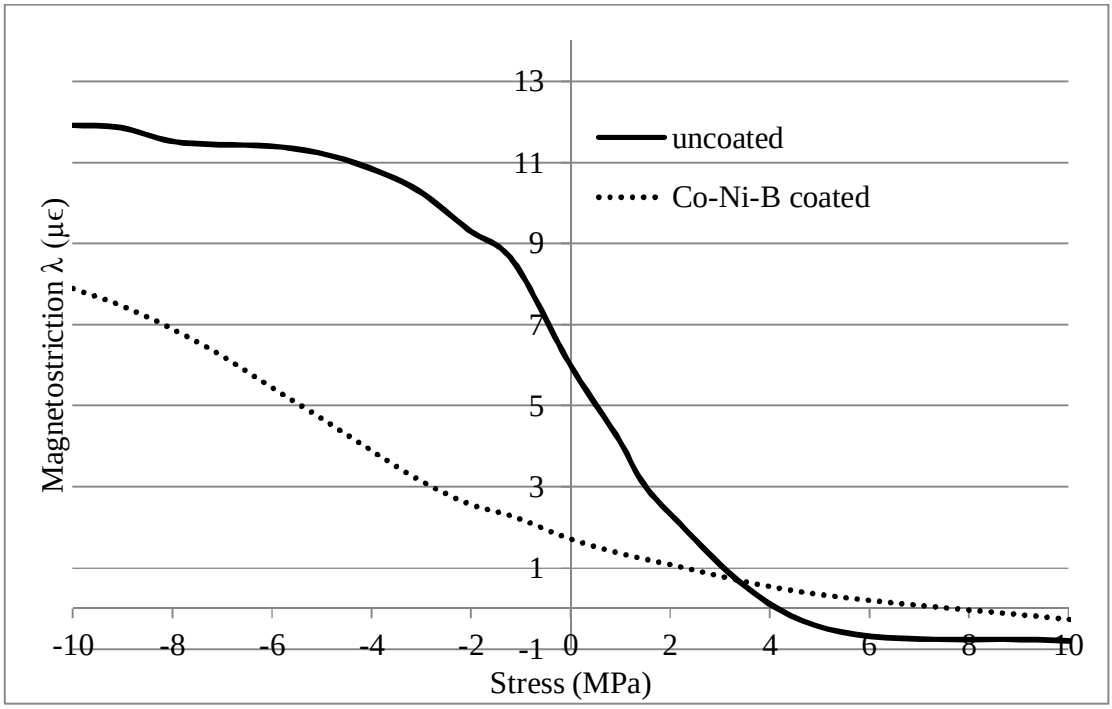

Figure 5.30 Magnetostriction of a transverse cut sample coated with Co-Ni-B coating.

5.3.8 Stress and magnetic properties in rolling and transverse direction for Co-Ni-B coating

Co-Ni-B coating induced a compressive stress of 11 MPa in GOES coated along the rolling direction which affected the magnetic domains pattern which was completely destroyed by the stress and transformed to stress pattern I where the size of closure domains reduce due to the increase in magnetoelastic energy of those domains. The power loss was increased by 60-65 % at 1.5 T magnetic flux density and Moses [18] has shown that a compressive stress of 10 MPa results in increase of loss up to 60 % after which it saturates. The increase in power loss was the combined contribution of anomalous and hysteresis loss which was due to the effect of compressive stress and the surface roughness of the coating. On isolating the effect of compressive stress on power loss it was found that the contribution was 75 % from stress and 25 % from the roughness of the coating. The compressive stress shifted the magnetostriction curve by 7 MPa and the results were in agreement with Moses [17] who observed a stress shift of 8 MPa for applied compressive stress of 10 MPa.

Co-Ni-B coating on the transverse samples improved the power loss by 21-23 % at 1 T magnetic flux density and the magnetostriction was improved by a stress shift of 6 MPa and this affect was due to the removal of supplementary domain structure, decrease in lancet domain density and stress pattern I, and domain refinement [21]. Application of compressive stress in the transverse direction improves the domain orientation in the rolling direction and upon magnetization in transverse direction it switches from rolling to transverse direction by 90° and finally 180° rotation [8].

5.4 Conclusion

GOES was coated with Co-Ni-P using electroless plating. Power loss testing was performed before and after the application of coating. An improvement of approximately 9-11 % in power loss was observed. The mean thickness of the coating was found to be 2.15±0.15 μm from ESEM images. The VSM results confirmed the magnetic nature of the coating. Shifts of magnetostriction stress sensitivity curves confirmed that stress was acting on the substrate. XRD results showed peaks of α-Iron in uncoated sample, α-Iron-Cobalt and α-Iron in Co-Ni-P coated sample. The shift in XRD peaks after coating further corroborates the stress in the substrate. Magnetic pattern viewer clearly showed the narrowing of the domains after the samples were coated. This narrowing of domains after coating reduced the anomalous loss. The Talysurf profilometer showed a decrease in surface roughness (Ra) values after coating the sample which reduced the hysteresis loss. The AFM images further endorse the roughness values showing regions of higher roughness for the uncoated surface and reduced roughness for Co-Ni-P coated sample at pH of 9.0.

Co-Ni-B was coated on GOES using electroless plating at a pH of 8 and 8.8. The Co content increased with the pH and Ni was decreased. SEM analysis showed that the coating was found to be agglomerated for both the pH values. One sided coating GOES samples showed that compressive stress was applied on GOES by the coating. Magnetic domain imaging showed the development of stress pattern I after coating where the main domains rotate from [001] to [100] and the material becomes hard to magnetize. The power loss was increased by 60-65% after coating and the loss separation calculation showed the increase of anomalous and hysteresis loss. The increase in anomalous and hysteresis loss was due to the compressive stress and higher roughness after coating. For zero stress the magnetostriction curves showed an increase in magnetostriction from 0 μϵ to 10 μϵ after coating. The increase in magnetostriction was due to the development of compressive stress in GOES. This coating is not suitable for GOES.

5.5 References

[1] T. Homma, J. Shiokawa, Y. Sezai, and T. Osaka, "In situ analysis of the deposition process of electroless CoNiP perpendicular magnetic recording media," *Electroechemical society proceedings,* vol. 95, p. PV 181, 1996.

[2] K. S. Lew, M. Raja, S. Thanikaikarasan, T. Kim, Y. D. Kim, and T. Mahalingam, "Effect of pH and current density in electrodeposited Co–Ni–P alloy thin films," *Materials Chemistry and Physics,* vol. 112, pp. 249-253, 2008.

[3] N. Fenineche, A. M. Chaze, and C. Coddet, "Effect of pH and current density on the magnetic properties of electrodeposited Co-N-P alloys," *Surface and Coatings Technology,* vol. 88, pp. 264-268, 1996.

[4] G. O. Mallory and J. B. Hajdu, "Electroless Plating Fundamentals & Applications," *American electroplaters and surface finishers society,* vol. chapter 4, pp. 121-122, 1990.

[5] K. Parker and H.Shah, "The stress of electroless nickel deposits on beryllium," *Journal of the Electrochemical Society,* vol. 117, pp. 1091-1094, 1971.

[6] J. Y. Song and J. Yu, "Residual stress measurements in electroless plated Ni–P films," *Thin Solid Films,* vol. 415, pp. 167-172, 2002.

[7] E. Beyer, L.Lahn, C.Schepers, and T.Stucky, "The influence of compressive stress applied by hard coatings on the power loss of grain oriented electrical steel sheet," *Journal of Magnetism and Magnetic Materials,* vol. 323, pp. 1985-1991, 2011.

[8] P. Klimczyk, "Novel Techniques for Characterisation and Control of Magnetostriction in G.O.S.S," *PhD Thesis, Cardiff University, Cardiff,* 2012.

[9] R. A. Fisher, "Frequency Distribution of the Values of the Correlation Coefficient in Samples from an Indefinitely Large Population," *Biometrika,* vol. 10, pp. 507-521, May 1915.

[10] K. Toshiya Wada, T. N. Munakata, and T. T. Kitakyushu, "Method for producing a super low watt loss grain oriented electrical steel sheet," *US Patent,* vol. 3,932,236, January 13, 1976.

[11] T. Yamamoto and T. Nozawa, "Effects of Tensile Stress on Total Loss of Single Crystals of 3% Silicon-Iron," *Journal of Applied Physics,* vol. 41, pp. 2981-2984, June 1970.

[12] C. R. Boon and J. A. Robey, "Effect of domain-wall motion on power loss in grainoriented silicon-iron sheet," *Proceedings of the IEEE,* vol. 115, pp. 1535-1540, October 1968.

[13] M. N. Obrovac and L. Christensen, "Structural Changes in Silicon Anodes during Lithium Insertion/Extraction," *Electrochemical and Solid-State Letters,* vol. 7, pp. A93-A96, 2004.

[14] W. L. Bragg, "The Diffraction of Short Electromagnetic Waves by a Crystal," *Proceedings of the Cambridge Philosophical Society,* vol. 17, pp. 43-57, 1913.

[15] W. D. Corner and J. J. Mason, "Effect of stress on domain structure of goss textured silicon iron," *British Journal of Applied Physics,* vol. 15, pp. 709-722, 1964.

[16] J. W. Shilling, "Domain Structure During Magnetization of Grian-Oriented 3% Si-Fe as a function of Applied Tensile Stress," *Journal of Applied Physics,* vol. 42, pp. 1787-1789, 15 Mach 1971.

[17] A. J. Moses, "Effects of applied stress on the magnetic properties of high permeability silicon-iron," *IEEE transactions on magnetics,* vol. MAG-15, pp. 1575-1579, November 1979.

[18] A. J. Moses, "Effects of stresses on the magnetic properties of silicon-iron laminations," *Journal of Materials science,* vol. 9, pp. 217-222, 1974.

[19] R. C. Agarwala and V. Agarwala, "Electroless alloy/composite coatings: A review," *Sadhana,* vol. 28, pp. 475-493, 2003.

[20] K. H. Lee, D. Chang, and S. C. Kwon, "Properties of electrodeposited nanocrystalline Ni–B alloy films," *Electrochimica Acta,* vol. 50, pp. 4538-4543, 2005.

[21] O. Perevertov and R. Schafer, "Influence of applied compressive stress on the hysteresis curves and magnetic domain structure of grain-oriented transverse Fe–3%Si steel," *Journal Of Physics D: Applied Physics,* vol. 45, pp. 1-11, 2012.

6 Electroless Co-P-Carbon Nanotube composite coating to enhance magnetic properties of grain-oriented electrical steel

6.1 Introduction

The aim of this work was to optimise Co-P-CNT coating for power loss reduction in grain-oriented electrical steel which was measured using a single strip tester. The coating was characterised using a number of techniques including Environmental Scanning Electron Microscope (ESEM), vibrating sample magnetometer, Raman spectroscopy, four point probe resistivity measurement, Talysurf surface profilometer and X-ray diffraction to measure the thickness, chemical composition, magnetic activity, resistivity and roughness which effect the power loss.

6.2 Co-P-CNT coating deposition

Table 6.1 highlights the sample id's along with the time and condition of solution.

Sample ID	Time for electroless plating (min)	Solution condition
CoP1	60	With CNTs
CoP2	80	With CNTs
CoP3	60	Without CNTs

Table 6.1 shows the sample identities for different times and treatments. The coating was deposited on electrical steel as it was an active surface to attract the reduced Co which then acted as a nucleation site for further deposition of the coating. Phosphorus got trapped during the deposition. The CNTs dispersed in the solution bonded to the surface of coating due to the force of adhesion. The coating grew trapping the CNTs in it and hence Co-P-CNT was formed. The thickness of coating was dependent on the time during which GOES was in the solution.

6.3 Raman spectroscopy

Raman spectroscopy was carried out to show the presence of CNTs in the coating. The Raman spectrum of the coated samples is shown in the Figure 6.1. The main characteristic bands obtained were the D and G bands at around 1360 and 1590 cm^{-1}, respectively. The D band represents the disorder/distortions in the MWCNTs or the sp^3 bonds in the coating whereas the G band confirms the presence of graphite or the sp^2 bonds in the coating. These two bands confirm that the MWCNTs were present in the coating. All the five spots in the coated sample showed the same characteristic D and G bands which confirms that the MWCNTs were uniformly distributed in the coating. The uncoated sample did not show any characteristic D and G bands. The weight percentage of CNT in the solution was calculated to be 0.24% by the equation 6.1 shown below.

$$\frac{weight\ of\ CNTs\ in\ solution}{weight\ of\ all\ components\ in\ solution} * 100 \qquad (6.1)$$

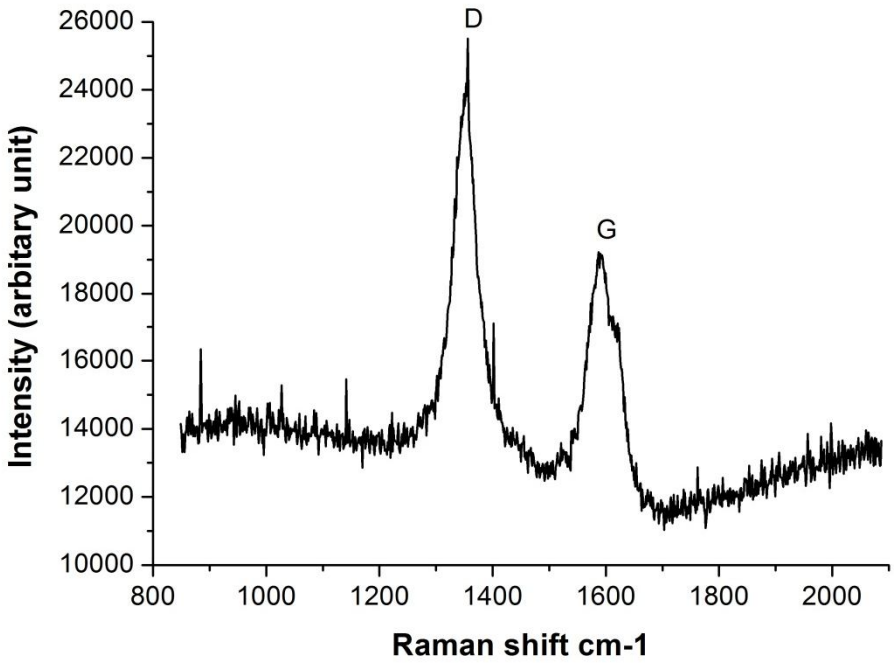

Figure 6.1 Raman spectra of the Co-P-CNT coated sample showing the D and G bands.

6.4 Scanning Electron Microscopy

Figure 6.2 shows the SEM image of a CoP1 sample. The grey area shows the substrate while the white area shows the coating. It can be seen from the SEM images that the coating makes the surface smoother by variable deposition based on the surface contours. On visual inspection the adherence between the coating and the sample was found to be intact and continuous. No gaps or cracks were found. The mean thickness of the coating was measured to be around 412 nm with a standard deviation of 26 nm for three CoP1 samples.

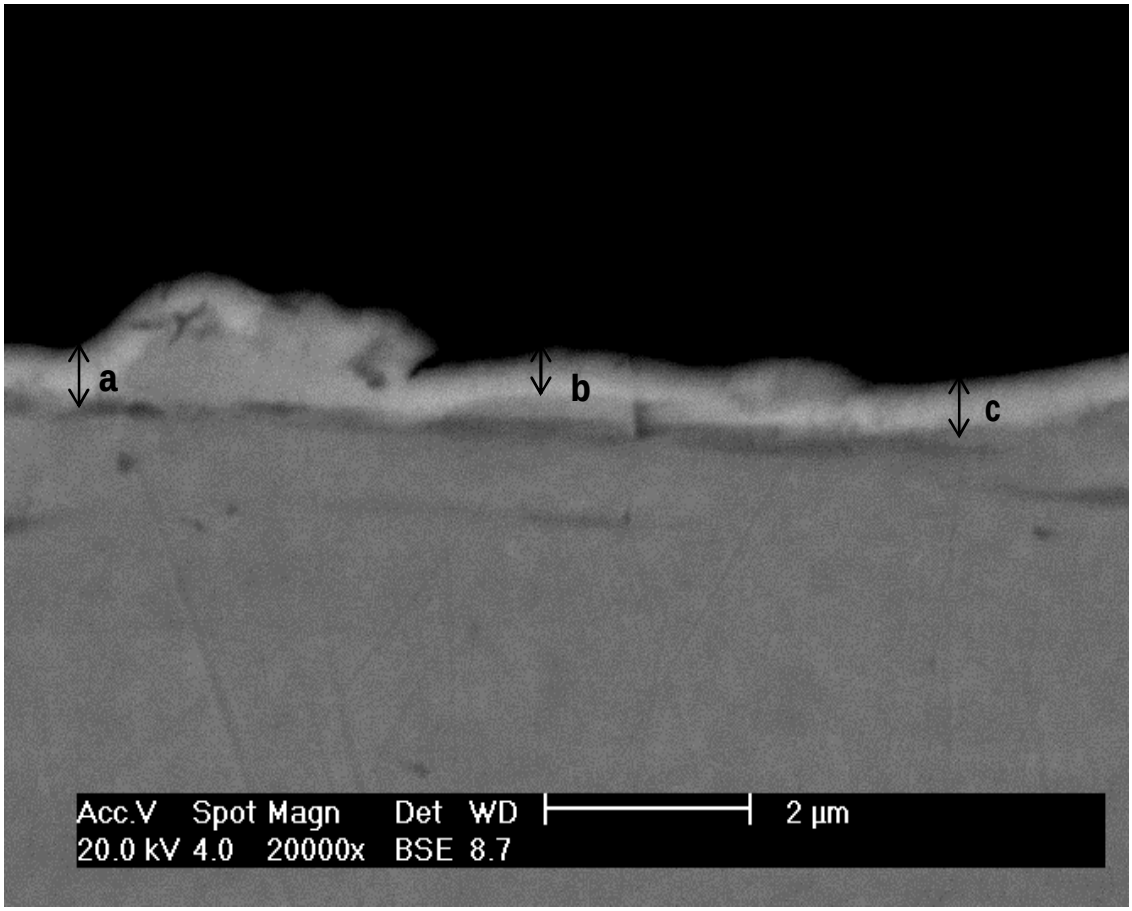

Figure 6.2 SEM image of the sample coated with Co-P-CNT for CoP1 showing thickness a= 452 nm, b= 376 nm & c=414 nm**.**

To investigate the state of CNTs in the coating high resolution SEM images were taken for the sample coated with Co-P-CNT. In Figure 6.3 it can be seen that the CNTs were not agglomerated but dispersed well throughout the coating. The dispersion of CNTs in the solution was influenced by the pH of the solution which changes the zeta potential which is the potential difference between the medium of dispersion and the particle

dispersed. The higher the magnitude of zeta potential the higher the repulsive forces between like particles and they are less likely to stick together and agglomerate. The magnitude of zeta potential of CNTs in solution increases with increase in pH value [1, 2]. The high value of pH at 9.7 did not allow the CNTs to agglomerate together in the solution and hence a good dispersion was observed in the coating.

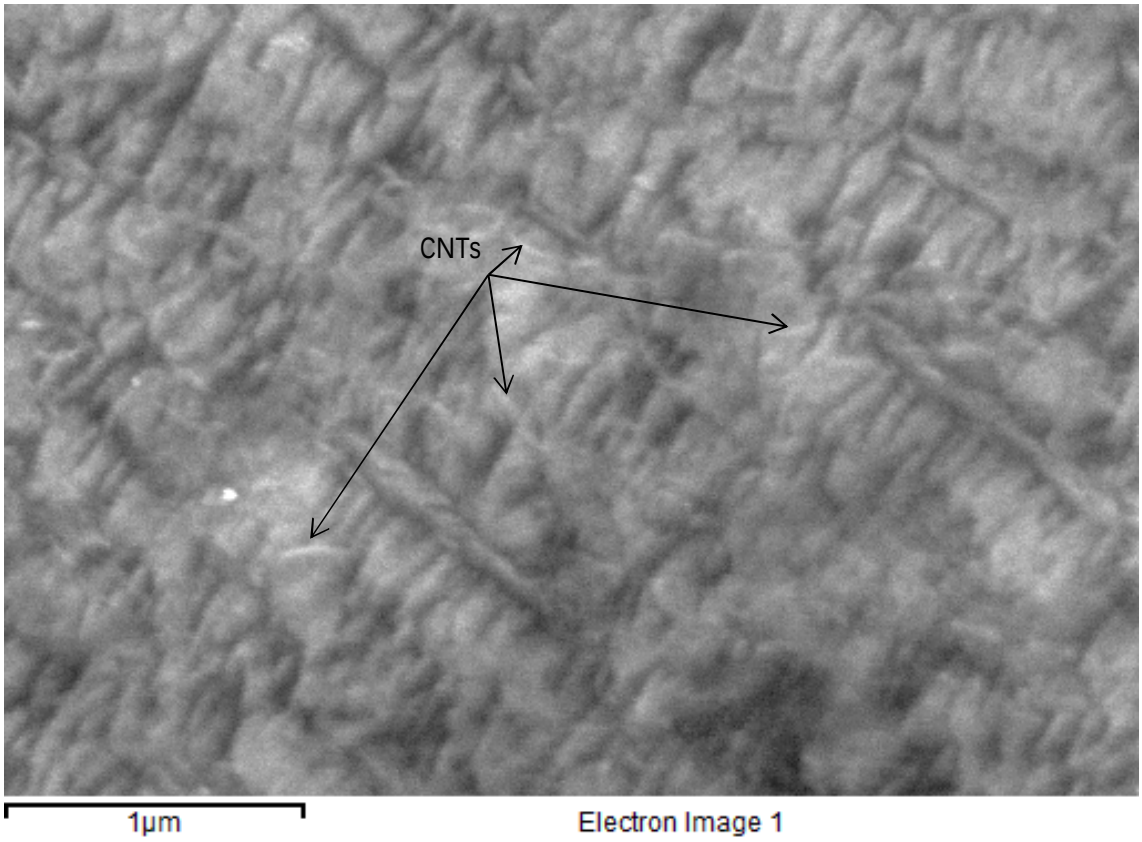

Figure 6.3 SEM image showing the CNTs dispersed in the coating.

Figure 6.4 and Figure 6.5 show the uncoated and CoP1. The rolling direction could be easily identified by the horizontal lines in both the samples. The uncoated sample had regions of elevation and depression which occurs during the rolling process. This makes the sample uneven and hence the surface roughness varies widely. On coating the sample with Co-P-CNT the depressions disappear as the coating grows in these regions while a small amount of coating grows at elevations as shown in Figure 6.5. This process makes the surface smoother than the uncoated surface and hence contributes to the improvement in surface roughness of GOES.

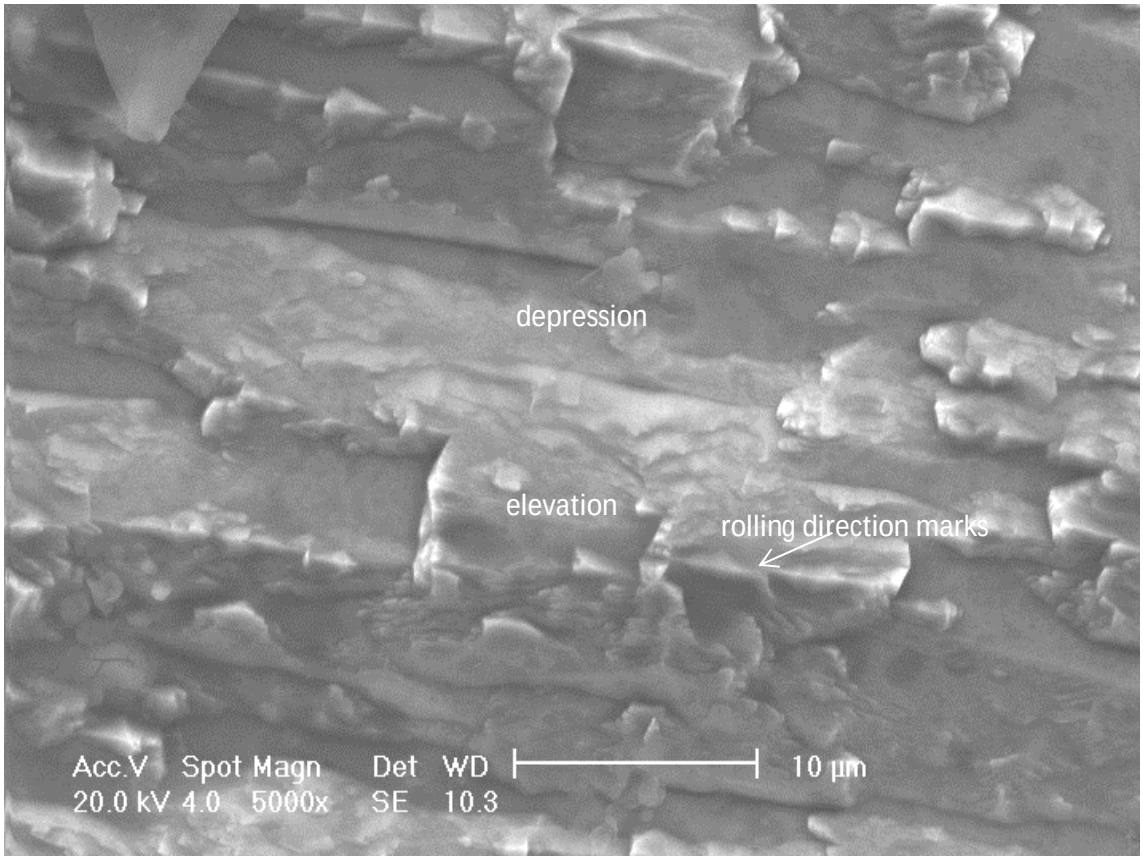

Figure 6.4 SEM image showing the surface of uncoated sample.

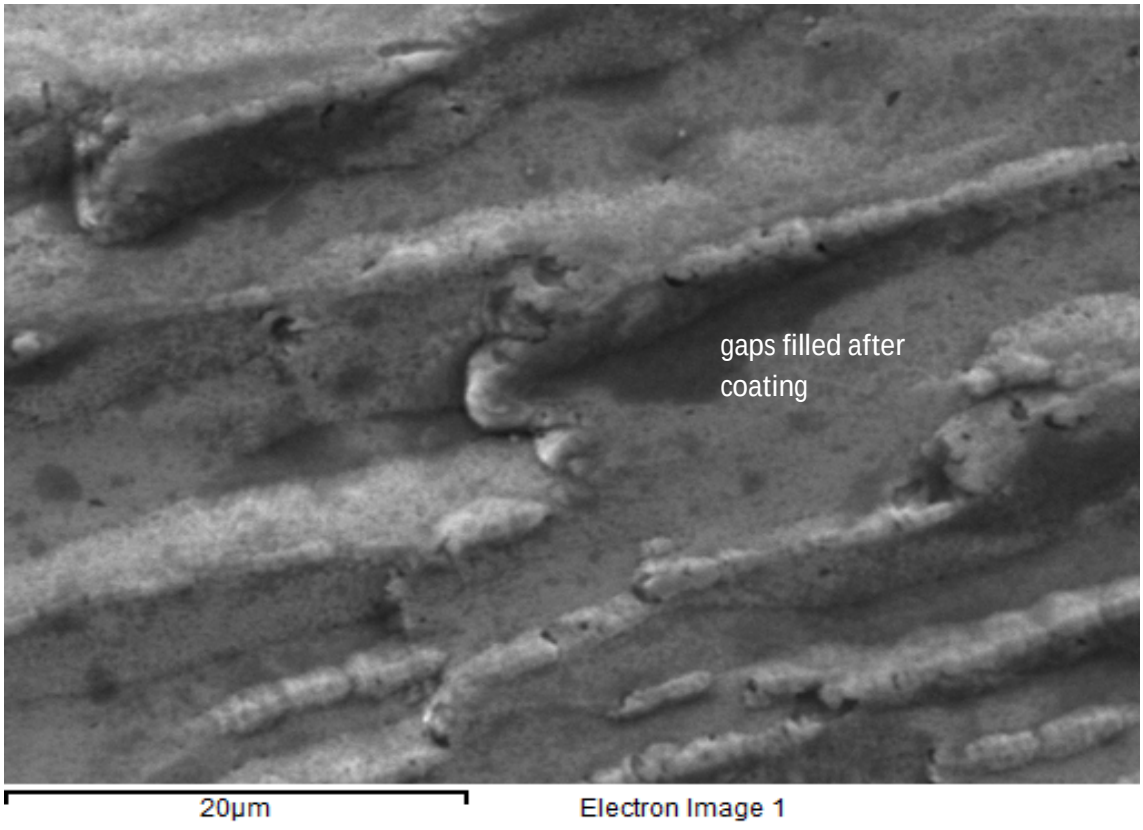

Figure 6.5 SEM image showing the surface of sample after coating with Co-P-CNT

6.5 Surface profiling

The surface roughness affects the magnetization of core material by pinning the domain walls [3]. A larger pinning occurs for samples showing high surface roughness and vice versa. The surface roughness (Ra) of uncoated, CoP3 and CoP1 was measured to be 695 ± 10 nm, 631 ± 6 nm and 437 ± 3 nm respectively as shown in Figure 6.6. The values for surface roughness of CoP1 and CoP3 were the combined values of steel substrate and the coating.

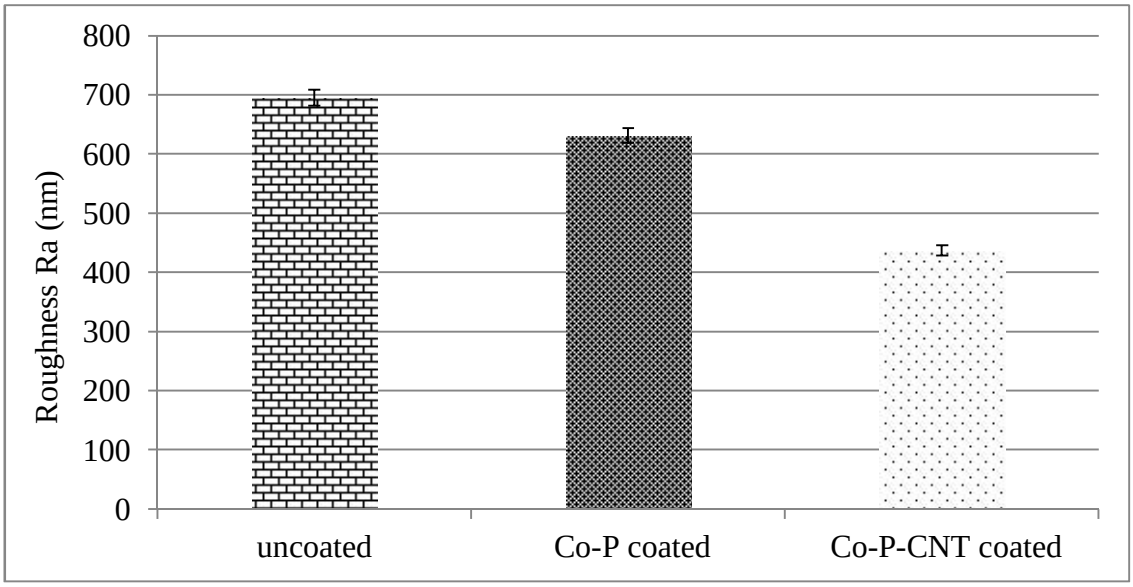

Figure 6.6 Surface roughness of uncoated, Co-P and Co-P-CNT coated GOES.

6.6 Magnetic properties of the Co-P-CNT coating

Figure 6.7 shows a hysteresis loop for the Co-P-CNT coating sample CoP1. The B-H loop measured in the VSM validates the magnetic nature of the coating. The coercivity of the coating was calculated to be 7958 A/m which is higher than that of GOES but since the coating was extremely thin the contribution of coating for power loss was negligible. The coercivity of cobalt varies widely depending upon the type of alloying elements and also upon the process route to make the material. The addition elements such as phosphorus and CNTs in the coating raise the coercivity due to the non-magnetic nature of these elements. The saturation magnetization of the CoP1 coating was measured by VSM to be 0.85T for a sample of volume (3mm x 3mm x 2µm). The saturation magnetization measured for grain oriented electrical steel was 2.0T.

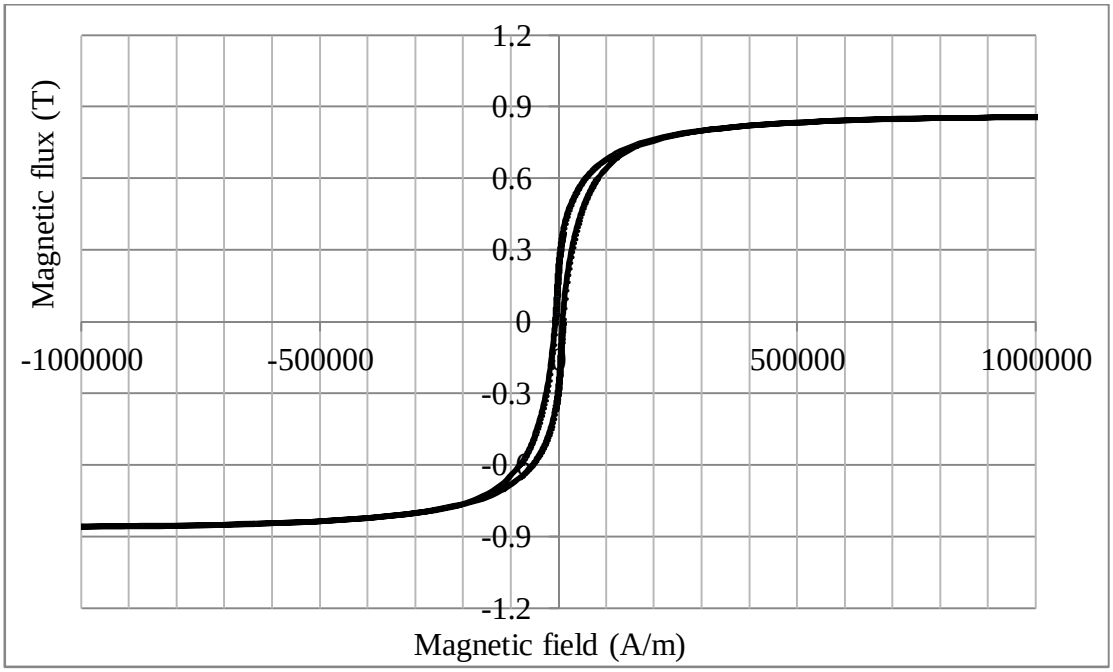

Figure 6.7 VSM measurement confirming the magnetic nature of CoP1 coating at pH of 9.7.

6.7 Power loss and resistivity of Co-P-CNT coated GOES samples

Figure 6.8 shows the average results of five uncoated, Co-P and Co-P-CNT coated samples for two magnetic flux densities of 1.5 and 1.7T. It can be seen from Figure 6.8 that the CoP1 samples show an improvement ranging 13 to 15 % in power loss at magnetic flux density of 1.7T and 50 Hz frequency. To study the effect of CNTs in the coating, a sample was coated with Co-P without the addition of CNTs (CoP3). The coated sample did not show any improvement in power loss as shown in Figure 6.8 which confirms that the improvement was only due to the presence of CNTs in the coating. The resistivity of the coating was calculated to be 10^4 μΩcm. It is proposed that the enhancement in electrical resistivity was due to the disorder in the lattice structure of cobalt by co-deposition of phosphorus and CNTs in the coating.

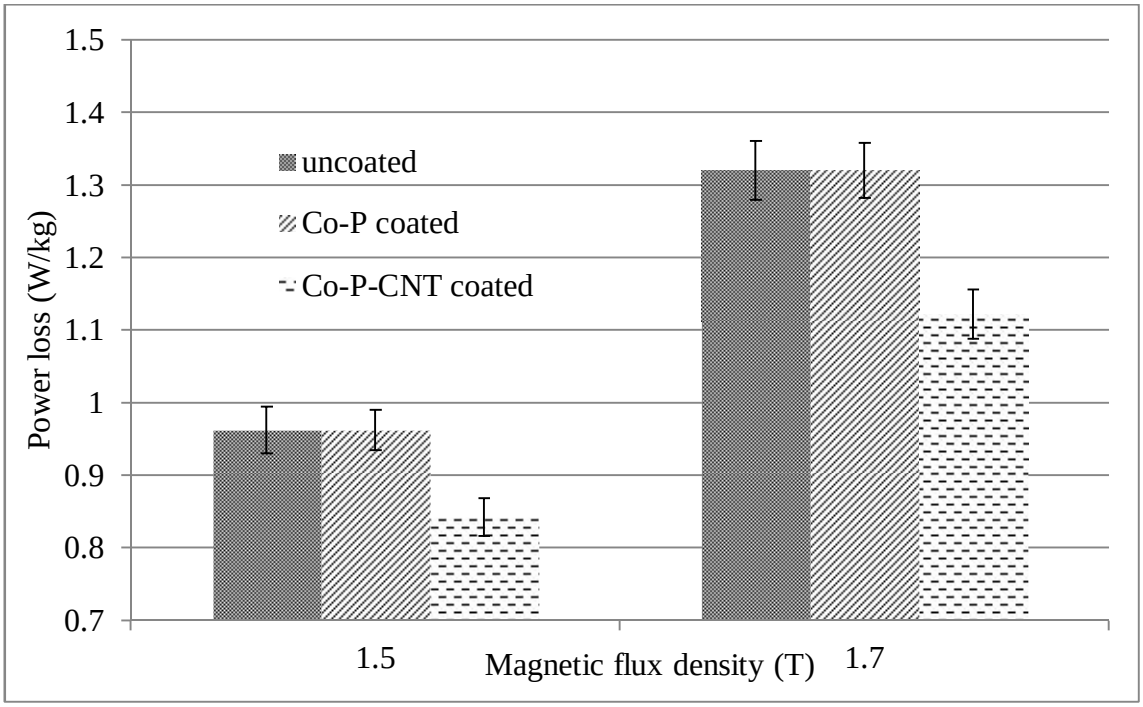

Figure 6.8 Power loss of uncoated, CoP3 and CoP1 sample at 1.5 and 1.7T flux densities and 50Hz frequency (average of five samples).

6.8 Loss separation

The power loss was separated as described in section 2.4.4. The values were plotted over a range of frequencies from 10Hz to 1000Hz. The value of correlation coefficient r^2 [4] was 0.9994 & 0.9998 for the uncoated and Co-P-CNT coated sample. On plotting the loss separation graph before and after coating, the results shown in Figure 6.9 were obtained. It can be clearly seen from the figure that the coated sample shows a significant reduction of 0.27 W/kg in hysteresis loss while the eddy current and anomalous loss increase was insignificant.

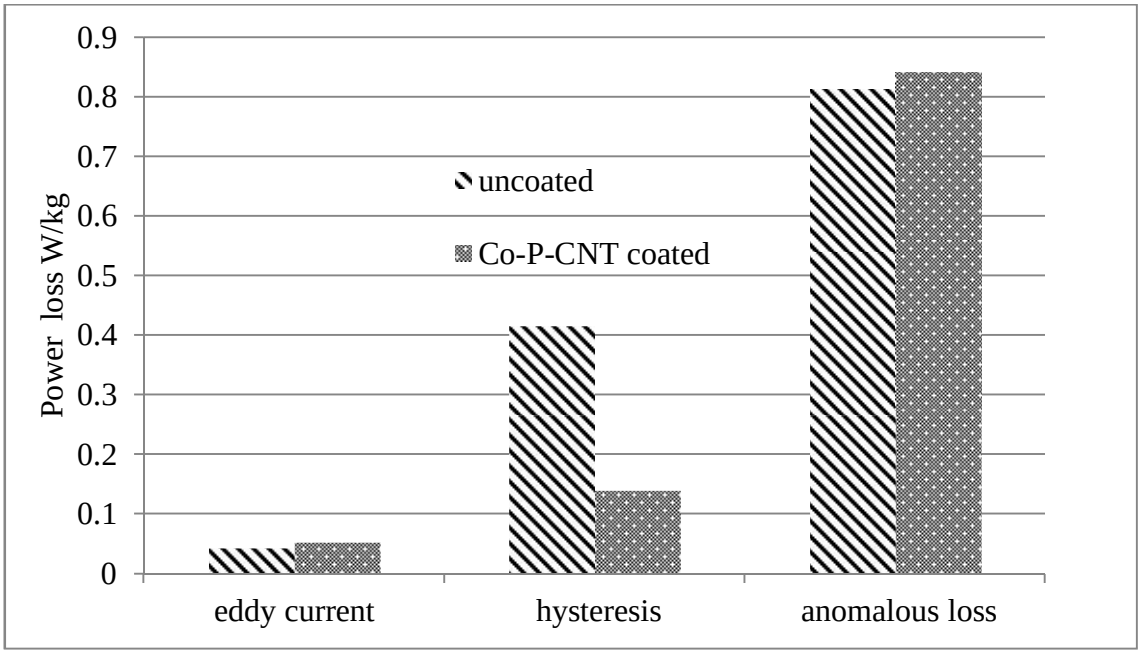

Figure 6.9 Loss separation for the uncoated and CoP1 sample at a flux density of 1.7T and 50Hz frequency.

The surface roughness affects the hysteresis loss as explained in section 5.2.9. Improvement in surface roughness would lead to an increase in the number of mobile domains and reduce the energy consumption which reduces the total loss. The improvement in surface roughness by chemical polishing of the sample to a mirror finish [5] is a tedious method and could not be applied on a production line. The use of electroless plating for depositing Co-P-CNT composite coating on the surface of grain oriented electrical steel to improve the surface roughness could be used as a replacement method instead of mechanical polishing. Improving the surface roughness with a non-magnetic coating would not contribute to an improvement in magnetic properties of the material as the magnetic path on the surface of grain oriented electrical steel remains the same so a magnetic material could only be used. It is proposed that the enhancement of magnetic properties in Co-P-CNT coated sample was due to the improvement in surface roughness by the magnetically active coating. Jiang et. al [6] deposited Co films on smooth and rough surface and found that the coercivity was three times higher when the films were deposited on rough surface. M. Li et. al [7] deposited Co films on plasma etched (0-100 min) Si substrates and found that the hysteresis loop was widened in 100 min etched sample as the roughness increased due to etching. In smoother films the magnetic reversal was dominated by magnetization rotation whereas

in rough films the predominant phenomenon was domain wall motion where pinning of mobile domains leads to loss of energy.

6.9 Stacking factor

The stacking factor calculated for 414 nm thick coating by joining sheets of 0.3 mm thickness was 99.73% as compared to 97.4% for conventional coating assuming it be 4 µm thick as shown below.

$$stacking\ factor(\%) = (1 - \frac{Non - magnetic\ material\ in\ the\ core}{Total\ material\ in\ the\ transformer}) * 100$$

If the coating was non-magnetic, the thickness of coating on both sides = 800 nm

The thickness of Epstein strip without coating = 300 micron

Thickness with coating = 300.8 micron

$$stacking\ factor(\%) = (1 - \frac{0.8}{300.8}) * 100$$

$$stacking\ factor(\%) = 99.73$$

The replacement of a non-magnetic coating by Co-P-CNT would further increase the stacking factor by adding a soft magnetic material in the transformer core as compared to the non-magnetic coating material. The new value of stacking factor calculated by considering the saturation magnetization of Co-P-CNT coating (0.86T) and that of GOES as 2 T was 99.85 % as shown below. The increment in stacking factor due to the magnetic activity of the coating was insignificant.

$$Net\ magnetic\ contribution\ of\ the\ coating\ as\ compared\ to\ GOES = (\frac{0.86}{2}) * 100)$$

$$Net\ magnetic\ contribution\ of\ the\ coating\ as\ compared\ to\ GOES = 43\%$$

$$New\ stacking\ factor(\%) = 99.73 + ((\frac{100 - 99.73}{100}) * 43)$$

$$New\ stacking\ factor(\%) = 99.85$$

6.10 X-Ray Diffraction

The XRD histograms of the uncoated and CoP1 samples are compared in Figure 6.10. The peaks observed in the coated sample were that of cobalt and iron while only iron peak was noticed in the uncoated sample. The diffusive nature of cobalt and iron peak suggests that the coating was amorphous in nature. The iron peak in Co-P-CNT coated sample was not shifted with respect to their position for the uncoated particles. This suggests that no stress was developed during the coating process.

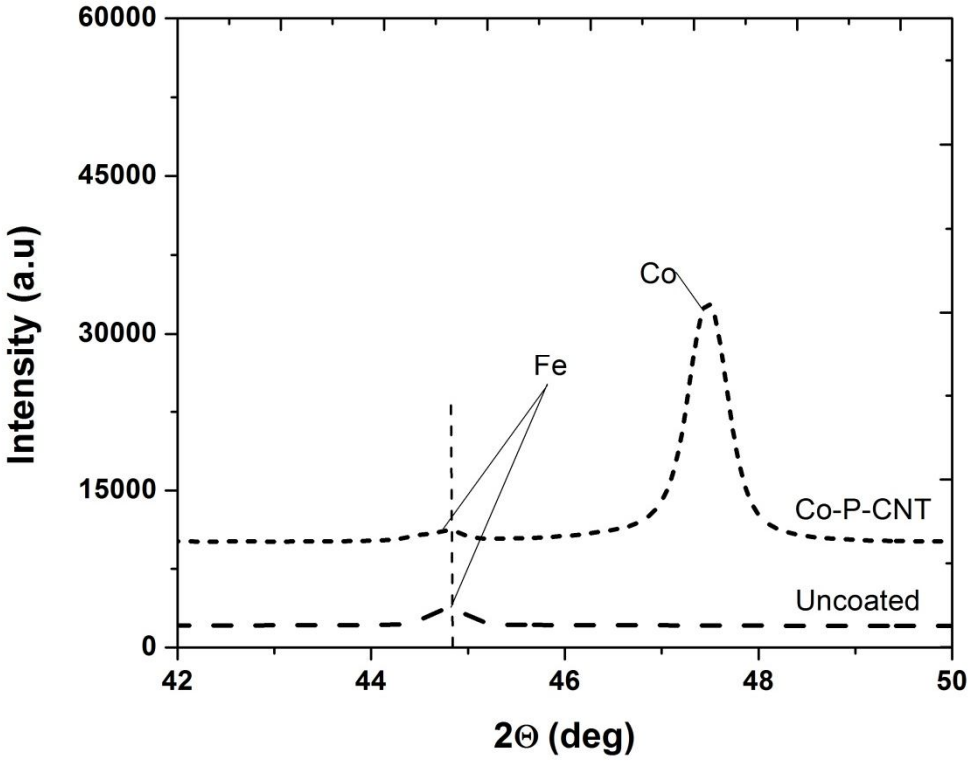

Figure 6.10 XRD of uncoated and Co-P-CNT coated sample.

6.11 Conclusions

The effect of Co-P-CNT coating on the magnetic properties of GOES was investigated. To analyse the coating, Raman spectroscopy, Vibrating Sample Magnetometer (VSM), single strip testing, scanning electron microscopy (SEM) and talysurf surface profilometry were performed. Raman spectra showed the D and G band which corroborates the presence of MWCNTs in the coating. The magnetic nature of the coating was confirmed by VSM results. Power loss results show an improvement ranging 13-15% after coating with Co-P-CNT compared to 4-6 % improvement by the conventional coating. The resistivity of the coating was measured to be 10^4 μΩcm which is higher than that of GOES with resistivity of 48 μΩcm. The loss separation data plotted before and after coating shows that the hysteresis loss was reduced after coating. The thickness of the coating was found to be 414 ± 40 nm by the SEM. The surface profilometry results showed that the surface roughness improved after coating the sample.

6.12 References

[1] H. Xie, H. Lee, W. Youn, and M. Choi, "Nanofluids containing multiwalled carbon nanotubes and their enhanced thermal conductivities," *Journal of Applied Physics*, vol. 94, pp. 4967-4971, 15 October 2003.

[2] J. Sun and L. Gao, " Development of a dispersion process for carbon nanotubes in ceramic matrix by heterocoagulation," *Carbon*, vol. 41, pp. 1063-1068, 2003.

[3] T. Wada, T. Nozawa, and T. Takata, "Method for producing a super low watt loss grain oriented electrical steel sheet," *US Patent*, vol. 3932236, January 13, 1976.

[4] R. Taylor, "Interpretation of the correlation coefficient: A basic review," *Journal of diagnostic medical sonography*, vol. 6, pp. 35-39, 1990.

[5] H. Yamaguchi, M. Muraki, and M. Komatsubara, "Application of CVD method on grain-oriented electrical steel," *Surface & Coatings Technology*, vol. 200, pp. 3351-3354, 2006.

[6] Q. Jiang, H. N. Yang, and G. C. Wang, "Effect of interface roughness on hysteresis loops of ultrathin Co films from 2 to 30 ML on Cu(001) surfaces " *Surface Science*, vol. 373, pp. 181-194, 1997.

[7] M. Li, G. C. Wang, and H. G. Min, "Effect of surface roughness on magnetic properties of Co films on plasma-etched Si(100) substrates," *Journal of Applied Physics*, vol. 83, pp. 5313-5320, 1998.

7 Ceramic coatings to improve the magnetic properties of GOES

7.1 Introduction

The aim of this work was to investigate different ceramic coatings (CrN, CrAlN and TiAlN) on GOES to reduce power loss and magnetostriction. The coatings were tested in single strip tester and magnetostriction measuring system to compare the magnetic properties of conventional coated, ceramic coated on top of forsterite and ceramic coated on uncoated samples. These coatings were characterised using optical microscopy, GDOES and magnetic domain viewer to measure the thickness, chemical composition and domain behaviour.

7.2 Characterisation of coatings

Table 7.1 highlights the sample id's with the coating type and starting surface condition.

Sample ID	Type of coating	Surface before coating
CrN1	CrN	Forsterite
CrAlN1	CrAlN	Forsterite
TiAlN1	TiAlN	Forsterite
CrN2	CrN	Uncoated
TiAlN2	CrAlN	Uncoated

Table 7.2 Highlights the main characteristics of the ceramic coatings.

Properties	**CrN**	**CrAlN**	**TiAlN**
Thickness on forsterite (µm)	2.65 ± 0.15	1.9 ± 0.2	3.20 ± 0.10
Thickness on uncoated (µm)	2.15 ± 0.15	NA	2.55 ± 0.15
Young's modulus (GPA)	200	270	632
Bonding with forsterite	Not good	Not good	good
Bonding with uncoated	good	NA	good
Colour	silver	Pale bule/silver	Bright blue/black
Hardness	2700 HV	3000 HV	3000 HV

Table 7.1 shows the sample identities for different types of ceramic coatings and the starting surface before coating. The important characteristics of the ceramic coating are shown in Table 7.2. The CrN1 and CrAlN1 did not show good bonding as gaps were found between the forsterite and the ceramic coating as shown in Figure 7.1(a-c). To overcome this problem samples were prepared on uncoated surface namely CrN2 and TiAlN 2 as shown in Figure 7.2 (a) and (b). It can be seen from the figures that the coating was completely bonded with the substrate showing no gaps in between. The bonding between the substrate and the ceramic coating affects the magnitude of stress applied by the coating on GOES.

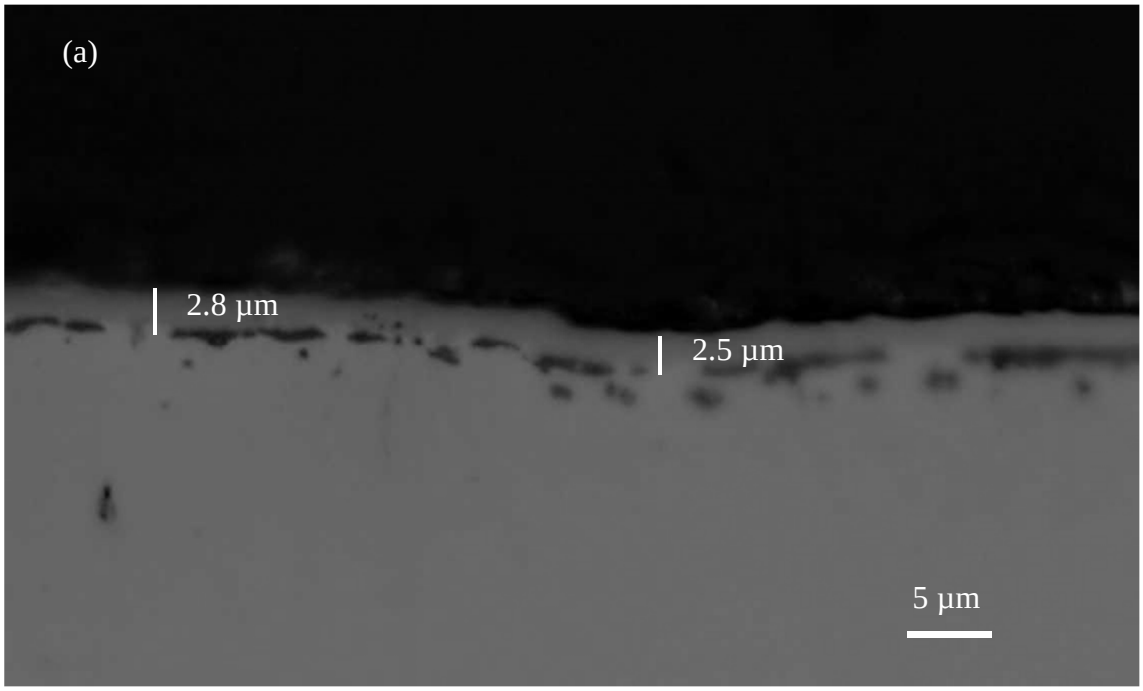

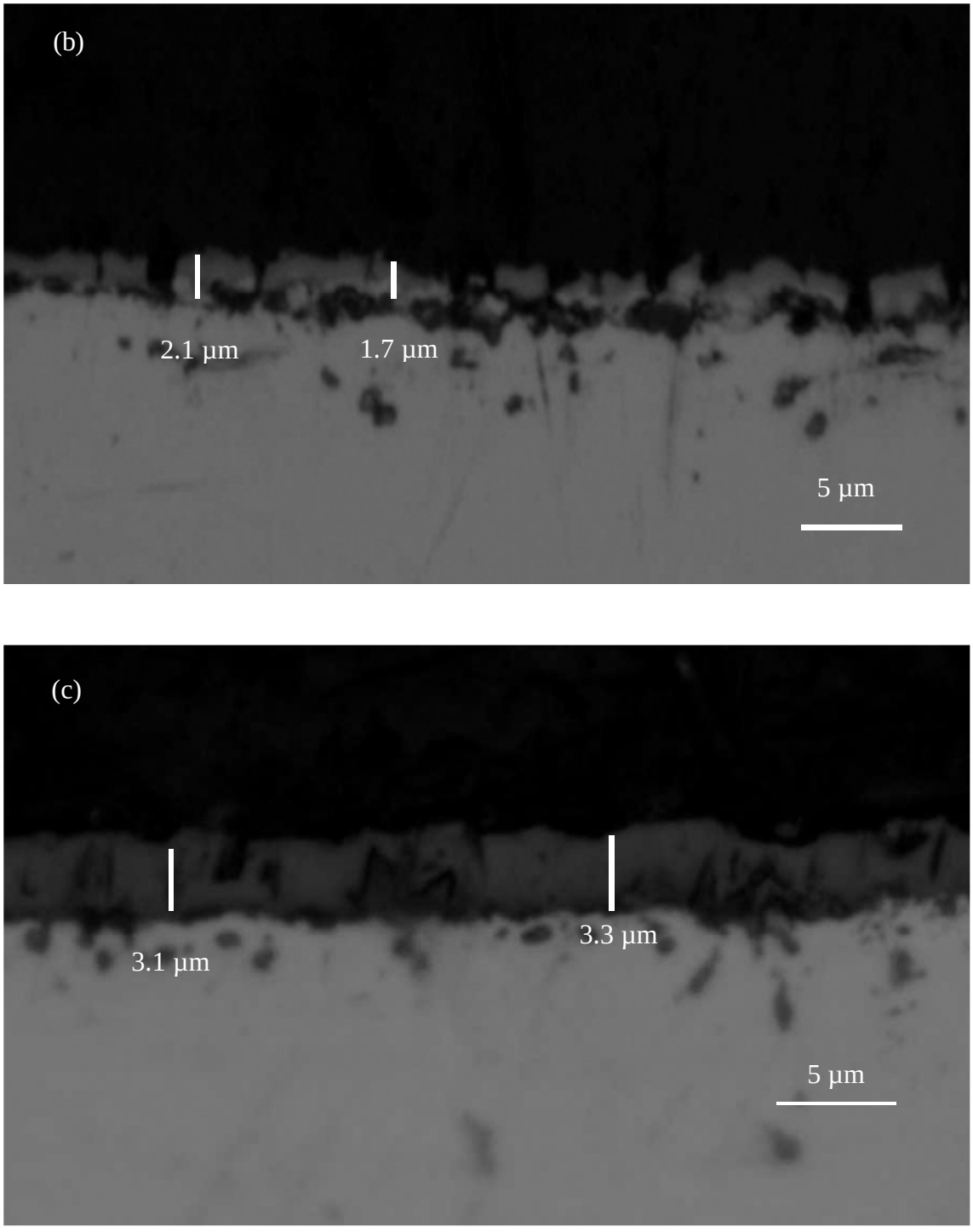

Figure 7.1 Optical microscopy image of (a) CrN1 (b) CrAlN1 (c) TiAlN1.

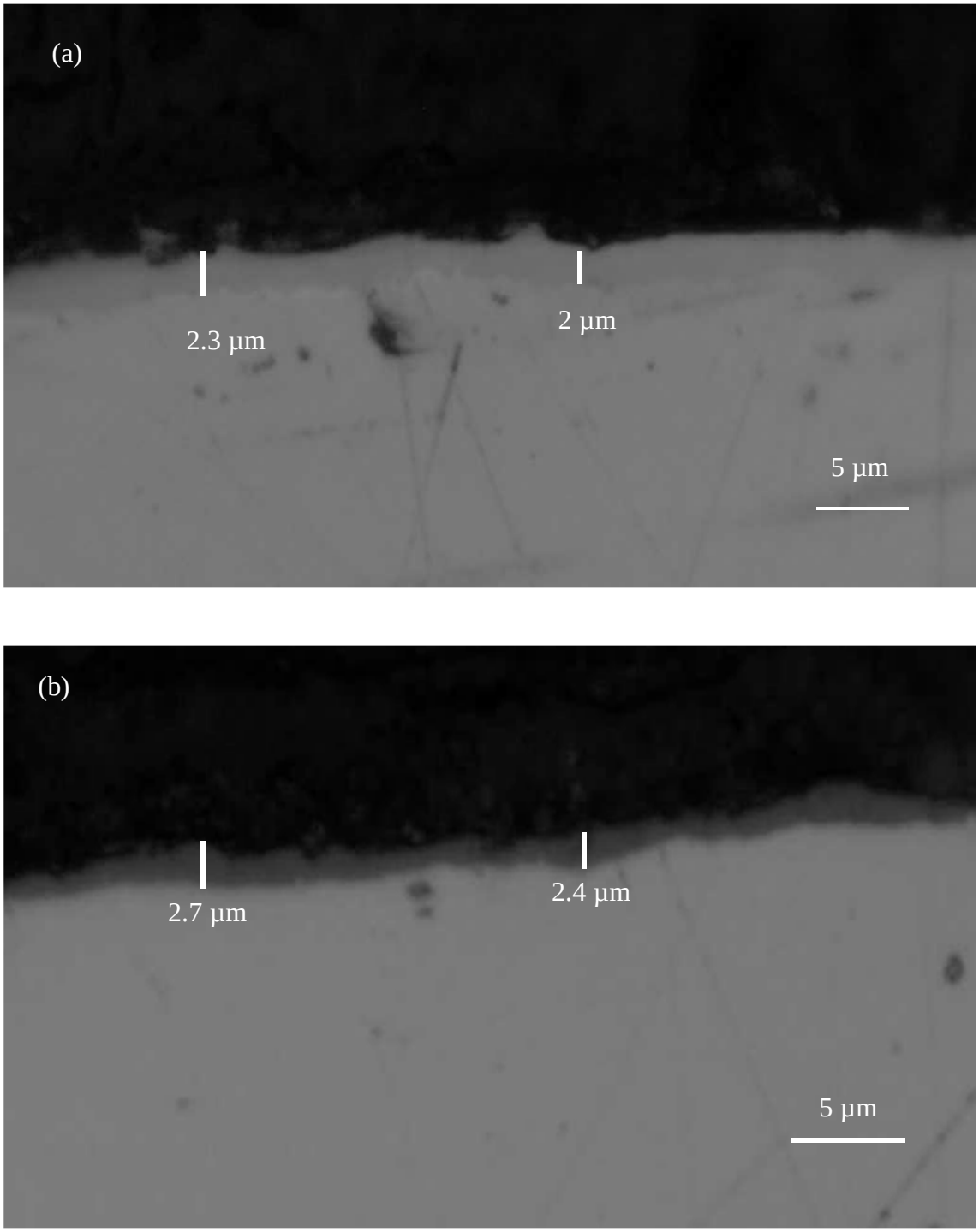

Figure 7.2 Optical microscopy image of (a) CrN2 (b) TiAlN2 coating.

7.3 Spectroscopy

The chemical composition of the coating was determined by using Glow Discharge Optical Emission Spectroscopy (GDOES) as described in section 4.15. The results obtained for the CrN1 coating are shown in Figure 7.3 (a) and (b). The coating thickness was estimated to be around 2.5-3 µm based upon the chromium and nitrogen emission in the GDOES which corroborates the optical microscopy images. Figure 7.3 (a) shows chromium content in the coating ranges from 60-68 % and the nitrogen varied accordingly up to a thickness of 2 µm. In the thickness range of 2 to 3 µm the Cr and N content decreased and Mg, O and Si increased which means that during the deposition process some amount of Cr and N penetrated in the forsterite layer which is shown in Figure 7.3 (b). This penetration disturbs the bond structure of the forsterite which introduces stress in the coating [1].

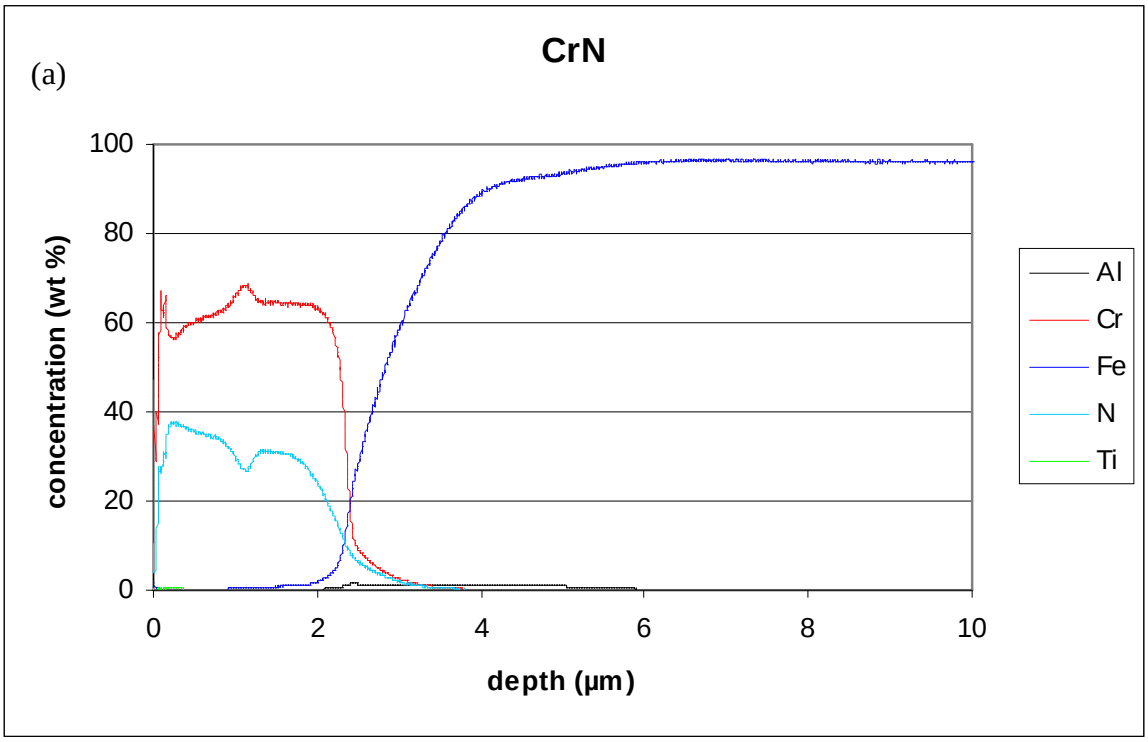

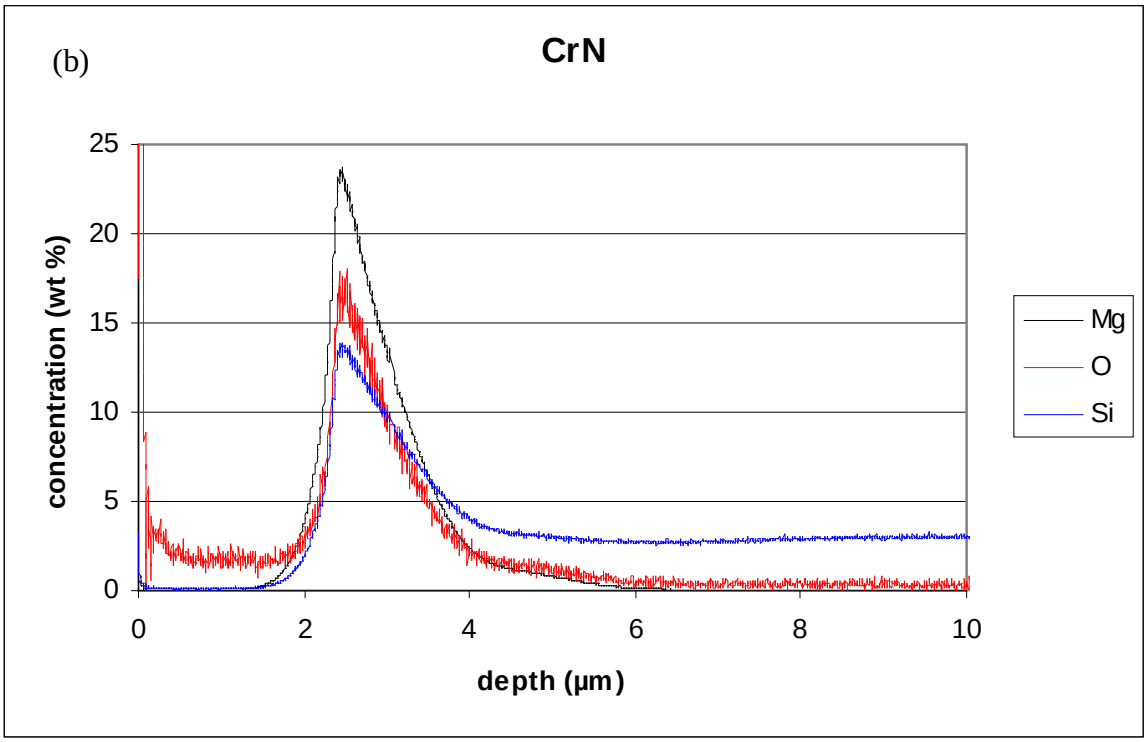

Figure 7.3 Chemical composition of the coating through thickness (a) chromium nitride layer (b) forsterite layer.

The results obtained for CrAlN1 from the GDOES are shown in Figure 7.4 (a) and (b). The thickness of the coating was approximated to be around 1.9 ± 0.2 µm from this technique and contained two distinct areas. The percentage of Cr in the coating varied from 40-60% with higher percentage near the interface. The aluminium and nitrogen contents followed an opposite concentration gradient, i.e. higher concentrations at the surface with the aluminium increasing from 0% at the interface to around 20 % at the surface. This behaviour suggested that during deposition a thin layer of CrN was laid first on which a layer of CrAlN was deposited. In the region from 1.5-2 µm there was an overlap of chemicals from the forsterite coating and CrAlN coating as shown in Figure 7.4 (a, b) which suggests that the Cr, Al and N atoms of the CrAlN coating were embedded in the forsterite layer which disturbs the bond structure of the forsterite coating and introduces stress in the coating.

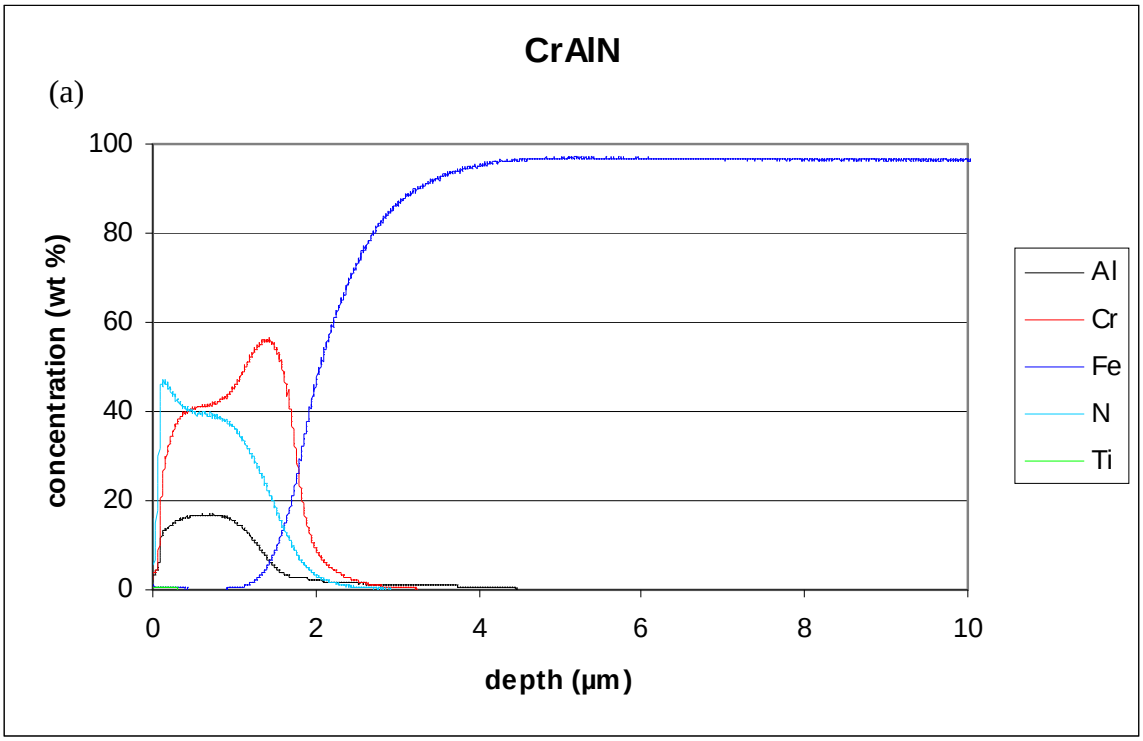

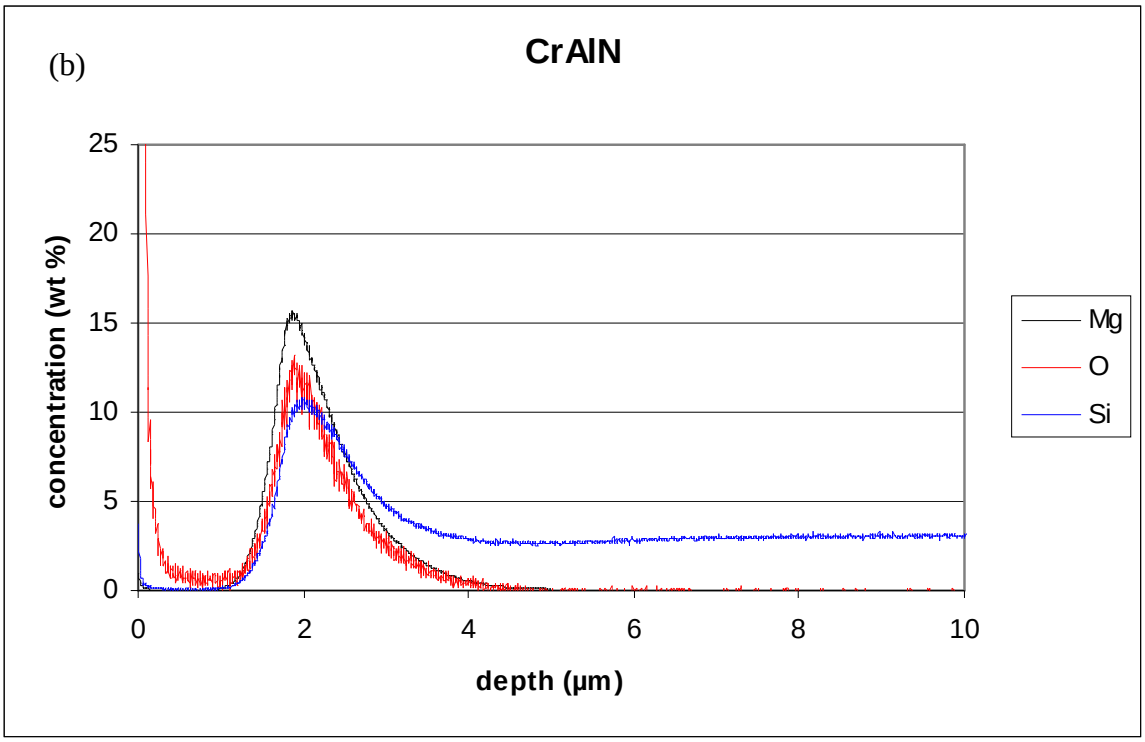

Figure 7.4 Chemical composition of the coating through thickness (a) chromium aluminium nitride layer (b) fayalite/forsterite layer.

The results obtained for TiAlN1 from the GDOES are shown in Figure 7.5 (a) and (b). The coating was homogeneous, according to the depth profiles of Al, Ti and N, the signal of N decreasing slightly from surface to interface. The titanium content was found to be around 30-35%, aluminium was around 15-18% and the nitrogen content varied from 50% at the surface to around 40% at the interface. The coating was thicker than the other coatings as the thickness measured from the GDOES was around 3 µm. The penetration of TiAlN coating in forsterite was deeper because of the higher substrate temperature (Section 4.7.3) which allows more diffusion and it imparted more stress than the CrN and CrAlN coating system.

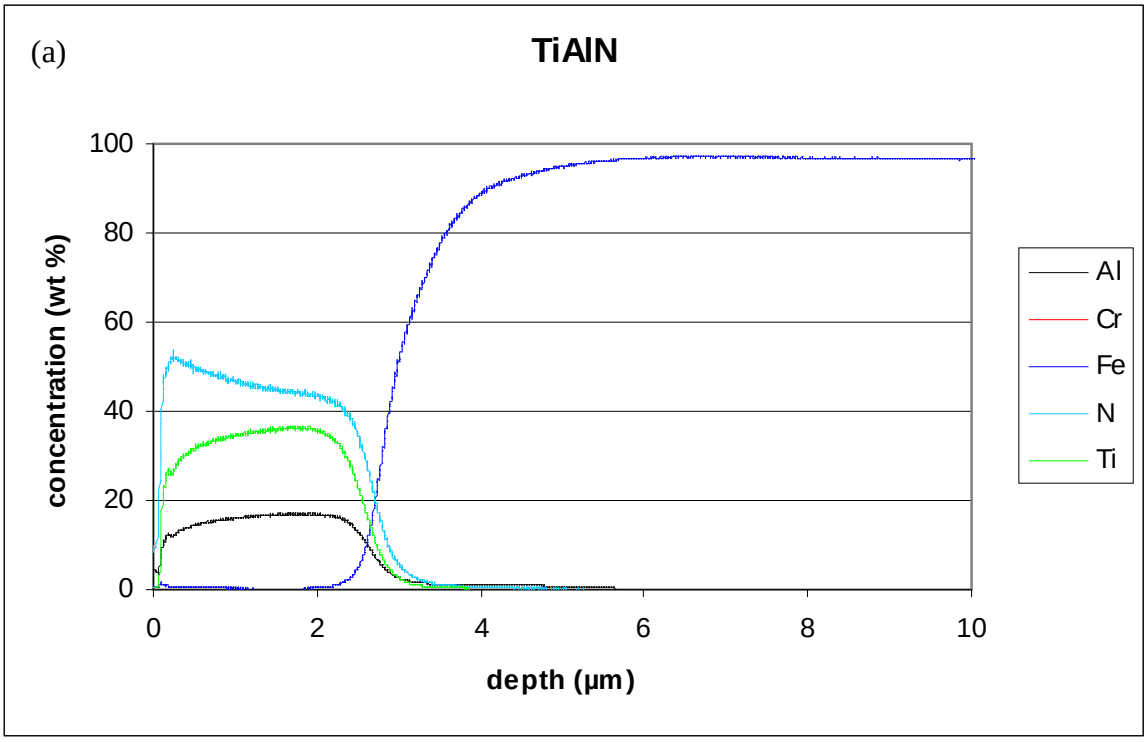

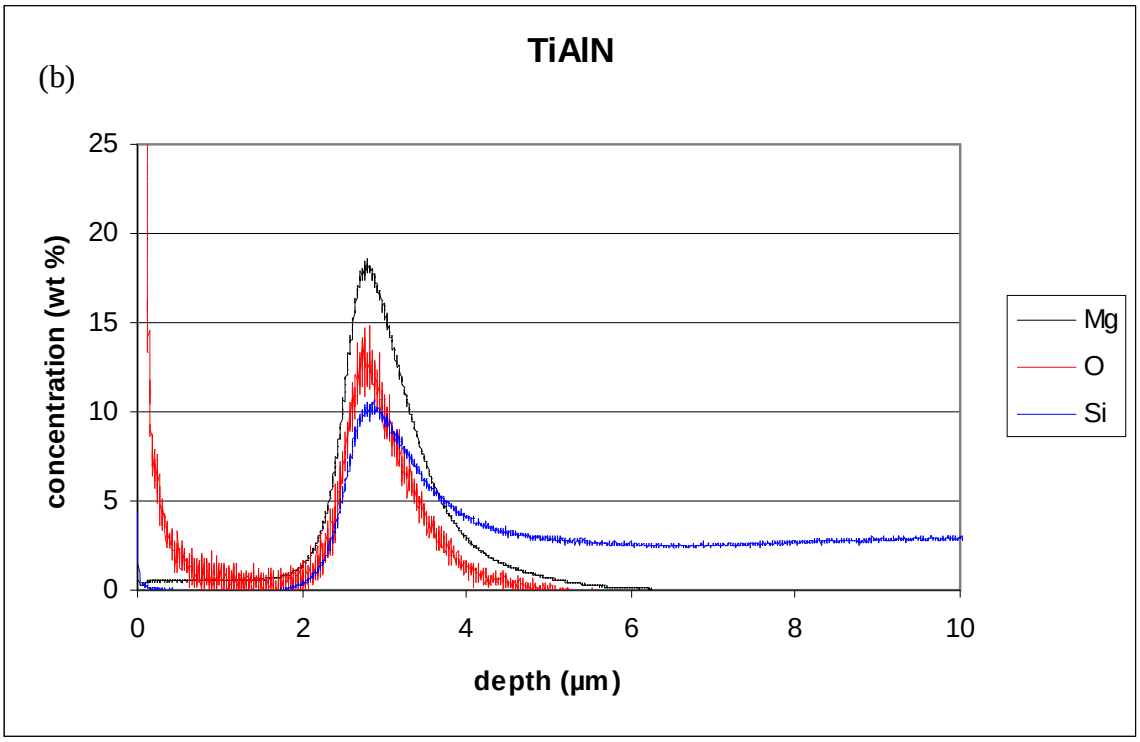

Figure 7.5 Chemical composition of the coating through thickness (a) Titanium aluminium nitride layer (b) fayalite/forsterite layer.

7.4 Stress calculation based on single side coated steel

The generation of stress in the ceramic coating was confirmed by coating the GOES samples on one side. GOES samples without any coating and with forsterite coating were coated with CrN and TiAlN coating as shown in Figure 7.6. The single side coated samples bent inwards forming a convex shape on the coating side. Stress was measured based upon the formula explained in section 5.2.9.

The Young's modulus (E) of GOES in rolling direction was 113 GPa,

Thickness of the strip (t) was 0.27 mm,

Radius of curvature calculated for TiAlN2 using x = 38 mm and a = 145 mm was 276.65 mm.

$$\sigma_{max(TiAlN)} = 55.11 \text{ MPa}$$

Similarly the maximum stress for CrN2 was calculated to be 20.33 MPa using

Radius of curvature =750.135 mm with x = 15 mm, a= 150 mm

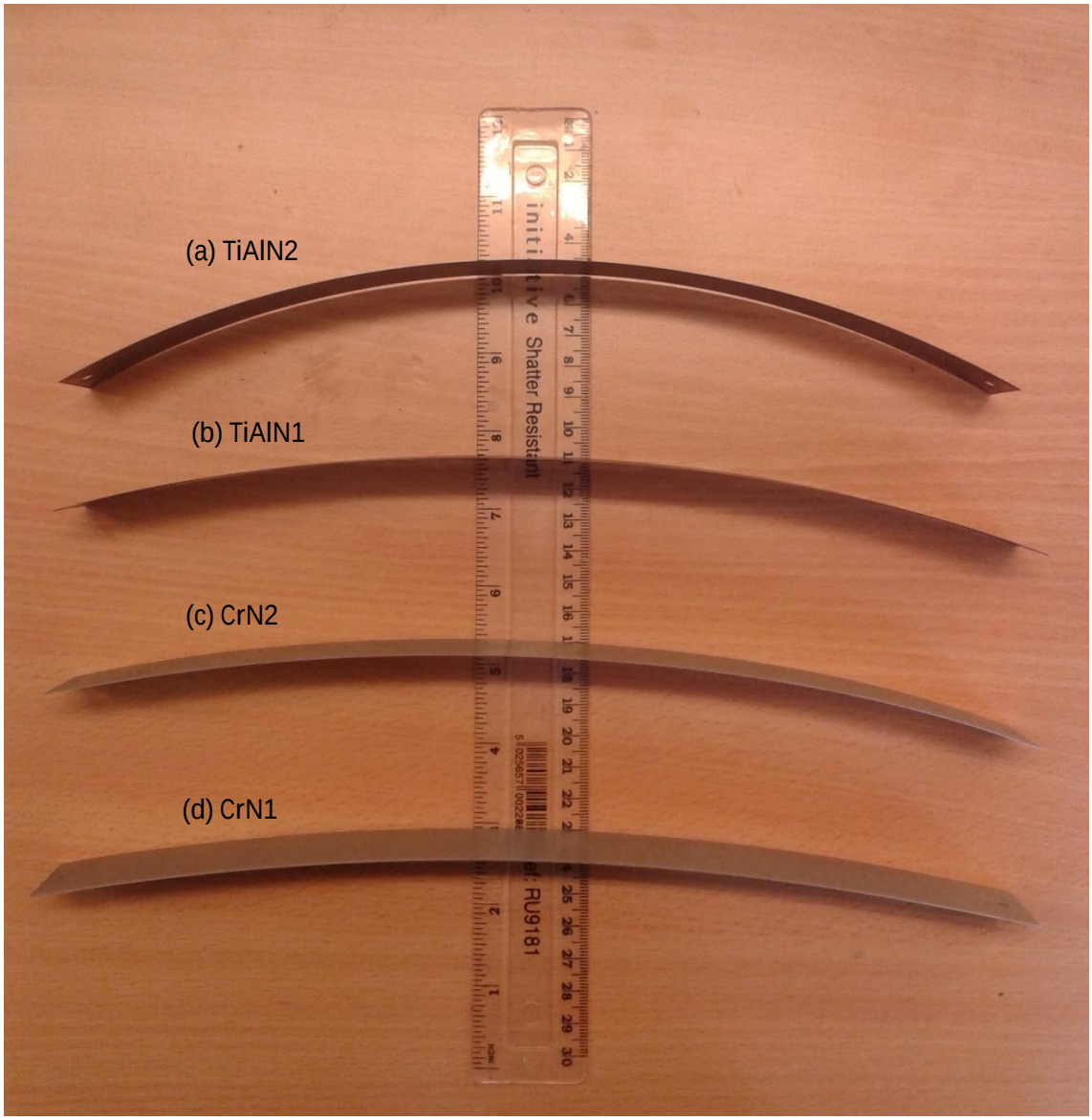

Figure 7.6 Single side coated (a) TiAlN2 (b) TiAlN1 (c) CrN2 (d) CrN1 showing generation of compressive stress in the coating.

The radius of curvature and stress was also calculated for CrN1 and TiAlN1 separately as R = 508 mm, $\sigma_{max(TiAlN)}$ = 30.02 and R = 814 mm and $\sigma_{max(CrN)}$ = 18.73MPa respectively. The samples were not as bent for the forsterite coated with ceramic as compared to ceramic on uncoated GOES. This was explained in section 7.2.

7.5 Magnetic Domain imaging

To understand the effect of coating stress on GOES, all ceramic coated samples were imaged under a magnetic domain viewer. Figure 7.7 shows domain images of (a) uncoated sample (b) forsterite coated (c) CrN2 (d) CrN1 (e) CrAlN1 (f) TiAlN2 (g) TiAlN1. The results obtained from domain imaging were in agreement with the stress calculations made in section 7.4 as the domain width was narrowed upon the application of stress shown in Figure 7.8. The uncoated sample had wide domain spacing with a domain width of 1.2 mm which was narrowed after coating it with forsterite coating to 0.76 mm. The CrN1 and CrAlN1 coated samples reduced the domain spacing further to 0.42 mm but the best results were obtained when the GOES samples without the forsterite coating were coated with ceramic coating which reduced the domain width to 0.31mm. This could be explained on the basis of bonding tendencies of the coating and the substrate. The CrN and CrAlN coating did not bond well with forsterite coated GOES as shown in Figure 7.1 (a) and (b) but these ceramic coating were well bonded with uncoated steel so the magnitude of stress applied by the coating on GOES was more when the bonding was good. For TiAlN1 and TiAlN2 the bonding was similar so same stress was applied each time and hence similar domain narrowing was achieved in both the cases.

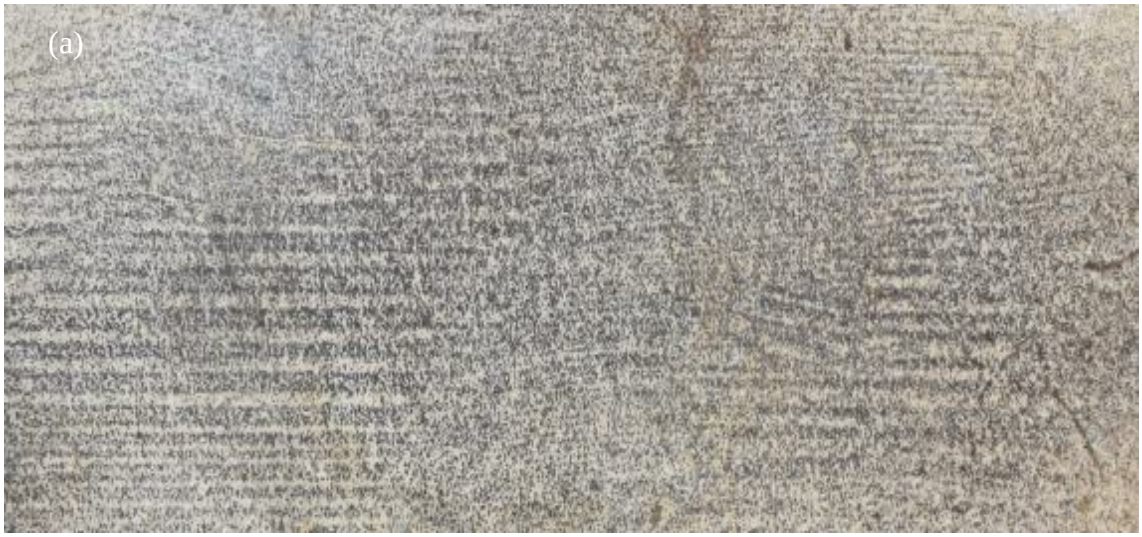

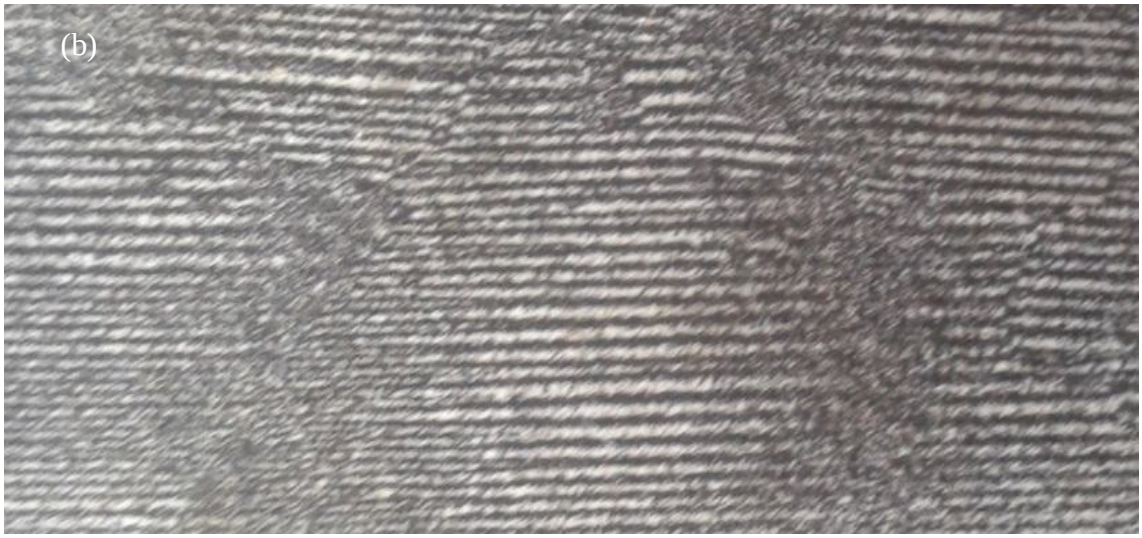
(b)

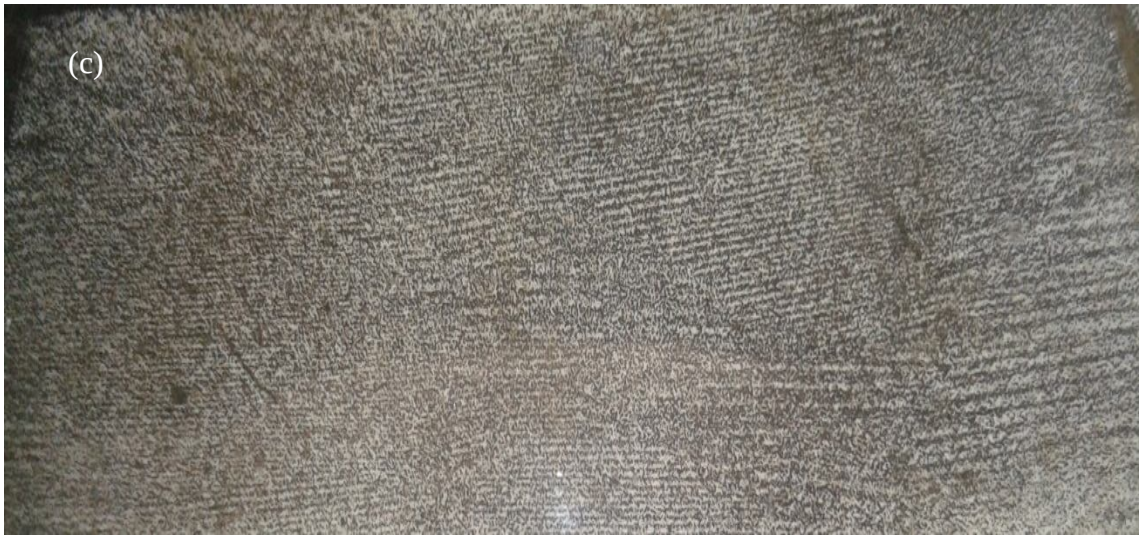
(c)


(d)

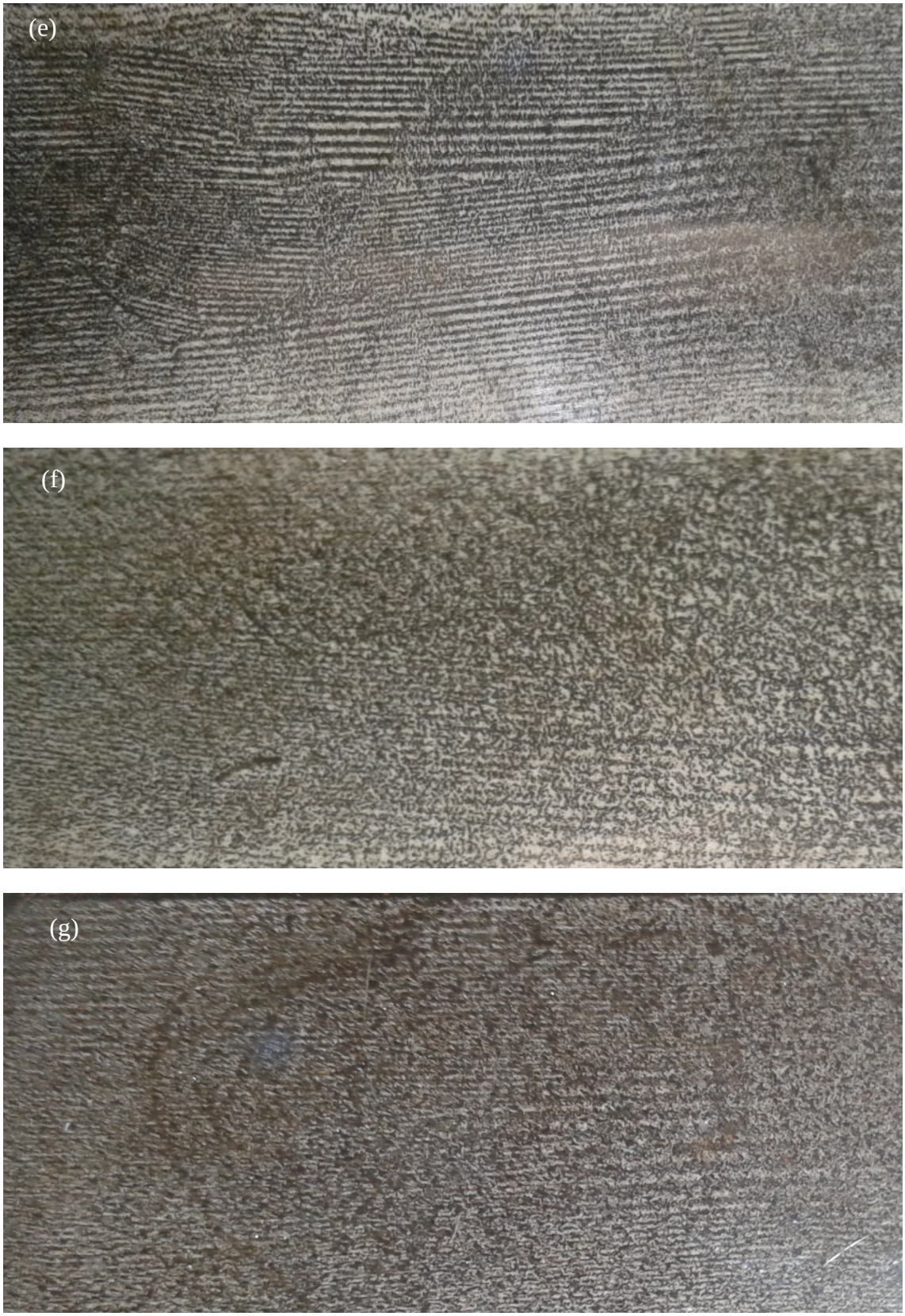

Figure 7.7 Magnetic domain images of the (a) uncoated sample (b) forsterite coated (c) CrN2(d) CrN1 (e) CrAlN1 (f) TiAlN2 (g) TiAlN1.

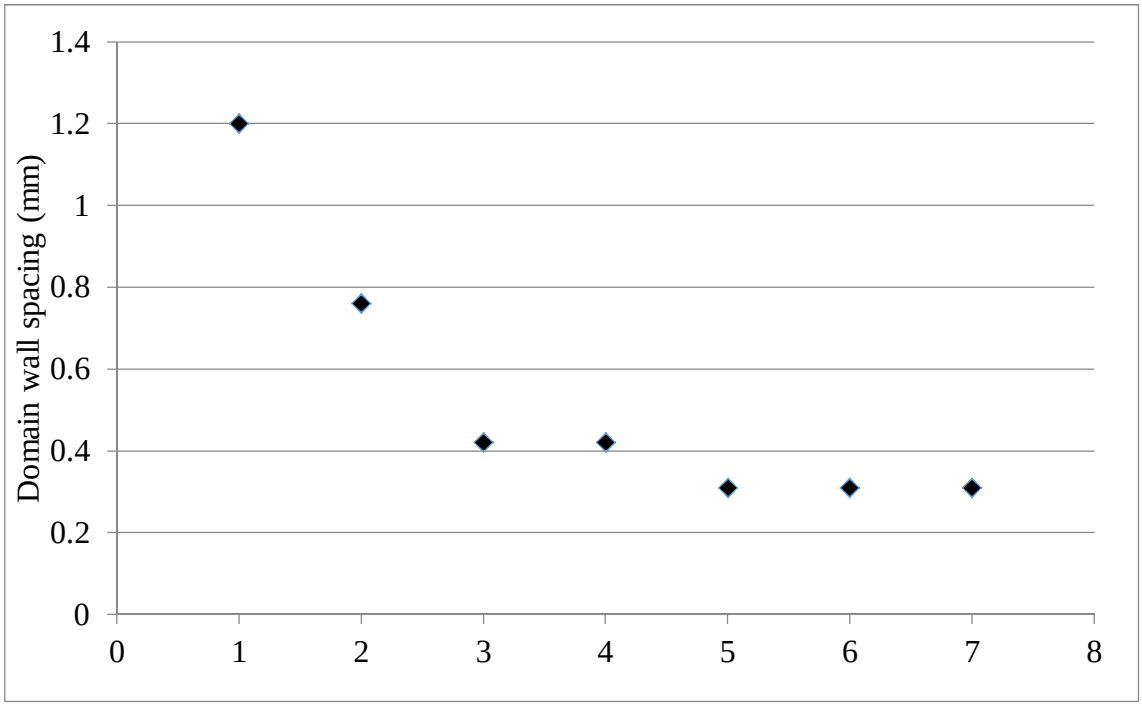

Figure 7.8 shows the domain wall spacing before and after coating. (1) uncoated (2) forsterite coating (3) CrN1 (4) CrAlN1 (5) CrN2 (6) TiAlN1 (7) TiAlN2.

7.6 Power loss

The power loss results of all the ceramic coated samples showed reduction after coating and further reduction after annealing as shown in Figure 7.9. The two types of substrate shown in the figure are uncoated and forsterite coated. The ceramic coated samples without the forsterite layer (uncoated) showed greater reduction in power loss as compared to the samples with forsterite layer which was due to the gaps in bonding between the forsterite and ceramic coatings. The annealing of the samples was performed to remove the bend in Epstein strip which affects power loss results. Post annealed samples showed further reduction in power loss. The TiAlN coated samples after annealing were not flat so the power loss reduction after annealing was not as good as that observed in CrN coated and annealed sample. CrN2 sample showed largest reduction in power loss of 8-9 % and further 3-4% reduction after annealing. The average reduction in power loss was around 3-4% after coating and 2-3% post annealing. Overall the ceramic coated samples showed a reduction in power loss and this was due to the domain narrowing [2] after coating which was explained in section 5.2.9.

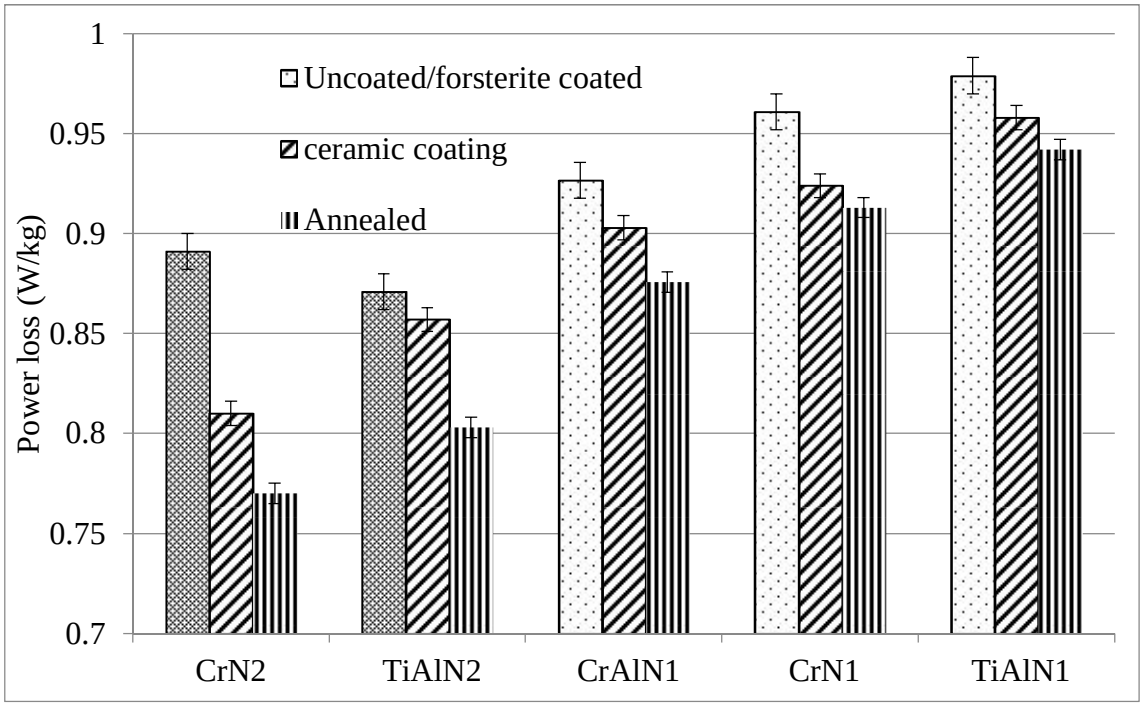

Figure 7.9 power loss for uncoated/forsterite, ceramic coated and annealed sample at 1.5T and 50 Hz frequency.

7.7 Power loss and magnetic domain behaviour

The narrowing of domains after coating leads to reduction in power loss. The relationship between domain behaviour after coating and its effect on power loss is shown in Figure 7.10. The highest improvement in power loss seen in CrN2 corresponds to the maximum reduction in domain width after coating. In samples TiAlN1 and TiAlN2 the domains were as narrow as seen in CrN2 but the improvement in power loss was lower, this was due to significant amount of bend in TiAlN coated samples which was not removed even after annealing the samples. Samples CrAlN1 and CrN1 showed equal domain refinement and lesser than that of CrN1 samples and hence the improvement in power loss for these samples was lower than CrN2 but similar to each other.

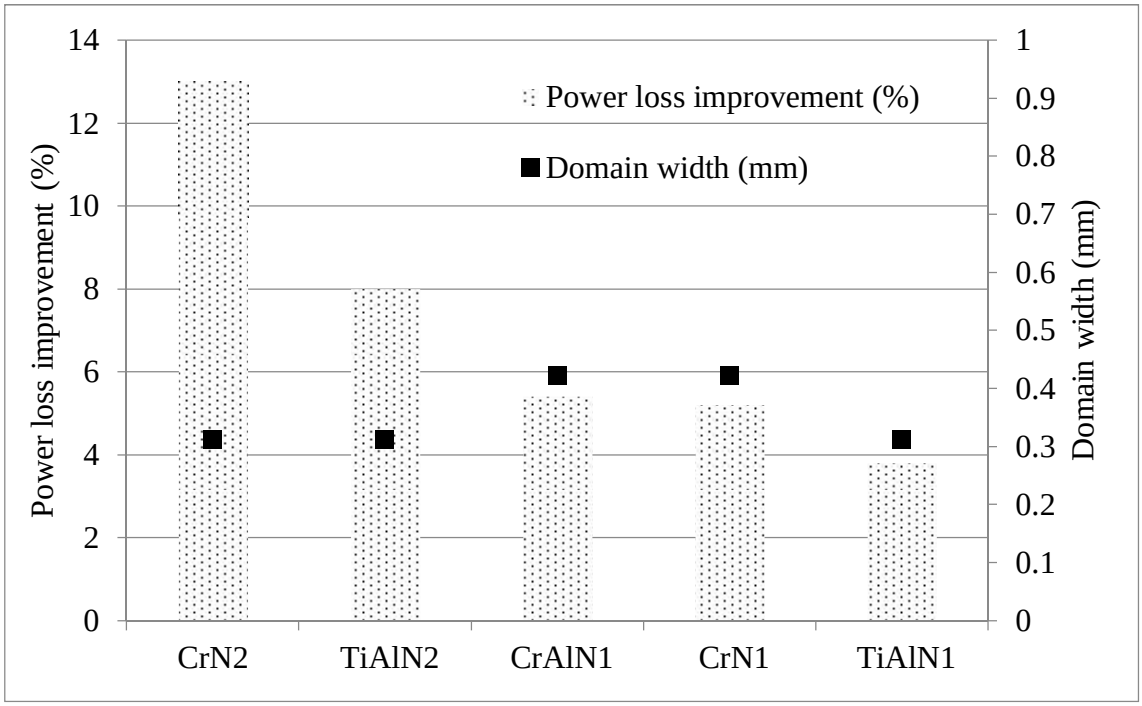

Figure 7.10 Variation in the improvement in power loss and domain narrowing after coating.

7.8 Magnetostriction and stress

Table 7.3 The table below shows the magnetostriction shifts of ceramic coatings with the amount of stress generated.

Coating	Stress (MPa)	Magnetostriction shift (MPa)
CrN1	18	-6
TiAlN1	30	-8
CrN2	20	-8
CrAlN1	NA	-8
TiAlN2	55	-10

The ceramic coated samples generated tensile stress in the substrate and hence the magnetostriction was improved based upon the magnitude of stress applied. The magnetostriction vs stress results for the uncoated, forsterite coated and ceramic coated samples is shown in Figure 7.11. From the figure it could be clearly interpreted that the magnetostriction was reduced after coating GOES with forsterite coating and further reduced after coating with ceramic coatings. A greater reduction was observed if the coating was applied on uncoated steel than forsterite coated steel. The highest reduction

in magnetostriction was noted for TiAlN2 with a stress shift of 10 MPa (due to machine constraints it could not be measured after 10 MPa). For an applied compressive stress of 6 MPa all the ceramic coated samples showed near zero magnetostriction. The reduction in magnetostriction was different for all the ceramic coatings and was dependent upon the starting surface which was uncoated steel or forsterite coated steel as shown in Table 7.3. The stress shifts in magnetostriction could be related to the stress generation results in Table 7.3 where TiAlN2 coating on single side generated a stress of 55 MPa and shifted the magnetostriction curve by 10 MPa and the CrN1 generated a stress of 18 MPa and shifted the magnetostriction curve by 6 MPa. The large reduction in magnetostriction was believed to be due to the high Young's modulus of the CrN (200GPa), CrAlN (270GPa) and TiAlN (632GPa) coating as compared to GOES (113GPa) [3]. The Young's modulus (E) is dependent upon strain as shown in the equation below; for constant stress the product of Young's modulus and strain is constant and hence increase in Young's modulus decreases the magnetostrictive strain which prevented the GOES sample to expand under the influence of applied magnetic field. No change in magnetostriction was observed after annealing.

$$E \propto \frac{\sigma}{\epsilon} \tag{7.1}$$

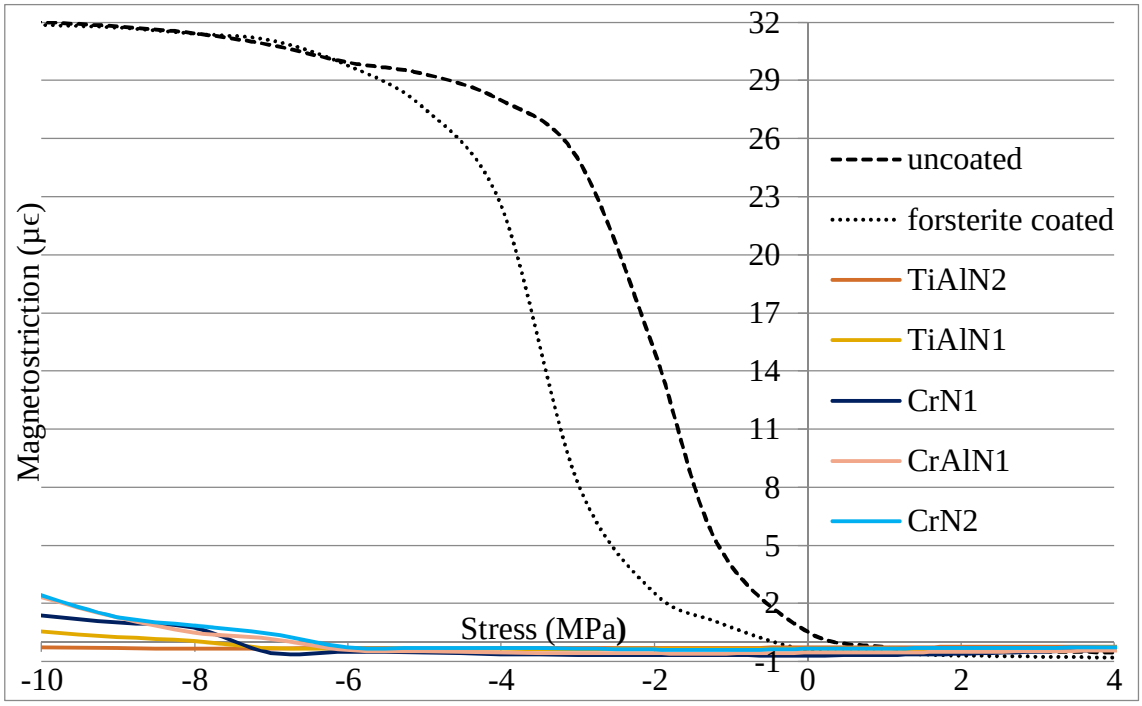

Figure 7.11 Magnetostriction vs stress curves for the uncoated, forsterite coated and different ceramic coated samples showing reduction in magnetostriction after the application of ceramic coatings.

7.9 Conclusions

The ceramic coatings could be effectively used to coat GOES as the coatings were able to reduce the power loss and magnetostriction. The average reduction in power loss was 3-4% after coating and 2-3% post annealing. The best results for power loss reduction were observed for CrN2 which was 8-9 % after coating and 3-4% post annealing. The magnetostriction was reduced to zero for 6 MPa of compressive stress by all the ceramic coatings. The TiAlN coating was able to reduce the magnetostriction to less than zero for an applied compressive stress of 10 MPa. The reduction in power loss was due to the tensile stress developed in the electrical steel by the ceramic coatings which reduced the domain width. The magnetostriction was reduced by the higher Young's modulus of the coatings as compared to electrical steel which did not allow the expansion of steel under magnetisation. The bonding between the substrate and the coating was a dominant factor in controlling magnetic properties. The ceramic coatings were well bonded with the uncoated substrate as compared to the forsterite coated substrate and that is why more stress was generated in the uncoated substrates coated with ceramic coatings. The thickness of the different ceramic coatings varied between 2 to 3.5 µm but the thicker coatings did not show additional effect on the stress generation as TiAlN2 with a thickness of 2.55 ± 0.15 µm showed the highest stress generation of 55 MPa.

7.10 References

[1] O.Knotek, R.Elsing, G.Kramer, and F.Jungblut, "On the origin of compressive stress in PVD coatings — an explicative model," *Surface & Coatings Technology*, vol. 46, pp. 265-274, September 1991.

[2] C. R. Boon and J. A. Robey, "Effect of domain-wall motion on power loss in grainoriented silicon-iron sheet," *Proceedings of the IEEE*, vol. 115, pp. 1535-1540, October 1968.

[3] Y. Chen, J. E. Snyder, C. R. Schwichtenberg, K. W. Dennis, D.K.Falzgraf, R.W.McCallum, *et al.*, "Effect of the elastic modulus of the matrix on magnetostrictive strain in composites," *Applied Physics Letters*, vol. 74, p. 1159, 1999.

8 Conclusions and Industrial impact

8.1 Conclusions

This work assessed the effect of applying different types of coatings using two different coating techniques namely electroless plating and PVD to improve the magnetic properties of GOES. The influence of stress, surface roughness and thickness of coatings on GOES's magnetic properties is investigated in this thesis. The main findings of the research include five different types of coatings (Co-Ni-P, Co-P-CNT, CrN, TiAlN and CrAlN) for GOES to enhance the magnetic properties. The most effective coatings were able to reduce the power loss by 13-15 % and reduce the magnetostriction to less than zero at 10 MPa of compressive stress which would be beneficial to reduce the overall consumption of power and noise in the machine applications. The main results are summarised in Table 8.1 and the conclusions drawn from this research are divided into three sub categories as follows:

Table 8.1 Highlights the main coatings with the magnetic properties

Coating	Method	Thickness	Power loss	Magnetostriction
Co-Ni-P	Electroless	2 µm	-9-11%	-1.8 MPa
Co-Ni-B	Electroless	3 µm	+60-65%	+7 MPa
Co-P-CNT	Electroless	0.4 µm	-13-15%	NA
CrN	PVD	2.5 µm	-13-15%	-8 MPa
CrAlN	PVD	2 µm	-6-7%	-8 MPa
TiAlN	PVD	3 µm	-6-7%	-10 MPa

8.1.1 Co-Ni-P coating on GOES

An electroless deposition of Co-Ni-P was shown to provide an effective coating for electrical steels as the power loss was reduced by 9-11 % after coating and the magnetostrictive stress was reduced by 1.8 ± 0.2 MPa. The reason for the improvement in magnetic properties was due to two main factors; improvement in 30% surface roughness after coating and development of 3.9 MPa of tensile stress. The stacking factor was enhanced as the coating thickness was half the conventional coating and its magnetic nature also contributed further to it.

8.1.2 Co-Ni-B coating on GOES

Co-Ni-B coating on GOES showed the reverse effect as that of Co-Ni-P coating. A compressive stress of 11 MPa and fivefold increase in roughness increased the power loss by 60-65% and the magnetostriction by a stress shift by 7 MPa. This coating would be suitable for fatigue resistance of materials where compressive stress is required to close the surface cracks to prevent failure.

8.1.3 Co-P-CNT coating on GOES

The coating reduced the total power loss in GOES ranging 13 to 15 % due to the smoothing of surface roughness by 37 % after coating. The stacking factor was improved to 99.85%.

8.1.4 Ceramic coatings (CrN, CrAlN and TiAlN) on GOES

Ceramic coated samples showed a maximum power loss improvement of 11-13 % and an average of 6-7 % which was due to the generation of compressive stress in the coating. Annealing reduced power loss by 2-3% as the samples were flattened. No magnetostriction was observed for an applied compressive stress of 10 MPa due to the high Young's modulus of the coating as compared to GOES.

8.2 Industrial impact and future research

8.2.1 Electroplating with Co-Ni-P and Co-P-CNT

To make Co-Ni-P and Co-P-CNT coatings industrially viable a faster and better controlled process is required than electroless plating. Electroplating can be used as an alternate as the process is much faster than electroless plating with deposition rates of 1.25 µm/min as compared to 1.25 µm/hour also the process is much cheaper than electroless plating. Switching from one process to another requires a thorough investigation because the desired chemistry of the coating with desired phosphorus content and lower surface roughness is required for reduction in power loss. A faster process may lead to agglomeration and variable phosphorus throughout the coating which will be harmful to magnetic properties.

Co-Ni-P coating can replace the dual layer coating system with one coating by employing the process after the formation or the final grain structure but would require that the forsterite layer is not formed or removed.

This would make it ideal for a shortened process route where decarburising, secondary grain growth and coating all take place in a single continuous process.

8.2.2 Recycling of CNT in Co-Ni-CNT coating

The use of CNT in the coating produced better magnetic properties but it is a very costly material. Although a small amount of CNT's goes in the coating but a large amount of it is required in the solution and much of it is wasted after the solution is discarded. A study on recycling of CNT's from the solution would make it a cost effective and industrially viable process.

8.2.3 Ceramic coatings deposited by sputtering or CVD

The ceramic coatings were deposited with electron beam PVD, to generate larger compressive stress magnetron sputtering of the ceramic material on GOES can be investigated. Sputtering atoms travel with greater force towards the target material and impinge with high velocity to interfere with the bond structure which generates a greater compressive stress in the coating. Also a negative bias voltage applied to the substrate attracts positive ions and develops larger value of compressive stress in the coating which imparts tensile strength to GOES and could enhance the magnetic properties. To employ ceramic coatings in the production line, these coatings could replace the phosphate layer after the HTCA in the current process route with a continuous CVD/PVD process.

8.3 Environmental impact

The impact of reduction in power loss on the environment can be calculated as shown below.

Consumption of electricity in UK = 400 TWh/year [1]
Loss of electricity in the grid = 29 TWh/year [1]
40% of grid loss is due to transformers = 11.6 TWh/year
Improvement of 15 % in power loss = 1.74 TWh/year
Greenhouse gas emission for 1 kWh = 0.504 kg CO_2 [2]
Greenhouse gas emission for 1.74 TWh = 87.7×10^{10} kg CO_2
This is based upon the assumption if all transformers in the UK are replaced with new coatings, however this is offset by the fact that many transformers are up to 50 years old and will have loss more than four times the current levels.

8.4 References

[1] "The CO_2 benefits of grain oriented electrical steel in transformers," *Cogent Power internal report.*

[2] "IEA statistics: CO_2 emissions from fuel combustion," 2011.

List of publications

1. Vishu Goel, Philip Anderson, Jeremy Hall, Fiona Robinson and Siva Bohm, Electroless Co-P-CNT composite coating to enhance magnetic properties of GOES, Journal of Magnetism and Magnetic Materials, volume 407, 1 June 2016, Pages 42-45, DOI 10.1016/j.jmmm.2015.12.076
2. Vishu Goel, Philip Anderson, Jeremy Hall, Fiona Robinson and Siva Bohm, Application of Co-Ni-P coating on grain-oriented electrical steel, IEEE Transactions on Magnetics DOI 10.1109/TMAG.2015.2496315
3. Vishu Goel, Philip Anderson, Jeremy Hall, Fiona Robinson and Siva Bohm, Electroless plating: A versatile technique to deposit coatings on electrical steel, SMM-22 magnetics conference, Sept 13-16, 2015 at Sao Paulo, Brazil, published in IEEE Transactions on Magnetics April 2016, volume 52, issue 5, page 1-4, DOI 10.1109/TMAG.2016.2514745
4. Vishu Goel, Philip Anderson, Jeremy Hall, Fiona Robinson and Siva Bohm, CrAlN coating to enhance the power loss and magnetostriction in grain oriented electrical steel, InterMag 2016 conference in San Diego, Jan 11-15 2016, published in AIP Advances 6, 055924 (2016), DOI: 10.1063/1.4944340
5. Vishu Goel, Philip Anderson, Keith Jenkins, Jeremy Hall and Siva Bohm, Novel coating technologies for electrical steels, WMM 14 conference proceedings, June 17-19, 2014 at Cardiff, UK

Application of Co–Ni–P Coating on Grain-Oriented Electrical Steel

Vishu Goel[1], Philip Anderson[1], Jeremy Hall[1], Fiona Robinson[2], and Siva Bohm[3]

[1]Wolfson Centre for Magnetics, Cardiff University, Cardiff CF24 3AA, U.K.
[2]Cogent Power, Newport NP19 0RB, U.K.
[3]Tata Steel Research, Development and Technology, Rotherham S603 AR, U.K.

An electroless plating of Co–Ni–P was applied to a grain-oriented electrical steel substrate, resulting in a power loss improvement of ∼9%–11%. The mean thickness of the coating was found to be 2.15 ± 0.15 μm from environmental scanning electron microscopy images. Shifts of the magnetostriction stress sensitivity curves showed that stress was acting on the substrate and was corroborated by a shift in X-ray diffraction (XRD) peaks and narrowing of the domains after the samples were coated. The magnetic property measurement system results confirmed the magnetic nature of the coating and XRD results showed peaks of α-iron in the uncoated sample, α-iron-cobalt and α-iron in the Co-Ni-P-coated sample. The Talysurf profilometer showed a decrease in surface roughness values after coating the sample, which reduced the hysteresis loss.

Index Terms—**Electroless coating, grain-oriented electrical steel, magnetic coating, magnetostriction, power loss, stress.**

I. Introduction

EFFORTS are being made to produce high-performance electrical steel through several methods, including better secondary recrystallization methods [1], grain orientation control [2], increasing the electrical resistivity, gauge reduction [3], and understanding the magnetic domain structure [4]–[7]. Perhaps the greatest gains can be obtained by employing effective stress coatings [8], [9], which can play a dominant role in minimizing losses and magnetostriction.

Stress can be applied to the material with the help of coatings. Coating the steel helps in reducing both the losses and the magnetostriction. It is well known that the effect of magnetostriction can be suppressed by the application of tensile stresses. Tensile stress imparted from the coating on the steel sheet eliminates the surface closure domains, and losses are reduced as tensile stress helps in narrowing the domain-wall spacing in addition to minimizing the circulation of eddy currents by providing electrical insulation. Current coating systems on grain-oriented electrical steel comprise a two-layer coating with a forsterite layer (Mg_2SiO_4) below an aluminum orthophosphate layer. Conventionally, coatings that have low coefficient of thermal expansion are used, because when cooled from high temperature, they contract lesser than does the substrate. This difference in cooling applies a tensile stress on the substrate.

A number of different methods can be used to apply a coating on the surface of a steel sheet such as sol–gel [10], chemical vapor deposition [11], physical vapor deposition [12], plasma spraying, wet coating, printing, electroless plating, and electrochemical method.

This paper investigates electroless plating of Co–Ni–P, which has the advantages of corrosion resistance, uniform thickness, and wear and abrasion resistance. Stress develops in electroless plating due to the difference in the coefficient of thermal expansion between the substrate and the coating or develops in the deposition process. During deposition, the particles get deposited at a few places rather than forming a uniform atomic layer. The coating grows at those few places only. Surface tension binds the particles together. Rearrangement of these atoms due to surface tension changes the interatomic distance and hence develops tensile or compressive stress depending on the increase or decrease in the interatomic distance. Minimizing the coagulation could reduce the amount of tensile stress, and by introducing phosphorus, the stress can be changed from tensile to compressive, as can be seen in Fig. 1 [13]. The electroless deposition rates are very fast as compared with other chemical coating techniques, and being autocatalytic, no external current is supplied for the process to take place.

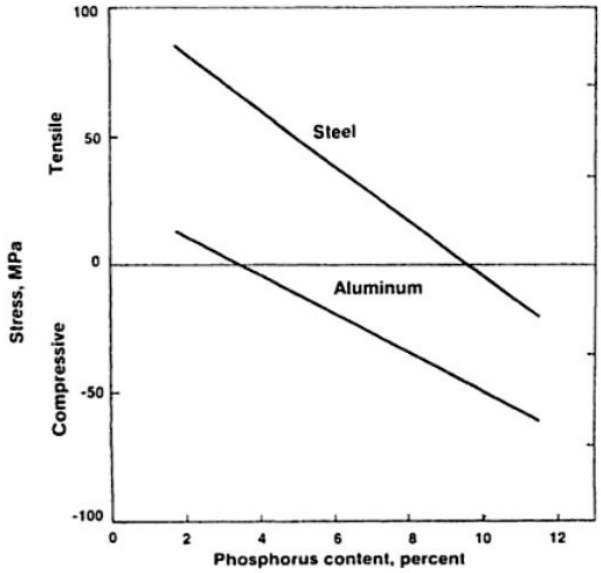

Fig. 1. Relationship between phosphorus content and stress in the coating.

Manuscript received May 7, 2015; revised August 27, 2015; accepted October 20, 2015. Corresponding author: V. Goel (e-mail: vishu.goel.nit@gmail.com).

Color versions of one or more of the figures in this paper are available online at http://ieeexplore.ieee.org.

Digital Object Identifier 10.1109/TMAG.2015.2496315

Chivavibul *et al*. [14] produced an electroless Ni–Co–P coating of 1 μm thickness on non-oriented electrical steel and found that the coating was effective in reducing losses by up to 4% at a magnetic flux density of 0.3 T and frequency of 400 Hz. The coating was able to minimize the eddy current loss at higher frequencies to reduce the overall loss. Power transformers operate at a flux density of 1.5 T and above and a frequency of 50 Hz. The component of eddy current loss decreases as the frequency decreases. It was also found that as the thickness of Ni–Co–P coating increased, hysteresis loss increased and hence Ni–Co–P may not be suitable at lower frequencies, where hysteresis and anomalous loss dominate [15]. Co–Ni–P was chosen as a suitable coating. The amount of phosphorus could be balanced to develop compressive stress in the coating. The coating is also ferromagnetic, and its properties can be altered by varying the chemical content. The parameters used to deposit the Co–Ni–P coating determine the impact on final magnetic properties such as the coercivity and hysteresis loss [16]. The aim of this paper is to evaluate and optimize these coatings for transformer applications and compare them with conventional coatings.

II. Material and Methods

Grain-oriented (Fe-3%Si) samples (0.3 mm × 30 mm × 305 mm) were supplied by Cogent Power Ltd., Newport, and both the tension and insulation coating were removed with a solution of 7.5% sulphuric acid and 1% hydrofluoric acid for approximately 10 min and then in 4% nitric acid for approximately 7 min. The specific total loss was measured with a single strip tester [17] from a magnetic flux density of 1.1 T to 1.7 T at a frequency of 50 Hz. Flux closure was provided by a pair of high permeability wound yokes with a 255 mm pole gap, and the number of turns on the primary and secondary windings was 865 and 250, respectively. A mutual inductor was used to provide air flux compensation. The magnetostriction measurements were made on a magnetostriction measurement system using the procedure described in [18]. The stress induced by the coating was also calculated from the measured magnetostriction curves using the method outlined in [18]. The microscopy images were obtained from an XL30 ESEM field emission gun. The elemental analysis was performed with an Oxford Instruments energy-dispersive X-ray spectroscopy (EDX) analysis system. To study the structure and phases of the coating, X-ray diffraction (XRD) was carried out, with cobalt radiation at 30 kV and 40 mA. The magnetic domains were imaged with a magnetic pattern viewer [19]. The magnetic properties of the coating were measured at room temperature by the magnetic property measurement system (MPMS). The magnetic field was applied up to 20 000 Oe. The surface roughness of the uncoated and coated surfaces was measured by Talysurf surface profilometer. The measurement was made in the direction of rolling for a distance of 40 mm for all the samples. The samples were coated with Co–Ni–P using electroless plating. The composition of the bath and the operating conditions was referred from [20] and modified as shown in Table I. To study the effect of coating thickness on the substrate, four samples were immersed in the plating solution and were removed at 20, 35, 50, and 90 min, respectively. The pH of the solution was maintained by adding ammonium hydroxide. To ascertain the effect of pH on the power loss, five samples were prepared with pH values varying from 7.8 to 9.4. All five samples were immersed for 90 min, as it was found to be the optimum time for best results.

TABLE I
Electroless Plating Bath Conditions

Composition	Grams/litre
Nickel sulphate	7.5
Cobalt sulphate	15
Trisodium citrate	50
Sodium hypophosphite	25
Boric acid	30
Temperature 60 ± °5	

III. Results and Discussion

A. Power Loss Results for Various Thicknesses

Fig. 2 shows the difference in power loss of the coated and uncoated samples for different times. The uncoated power loss was different for different strips because the Epstein strips cut from a sheet material show a significant local variation in grain size, orientation, and pinning sites. The thickness of the coating deposited was proportional to the time for which the samples were kept in the plating solution. The dehydrogenation of hypophosphite provides the hydride ion (1a). The deposition of nickel and cobalt on the surface of grain-oriented electrical steel was triggered by the reduction of nickel and cobalt ions by the hydride ion as shown in reactions (1b) and (1c) [21]. These deposited particles act as nucleation sites for further deposition of coating and hence the time period of coating dictates the thickness of coating deposited

$$H_2PO_2^- + H_2O \rightarrow H^+ + HPO_3^{2-} + 2H \quad (1a)$$

$$Ni^{2+} + 2H \rightarrow Ni^0 + 2H^+ \quad (1b)$$

$$Co^{2+} + 2H \rightarrow Co^0 + 2H^+. \quad (1c)$$

Fig. 2(a)–(d) shows that the coating thickness plays a major role in determining the power loss with a thicker coating applying greater stress. For the sample coated for 20 min, the reduction in power loss was around 4%–5%. Material coated for 90 min had a reduction in loss of approximately 9%–11% at 1.5 T as compared with the uncoated sample. The values of stress calculated for 20 and 90 min coated samples were 0.86 and 2.10 MPa, respectively. Song and Yu [22] showed that stress was introduced to the substrate by the Ni–P coating, The stress can be tensile or compressive depending upon the amount of phosphorus in the coating; 8.5% phosphorus induces compressive stress in the coating [23]. The phosphorus gets trapped during the deposition and forms small grains monodomains, increasing the soft magnetic properties [24]. In this case, the stress in the coating was compressive as the amount of phosphorus was confirmed to be between 9% and 10%, and hence tensile stress acted on the substrate, which was

This article has been accepted for publication in a future issue of this journal, but has not been fully edited. Content may change prior to final publication. Citation information: DOI 10.1109/TMAG.2015.2496315, IEEE Transactions on Magnetics

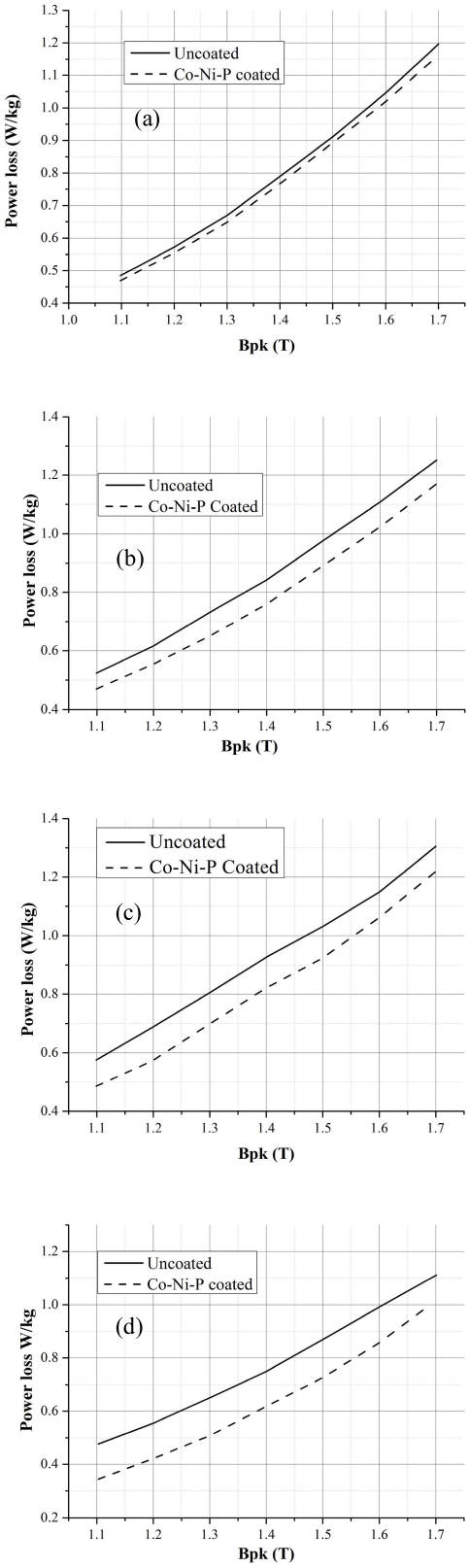

Fig. 2. Power loss testing for the uncoated and Co–Ni–P-coated samples for different times. (a) 20 min. (b) 35 min. (c) 50 min. (d) 90 min.

beneficial in terms of power loss reduction and magnetostriction. To minimize losses, coating thickness could be increased, but the stress decreases as the thickness increases [23] and

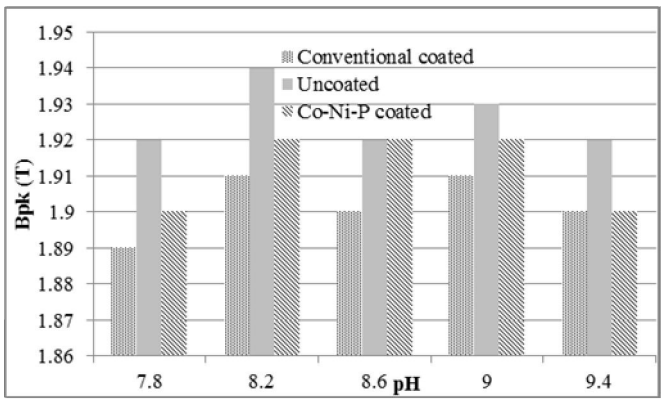

Fig. 3. Bpk measured at magnetic field strength of 800 A/m for different values of pH.

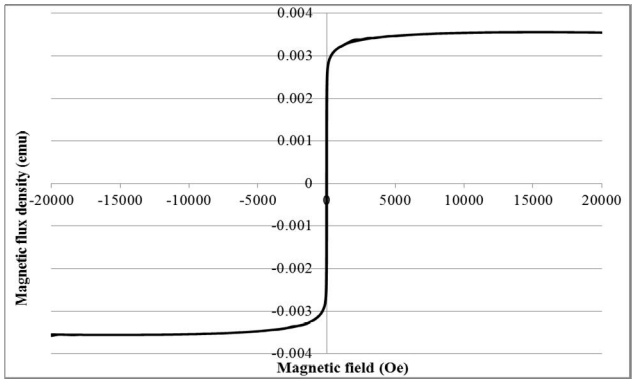

Fig. 4. Magnetic flux density measured for Co–Ni–P coated at pH 9.0.

it leads to unacceptable degradation of permeability shown in Fig. 3, where the Bpk (magnetic flux density at 800 A/m magnetic induction) was reduced after coating, and stacking factor gets affected.

B. Magnetic Properties

Fig. 4 shows a classical hysteresis loop for Co–Ni–P coating at pH 9.0. The B–H loop measured by the MPMS validates the magnetic nature of the coating. The coercivity of the coating was calculated to be 796 A/m. The saturation magnetization of the coating was calculated to be 0.0036 emu as compared with 0.0288 emu for grain-oriented electrical steel, considering same volume for both materials. The magnetic property of Co–Ni–P coating increases the stacking factor by adding a soft magnetic material in the transformer core as compared with the conventional non-magnetic coating.

C. Magnetostriction

Fig. 5 shows the magnetostriction curve for the uncoated and Co–Ni–P-coated samples for 90 min at pH 9.0. The threshold (point-of-zero magnetostriction) for the uncoated and Co–Ni–P-coated samples was around -1 and -3 MPa, respectively. A stress shift of 1.80 ± 0.20 MPa was observed after coating the sample. This shift in the magnetostriction curve toward the left infers that a significant amount of stress

This article has been accepted for publication in a future issue of this journal, but has not been fully edited. Content may change prior to final publication. Citation information: DOI 10.1109/TMAG.2015.2496315, IEEE Transactions on Magnetics

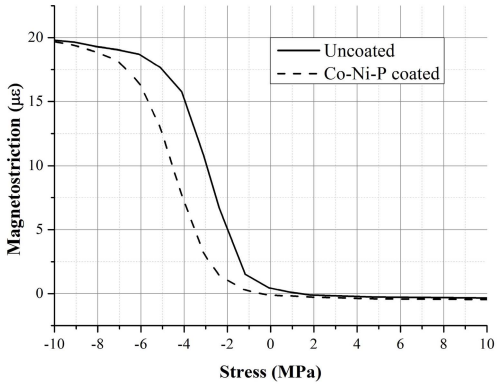

Fig. 5. Magnetostriction versus stress for uncoated and Co–Ni–P coated for 90 min.

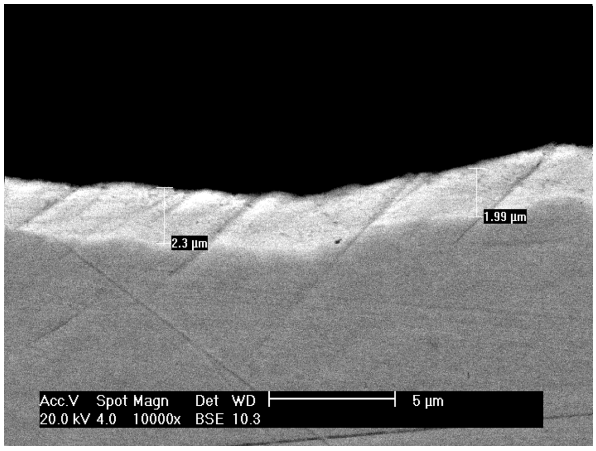

Fig. 6. Cross-sectional image of the substrate and the coating at pH 9.

was acting on the substrate. Applying a compressive coating on the substrate eliminates the surface closure domains. These surface closure domains are responsible for magnetostriction [18]. As the surface closure domains are minimized, the magnetostriction reduces.

D. Scanning Electron Microscopy

Fig. 6 shows the scanning electron microscopy (SEM) image of the 90 min coated sample at pH 9. The gray area shows the substrate, while the lighter area shows the coating. The coating was uniformly distributed across the sample. No gaps or cracks were found. The thickness of the coating was averaged to be around 2.15 ± 0.15 μm.

The stacking factor calculated for 2 μm-thick coating was 98.68%, as compared with 97.4% for 4 μm-thick conventional coating calculated as

$$\text{stacking factor} = \left(1 - \frac{\text{Non-magnetic material in the core}}{\text{Total material in the transformer}}\right) * 100.$$

If the coating was non-magnetic, the thickness of coating on both sides was 4 μm.

The thickness of Epstein strip without coating $= 300$ μm.

The thickness of total material in the transformer core $= 304$ μm

$$\text{stacking factor}(\%) = \left(1 - \frac{300}{304}\right) * 100$$
$$\text{stacking factor}(\%) = 98.68.$$

However, as the coating was also magnetic, it would contribute to the stacking factor, and hence the new value of stacking factor considering the saturation magnetization of Co–Ni–P coating to be 0.0036 emu and that of GOES to be 0.0288 emu was 98.84%. The increase in stacking factor by the magnetic nature of the coating was found to be insignificant

$$\text{Magnetic contribution of coating to GOES} = \frac{0.0036}{0.0288} * 100$$
$$\text{Magnetic contribution of coating to GOES} = 12.5\%$$
$$\text{New stacking factor}(\%) = 98.68 + \left(\frac{100 - 98.68}{100}\right) * 12.5$$
$$\text{New stacking factor}(\%) = 98.84.$$

Fig. 7 shows five SEM images of the samples prepared with coating at various pH values (7.8, 8.2, 8.6, 9, and 9.4). pH plays a major role in determining the type of coating (hard or soft magnetic) and controls the coating mechanism [25]. At pH 1.5, the coating was found to be having a coercivity of 11,937 A/m and at pH 3.5, value the coating had a coercivity of 47,747 A/m [24], [26]. As can be seen from the images at a pH of 7.8, the Co–Ni–P coating coagulates in some areas rather than forming a uniform coating. The nucleation of Ni and Co on the surface of grain-oriented electrical steel is not distributed throughout the sample; instead the metal particles nucleate at a few sites. The coating grows at those sites only. The surface tension binds the particle together and changes the interatomic spacing. The change in interatomic spacing introduces tensile or compressive stress in the coating [13]. A reduction in interatomic spacing would lead to a compressive stress in the coating and therefore a tensile stress in the substrate. As the pH of the solution was increased, there was a reduction in size of the particles and a more uniform coating was formed. At pH 9, nucleation occurs throughout the sample and we could see a uniform coating on the substrate and a minimal amount of coagulation in the coating. The stress applied by the coating on the substrate was uniform and a reduction in power loss was observed. The pH was increased further and the coating was again found to be coagulated at various places.

E. Surface Profiling

The surface roughness values in Fig. 8 validate the SEM results. The value of roughness was largely dependent on the pH of the coating solution. The surface of the sample coated with a pH value of 7.8 was found to be rougher than the uncoated sample. The least value of roughness was measured at a pH of 9.0. The surface roughness effects the hysteresis loss [27]. The increase in surface roughness increases the number of free poles on the surface, and these free poles pin the domain walls. It leads to reduction of domains, and the motion of domain wall is inhomogeneous [9]. Energy is

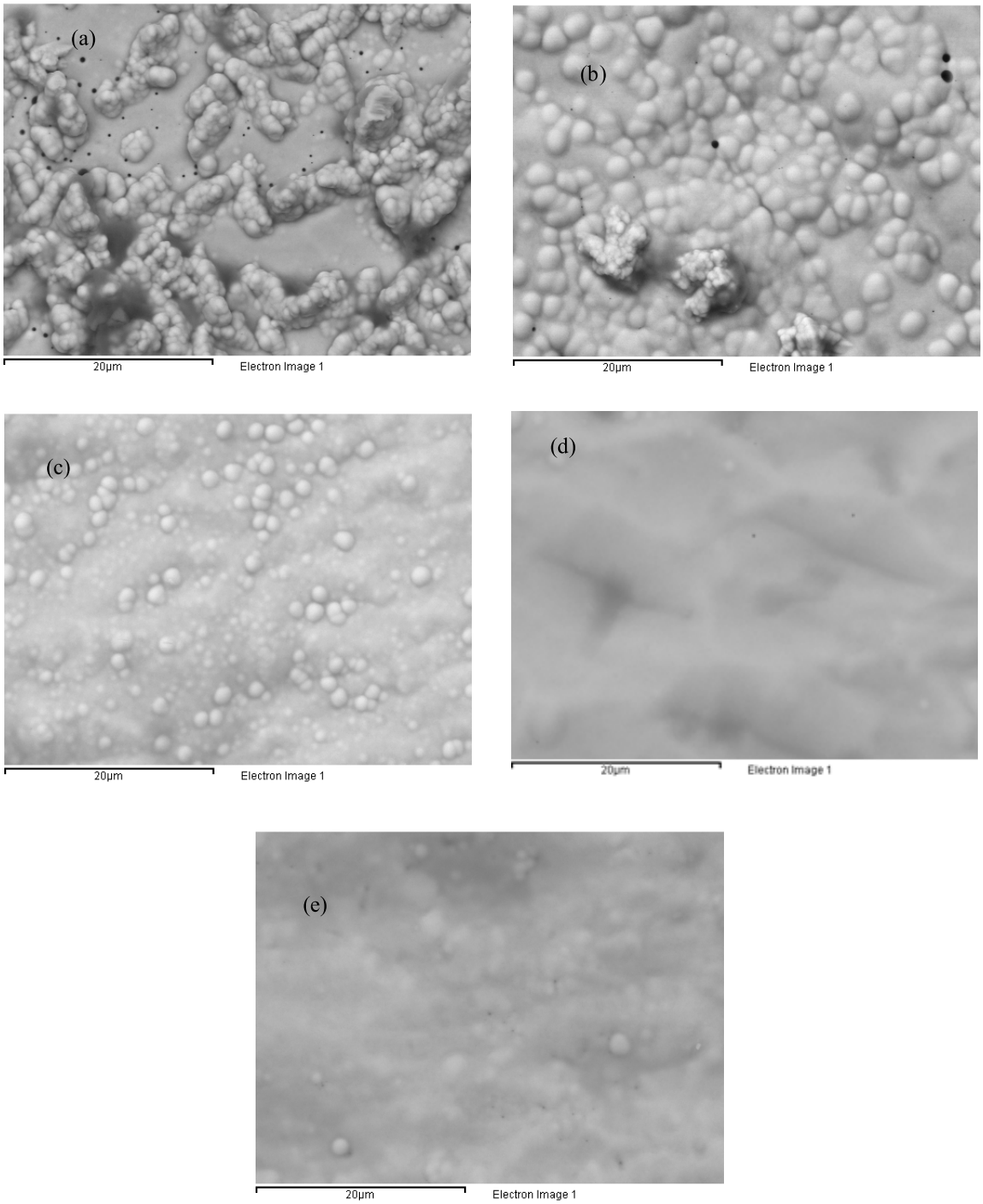

Fig. 7. SEM images for the samples coated with different pH values. (a) 7.8. (b) 8.2. (c) 8.6. (d) 9. (e) 9.4.

dissipated in freeing these domain walls, and this energy contributes to specific total loss. It was assumed that the enhancement of magnetic properties at pH 9.0 was due to the improvement in surface roughness by magnetically active coating.

F. Effect of pH on Coating Composition and Power Loss

Fig. 9 shows the power loss results of the different samples. As expected and endorsed by the SEM images, the sample coated at a pH of 9 shows the highest reduction in power loss, because a uniform coating could be achieved only at this value. Changing the pH value either way affects the coating formation, which generates tensile stress in the coating and the improvement in power loss reduction gets reduced. Table II highlights the elements present in the coating at different pH values. The cobalt content in the coating increased as the pH was increased and reached a maximum of 60%–62% by weight for a pH of 9. On the other hand,

This article has been accepted for publication in a future issue of this journal, but has not been fully edited. Content may change prior to final publication. Citation information: DOI 10.1109/TMAG.2015.2496315, IEEE Transactions on Magnetics

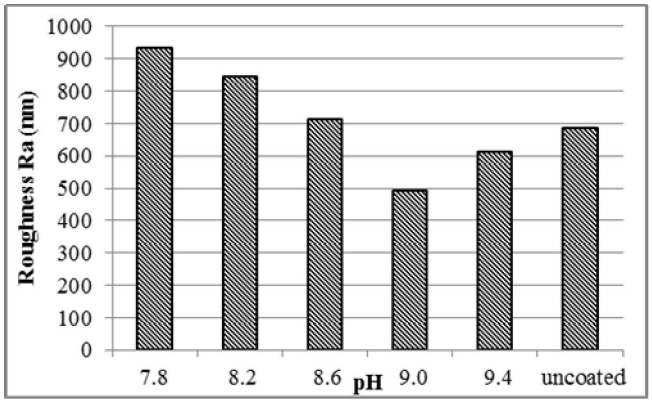

Fig. 8. Talysurf surface roughness values Co–Ni–P coating at different pH values.

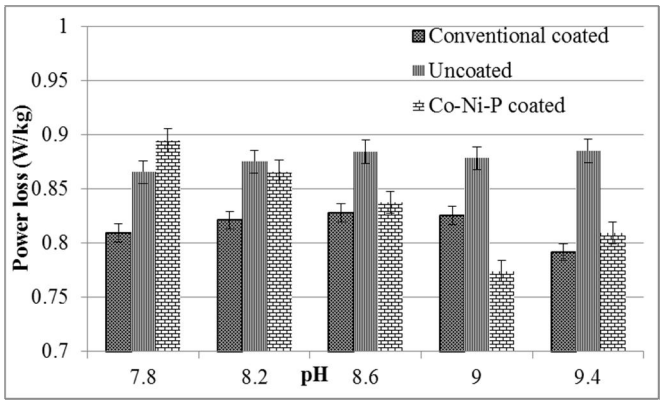

Fig. 9. Effect of pH on power loss measured at 1.5 T and 50 Hz frequency.

nickel content decreased. The results were in agreement with [26]. The saturation magnetization of cobalt (167 emu/g) was much higher than that of nickel (54 emu/g), and so, increasing cobalt content would result in better soft magnetic properties. The amount of phosphorus remains relatively unchanged except for the coating with a pH of 9.4 where sodium was introduced in the coating, and the compressive stress from the coating reduces, which may be the reason for the decrease in improvement of power loss at a pH value of 9.4.

G. Magnetic Domain Imaging and Loss Separation

To study the effect of coating on power loss, the domain images were recorded before and after coating the sample. The magnetic domain imaging clearly shows the narrowing of domains after coating with Co–Ni–P. The average domain width in the rectangular box in Fig. 10 for the uncoated sample was 0.73 mm as compared with 0.48 mm for the Co–Ni–P-coated sample. The narrowing of domain width decreases the anomalous loss. The anomalous loss is directly proportional to velocity of the domain wall. As the domain width decreases, the walls have to travel a shorter distance within the same time, so the velocity of the wall decreases [5].

The model used here for loss separation was proposed in [15]. The core loss equation is

$$W = k_h f \mathrm{B}^{\alpha} + k_e f^2 \mathrm{B}^2 + K_a f^{1.5} \mathrm{B}^{1.5} \tag{2a}$$

TABLE II
ELEMENTAL COMPOSITION (WEIGHT%) OF COATING AT DIFFERENT pH VALUES

pH	Nickel%	Cobalt%	Phosphorus%	Sodium%
7.8	41-43	48-50	9-10	0
8.2	33-35	54-56	9-10	0
8.6	32-34	55-57	9-10	0
9.0	29-31	60--62	9-10	0
9.4	28-30	58-60	7-8	4-5

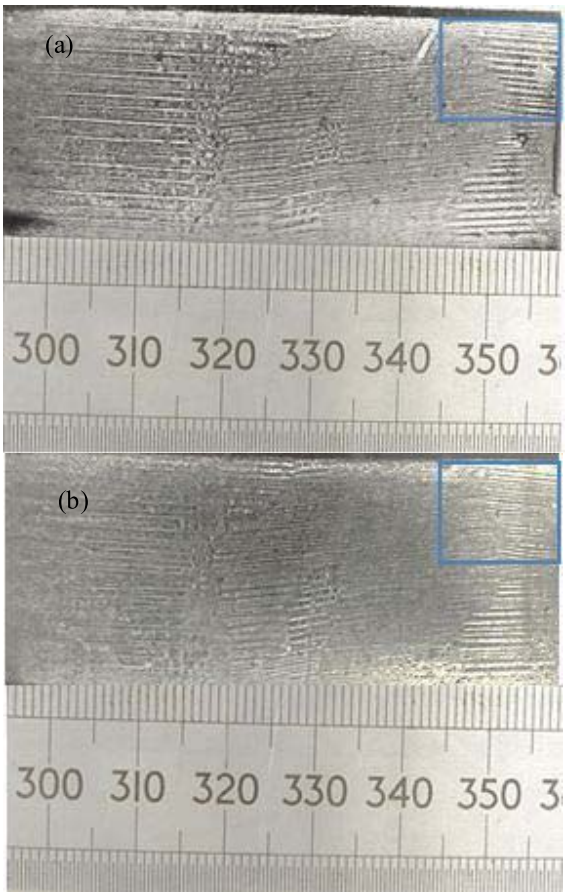

Fig. 10. Magnetic domain imaging for the (a) uncoated and (b) Co–Ni–P-coated samples at pH 9.

where W is the total loss, $k_h f \mathrm{B}^{\alpha}$ is the hysteresis loss component, $k_e f^2 \mathrm{B}^2$ is the eddy current, and $K_a f^{1.5} \mathrm{B}^{1.5}$ is the anomalous loss component. The loss per cycle is given by

$$W/f = k_h \mathrm{B}^{\alpha} + k_e f \mathrm{B}^2 + K_a f^{0.5} \mathrm{B}^{1.5}. \tag{2b}$$

Equation (2b) can be compared to a quadratic equation of the type $a + bx + cx^2$ as shown in (2c), assuming that k_h, k_a, k_e, and α are constants that are independent of frequency and magnetic flux density. The coefficients of $f^{0.5}$ can be found by plotting a fitting curve

$$W = a + bf^{0.5} + cf \tag{2c}$$

where

$$a = k_h \mathrm{B}^{\alpha} \quad b = k_a \mathrm{B}^{1.5} \quad c = k_e \mathrm{B}^2.$$

This article has been accepted for publication in a future issue of this journal, but has not been fully edited. Content may change prior to final publication. Citation information: DOI 10.1109/TMAG.2015.2496315, IEEE Transactions on Magnetics

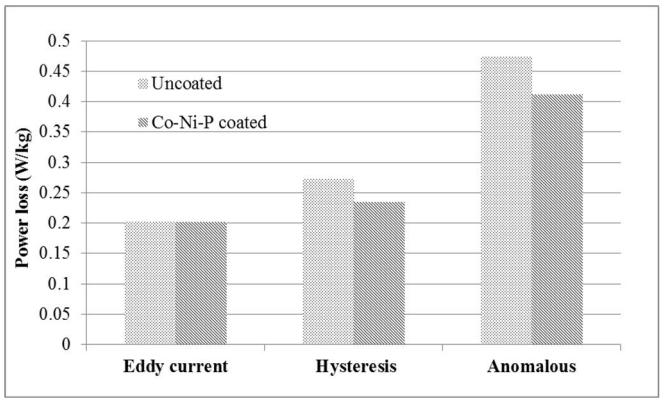

Fig. 11. Loss separation at 1.5 T magnetic flux density and 50 Hz frequency for the Co–Ni–P-coated sample at pH 9.

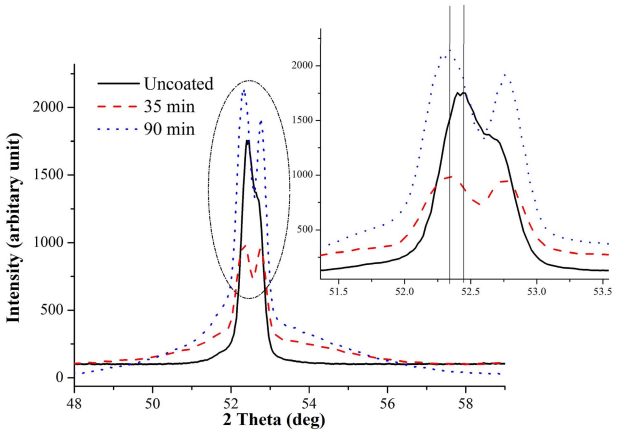

Fig. 12. XRD of the uncoated and Co–Ni–P-coated samples at pH 9.

The values were plotted over a range of frequencies from 10 to 1000 Hz to get a good approximation of the fitting. The value of the correlation coefficient [28] r^2 was 0.9997 and 0.99996 for the uncoated and Co–Ni–P-coated samples, respectively. Fig. 11 shows the loss separation data for the uncoated and coated samples. It can be clearly seen from the graph that the coated sample has a large reduction in anomalous loss, which is in agreement with the magnetic pattern viewer images.

H. X-Ray Diffraction

The XRD result in Fig. 12 shows the uncoated, 35-min and 90-min coated samples. The diffusive broad peaks in the histogram confirm the amorphous or nanocrystalline nature of the coating. The peaks may be Co–P or Co–Ni–P. The sharp peaks that were observed correspond to α-iron and α-iron-cobalt ($Fe_{0.3}Co_{0.7}$). The 110 reflection was shifted toward the lower angle in the coated sample, as can be seen in Fig. 12. Stress is introduced by the coating [22], which can expand the lattice of the substrate material.

The stress shift was interpreted from Bragg's law [29]. The shift in peaks toward a lower angle confirmed that the inter planer distance d increases and hence compressive stress developed in the coating. An equivalent tensile stress acted on the grain-oriented electrical steel surface to compensate the compressive residual stresses due to which there was an improvement in magnetic properties.

IV. Conclusion

An effective coating on grain-oriented electrical steel provides sufficient tension and insulation to reduce the specific total loss and magnetostriction. In addition to that, the magnetic activity and reduced thickness improves the stacking factor. An electroless deposition of Co–Ni–P was shown to provide an effective coating for electrical steels. The thickness of the coating was half the thickness of conventional coatings and being magnetic in nature, it further improves the stacking factor in the transformers to 98.83%. The threshold value of magnetostriction was shifted by 1.8 ± 0.20 MPa toward left after coating the sample. The time period for the electroless deposition dictates the thickness of the coating and hence the power loss reduction. A reduction of power loss by 4%–5% was observed for samples coated for 20 min as compared with a reduction of 9%–11% for samples coated for 90 min. The increase in pH of the solution from 7.8 to 9.0 decreases the surface roughness of the coating, which reduces the hysteresis loss. The domain structure was also narrowed, which reduces the anomalous loss; hence the overall total loss for grain-oriented electrical steel was reduced. It is suggested that these coatings could be scaled cost effectively to production material due to the simple autocatalytic process.

Acknowledgment

This work was supported by Tata Steel RD&T, Rotherham and Cogent Power Ltd., Newport.

References

[1] S. Turner, A. Moses, J. Hall, and K. Jenkins, "The effect of precipitate size on magnetic domain behavior in grain-oriented electrical steels," *J. Appl. Phys.*, vol. 107, no. 9, p. 09A307, 2010.

[2] J.-T. Park and J. A. Szpunar, "Effect of initial grain size on texture evolution and magnetic properties in nonoriented electrical steels," *J. Magn. Magn. Mater.*, vol. 321, no. 13, pp. 1928–1932, 2009.

[3] H. Haiji, K. Okada, T. Hiratani, M. Abe, and M. Ninomiya, "Magnetic properties and workability of 6.5% Si steel sheet," *J. Magn. Magn. Mater.*, vol. 160, pp. 109–114, Jul. 1996.

[4] J. W. Shilling, "Domain structure during magnetization of grain-oriented 3% Si–Fe as a function of applied tensile stress," *J. Appl. Phys.*, vol. 42, no. 4, pp. 1787–1789, 1971.

[5] C. R. Boon and J. A. Robey, "Effect of domain-wall motion on power loss in grain-oriented silicon-iron sheet," *Proc. Inst. Electr. Eng.*, vol. 115, no. 10, pp. 1535–1540, Oct. 1968.

[6] K. Tone, H. Shimoji, S. Urata, M. Enokizono, and T. Todaka, "Magnetic characteristic analysis considering the crystal grain of grain-oriented electrical steel sheet," *IEEE Trans. Magn.*, vol. 41, no. 5, pp. 1704–1707, May 2005.

[7] B. N. Filippov, S. V. Zhakov, and Y. G. Lebedev, "Influence of domain structure on some dynamic properties of ferromagnets," *IEEE Trans. Magn.*, vol. 15, no. 6, pp. 1849–1854, Nov. 1979.

[8] R. Langman, "The effect of stress on the magnetization of mild steel at moderate field strengths," *IEEE Trans. Magn.*, vol. 21, no. 4, pp. 1314–1320, Jul. 1985.

[9] T. Yamamoto and T. Nozawa, "Effects of tensile stress on total loss of single crystals of 3% silicon-iron," *J. Appl. Phys.*, vol. 41, no. 7, pp. 2981–2984, Jun. 1970.

[10] T. Olding, M. Sayer, and D. Barrow, "Ceramic sol–gel composite coatings for electrical insulation," *Thin Solid Films*, vols. 398–399, pp. 581–586, Nov. 2001.

[11] H. Yamaguchi, M. Muraki, and M. Komatsubara, "Application of CVD method on grain-oriented electrical steel," *Surf. Coat. Technol.*, vol. 200, no. 10, pp. 3351–3354, 2006.

[12] X. D. He, X. Li, and Y. Sun, "Microstructure and magnetic properties of high silicon electrical steel produced by electron beam physical vapor deposition," *J. Magn. Magn. Mater.*, vol. 320, nos. 3–4, pp. 217–221, 2008.

[13] G. O. Mallory and J. B. Hajdu, Eds., *Electroless Plating: Fundamentals and Applications*. FL, USA: American Electroplaters and Surface Finishers Society, 1990, ch. 4, pp. 121–122.

[14] P. Chivavibul, M. Enoki, S. Konda, Y. Inada, T. Tomizawa, and A. Toda, "Reduction of core loss in non-oriented (NO) electrical steel by electroless-plated magnetic coating," *J. Magn. Magn. Mater.*, vol. 323, nos. 3–4, pp. 306–310, 2011.

[15] D. M. Ionel, M. Popescu, S. J. Dellinger, T. J. E. Miller, R. J. Heideman, and M. I. McGilp, "On the variation with flux and frequency of the core loss coefficients in electrical machines," *IEEE Trans. Ind. Appl.*, vol. 42, no. 3, pp. 658–667, May/Jun. 2006.

[16] D.-H. Kim, K. Aoki, and O. Takano, "Soft magnetic films by electroless Ni-Co-P plating," *J. Electrochem. Soc.*, vol. 142, no. 11, pp. 3763–3767, 1995.

[17] P. I. Anderson, "Measurement techniques for the assessment of materials under complex magnetising conditions," *Electr. Rev.*, vol. 87, no. 9b, pp. 61–64, 2011.

[18] P. I. Anderson, A. J. Moses, and H. J. Stanbury, "Assessment of the stress sensitivity of magnetostriction in grain-oriented silicon steel," *IEEE Trans. Magn.*, vol. 43, no. 8, pp. 3467–3476, Aug. 2007.

[19] R. J. Taylor and J. A. Watt, "Magnetic pattern viewer," U.S. Patent 5 034 754, Jul. 23, 1991.

[20] A. A. Aal, A. Shaaban, and Z. A. Hamid, "Nanocrystalline soft ferromagnetic Ni–Co–P thin film on Al alloy by low temperature electroless deposition," *Appl. Surf. Sci.*, vol. 254, no. 7, pp. 1966–1971, 2008.

[21] A. K. Sharma, M. R. Suresh, H. Bhojraj, H. Narayanamurthy, and R. P. Sahu, "Electroless nickel plating on magnesium alloy," *Metal Finishing*, vol. 96, no. 3, pp. 10, 12, 14, and 16–18, 1998.

[22] J. Y. Song and J. Yu, "Residual stress measurements in electroless plated Ni–P films," *Thin Solid Films*, vol. 415, nos. 1–2, pp. 167–172, 2002.

[23] K. Parker and H. Shah, "The stress of electroless nickel deposits on beryllium," *J. Electrochem. Soc.*, vol. 117, no. 8, pp. 1091–1094, 1970.

[24] N. Fenineche, A. M. Chaze, and C. Coddet, "Effect of pH and current density on the magnetic properties of electrodeposited Co-Ni-P alloys," *Surf. Coat. Technol.*, vol. 88, nos. 1–3, pp. 264–268, 1997.

[25] T. Homma, J. Shiokawa, Y. Sezai, and T. Osaka, "*In situ* analysis of the deposition process of electroless CoNiP perpendicular magnetic recording media," in *Proc. Electroechem. Soc.*, 1995, pp. 181–190.

[26] K. S. Lew, M. Raja, S. Thanikaikarasan, T. Kim, Y. D. Kim, and T. Mahalingam, "Effect of pH and current density in electrodeposited Co–Ni–P alloy thin films," *Mater. Chem. Phys.*, vol. 112, no. 1, pp. 249–253, 2008.

[27] T. Wada, T. Nozawa, and T. Takata, "Method for producing a super low watt loss grain oriented electrical steel sheet," U.S. Patent 3 932 236, Jan. 13, 1976.

[28] R. A. Fisher, "Frequency distribution of the values of the correlation coefficient in samples from an indefinitely large population," *Biometrika*, vol. 10, no. 4, pp. 507–521, May 1915.

[29] W. L. Bragg, "The diffraction of short electromagnetic waves by a crystal," in *Proc. Cambridge Philos. Soc.*, vol. 17. 1913, pp. 43–57.

Journal of Magnetism and Magnetic Materials 407 (2016) 42–45

Contents lists available at ScienceDirect

Journal of Magnetism and Magnetic Materials

journal homepage: www.elsevier.com/locate/jmmm

Current Perspectives

Electroless Co–P-Carbon Nanotube composite coating to enhance magnetic properties of grain-oriented electrical steel

Vishu Goel [a,*], Philip Anderson [a], Jeremy Hall [a], Fiona Robinson [b], Siva Bohm [c]

[a] Wolfson Centre for Magnetics, Cardiff University, Cardiff CF243AA, United Kingdom
[b] Cogent power Ltd., Newport NP19 0RB, United Kingdom
[c] IIT Bombay, Mumbai 400076, India

ARTICLE INFO

Article history:
Received 5 May 2015
Received in revised form
9 October 2015
Accepted 21 December 2015
Available online 12 January 2016

Keywords:
Power loss
Surface roughness
Electroless
Grain-oriented

ABSTRACT

The effect of Co–P-CNT coating on the magnetic properties of grain oriented electrical steel was investigated. To analyse the coating, Raman spectroscopy, Superconducting QUantum Interference Device (SQUID), single strip testing, Scanning Electron Microscopy (SEM) and talysurf surface profilometry were performed. Raman spectra showed the D and G band which corroborates the presence of Multi-Walled Carbon Nanotubes (MWCNT) in the coating. The magnetic nature of the coating was confirmed by SQUID results. Power loss results show an improvement ranging 13–15% after coating with Co–P-CNT. The resistivity of the coating was measured to be 10^4 μΩ cm. Loss separation graphs were plotted before and after coating to study the improvement in power loss. It was found that the coating helps in reducing the hysteresis loss. The thickness of the coating was found to be 414 ± 40 nm. The surface profilometry results showed that the surface roughness improved after coating the sample.

1. Introduction

Grain-oriented electrical steel (GOES) laminations are utilized in the ferromagnetic cores of the majority of high efficiency power and distribution transformers. They are characterised by low power losses and high permeability which maximize the performance of these essential devices.

Improvements in the chemistry and process technologies for these materials have brought large improvements in their properties over the last 20 years [1]. However further optimization is likely to bring only incremental improvements. Coatings applied to these steels have the potential to provide far larger gains and are therefore the subject of significant research effort.

The main role of the steel coating is to reduce power loss which is achieved by two main mechanisms. Firstly the coatings provide an insulating layer between laminations which reduces the eddy currents circulating in the device. Secondly there is reduction in both the hysteresis [2] and anomalous loss as a result of beneficial tensile stress [3] to the substrate. A tensile stress applied on GOES helps in minimizing the losses by reducing the domains perpendicular to the direction of magnetization. The tensile stress also results in narrowing the domain wall spacing which decreases the anomalous loss due to a reduction in average wall velocity. The reverse happens when compressive stress is applied to GOES i.e. domain width increases as does the volume of perpendicular structure due to a switch to new domain configurations known as stress patterns [4]. Thus coatings which provide high levels of tension to the steel substrate or that have a high strength such that the substrate is protected from in-plane compressive stress are particularly attractive for this application.

Carbon Nanotubes (CNTs) are known for their mechanical properties such as high strength, elastic modulus, elastic strain bearing tendency [5,6], flexibility [7] and many other properties which make CNTs favourable for a number of applications. The calculation of the theoretical Young's modulus of single walled CNT of 5 GPa [8] and its bending strength of 14.2 GPa [9] make it ideal for use in a composite coating. CNTs are mostly used in composite coatings for improving the tribological properties of the material [10–14]. For example, Chen et. al. [10] showed that the addition of CNTs in the coating increases the hardness of the coating.

This work presents the use of electroless plating for depositing Co–P-CNT composite coating on the surface of grain oriented electrical steel. Cobalt was chosen as it is magnetically active and has a comparable saturation magnetization of 167 emu/g as that of iron (221 emu/g). This could offer a significant additional advantage in that it would increase the core stacking factor defined as the ratio of magnetic to non-magnetic material in the transformer core and could thus also be increased through a reduction

* Corresponding author.
E-mail addresses: vishu.goel.nit@gmail.com (V. Goel), AndersonPI1@cf.ac.uk (P. Anderson), HallJP@cf.ac.uk (J. Hall), fiona.cj.robinson@tatasteel.com (F. Robinson), siva.bohm@tatasteel.com (S. Bohm).

http://dx.doi.org/10.1016/j.jmmm.2015.12.076

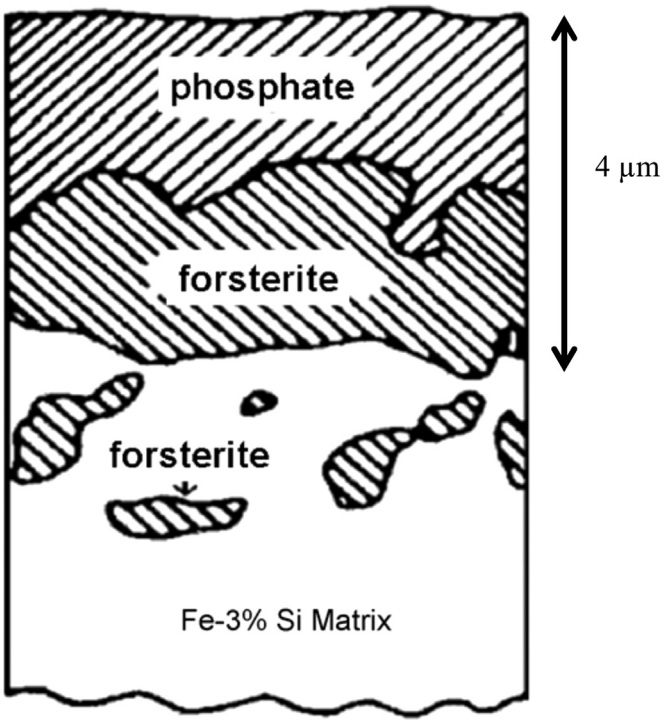

Fig. 1. Conventional coated Iron–3% Silicon showing layers of phosphate and forsterite.

in overall coating thickness. The current coating system of forsterite (Mg_2SiO_4) and aluminium orthophosphate coating, with a total thickness of 4 μm per side as shown in Fig. 1, are non-magnetic and hence reduce the stacking factor.

2. Material and method

Fully finished grain oriented (Fe–3%Si) samples (0.3 mm × 30 mm × 305 mm) were supplied by Cogent Power Ltd., Newport UK and both the coatings were removed with a solution of 7.5% sulphuric acid + 1% Hydrofluoric acid for approximately 10 min and then in 4% Nitric acid solution for approximately 7 min. The samples were then cut into 0.3 mm × 30 mm × 75 mm. Samples were coated with Co–P-CNT coating. The solution was stirred with magnetic stirrer to suspend the MWCNTs in the solution. The composition of the bath was taken from [15] and modified by adding 0.2 g/l of MWCNTs in the solution. The modified bath and operating conditions are shown in Table 1. The pH of the solution was maintained by adding ammonia hydroxide. The samples were immersed in the bath at a temperature of 50 °C and the final bath temperature recorded was 62 ± 1 °C.

The samples were coated for different time periods and optimized to get best improvement of power loss. Samples were also coated without CNTs in the plating solution to study the effect of Co–P coating on grain oriented electrical steel.

Table 1
Bath Composition and conditions.

Chemical reagent	Concentrations (g/l)
Cobalt sulphate	14
Sodium hypophosphite	25
Trisodium citrate	45
MWCNT	0.2
pH at 25 °C	9.7
Temperature	62 ± 1 °C

The MWCNTs used in coating the samples were supplied by M/s Haydale Ltd UK. The MWCNTs were used in the as received condition. The power loss testing was performed with the single strip tester (SST) [16] from a magnetic flux density of 0.1 T to 1.8 T and a frequency of 50 Hz. The results are shown at 1.5 and 1.7 T magnetic flux density and 50 Hz frequency as these are common operational parameters for distribution transformers in the UK. The resistivity of the coating was measured by a four point probe method using a glass sheet coated with Co–P-CNT. The induced voltage across two probes under controlled current excitation was measured in the coating and the resistance was calculated.

The microscopy images were obtained from a Philips XL30 Environmental Scanning Electron Microscope (ESEM) Field Emission Gun (FEG). The magnetic properties of the coating were measured at room temperature by Superconducting QUantum Interference Device (SQUID) based magnetometer from Digital Instruments. The magnetic field was applied up to ± 20,000 Oe. From −100 to +100 the rate of change in field was 0.25 Oe/s, between ±1000 and ±100 the rate of change was 1.5 Oe/s and from ±20,000 to ±1000 the rate of change was 15.15 Oe/s. The sample was manufactured from a square glass slide coated with Co–P-CNT such that the magnetic field was applied in the plane of sample.

The surface roughness of the uncoated and coated surfaces was measured by talysurf surface profilometer. The measurement was made in the direction of rolling for a distance of 40 mm for all the samples.

To determine the presence of MWCNTs in the coating the samples were analysed using a Renishaw inVia Raman microscope. The coated samples were excited with a 514 nm argon laser with the power maintained at 12.5 mW and a spot size of 5 μm. The Raman spectra spanning between 800 and 2100 cm^{-1} was obtained at five different spots.

2.1. Raman spectroscopy

The Raman spectrum of the coated samples is shown in Fig. 2. The main characteristic bands obtained were the D and G bands at around 1360 and 1590 cm^{-1}, respectively. The D band represents the disorder/distortions in the MWCNTs or the sp^3 bonds whereas the G band confirms the presence of graphite or the sp^2 bonds, both confirming a significant volume fraction of MWCNTs in the coating. All five characterised areas showed the same characteristic D and G bands which confirms that the MWCNTs were uniformly distributed in the coating whilst the uncoated sample did not show either D or G bands. The percentage, by weight, of CNTs

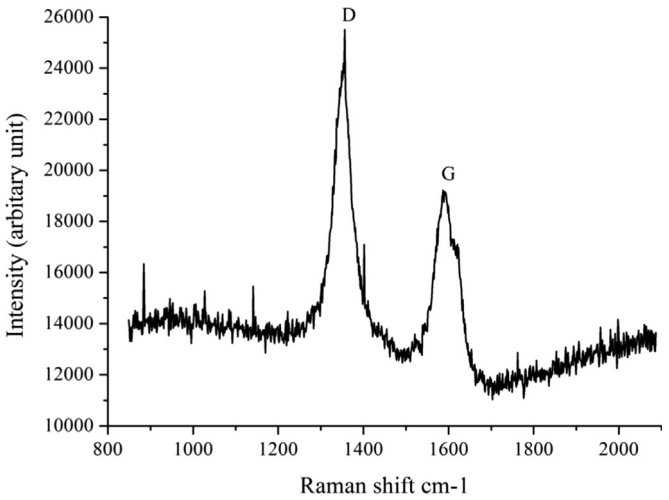

Fig. 2. Raman spectra of the Co–P-CNT coated sample showing the D and G bands.

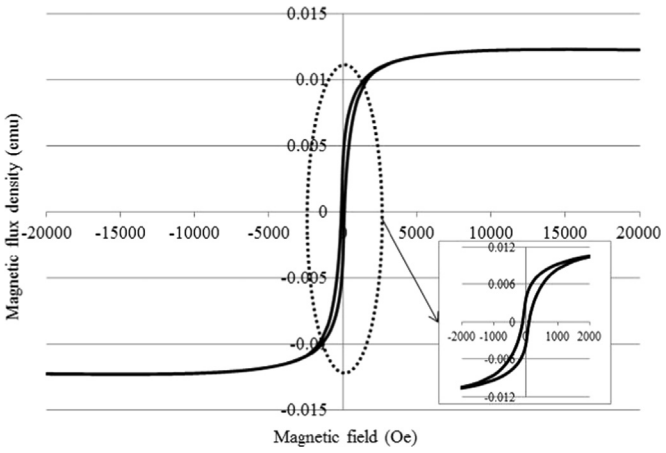

Fig. 3. Magnetic characterization of Co–P-CNT coated at pH of 9.7.

in the solution was calculated to be 0.24% by adding the weight of different components in the solution and then dividing the CNTs weight by added components.

2.2. Magnetic properties

Fig. 3 shows a hysteresis loop for Co–P-CNT coating (with a sample of volume 3 mm × 3 mm × 2 μm) at a pH of 9.7. The B–H loop measured in the SQUID confirms that the coating is ferromagnetic with coercivity 100 Oe and saturation magnetization of 683 emu/cm^3. The coercivity of cobalt varies widely depending upon the process route and alloying elements with the addition of non-magnetic elements such as phosphorus and CNT's in the coating raising the coercivity.

2.3. Power loss and resistivity

Fig. 4 shows the average results of five uncoated and Co–P-CNT coated samples for two magnetic flux densities of 1.5 and 1.7 T. It can be seen from Fig. 4 that the coated samples show a power loss improvement ranging from 13% to 15% at 1.7 T, 50 Hz. To isolate the effect of CNTs a sample was coated with Co–P without the addition of CNTs. The coated sample did not show any improvement in power loss which confirms that the improvement was only due to the presence of CNTs in the coating.

The measured resistivity of the coating was approximately 10^4 μΩ cm due to the disorder in the lattice structure of cobalt by co-deposition of phosphorus and CNTs.

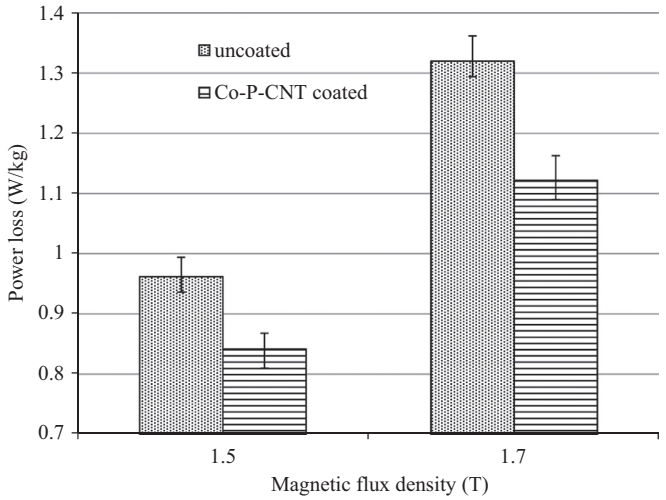

Fig. 4. Power loss of uncoated and Co–P-CNT coated sample at various flux densities and 50 Hz frequency (average of five samples).

2.4. Loss separation

The model used here for loss separation was proposed by Ionel et al. [17]. The power loss equation can be written as

$$W = k_h f B^{\alpha} + k_e f^2 B^2 + K_a f^{1.5} B^{1.5} \quad (1)$$

where W is the total loss (W/kg), f is the frequency (Hz), B is the magnetic flux density (T),

k_h, k_e, k_a are coefficients for hysteresis, eddy current and anomalous loss respectively,

$k_h f B^{\alpha}$ is the hysteresis loss, $k_e f^2 B^2$ is the eddy current, $K_a f^{1.5} B^{1.5}$ is the anomalous loss and α is a constant.

In order to extract the individual components, the total loss per cycle can be calculated from (1) as below

$$W/f = k_h B^{\alpha} + k_e f B^2 + K_a f^{0.5} B^{1.5} \quad (2)$$

$$W = a + bf^{0.5} + cf \quad (3)$$

Eq. (2) can be compared to a quadratic equation of the type $a+bx+cx^2$ as shown in (3) and the coefficients of $f^{0.5}$ can be found by plotting a fitting curve. The values were plotted over a range of frequencies from 10 Hz to 1000 Hz. The value of correlation coefficient r^2 [18] was 0.9994 and 0.9998 for the uncoated and Co–P-CNT coated sample. On plotting the loss separation graph before and after coating, the results shown in Fig. 5 were obtained. It can be clearly seen from the figure that the coated sample shows a significant reduction of 0.27 W/kg in hysteresis loss while the eddy current and anomalous loss increase was insignificant.

2.5. Scanning Electron Microscopy

Fig. 6 shows the SEM image of a 60 min coated sample. It can be seen from the image that the coating, the white area in the image, makes the surface smoother by variable deposition based on the surface contours. On visual inspection the adherence between the coating and the sample was found to be good with no gaps or cracks. The average thickness of the coating was measured to be around 414 ± 40 nm for sample coated for 60 min giving a stacking factor of 99.73% compared to 97.4% for a conventional 4 μm coating. Considering the saturation magnetization of Co–P-CNT coating (0.0123 emu) the stacking factor rises to 99.85%.

2.6. Surface profiling

A higher surface roughness affects the magnetization of core

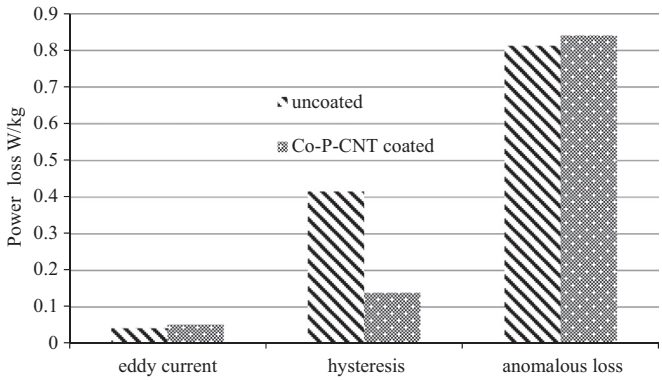

Fig. 5. Loss separation for the uncoated and Co–P-CNT coated sample at a flux density of 1.7 T and 50 Hz frequency.

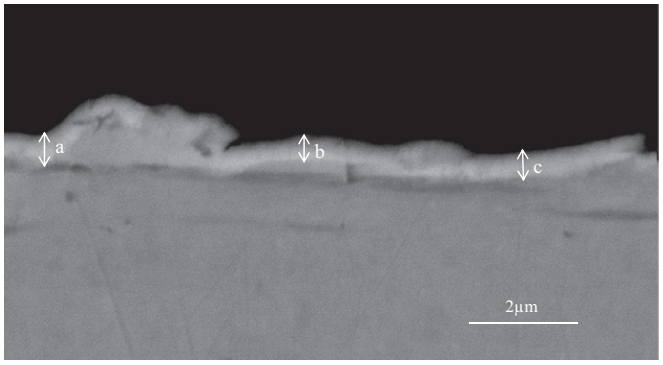

Fig. 6. SEM image of the sample coated with Co–P-CNT for 60 min showing thickness $a=452$ nm, $b=376$ nm and $c=414$ nm.

material by pinning the domain walls [2]. The surface roughness (Ra) of uncoated, Co–P and Co–P-CNT coated surfaces was measured to be 695 ± 10 nm, 631 ± 6 nm and 437 ± 3 nm respectively with the coated values being a combination of substrate and coating roughness.

Wang et al. [11] performed surface roughness measurements on Ni–P-CNT coated samples and found they were between 100 and 300 nm whilst Alishahi et al. [19] reported that wear properties of the surface could be enhanced by an improvement in surface roughness from a CNT coating. The surface roughness (Ra) of Ni–P and Ni–P-CNT coated sample was shown to be reduced from 192 nm to 129 nm and corrosion resistance of Ni–P coatings was improved with the incorporation of CNTs due to their high chemical stability. The improvement in surface roughness was thought to be due to the reduction in deposited particle size by addition of CNTs [20].

The surface roughness has been shown to directly affect the hysteresis loss. Wada et al. [2] showed that power losses could be reduced by 30–40% on improving the surface roughness due to a reduction in the number of free poles at the surface. These free poles pin the domain wall reducing the number of mobile walls leading to inhomogeneous domain wall motion. Freeing up these domains leads to a significant reduction in the total loss. Improving the surface roughness with a non-magnetic coating would not contribute to an improvement in magnetic properties of the material as the magnetic path on the surface would remain unchanged.

2.7. Conclusions

In general two stage non-magnetic coatings are used to impart tensile stress to grain oriented electrical steel in order to reduce power losses. In this work a novel attempt was made to improve the power loss in the range of 13–15% by enhancing the surface roughness with a magnetically active Co–P-CNT coating. The coating was shown to exhibit the desirable insulation properties with a resistivity of 10^4 μΩ cm. The loss separation data showed that hysteresis loss was reduced by the coating which was attributed mainly to a surface roughness improvement. The stacking factor was improved to 99.85% based on two factors. The thickness of Co–P-CNT coating was reduced by almost 90% to 414 nm as compared to the conventional coating of 4 μm. The high value of saturation magnetization of the coating further raised the stacking factor by replacing non-magnetic material in the core by a magnetic material.

Acknowledgement

This work was supported by Tata Steel RD&T, Rotherham and Cogent Power Ltd., Newport.

References

[1] A.J. Moses, Energy efficient electrical steels: magnetic performance prediction and optimization, Scr. Mater. 67 (2012) 560–565.
[2] T. Wada, T. Nozawa, T. Takata, Method for producing a super low watt loss grain oriented electrical steel sheet, US Patent, vol. 3932236, January 13, 1976.
[3] T. Yamamoto, T. Nozawa, Effects of tensile stress on total loss of single crystals of 3% Silicon–Iron, J. Appl. Phys. 41 (1970) 2981–2984.
[4] L.J. Dijkstra, U.M. Martius, Domain patterns in silicon iron under stress, Rev. Mod. Phys. 25 (1953) 146–150.
[5] G. Overney, W. Zhong, D. Tomamek, Structural rigidity and low frequency vibrational modes of long carbon tubules, Z. Phys. D 27 (1993) 93–96.
[6] J.P. Salvetat, J.M. Bonard, N.H. Thomson, A.J. Kulik, L. Forr´o, W. Benoit, et al., Mechanical properties of carbon nanotubes, Appl. Phys. A 69 (1999) 255–260.
[7] S. Iijima, Structural flexibility of carbon nanotubes, J. Chem. Phys. 104 (1996) 2089–2092.
[8] M.M.J. Treacy, T.W. Ebbesen, J.M. Gibson, Exceptionally high Young's modulus observed for individual carbon nanotubes, Nature 381 (1996) 678–680.
[9] E.W. Wong, P.E. Sheehan, C.M. Lieber, Nanobeam mechanics: elasticity, strength and toughness of nanorods and nanotubes, Science 277 (1997) 1971–1975.
[10] W.X. Chen, J.P. Tu, Z.D. Xu, W.L. Chen, X.B. Zhang, D.H. Cheng, Tribological properties of Ni–P-multi-walled carbon nanotubes electroless composite coating, Mater. Lett. 57 (2003) 1256–1260.
[11] L.Y. Wang, J.P. Tu, W.X. Chen, Y.C. Wang, X.K. Liu, C. Olk, et al., Friction and wear behavior of electroless Ni-based CNT composite coatings, Wear 254 (2003) 1289–1293.
[12] W.X. Chen, J.P. Tu, H.Y. Ga, Z.D. Xu, Q.G. Wang, J.Y. Lee, et al., Electroless preparation and tribological properties of Ni–P-Carbon nanotube composite coatings under lubricated condition, Surf. Coat. Technol. 160 (2002) 68–73.
[13] X.H. Chen, C.S. Chen, H.N. Xiao, H.B. Liu, L.P. Zhou, S.L. Li, et al., Dry friction and wear characteristics of nickel/carbon nanotube electroless composite deposits, Tribol. Int. 39 (2006) 22–28.
[14] X. Chen, J. Xia, J. Peng, W. Li, S. Xie, Carbon-nanotube metal-matrix composites prepared by electroless plating, Compos. Sci. Technol. 60 (2000) 301–306.
[15] Z. Li, B. Shen, Y. Deng, L. Liu, W. Hu, Preparation and microwave absorption properties of electroless Co–P-coated nickel hollow spheres, Appl. Surf. Sci. 255 (2009) 4542–4546.
[16] P. Anderson, Measurement techniques for the assessment of materials under complex magnetising conditions, Electr. Rev. 87 (2011) 61–64.
[17] D.M. Ionel, M. Popescu, S.J. Dellinger, T.J.E. Miller, R.J. Heideman, M.I. McGilp, On the variation with flux and frequency of the core loss coefficients in electrical machines, IEEE Trans. Ind. Appl. 42 (2006) 658–667.
[18] R. Taylor, Interpretation of the correlation coefficient: a basic review, J. Diagn. Med. Sonogr. 6 (1990) 35–39.
[19] M. Alishahi, S.M. Monirvaghefi, A. Saatchi, S.M. Hosseini, The effect of carbon nanotubes on the corrosion and tribological behavior of electroless Ni–P-CNT composite coating, Appl. Surf. Sci. 258 (2012) 2439–2446.
[20] Z. Yang, H. Xu, M.-K. Li, Y.-L. Shi, Y. Huang, H.-L. Li, Preparation and properties of Ni/P/single-walled carbon nanotubes composite coatings by means of electroless plating, Thin Solid Films 466 (2004) 86–91.

AIP Advances

CrAlN coating to enhance the power loss and magnetostriction in grain oriented electrical steel

Vishu Goel, Philip Anderson, Jeremy Hall, Fiona Robinson, and Siva Bohm

Citation: AIP Advances **6**, 055924 (2016); doi: 10.1063/1.4944340
View online: http://dx.doi.org/10.1063/1.4944340
View Table of Contents: http://scitation.aip.org/content/aip/journal/adva/6/5?ver=pdfcov
Published by the AIP Publishing

CrAlN coating to enhance the power loss and magnetostriction in grain oriented electrical steel

Vishu Goel,[1] Philip Anderson,[1] Jeremy Hall,[1] Fiona Robinson,[2] and Siva Bohm[3]
[1]*Wolfson Centre for Magnetics, Cardiff University, Cardiff- CF243AA, United Kingdom*
[2]*Cogent power Ltd., Newport-NP190RB, United Kingdom*
[3]*Dept. of metallurgical engineering & materials science, IIT Bombay, Mumbai-400076, India*

(Presented 13 January 2016; received 5 November 2015; accepted 6 January 2016; published online 11 March 2016)

Grain oriented electrical steels (GOES) are coated with aluminium orthophosphate on top of a forsterite (Mg_2SiO_4) layer to provide stress and insulation resistance to reduce the power loss and magnetostriction. In this work Chromium Aluminium Nitride (CrAlN) was coated on GOES samples with electron beam physical vapour deposition and was tested in the single strip and magnetostriction tester to measure the power loss and magnetostriction before and after coating. Power loss was reduced by 2% after coating and 6 % post annealing at 800 °C. For applied compressive stress of 6 MPa, the magnetostrictive strain was zero with the CrAlN coating as compared to 22 and 24 με for fully finished GOES and GOES without phosphate coating. The thickness of the coating was found to be 1.9 ± 0.2 μm estimated with Glow Discharge Optical Emission Spectroscopy (GDOES). The magnetic domain imaging showed domain narrowing after coating. The reduction in power loss and magnetostriction was due to the large residual compressive stress and Young's modulus (270 GPa) of the coating. [http://dx.doi.org/10.1063/1.4944340]

I. INTRODUCTION

Grain oriented electrical steel (GOES) (Fe + 3% Si) is used in transformer cores where it undergoes a cycle of magnetization and demagnetization leading to a loss of energy. Additionally it expands and contracts due to the phenomenon of magnetostriction and causes acoustic noise. Advancement in steel making technologies,[1] better understanding of the domain behaviour[2] and, gauge reduction[3] have led to large improvements in these magnetic properties but continued improvements will be most likely introduced by new coatings[4] technologies. Coatings fulfil two roles: providing insulation resistance to minimise the eddy currents and imparting tensile stress to refine the domain structure which minimises the anomalous loss and magnetostriction. The current coating system comprises a forsterite layer (Mg_2SiO_4) formed during a high temperature batch anneal and aluminium orthophosphate layer which is roller coated and cured.

Research at Cardiff has focused on identifying new coating materials which would lead to significant improvements in the steel magnetic performance. Previously the authors have described the application of Co-Ni-P coating on GOES which showed 9-11% reduction in power loss and an improvement of 2MPa in magnetostriction.[5] The research has also identified a class of coatings described by $Cr_{1-x}Al_xN$. This ceramic material possesses ideal characteristics for providing high tension and inter laminar insulation. The residual compressive stress generated by $Cr_{1-x}Al_xN$ coating is quoted in the range of 4.5 to 5.6 GPa based upon the type of deposition process, parameters and chemical composition of the coating.[6] Reiter et al.[7] has varied the aluminium content in the coating and found that a compressive residual stress of around 5 GPa and microhardness of 37000 N/mm^2 was observed at x=0.46. This compressive stress in the coating results in a tensile stress being applied to the substrate. As an electrical steel coating is required to provide

electrical insulation the resistivity of any new coating is important. The resistivity of GOES is 4.6 x 10^{-7} Ωm and that of $Cr_{1-x}Al_xN$ coating depends upon the amount of aluminium content in the coating and increases from 3.5 x 10^{-3} to 2 x 10^{-1} Ωm for x=0 to x=0.55[8] respectively at room temperature.

The coating can be deposited by a number of Physical/Chemical Vapour Deposition (P/CVD) techniques. For this study electron beam PVD was utilised to enable a range of material parameters to be trialled. Production quantities of coated materials can be produced on industrial scale electron beam PVD systems such as that available in Tata steel Ijmuiden. The system also offers high deposition rates, manipulation of the composition and microstructure and, low impurity content.

II. EXPERIMENTAL PROCEDURE

GOES samples (305mm x 30mm x 0.3mm) with forsterite layer and without the aluminium orthophosphate coating were supplied by Cogent Power Ltd., Newport.

CrAlN coatings were deposited on the samples by electron beam physical vapour deposition (EB-PVD) under vacuum by Wallwork Cambridge. The samples were vapour blasted to remove any dust/grease from the surface and were then sputter cleaned in the argon filled chamber at 450 °C removing any oxide layer present and enhancing the bonding capabilities of the steel for further deposition. The deposition temperature was set to 350-450 °C and pure chromium was deposited on the substrate. Nitrogen was then injected into the chamber and the opening of the chromium and aluminium shutters were controlled to get the final deposition of CrAlN. The whole process took around 6 hours.

To characterise the samples, power loss testing was performed before and after coating at a magnetic flux density of 1.7T and 50Hz frequency in a single strip tester[9] with 865 primary and 250 secondary turns. The resistivity of the coating was calculated from a 4 probe resistance measurement over a 70 mm length. The magnetostriction was measured with a magnetostriction measurement system[10] over a range of applied stress from -10 to 10 MPa. The magnetic domain structure was imaged with magnetic pattern viewer based on the bitter technique.[11] The chemical composition of the coating was analysed with Glow Discharge Optical Emission Spectroscopy (GDOES) JY 5000RF at 30 W, 3.0 mbar. Samples were thermal flattened in the high temperature annealing furnace at 800 ° C for 1 hour in vacuum for magnetic testing.

III. RESULTS AND DISCUSSION

A. Coating properties

The coating had a very distinctive pale blue/silver appearance and no gaps or cracks were observed inferring good bonding between coating and substrate. The hardness and Young's modulus of the coating were 3000 HV and 270 GPa respectively.

B. Magnetostriction

The magnetostriction result for a typical GOES, without phosphate coating, with CrAlN coating and projected value of CrAlN magnetostriction is shown in figure 1. The value was projected to estimate the shift in the magnetostriction characteristic after coating. The threshold magnetostriction (magnetostriction <= 0) was shifted from 2 MPa in GOES without phosphate layer to -6 MPa in CrAlN coated sample. The large reduction in magnetostriction was believed to be due to the high Young's modulus of the coating (270GPa) as compared to GOES (113GPa) which restricts the expansion of GOES sample under the influence of applied magnetic field. The high value of Young's modulus was due to the dissolution of aluminium atoms in the face centred cubic-chromium nitride lattice structure which strains it. This hindered the movement of dislocations which increased the Young's modulus.

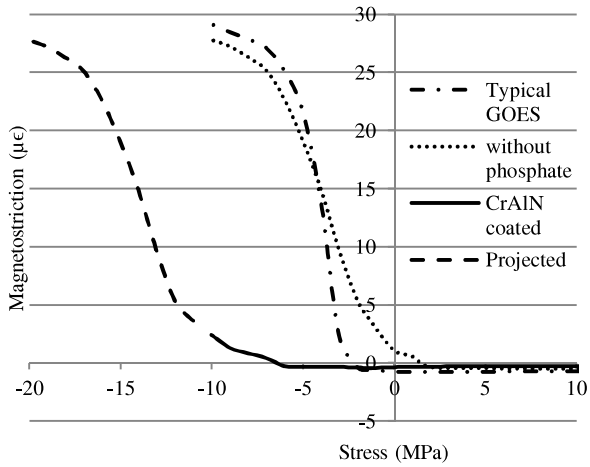

FIG. 1. Effect of stress on magnetostriction for typical GOES, GOES without phosphate and CrAlN coated samples.

C. Power loss

The power loss result of the GOES, GOES without phosphate coating, CrAlN coated and annealed sample is shown in figure 2. The power loss increased after removal of phosphate coating and it was reduced by 2.0% after coating the sample with CrAlN thin film. The samples showed further reduction in power loss of about 4% after annealing. The resistivity of the coating was measured to be 4.29 x 10^{-2} Ωm. The reduction in power loss was due to the residual compressive stress in the coating which applies beneficial tensile stress on GOES and hence reduces the power loss.

D. Magnetic Domain Imaging

To understand the effect of coating stress on GOES, samples were imaged under a magnetic domain viewer. The domain images of the GOES without phosphate coating (a) and CrAlN coated (b) are shown in figure 3. The domains were narrowed after coating and the average domain width reduced from 0.76 mm to 0.42 mm. The reduction in domain width reduces the domain wall velocity as the walls travel less distance in the given time. This reduces the anomalous loss as the loss is directly proportional to square of wall velocity.[12] Hence the total loss was reduced.

E. Chemical composition and thickness

The results obtained from the GDOES are shown in Figure 4. The thickness of the coating was approximated to be around 1.9 ± 0.2 μm from this technique and contained two distinct areas. The

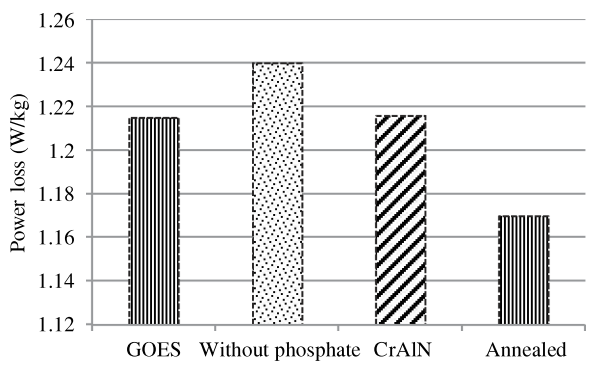

FIG. 2. Power losses for the GOES, without phosphate coating, CrAlN coated and CrAlN annealed samples.

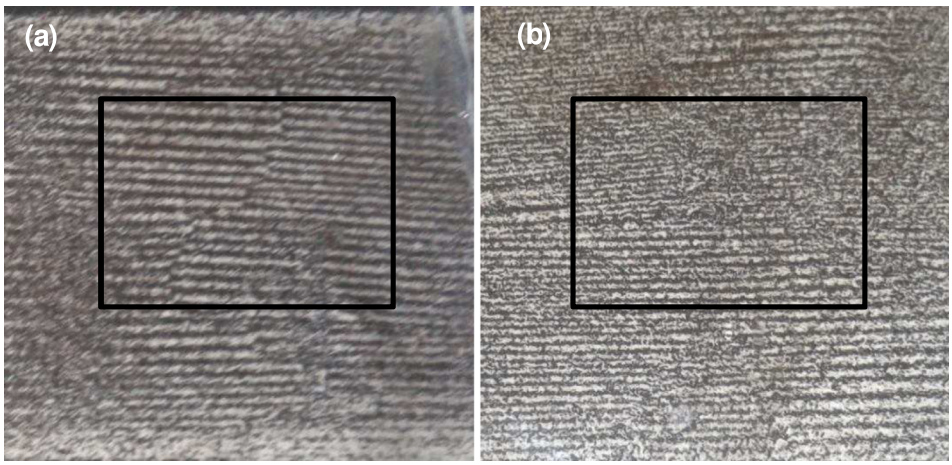

FIG. 3. Magnetic domain imaging showing GOES without phosphate coating (a) and narrowing of domain after coating (b).

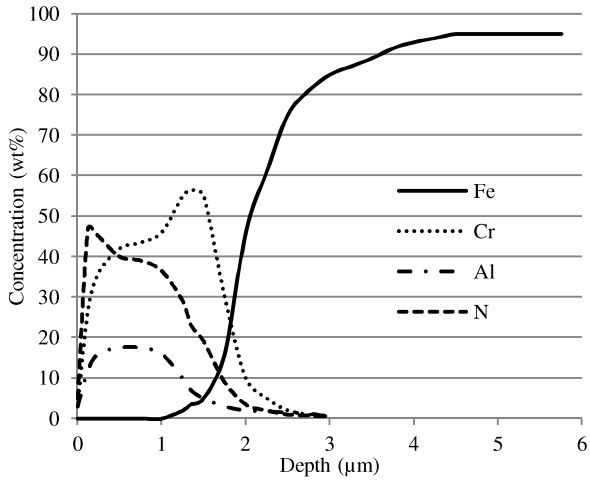

FIG. 4. In-depth spectroscopy of CrAlN coating.

percentage of Cr in the coating varied from 40-60 with a lower percentage near the surface than to the interface. The aluminium and nitrogen contents followed an opposite concentration gradient, i.e. higher concentrations at the surface with the aluminium increasing from 0% at the interface to around 20 % at the surface. This behaviour suggested that during deposition a thin layer of CrN was laid first on which a layer of CrAlN was deposited. In the region from 1.5-2 μm there was an overlap of chemicals from the forsterite coating and CrAlN coating as shown in Figure 4 which suggests that the Cr, Al and N atoms of the CrAlN coating were embedded in the forsterite layer which disturbs the bond structure of the forsterite coating and introduces stress in the coating. It is proposed that this stress was able to reduce the power loss.

IV. CONCLUSION

CrAlN coating of 1.9 ± 0.2 μm thickness was applied on GOES by EB-PVD process which is an industrially viable technique. The coating was able to reduce the power loss by 6% post annealing. The magnetostriction was reduced to 3 με from 27 με for applied compressive stress of 10 MPa by coating. The reduction in the power loss was due to the beneficial tensile stress applied on GOES by the coating. The magnetostriction was largely reduced due to the higher Young's modulus of the coating.

[1] A. J. Moses, "Energy efficient electrical steels: Magnetic performance prediction and optimization," Scripta Materialia **67**, 560-565 (2012).
[2] J. W. Shilling, "Domain Structure During Magnetization of Grian-Oriented 3% Si-Fe as a function of Applied Tensile Stress," Journal of Applied Physics **42**, 1787-1789 15 Mach 1971.
[3] H. Haiji, K. Okada, T. Hiratani, M. Abe, and M. Ninomiya, "Magnetic properties and workability of 6.5% Si steel sheet," Journal of Magnetism and Magnetic Materials **160**, 109-114 (1996).
[4] E. Beyer, L. Lahn, C. Schepers, and T. Stucky, "The influence of compressive stress applied by hard coatings on the power loss of grain oriented electrical steel sheet," Journal of Magnetism and Magnetic Materials **323**, 1985-1991 (2011).
[5] V. Goel, P. Anderson, J. Hall, F. Robinson, and S. Bohm, "Application of Co-Ni-P coating on grain-oriented electrical steel," IEEE transactions on magnetics (2015) (DOI 10.1109/TMAG.2015.2496315).
[6] G. S. Kim and S. Y. Lee, "Microstructure and mechanical properties of AlCrN films deposited by CFUBMS," Surface & Coatings Technology **201**, 4361-4366 (2006).
[7] A. E. Reiter, V. H. Derflinger, B. Hanselmann, T. Bachmann, and B. Sartory, "Investigation of the properties of $Al_{1-x}Cr_xN$ coatings prepared by cathodic arc evaporation," Surface & Coatings Technology **200**, 2114-2122 (2005).
[8] R. Sanjine's, O. Banakh, C. Rojas, P. E. Schmid, and F. Lévy, "Electronic properties of Cr1yxAlxN thin films deposited by reactive magnetron sputtering," Thin Solid Films **420-421**, 312-317 (2002).
[9] P. Anderson, "Measurement techniques for the assessment of materials under complex magnetising conditions," Electrical review **87**, 61-64 (2011).
[10] P. I. Anderson, A. J. Moses, and H. J. Stanbury, "Assessment of the Stress Sensitivity of Magnetostriction in Grain-Oriented Silicon Steel," IEEE Transactions on Magnetics **43**, 3467-3476 (2007).
[11] R. J. Taylor and J. A. Watt, "Magnetic pattern viewer," US Patent 034754 A (1991).
[12] C. R. Boon and J. A. Robey, "Effect of domain-wall motion on power loss in grainoriented silicon-iron sheet," Proceedings of the IEEE **115**, 1535-1540 (1968).

Electroless Plating: A Versatile Technique to Deposit Coatings on Electrical Steel

Vishu Goel[1], Philip Anderson[1], Jeremy Hall[1], Fiona Robinson[2], and Siva Bohm[3]

[1]Wolfson Centre for Magnetics, Cardiff University, Cardiff CF243AA, U.K.
[2]Cogent Power, Newport NP19 0RB, U.K.
[3]Tata Steel Research, Development and Technology, Rotherham S603AR, U.K.

Coatings on grain-oriented electrical steel (GOES) are produced primarily by roller coating deposition of aluminum orthophosphate on the top of forsterite. These coatings provide the insulation resistance and stress to improve the magnetic properties. Electroless deposition of nickel- and cobalt-based coatings could be used as an alternative, because these coatings can be made insulated and stress can be generated and tailored in these coatings. The rate of deposition in electroless plating is faster when compared with other chemical coating techniques, and the process is autocatalytic (no external current required). The coatings are corrosion resistant, and the magnetic properties of the coatings can be varied by simply changing the pH of the solution. Addition of alloying elements, such as phosphorus and boron, can manipulate the stress generated in the coating from tensile to compressive and vice versa. A 2.15 ± 0.15 μm thick Co–Ni–P coating on GOES was able to reduce the power loss by 9%–11%. Similarly, a 414 ± 40 nm thick coating of Co–P-carbon nanotube (CNT) on GOES was able to reduce the power losses ranging 13%–15%. The reduction in power loss in a Co–Ni–P coated sample was due to the tensile stress applied to GOES by the coating that reduced the anomalous loss. The surface roughness was improved for both the Co–Ni–P and Co–P-CNT coatings. An improvement in the surface roughness contributed to the reduction of hysteresis loss.

Index Terms— **Electroless coating, magnetostriction, power loss, stress.**

I. Introduction

GRAIN-ORIENTED electrical steels (GOESs) are used in the transformer cores, and have grains oriented along the length of the sample, which make it easy to magnetize and demagnetize under the ac operating conditions. These steels are coated with an aluminum orthophosphate-based coating on the top of a forsterite layer, which provides the desired tension [1] and insulation to the steel substrate reducing power losses in the B–H magnetizing cycle. In order to improve on these conventional roller coating methods, several other coating techniques have been investigated, including physical vapor deposition [2] and electroless plating [3].

The electroless plating is a commonly used technique for coating a wide variety of materials. It is a coating technique, in which the metal to be deposited is reduced on the substrate with the help of a reducing agent. No external current is supplied for the process to take place, and so it is also known as autocatalytic. The process is monitored by supplying the metal ions or a reducing agent. The substrate is made as cathode and the metal salt as anode. The exact process parameters for electroless deposition were given in [4]. Pure nickel is highly conductive, and thus, a nickel coating would lead to the generation of eddy currents if coated on the electrical steels. Alloying it with elements, such as phosphorus, boron, and cobalt, was shown to significantly affect the final properties [5]. Addition of phosphorus to nickel coating increased the overall resistivity [6].

The properties of these coatings could be highly beneficial to the electrical steels due to their high resistivity and high-compressive stress developed in the coating.

Manuscript received August 25, 2015; revised December 11, 2015; accepted January 3, 2016. Date of publication January 8, 2016; date of current version April 15, 2016. Corresponding author: V. Goel (e-mail: vishu.goel.nit@gmail.com).

Digital Object Identifier 10.1109/TMAG.2016.2514745

In the investigation, two coatings were chosen to be deposited by the electroless plating on GOES.

A. Co–Ni–P Coating

Ni–Co–P (nickel > cobalt) has high saturation magnetization, permeability, and low coercive force [5]. The resistivity of these coatings ranges from 7.9 to 13.6×10^{-7} Ωm depending upon the amount of cobalt used, and is higher than the typical 3% Si steel (4.5×10^{-7} Ωm). Chivavibul *et al.* [3] produced an electroless Ni–Co–P (56%–59% Ni, 32%–35% Co, and 8%–10% P by mass) coating of 1 μm thickness on non-oriented electrical steel and found that the coating was effective in reducing losses by up to 4% at a magnetic flux density of 0.3 T and a frequency of 400 Hz. The coating was able to provide insulation resistance and minimize the eddy current loss at higher frequencies to reduce the overall loss. As the thickness of the coating was increased, there was an increase in the hysteresis loss. This was because the soft magnetic coating was part of the power loss measurement, and so the loss from the coating also contributes to the total power loss.

Ni–Co–P coating may not be suitable for transformer application, because transformers operate at a flux density of 1.5 T and above and a frequency of 50 Hz. By changing the frequency from 400 to 50 Hz, the contribution of eddy current loss in the total power loss reduces, because it is directly proportional to the square of frequency. Hence, hysteresis and anomalous losses dominate at low frequencies, and so Ni–Co–P may not be suitable at these frequencies. Instead of Ni–Co–P, Co–Ni–P (cobalt > nickel) was chosen as a suitable coating, because cobalt has higher saturation magnetization than nickel. The amount of phosphorus could be balanced to develop the compressive stress in the coating. The parameters used to deposit the Co–Ni–P coating determine

the impact on final magnetic properties, such as the coercivity loss and the hysteresis loss [7].

B. Co–P-CNT Coating

Carbon nanotubes (CNTs) are known for their mechanical properties, such as high strength, elastic modulus, elastic strain bearing tendency, and many other properties, which make CNTs favorable for a number of applications. The calculation of the theoretical Young's modulus of single walled CNT of 5 GPa and its bending strength of 14.2 GPa makes it ideal for use in a composite coating. CNTs are mostly used in the composite coatings for improving the tribological properties of the material. Wang *et al.* [8] performed the surface roughness measurements of uncoated pins and Ni–P-CNT coated pins and found that the surface roughness was improved from 4 μm to between 0.1 and 0.3 μm after coating. Alishahi *et al.* [9] had reported that wear properties of the surface could be enhanced by an improvement in surface roughness from CNT coating. The surface roughness of a Ni–P coated sample was shown to improve from 192 to 129 nm with the addition of CNTs. The aim of this coating was to study the effect of improvement in the surface roughness by a CNT coating on power loss.

II. Experimental Procedure

GOES samples were supplied by Cogent Power Ltd., Newport. The aluminum orthophosphate and forsterite coating was removed by dipping it in a solution of 7.5% sulphuric acid with 1% hydrofluoric acid for approximately 10 min and then in 4% nitric acid solution for approximately 7 min. Samples were precleaned with ethanol to remove dust and stains. The samples were then coated with Co–Ni–P by the electroless plating using five different pH values (7.8, 8.2, 8.6, 9, and 9.4) at a temperature of 60 ± 5 °C. The samples were also coated separately with Co–P-CNT at a pH of 9.7 and a temperature of 62 ± 5 °C. The samples were tested with a single strip tester at magnetic flux densities of 1.5 and 1.7 T and a frequency of 50 Hz to study the power loss. Scanning electron microscopy (SEM) was used to determine the thickness of the coating deposited. Energy dispersive X-ray spectroscopy (EDS) was used to study the chemical composition of Co–Ni–P coating. The surface roughness of the uncoated and coated samples was measured by a Talysurf surface profilometer.

III. Results

A. Power Loss

The results of power loss test with an aluminum orthophosphate and forsterite coating (conventional coated), without coating, and with a Co–Ni–P coating are shown in Fig. 1. From Fig. 1, it can be seen that the power loss increases after removing the conventional coating. On coating with Co–Ni–P, the loss increases for a pH of 7.8 and 8.2. At a pH of 9, the power loss was reduced to a minimum value. Similarly, uncoated and Co–P-CNT coated samples were tested for power loss, as shown in Fig. 2. It can be seen from Fig. 2 that the loss was reduced by 13%–15% after coating it with Co–P-CNT at a magnetic flux density of 1.7 T and a frequency of 50 Hz.

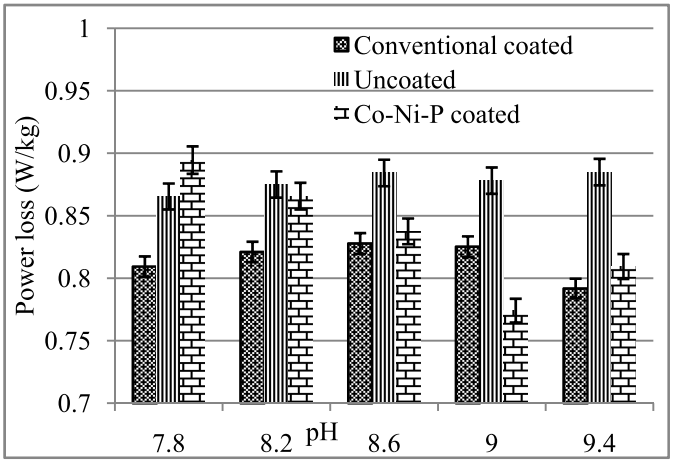

Fig. 1. Effect of pH on power loss measured at a magnetic flux density of 1.5 T and a frequency of 50 Hz.

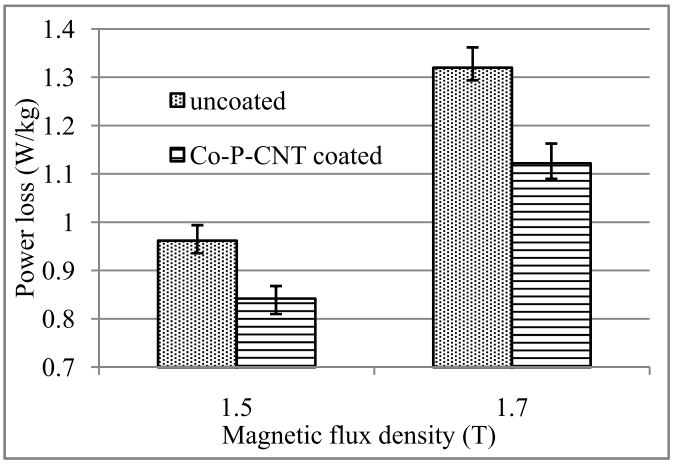

Fig. 2. Power loss of uncoated and Co–P-CNT coated samples at various flux densities and a frequency of 50 Hz (average of five samples).

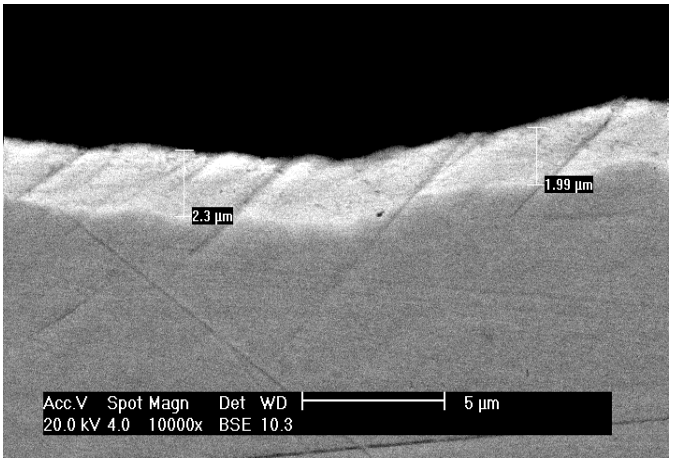

Fig. 3. SEM image of a Co–Ni–P coating on the electrical steel at a pH of 9.

B. Surface Studies

SEM was used to measure the thickness of the coatings. The gray area shows the substrate, while the light area shows the coating in Figs. 3 and 4. The thickness of Co–Ni–P and Co–P-CNT coatings was measured to be 2.15 ± 0.15 μm and 414 ± 40 nm, respectively, as shown in Figs. 3 and 4.

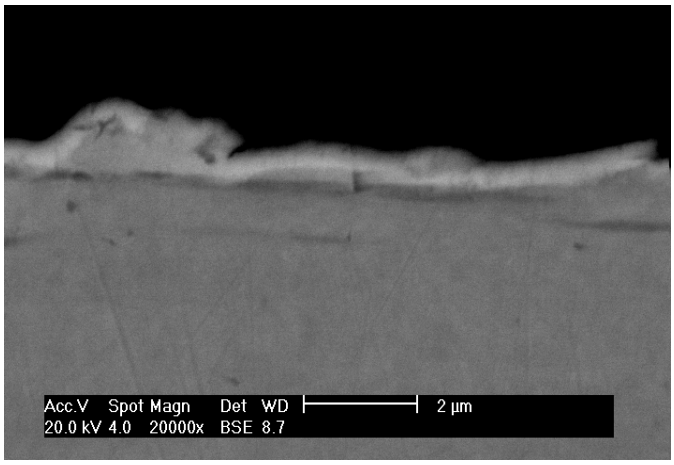

Fig. 4. SEM image of a Co–P-CNT coating on the electrical steel at a pH of 9.7.

TABLE I
ELEMENTAL COMPOSITION (WEIGHT %) OF THE COATING AT DIFFERENT pH VALUES

pH	Nickel%	Cobalt%	Phosphorus%	Sodium%
7.8	41-43	48-50	9-10	0
8.2	33-35	54-56	9-10	0
8.6	32-34	55-57	9-10	0
9.0	29-31	60--62	9-10	0
9.4	28-30	58-60	7-8	4-5

EDS results for a Co–Ni–P coating are shown in Table I. Cobalt content increases and nickel content decreases with increase in pH value. Phosphorus content was constant for all pH values except at a pH of 9.4, where sodium was introduced in the coating.

The surface roughness of uncoated and Co–Ni–P coated at different pH values is shown in Fig. 5. The surface roughness increased after coating with a Co–Ni–P coating at a pH of 7.8. It started decreasing and reached a minimum at a pH of 9, increased again as the pH increased. The surface roughness of the uncoated and Co–P-CNT coated samples was noted to be 695 ± 10 and 437 ± 3 nm, respectively.

C. Loss Separation

The power loss was separated using the model described in [10] to understand the mechanism of loss reduction after coating the samples with Co–Ni–P and Co–P-CNT coatings. The core loss was

$$W = k_h f B^{\alpha} + k_e f^2 B^2 + K_a f^{1.5} B^{1.5} \tag{1}$$

where W was the total loss, $k_h f B^{\alpha}$ was the hysteresis loss component, $k_e f^2 B^2$ was the eddy current, and $K_a f^{1.5} B^{1.5}$ was the anomalous loss component. The loss per cycle was given by

$$W/f = k_h B^{\alpha} + k_e f B^2 + K_a f^{0.5} B^{1.5}. \tag{2}$$

Equation (2) was compared with a quadratic equation of the type $a + bx + cx^2$ as shown in (3), assuming k_h, k_a, k_e, and α were constants independent of frequency and magnetic flux density. The coefficients of $f^{0.5}$ were found by plotting a fitting curve

$$W = a + bf^{0.5} + cf \tag{3}$$

where

$$a = k_h B^{\alpha} \quad b = k_a B^{1.5} \quad c = k_e B^2.$$

The values were plotted over a range of frequencies from 10 to 1000 Hz to get a good approximation of the fitting.

In Fig. 6, the power loss of the uncoated and Co–Ni–P coated samples is shown. It was observed that the hysteresis and anomalous losses reduced after coating the sample with a Co–Ni–P coating. Similarly, the power loss of uncoated and Co–P-CNT coated samples is shown in Fig. 7. After coating the sample with a Co–P-CNT coating, the hysteresis loss was reduced.

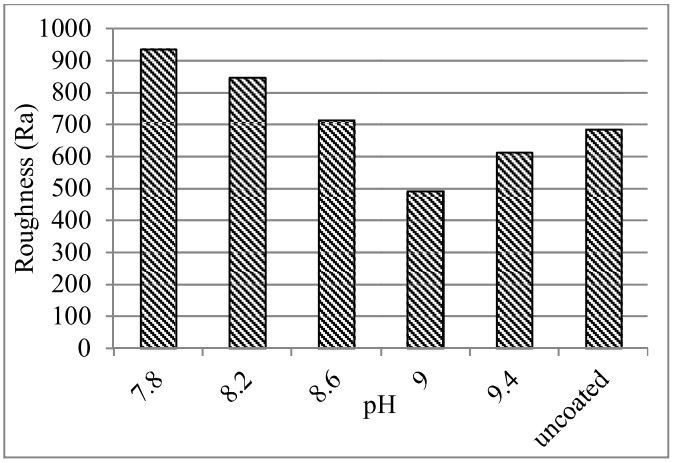

Fig. 5. Surface roughness readings for different pH values and the uncoated sample.

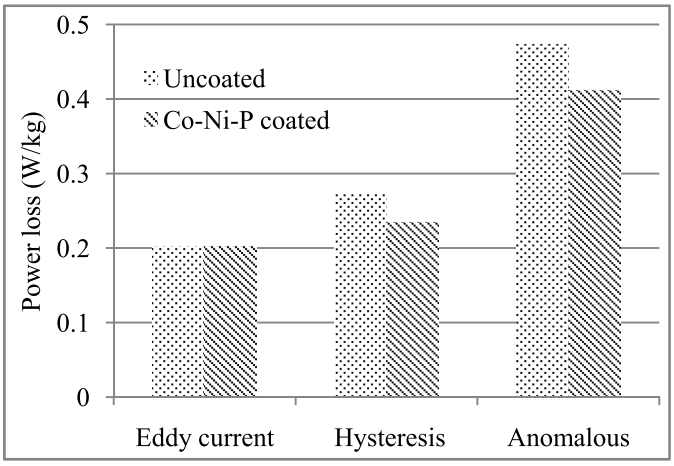

Fig. 6. Power loss separation at a frequency of 50 Hz for uncoated and Co–Ni–P coated samples at a pH of 9.

IV. DISCUSSION

A. Effect of Stress on Power Loss

Stresses develop in the electroless plating and are generated either due to the difference in the coefficient of thermal

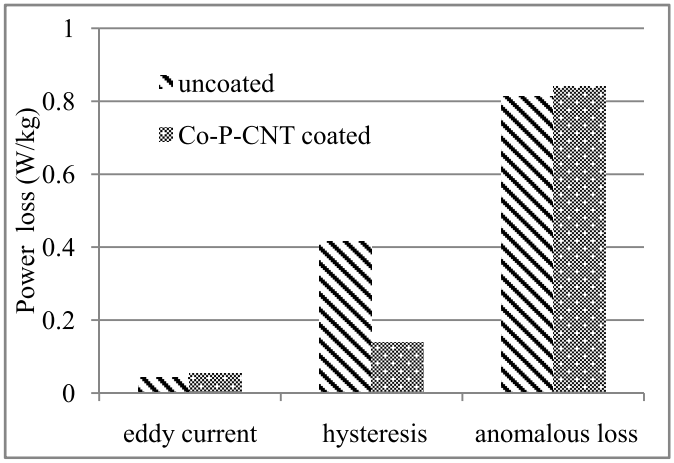

Fig. 7. Power loss separation at a frequency of 50 Hz for uncoated and Co–P-CNT coated samples at a pH of 9.7.

expansion between the substrate and the coating or during the deposition process. Duncan [11] has explained the origin of stress in the coating with relation to microstructure. Any nickel plating consists of two phases known as the beta (β) or the gamma (γ) phase. The phosphorus content dictates the relative volume of these phases. Below 5% phosphorus, the phase is entirely β, above 8.5% phosphorus, the phase is entirely γ, and between 5% and 8.5%, the microstructure consists of both β and γ. β phase is a crystalline solid solution of phosphorus in nickel, whereas γ is an amorphous phase. The two phases together make the structure incoherent, brittle and provide a tensile stress to the coating, but the individual phases alone are coherent, ductile, and impart compressive stress. The compressive stress in the coating provides the tensile stress in the electrical steel, which refines the domain structure and reduces the power loss. The phosphorus content in a Co–Ni–P coating was 9%–10% for all coatings except for the coating at a pH of 9.4. The power loss results were not in agreement with the stress generated, because another factor of surface roughness also plays an important role in the power loss as described below.

B. Surface Roughness

Wada *et al.* [12] had shown that the power loss could be reduced by 30%–40% on improving the surface roughness. The rough surface interacts with the domain walls with increased roughness leading to increased pinning and therefore, increased hysteresis loss. Improving the surface reduces the amount of domain pinning. The obtained results of power loss from Fig. 1 for the Co–Ni–P coating were in agreement with the surface roughness values in Fig. 5.

Similarly, for the sample coated with a Co–P-CNT coating, the surface roughness values in Section III-B (which improved from 695 ± 10 to 437 ± 3 nm after coating) corroborated the power loss results in Fig. 2. This improvement in surface roughness after coating reduced the power loss.

C. Loss Separation

The hysteresis and anomalous losses reduced by 15% and 13%, respectively, after coating with Co–Ni–P, as shown in Fig. 6. The application of stress by the coating on the electrical steel reduced the domain width and hence, the domain wall velocity was reduced. The anomalous loss being proportional to the domain wall velocity was reduced as a result of it. The improvement in surface roughness after the coating improved the hysteresis loss. For the sample coated with Co–P-CNT, the hysteresis loss was reduced by around 65%. This reduction of hysteresis loss was also due to the improvement in surface roughness of the electrical steel after coating it with Co–P-CNT.

V. Conclusion

The electroless plating could be considered as an effective method to coat GOES. The process offers the advantage of improving surface roughness of material after coating. Tensile or compressive stress can also be generated and tailored as per the required application. The composition of the coating can be varied by changing the pH of the solution and hence, different magnetic properties could be obtained. The process shows the capability of depositing thin and thick coatings in the range of nanometers to few micrometers. The coatings can be produced very cost effectively and no special equipment is required to develop the coating.

Acknowledgment

This work was supported by in part by Tata Steel RD&T, Rotherham, and in part by Cogent Power Ltd., Newport.

References

[1] R. Langman, "The effect of stress on the magnetization of mild steel at moderate field strengths," *IEEE Trans. Magn.*, vol. 21, no. 4, pp. 1314–1320, Jul. 1985.

[2] X. D. He, X. Li, and Y. Sun, "Microstructure and magnetic properties of high silicon electrical steel produced by electron beam physical vapor deposition," *J. Magn. Magn. Mater.*, vol. 320, nos. 3–4, pp. 217–221, 2008.

[3] P. Chivavibul, M. Enoki, S. Konda, Y. Inada, T. Tomizawa, and A. Toda, "Reduction of core loss in non-oriented (NO) electrical steel by electroless-plated magnetic coating," *J. Magn. Magn. Mater.*, vol. 323, pp. 306–310, Feb. 2011.

[4] A. Brenner and G. E. Riddell, "Deposition of nickel and cobalt by chemical reduction," *J. Res. Nat. Bureau Standards*, vol. 39, no. 5, p. 385, Nov. 1946.

[5] J. Pang, Q. Li, W. Wang, X. Xu, and J. Zhai, "Preparation and characterization of electroless Ni–Co–P ternary alloy on fly ash cenospheres," *Surf. Coatings Technol.*, vol. 205, pp. 4237–4242, May 2011.

[6] T. Osaka, M. Usuda, I. Koiwa, and H. Sawai, "Effect of phosphorus content of the magnetic and electric properties of electroless Ni–P film after heat treatment," *Jpn. J. Appl. Phys.*, vol. 27, no. 10, pp. 1885–1889, 1988.

[7] D.-H. Kim, K. Aoki, and O. Takano, "Soft magnetic films by electroless Ni–Co–P plating," *J. Electrochem. Soc.*, vol. 142, no. 11, pp. 3763–3767, 1995.

[8] L. Y. Wang *et al.*, "Friction and wear behavior of electroless Ni-based CNT composite coatings," *Wear*, vol. 254, no. 12, pp. 1289–1293, 2003.

[9] M. Alishahi, S. M. Monirvaghefi, A. Saatchi, and S. M. Hosseini, "The effect of carbon nanotubes on the corrosion and tribological behavior of electroless Ni–P–CNT composite coating," *Appl. Surf. Sci.*, vol. 258, no. 7, pp. 2439–2446, 2012.

[10] D. M. Ionel, M. Popescu, S. J. Dellinger, T. J. E. Miller, R. J. Heideman, and M. I. McGilp, "On the variation with flux and frequency of the core loss coefficients in electrical machines," *IEEE Trans. Ind. Appl.*, vol. 42, no. 3, pp. 658–667, May/Jun. 2006.

[11] R. N. Duncan, "Metallurgical structure of EN deposit," *Plating Surf. Finishing*, vol. 83, no. 11, p. 65, 1996.

[12] T. Wada, T. Nozawa, and T. Takata, "Method for producing a super low watt loss grain oriented electrical steel sheet," U.S. Patent 3 932 236, Jan. 13, 1976.